1986

RIB-STIFFENED CORRUGATED "SOIL-STEEL STRUCTURES".

SHANTARAM G. EKHANDE
University of Windsor

CANADIAN THESES

THÈSES CANADIENNES

NOTICE

The quality of this microfiche is heavily dependent upon the quality of the original thesis submitted for microfilming. Every effort has been made to ensure the highest quality of reproduction possible.

If pages are missing, contact the university which granted the degree.

Some pages may have indistinct print especially if the original pages were typed with a poor typewriter ribbon or if the university sent us an inferior photocopy.

Previously copyrighted materials (journal articles, published tests, etc.) are not filmed.

Reproduction in full or in part of this film is governed by the Canadian Copyright Act, R.S.C. 1970, c. C-30.

AVIS

La qualité de cette microfiche dépend grandement de la qualité de la thèse soumise au microfilmage. Nous avons tout fait pour assurer une qualité supérieure de reproduction.

S'il manque des pages, veuillez communiquer avec l'université qui a conféré le grade.

La qualité d'impression de certaines pages peut laisser à désirer, surtout si les pages originales ont été dactylographiées à l'aide d'un ruban usé ou si l'université nous a fait parvenir une photocopie de qualité inférieure.

Les documents qui font déjà l'objet d'un droit d'auteur (articles de revue, examens publiés, etc.) ne sont pas microfilmés.

La reproduction, même partielle, de ce microfilm est soumise à la Loi canadienne sur le droit d'auteur, SRC 1970, c. C-30.

THIS DISSERTATION
HAS BEEN MICROFILMED
EXACTLY AS RECEIVED

LA THÈSE A ÉTÉ
MICROFILMÉE TELLE QUE
NOUS L'AVONS REÇUE

RIB-STIFFENED

CORRUGATED

"SOIL-STEEL STRUCTURES"

by

© SHANTARAM G. KHANDE

A Dissertation
Submitted to the Faculty of Graduate Studies
through the Department of
Civil Engineering in partial fulfillment
of the requirments for the Degree of
DOCTOR of PHILOSOPHY
at
The University of Windsor

Windsor, Ontario, 1986

ISBN 0-315-29293-3

I hereby declare that I am the sole author of this thesis. I authorize the University of Windsor to lend this thesis to other institutions or individuals for the purpose of scholarly research.

SHANTARAM G. EKHANDE

I further authorize the University of Windsor to reproduce this thesis by photocopying or by other means, in total or in part, at the request of other institutions or individuals for the purpose of scholarly research.

SHANTARAM G. EKHANDE

The University of Windsor requires the signatures of all persons using or photocopying this thesis. Please sign below, and give address and date.

To my parents, wife and son

ABSTRACT

The method of Finite Strip is modified and applied to the three dimensional analysis of rib stiffened soil-steel structure. The strips are oriented in the curved direction, so that the effect of stiffeners is determined by considering them as individual strips. The stiffened and non-stiffened strips are treated as if being made of orthotropic material in which the properties of each strip are calculated as the average mechanical properties of its section. Herein, it is to be noted that the middle surface of the shell is not continuous along the common edge between the stiffened and non-stiffened curved elements. The eccentricity between the middle surfaces of the adjacent elements is taken into consideration in the displacement functions so that the continuity of the shell is satisfied between the strips.

The soil medium is replaced by radial and tangential extensional springs acting over the shell. The spring coefficients are dependent on the type and depth of soil, as well as the direction of displacement of the conduit wall.

The finite strip formulation is based on assumed displacement functions composed of polynomial-type shape functions and Fourier series-type basic functions. Functions

are developed to model a soil-steel structure during side filling and under the traffic loads. A structure under traffic load is modelled as a shell with hinge supports along both longitudinal edges with α representing the enclosed angle of the arch section. This formulation can also be applied to the analysis of closed conduits by considering the angle α to be in the order of 230° to 270°, depending on the relative stiffness of conduit wall with respect to the surrounding soil. This assumption of hinged supports at the invert of the conduit is valid since the bending moment and deflections are negligible in the bottom portion of the conduit. The developed formulation has been verified by the laboratory scale model tests as well as by prototype test results.

It has been observed that the provision of stiffeners at closer spacing (say 3' or 1.0m c/c) in the upper zone of the conduitshas considerable effect in reducing the conduit deformation and the combined stresses during construction. However, if the stiffener spacing is more than 9' (2.75m) c/c, the bending load carrying capacity of the stiffened upper zone is increased but slightly when compared with the capacity of non-stiffened conduits.

The practice of analysing the conduit as a plane structure is found to be approximately valid if the ratio of conduit radius (R) to stiffener spacing (S) is greater than 0.6. If $S/R \leq 0.2$, the stiffeners are considered to be fully

acting with the main shell, while for $0.2 < S/B < 0.6$, the stiffeners are considered to be partially acting with the main shell. Analysis procedures have been suggested for stiffened soil-steel structures during and after backfilling.

The failure tests of a laboratory scale model indicated that the stiffeners have considerable effect on the overall buckling of the conduit but little effect on the local buckling in the zone between the stiffeners, especially when localized live load is applied.

ACKNOWLEDGEMENTS

The author wishes to express his sincere gratitude to Dr. G. Abdel-Sayed who kindly supervised this research, for his enlightening guidance, continuous encouragement and most of all, many valuable suggestions, during the preparation of this dissertation.

The author also records his special thanks to the Civil Engineering Faculty members, especially Dr. G.R. Monforton, at the University of Windsor for their indirect inspiration through the valuable courses.

The author is grateful to the Ontario Ministry of Transportation and Communications for their financial support in sponsoring this research and providing useful prototype test results.

Thanks are due to the members of the Academic Programming Group, Computer Center, University of Windsor, for their help in running the computer programs developed during the course of this study.

Thanks are also due to Mr. Frank Kiss and Chris Allen for their assistance in conducting the laboratory model tests.

And finally, my wife, my son and my parents deserve my heartfelt thanks for their continued support and encouragement during my educational career.

TABLE OF CONTENTS

LIST OF FIGURES

LIST OF TABLES

NOMENCLATURE

A	= area of cross section of conduit wall, $in^2/in.$
A'	= unit area of cross section of unstiffened portion $in.^2/in.$
A'_s	= unit area of cross section of stiffened portion, $in.^2/in.$
b	= width of strip element, in.
$[B]$	= strain matrix
B_1	= νBx
B_l	= constant in Eq. 2.7 depending on active and passive zones.
Bx	= bending rigidity in X direction $lb.in^2/in.$
$B\theta$	= bending rigidity in ϕ direction $lb.in^2/in.$
$Bx\theta$	= torsional rigidity, $lb.in^2/in.$
C	= pitch of the corrugation profile, in.
c	= extreme fibre distance from neutral axis, in.
C_d	= constant involved in Eq. 3.32 for calculating coefficient of soil reaction.
C_o	= constant involved in Eq. 3.32 for calculating coefficient of soil reaction.
c_s	= extreme fibre distance for stiffened portion from neutral axis, in.

D = span of conduit, in.

d = deflection of conduit in Eq. 2.1, in.
depth of corrugation in Figure 3.9

$[D]$ = property matrix (both axil and bending rigidities)

D_1 = νDx

$[Db]$ = bending rigidity matrix

$[Dp]$ = axial rigidity matrix

Dx = axial rigidity in X direction, lb/in.

$D\theta$ = axial rigidity in ϕ direction, ib/in.

$Dx\theta$ = shear rigidity, ib/in.

E = modulus of elasticity of conduit material lb/in^2

E' = modulus of soil reaction, lb/in^2

F = eccentricity of stiffeners, in.

f = half depth of corrugations, in. (Figure 3.9)

$\{F\}$ = external load vectors.

F_s = factor involved in Eq. 3.62 for calculating shear coefficient in top soil.

f_b = buckling stress of conduit wall, lb/in^2

fy = yield stress of conduit material, ib/in^2

$Fu^{(a)}(\eta)$ = shape function for u displacement

$Fv^{(a)}(\eta)$ = shape function for v displacement

$Fw^{(a)}(\eta)$ = shape function for w displacement

h, Hc = height of cover over conduit, in.

I, I', I_s and I'_s = moment of inertias of conduit wall

i = i'th end of strip

j = j'th end of strip

K = factor in Eq. 2.7 depending on the relative stiffness of conduit wall and the soil.

= a proportionality constant in Eq. 5.2

K_o = coefficient of earth pressure at rest (Eq. 3.58)

K_1 = bedding constant in Eq. 2.1

K_I = factor in Eq. 5.21

K_c = load reduction factor in Eq. 5.23

K_n = normal coefficient of soil reaction (lb/in^3)

K_s = tangential coefficient of soil reaction (lb/in^3)

l = length as defined in Figure 3.9

L = length of beam between two supports, in.

l_1 = arc length of shell, Eq. 5.5, 5.6 (in.)

L_i = length of spring, in.

m,n = fourier series terms in basic functions

M = total number of fourier series terms.

$\{M\}$ = bendig stress array (M_x, M_θ, $M_{x\theta}$)

M_x = bending moment in X direction, lb.in/in.

M_θ = bending moment in ϕ direction, lb.in/in.

$M_{x\theta}$ = torsional moment, lb.in/in.

$\{N\}$ = axial stress array (N_x, N_θ and $N_{x\theta}$)

N = total number of strips

NDF = number of degrees of freedom

N_x = axial force in X direction, lb/in.

N_θ = axial force in ϕ direction, lb/in.

$N_{x\theta}$ = shear force lb/in.

P_c = design soil pressure at the crown.

P_r = soil pressure arround the conduit, lb/in^2

P_i = horizontal force along the support of i'th strip. lb/in.

P_n = horizontal earth pressure.

$\{P_s\}$ = equivalent load vectors, Eq. 3.46

P_t = total horizontal force along the supports. lb.

P', P'_s = unit force along support, per unit width of unstiffened and stiffened shell respectively. lb/in

q_c = load intensity at the crown level.

q_w = radial component of total shear force T_o

q_θ = tangential component of total shear force T_o

R = radius of cylindrical shell, in.

R' = radius of shell at a given point, in.

r = radius of gyration, in.

$[S]$ = stiffness matrix

t = thickness of conduit wall, in.

T = axial thrust, lb/in.

T_o = shear force in the soil at crown level

u = in-plane displacement in X direction with respect to the surface 1-1

u_s = in-plane displacement in X direction with respect to the surface 2-2

ux = rate of change of u or u_s with respect to X

U_i = strain energy of i'th element

v = in-plane displacement in ϕ direction with respect to the surface 1-1

v_s = in-plane displacement in ϕ direction with respect to the surface 2-2

vx = rate of change of v or v_s with respect to X

v_c = v displacement correction

w = out-of-plane displacement in Z direction with respect to the surface 1-1, (Figure 3.6)

w_s = out-of-plane displacement in Z direction with respect to the surface 2-2, (Figure 3.6)

wx = rate of change of w or w_s with respect to X

w_c = w displacement correction

W = width of stiffener, in.

We = effective width of stiffener, in.

Wi = external work done on i'th element.

β = reduction factor accounting for the depth of cover in Eq. 2.5

= factor involved in an expression for calculating

the coefficient soil reaction (Eq. 3.35)

γ = unit weight of soil (lb/in^3)

η = variable, x/b, in/in.

ν = Poisson's ratio

α = intersection angle of the shell

α_{eq} = equivalent intersection angle of the closed shaped conduit.

λ = a parameter connected with the natural frequency of a beam.

ε_1, ε_2 = measured strains

$\{\varepsilon\}$ = strain array

εx = axial strain in X direction.

$\varepsilon\theta$ = axial strain in ϕ direction.

$\gamma_{x\theta}$ = shear strain

$\{\chi\}$ = curvature or bending strain array

χ_x = bending strain in X direction

χ_θ = bending strain in ϕ direction

$\chi_{x\theta}$ = torsional strain

Π_p = total potential energy

Π_{pi} = potential energy for i'th element

$\phi_{u(\theta)}^{(m)}$ = basic function for u displacement

$\phi_{v(\theta)}^{(m)}$ = basic function for v displacement

$\phi_{w(\theta)}^{(m)}$ = basic function for w displacement

= stress (axial or bending)

θ_o = angle between the point of contraflexure in the upper zone of conduit.

θ_1 = half intersection angle formed by the spread of the load at crown level and the vertical at crown (Figure 3.13)

$\{d_i^{(m)}\}$ = displacement degrees of freedom at i and j ends of strip.

d_o = applied horizontal displacement along the supports, in.

Chapter I

INTRODUCTION

1.1 General

Underground conduits are being built in large numbers in North America as highway and railroad bridges, tunnels and highway underpasses. An example is shown in Figure 1.1. This development is accompanied by a steady increase in the size of installed conduits [69,82][1]. Conduits with spans as large as 58 feet (17.68 m), have been successfully constructed and are performing satisfactorily. Here, the term soil-steel structures is being used for bridges and culverts which are composed of corrugated steel plate shells embedded in an envelope of engineered soil. Their high load carrying capacity is due to the interaction between their wall displacement and the pressure induced in the surrounding soil.

Long span soil-steel structures came to be regarded as an economical alternative to conventional short span bridges because of the ease and speed of their design and construction [42]. Construction of conventional bridges is labour intensive and much of this labour is highly skilled. Major capital plant equipments, such as cranes and the like,

---

[1] The bracketed numbers indicate the refernce number as listed in the bibliography.

are required and conventional bridge components are usually made of high grade material. In contrast, the major component in soil-steel structure is soil which is one of the lowest cost building materials and widely available. Furthermore, the high performance of earth moving equipment makes the construction of flexible buried conduits highly productive and economical. The cost of maintaining diversions and detours is reduced because of the very fast construction of such structures. Normal pavement and shoulders over the structure eliminate some problems such as bridge deck deteriorations [68].

A report by the United States Federal Highway Administration estimates that using these low cost bridges results in saving of 30% over the conventional short span bridges. Similar savings are reported in Canada [25], while the Australian experience found the cost of soil-steel bridges to be typically 1/3 of that of the conventional bridges [37]. Value analysis by a product designer [77], concludes that most conventional overpass structures do not represent optimum design. Alternative design using flexible metal arches and culverts were favored when considering all governing parameters. These parameters are economy in design, fabrication, construction, maintenance, appearance and safety.

The conduit walls are usually made of corrugated steel panels with a corrugation depth of 2 inches (51 mm), a pitch

of 6 inches (152mm) and a thickness upto 0.315 in. (8mm). The plates are corrugated, punched and then galvanized and curved. They are usually shipped unassembled and bolted together at the site. The panels are very flexible and the buried flexible conduits are constructed so as to induce beneficial interaction between the conduit walls and the surrounding soil. The soil acts as an integral part of the structural system. If the diameter (or span) of a soil-steel structure made of multi-plates exceeds 25 ft. (7.62m), the structure is referred to as superspan [56]. With the increase of span, problems arise due to large deflection during construction of the flexible panels and lower buckling load capacity at the upper zone when subjected to dead and live loads.

The building of long span conduits is made possible and their performance is improved by providing curved stiffeners (or ribs) placed at intervals in the longitudinal direction. One recent example of such a structure with stiffeners is the Cheese Factory Bridge in the county of Wellington, where the stiffeners are made of rolled W10x49 (W250mm x 73kg/m) sections, at 6' (1.83m) spacing, Figure 1.2. Also, Table 1.1 shows the list of long span rib-stiffened soil-steel structures in the United States, designed and fabricated by SYRO steel company [79]. In those structures the stiffeners were made of angle sections, bolted at the crest of shell corrugations.

Peaking is typical of long span behavior during placement of backfill. In very flexible shells without stiffeners, severe peaking is common, requiring special restraints such as the use of top loading to limit excessive deflections of crown (Figure 1.3). To overcome the problem of excessive deformation at crown during backfilling, several construction techniques have been developed [51] such as the provision of curved stiffeners. The stiffeners increase the ring stiffness[2] of the upper zone of the conduit, and this reduces significantly the problems of deflection during backfilling. Even stiffened long-span structures are quite flexible, and they derive considerable portion of their load carrying capacity through interaction with the surrounding backfill. Design of these structures requires an understanding of this interaction, and a means for estimating the loads in the structures. However, at present, a proper procedure is not available for the evaluation of the composite action of the stiffeners and the steel panels.

Furthermore, soil-steel structures are analysed by considering a unit transverse slice of the steel structure and the surrounding soil [8,11,33,42]. This approach of plane analysis is usually acceptable for non-stiffened conduits since their properties do not change in the longitudinal direction. This practical approach of plane analysis may also be used for stiffened conduits after

---

[2] Ring Stiffness is defined as $EI/2^3$ of conduit.

establishing a rational criteria for determining the stiffener's effect. With the installation of the stiffeners, the conduit properties vary in the longitudinal direction and hence plane analysis can be utilised if we know the equivalent rigidity (EI) of the stiffened conduit wall. The computation of EI would be easier if one knows the width of the shell plates that is acting together as an integral part of the stiffener section. As of now, the designer has the information of the magnitude of the effective width when the sheets are flat, in which case the effective width is affected mainly by the shear lag in the panels which lead to a very limited reduction of the width between the stiffeners. Due to the absence of proper procedure there are several practices of estimating the equivalent bending rigidity of the stiffened conduit wall. Some designers assume the equivalent bending rigidity to be the sum of the bending rigidities of the stiffener and the main shell, as if the stiffener is not acting together with the main shell, while others estimate the equivalent bending rigidity by assuming full effectiveness of the stiffener with the shell [79]. The actual rigidity is in between the above mentioned two approaches, i.e., considering a part of the main shell acting with the stiffeners. Therefore, one of the objectives is to determine the equivalent rigidity of the stiffened conduit. Also, the load distibution pattern in the stiffened shell needs to be studied, during and after backfilling.

1.2 Objectives

Usually the depth of soil cover over the conduit crown varies in its longitudinal direction, with no cover at the ends and maximum cover over the middle of the structure, due to the profile of the road cross section. Service loads are usually applied on small patch loads (wheel loads) on the embankment level. Both these facts demand three dimensional analysis. The use of finite element method of analysis for this purpose would be very cumbersome, expensive and time consuming. Therefore, an alternate method of three dimensional analysis, which is inexpensive with regards to time and computer storage, needs to be developed.

The need has also has been established for a study of the actual performance of the stiffened cylindrical shells embedded in soil. It is necessary to examine the parameters that influence the effectiveness of stiffeners, both for conduits under construction as well as when subjected to service loading.

The objectives of this research are classified mainly in two parts as follows:

1) During the Construction Stage,
   a) to determine the rigidity of the stiffened shell in order to predict the displacements of the crown.
   b) to study the Bending Moment Capacity of the stiffened shell.
2) Under Live Loads,

a) to establish the load distribution in stiffened conduit wall in the longitudinal direction.

b) to study the design aspects of stiffened shell considering, (a) axial thrust, and (b) bending moment and axial thrust.

c) to study the stability of the stiffened conduit.

In order to achieve these objectives, it is essential to develop a computer program for the analysis of soil-steel structure system with varying properties in the longitudinal direction. The program based on the finite strip method of analysis avoids the previously mentioned shortcomings by,

1) considering different strip properties for conduit wall and stiffener strips.

2) simulating varying depth of soil cover over each strip by means of equivalent extensional radial and tangential springs, the coefficients of which are dependent on the height of soil cover over each strip, density of soil and the deflection of the conduit wall.

Chapter II

HISTORICAL BACKGROUND

2.1 General

The following discussion reviews the contributions of the work which most influenced the present research. The literature devoted to the subject of soil-steel structure behavior, in general, is abundant, but the literature dealing with the stiffened soil-steel structure behavior, in particular, is minimal.

The behavior of soil-steel structures has been examined by employing diverse empirical and analytical techniques. These range from approximate empirical calculation of ring compression [93], to highly sophisticated finite element analysis incorporating nonlinear stress-dependent properties of the soil media [33,42,48]. In between these approaches, the physical idealization or analog modelling of the soil-structure interaction has been developed [32,49,65]. However, so far these studies were generally confined to non-stiffened soil-steel structures. Better understanding of the behavior of soil-steel structure has led to the development and usage of larger size of structures [14,56,60,68,71,79], and thereby, a number of constructional and functional problems have arisen. A brief review of the

enhancement in the understanding of soil-steel interaction is presented below.

2.2 Conventional Design Methods.

Here, the conventional design methods are summarized in order to provide an appreciation of the past thinking which eventually led to the more refined developments in the analysis and design of soil-steel structures of today.

Generally, the commonly used methods for flexible culvert design involved establishing a load distribution around the culvert and then using this load distribution to determine the stresses in the culvert wall. Marston [57] was the first to investigate the load induced on buried conduits. Spangler [73] modified and extended Marston's theory to flexible culverts. Figure 2.1 shows the assumed simple pressure distribution in their method. At the top and bottom of the conduit the vertical soil pressure is assumed uniform and at the sides, a parabolic horizontal pressure is considered with the maximum at mid-height. The vertical presure is distributed over the diameter and the horizontal pressure over the arc length subtending a 100° angle at the centre. The intensity of the effective uniform pressure is assumed to be equal to the weight of a sliding vertical soil column above the crown of the conduit plus or minus the shearing resistance on the sides of the soil column. The maximum horizontal pressure at the ends of the horizontal diameter

of the conduit is assumed to be directly proportional to the horizontal deflection of the sides. According to the assumed distribution, the circumferential thrust is a function of the radius of the circular cross-section of the conduit, R, and the intensity of the vertical pressure at the crown, P_c. Approximate values for thrust and moments at the crown and shoulders are estimated as well and are shown in the same figure.

The radial deflection under the assumed loading consists of a downward movement of the top and outward movement of the sides of the conduit. Spangler also developed an empirical formula, which is as follows, to compute the deformation of the culvert:

$$d = \frac{K_1 P_c R^4}{EI + 0.061E' R^3} \qquad [2.1]$$

where,

- E = Modulus of elasticity of the conduit wall material in psi.
- I = Moment of inertia per unit length of cross section of conduit in in^4/in.
- E' = Modulus of soil reaction, in psi.
- P_c = Design soil stress at the crown, force per unit area. (It is equivalent to the overburden pressure plus any distributed live load including impact at the top of the conduit due to the moving loads.)

and

- K_1= Constant, depending on bedding angle and deflection lag factor.

Spangler assumed the crown deflection of 5% or less of the diameter to be a safe deflection and accordingly gave a design procedure based on this deflection.

The ring compression theory, developed by White and Layer [83], assumes the conduit as a thin ring in compression, neglecting overburden stress distribution, interface friction and bending stiffness. Basically the theory states that the thrust per unit length in the culvert wall is constant and is equal to the overburden stress applied at the crown of the culvert multiplied by one-half of the span of the structure, (Figure 2.2).

$$T = P_c \cdot \frac{D}{2} \qquad [2.2]$$

in which,

- T= Thrust, force per unit length of conduit.

and

- D= Span, unit of length.

For a non-circular conduit, the radial pressure is considered to vary in such a way that the circumferential thrust in the wall remains constant throughout the circumference. Therefore, the soil pressure at any point around the conduit is given by:

$$P_r = \frac{T}{R'} \qquad [2.3]$$

where, R' is the radius of curvature at any point under consideration. Eq. 2.3 indicates that the soil pressure is maximum at the point of minimum radius.

Any circumferential thrust that occurs in the ring causes ring compression stress equal to T/A, which is considered as a basis for design. Watkins and Musser [79] have applied this concept of design to the rib-stiffened culverts and studied the adequacy of some of the existing structures by dead and live load testing in the light of ring compression theory.

In order to check the conduit walls against buckling, Booy [15] applied the buckling formula of an elastically supported beam to the soil-steel structure as given below:

$$f_b = \frac{2}{A}\left(\frac{E\,I\,E'}{R}\right)^{1/2} \qquad [2.4]$$

where,

- f_b = buckling stress, and
- A = cross-sectional area per unit length of the conduit wall.

Meyerhof and Baikie [61], and Luscher [55], suggested similar equations for calculating the buckling stresses of flexible pipes. Watkins [81] considered a modification of the buckling stress for a pipe under hydrostatic pressure to account for the friction in actual soil around the conduit.

Based on Watkins's equation and the studies of Glock & Kloppel [49]. Abdel-Sayed [1] suggested the following formula which considers the relative stiffness of the soil with respect to the rigidity of the conduit wall as well as the effect of shallow cover,

$$f_b = \frac{3 E \beta}{(K R/r)^2} \qquad [2.5]$$

where,

- r = radius of gyration of the conduit wall,

and

- β = a reduction factor accounting for the depth of cover.

β has a value equal to unity if soil cover is more than twice the radius of conduit; if less, then β has the following value:

$$\beta = \left(\frac{h}{2R} \right)^{1/2} \qquad [2.6]$$

The value of factor K, which depends upon the relative stiffness of the conduit wall with respect to the adjacent soil, is given by:

$$K = B_l \left(\frac{E I}{E' R^3} \right)^{1/4} \qquad [2.7]$$

and B_1 has value of 1.22 in passive pressure zone and it has the following value in the active pressure zone,

$$B_1 = 1.22 \left[1.0 + 2. \left(\frac{EI}{E' R^3}\right)^{1/4} \right] \qquad [2.8]$$

Inelastic buckling is considered to start when 'f_b' equals half the yield stress 'f_y' of the wall material. A parabolic equation is assumed for the transition zone between full yielding ($KR/r = 0$) and the elastic zone at $f_y/2$. The buckling stress in the transition zone is given by:

$$f_b = f_y - \frac{f_y^2}{12 E \beta} \left(\frac{K R}{r}\right)^2 \qquad [2.9]$$

where K and β have the same values as those for buckling in the elastic zone.

Design, based on the buckling criteria, is achieved by selecting the wall thickness so that it is capable of carrying the thrust with an adequate factor of safety against buckling stress.

All the above buckling considerations are incorporated in the design codes [64].

2.3 Elastic Theory Solutions.

Burns [18] presented mathematical closed form solution to the problem of ring inclusion in an elastic media. The method can consider or neglect the friction between the conduit and the surrounding soil. According to Burns, a circular pipe having a depth of soil cover more than 1.5 times the pipe diameter can be analysed by assuming it to be an elastic cylindrical shell encased in an isotropic, linearly elastic medium of infinite extent subjected to a surface overburden pressure. Over simplifications to achieve closed form mathematical solutions limit the range of application of this method.

2.4 Frame on Elastic Supports.

Considering the conduit problem as a frame on elastic supports was proposed by Drawsky [32]. He replaced the conduit by a segmented ring surrounded by a system of radial springs. Later, Kloppel & Glock [49] used this approach to evaluate the buckling load. Herein, the soil is replaced by discrete elastic springs and the conduit by two dimensional polygon as shown in Figure 2.3. The active pressure is due to the movement of the soil towards the conduit and passive pressure is activated by the movement of the conduit wall towards the supporting fill. The frame is loaded by a radial pressure in the form of sine wave. To determine the zone of passive earth pressure, an iterative process was applied wherein the springs experiencing tension were deleted.

Recently Ghobrial & Abdel-Sayed [39] applied this type of model to study the inelastic buckling of soil-steel structures. They made use of spring coefficients developed by Okeagu & Abdel-Sayed [66].

2.5 Improved Spring Analog Model for Soil.

Accuracy of the analog modelling is dependent on proper evaluation of the coefficients of soil reaction. The significant work in this area belongs to Meyerhof & Baikie [61], Kloppel & Glock [49], Okeagu & Abdel-Sayed [66]. Constant values of coefficient of soil reactions (Kn) have been considered by Meyerhof & Baike and Kloppel & Glock. Their studies were limited by considering circular conduits and isotropic, homogeneous and linear soil media. Expressions for coefficients of soil reactions (Kn and Ks), developed by Okeagu and Abdel-Sayed, incorporate the parameters such as depth of soil cover (H), degree of compaction (c), span of conduit (S), unit weight of soil (γ), and direction of soil normal to displacement (θ). All other parameters such as rigidity of conduit (EI), Poisson's ratio of soil (ν) etc. were found not to affect the coefficient of soil reactions. Okeagu's spring coefficients were based on the results from a finite element analysis by Hafez [43]. The expressions for Kn and Ks have certain limitations. Their applicability to non-circular and non-elliptical conduits is doubtful. However, the

development of such analog modelling presented a useful tool to investigate a number of otherwise difficult problems, such as three dimensional behavior of soil-steel structure.

2.6 Finite Element Analysis.

Plane-strain finite elements have been used extensively for the analysis of buried conduit problems. Brown [17] developed a finite element program for flexible culverts under high fill. Allgood & Takahashi [11], Abel, et al. [8], Hafez [43], Dessouki [30], Katona, et al. [48] have developed similar programs with different capabilities. The most general of these is CANDE (Culvert ANalysis and DEsign), developed by Katona, Smith, Odella and Allgood [48]. All finite element programs are written for a slice of unit width of the structure, thereby assuming no variation of loading as well as shell properties in the longitudinal direction. Changes in structural properties in the longitudinal direction are predominant for stiffened shell. Thus the stiffener effects cannot be predicted by such analysis. Due to the complexities in three dimensional finite element, the application of finite element has been limited to plane-strain problems in soil-steel interaction studies.

2.7 Field Performance Tests.

Until recently the analysis procedures for soil-steel structures were mainly verified by the laboratory model tests, with a definite type of boundary conditions imposed on the models. Therefore, there was a growing need for field performance tests on prototype structures in order to support the various analytical procedures. Field performance tests give true reflection of the behavior of full size soil-steel structures. Recently such tests have been conducted on existing soil-steel structures, both in Canada and the United States [13,14,33,60,71,72,79]. These field test results have led to a better understanding of the soil-steel interaction. In Canada, the Ontario Ministry of Transportation and Communications (MTC) is in the forefront in conducting the field tests. MTC has tested the existing soil-steel structures of different shapes and sizes. The existing structure tested first was the Deux Rivieres Structure made of 5 gauge steel sheets of 6x2 in. (152x51 mm) corrugated profile. The second tested structure was the Adelaide Creek structure, which is of horizontally elliptical cross section made of Westeel Bosco K-D plate pipe. The third tested structure was the White Ash Creek soil-steel structure located on highway 21 in Thamesville, Ontario. This too is a Westeel Bosco K-D plate pipe. The section is circular, 25 feet (7.62 m) in diameter. The soil cover is extremely shallow in comparison to its span,

ranging from 3' to 4'-1" (0.91-1.24 m). The shell is composed of 6x2 in. (152x51 mm) corrugated plate with a thickness of 0.184 inch (4.67 mm). The most recently tested structure is the Cheese Factory Bridge in the county of Wellington, near Guelph, Ontario. This structure is considered to be the largest soil-steel structure and is made of 6x2 in. (152x51 mm) standard corrugation profile with a thickness of 0.276 inch (7 mm). The speciality of this structure is that it is fitted with curved stiffeners, made of W10x49 (W250mm x 73kg/m) rolled sections [Figure 1.2 and Figure 3.16]. The test results of this structure were not available at the time of writing of this dissertation.

Table 1.1 shows the list of soil-steel structures that have been tested by SYBO Steel Company of the United States [79]. All these structures were fitted with angle stiffeners, with spacing varying from 3 to 4 feet (0.91-1.22 m). Herein, the test results were interpreted by assuming full interaction of stiffeners with the main shell.

2.8 Finite Strip Method of Analysis.

Recently, the finite strip method has been developed by Cheung (1968) [22] and used with considerable success for the analysis of certain type of structures. The work presented by Kantorovick and Krylov [47], and by Vlasov [78], represent two of the important studies that contributed to the development of finite strip method.

Thereafter, this method of analysis has been extensively applied to the flat plate problems [24,40,41,46,74,75]. Although the finite strip method is in its advanced stages of development, its application to the curved members is very limited.

In 1979 Ibrahim and Monforton [46], applied the finite strip method of analysis to sandwich shell roofs in which the basic functions chosen were in the longitudinal direction of shell. This type of formulation is suitable for shells with or without stiffeners in longitudinal direction. For soil-steel structure, besides longitudinal thrust beams, the practice is to provide curved stiffeners. This type of arrangement necessitates curved finite strip formulation.

The stiffened sections of soil-steel structure are usually eccentric to the centroidal surface of the main shell. So far, most of the analyses consider the stiffener centroidal surface to be coinciding with the centroidal surface of the rest of the shell. This does not predict exactly the interaction of stiffener with the shell. Therefore, a formulation is needed that can tie the behavior of eccentric stiffener with the centroidal surface of the main shell.

Many investigators have combined the spring analog model of soil with the finite element method (as discussed earlier) mainly to describe plane-strain behavior. If the spring analog model is coupled with the cylindrical shell

finite strip, it would lead to the prediction of three dimensional performance of the soil-steel structure.

It has been concluded that the finite strip method is a powerful and convenient approach for the analysis of some classes of structures (plates and shells).

Chapter III

THEORETICAL FORMULATION

3.1 Introduction

The discussion in this chapter is focused on the finite strip capability for predicting the behavior of the soil-steel structure and the formulation procedure. A substantial number of problems which arise in structural analysis are not amenable to closed form solutions. Numerical means of structural analysis such as the finite element method have become relatively routine in recent years. However, the finite element method, while proven versatile and powerful, has some shortcomings mainly in terms of computer storage and time needed to solve the large number of algebraic equations. Therefore, for certain types of structures it is worthwhile to develop an alternative numerical approach in which a reduced number of simultaneous equations are needed. One of these approaches is the finite strip method. By comparing both finite element and finite strip approaches, a saving in computer storage and time can be realised. The finite element method requires the division of the domain of the structure into elements in both directions and boundary conditions are imposed only after the overall stiffness matrix has been formed. In the finite

strip method, the domain is divided only in one direction into a number of strips along the total length of the structure, (Figure 3.1). The displacement functions are chosen such that both force and displacement boundary conditions at the two ends of the strip (i.e. $\theta = 0, \alpha$) are satisfied. The general two dimensional problem is then reduced to a one dimensional problem, with a relatively small number of undetermined edge displacement parameters along the two sides of the strip in the X direction. For certain types of structures, the size of strip stiffness matrix is relatively small with a narrow band width; thus, the finite strip method for these structures is ideally suitable for programming on small computers.

The finite strip method presented herein is based on the principle of minimum potential energy which can be stated as [63]:

> "Of all geometrically admissible displacement states satisfying compatibility in the interior and the displacement boundary conditions, that which makes the potential energy minimum satisfies the equilibrium conditions and the force boundary conditions and is therefore, the actual displacement state."

In order to guarantee that the finite strip method be a monotonically converging potential energy formulation, it is essential that the assumed displacement states satisfy the geometric admissibility conditions of the principle of minimum total potential energy. These conditions can be obtained by examining the potential energy formulations.

Since the nature of the energy is undefined until the boundary conditions are specified, satisfaction of the boundary conditions necessarily forms one of the admissibility conditions. In the finite strip method, both the force and geometric boundary conditions are satisfied at the two ends of strip "a priori", while in width direction no force boundary conditions are imposed. However, this does not represent a violation of the previously mentioned admissibility condition, since at a true minimum potential energy, the force boundary conditions will be inherently satisfied. The remaining geometric admissibility conditions involve continuity requirements on the assumed displacement patterns; that is, the displacement functions must have a sufficient number of bounded derivatives as required by the form of the total potential energy expression.

A strip stiffness matrix with preset end conditions can be developed by substituting the assumed displacement functions into the strain energy formulation. It is pointed out that the strip stiffness matrix is always non-singular because of the preset boundary conditions. The overall stiffness matrix of the structure can be obtained by imposing the geometric admissibility conditions between the adjacent strips. This is achieved by the integer variable correlation scheme (known as IVC), in which the degrees of freedom of the various strips are linked together in such a way that the displacements of the discretized structure are

physically compatible with those of the original structure. The potential of the applied loads is dealt with on a work equivalent basis, in which the work equivalent loads associated with the corresponding degree of freedom are derived.

The finite strip approach represents a comprcmise between the finite element approach and the classical methods such as Navier and Lavi's solutions of plate and shell analysis. As mentioned before, the finite element method requires large storage and computing time, while application of classical methods to shells becomes cumbersome. In fact the finite strip method seems to be the best analysis tool for the problem under consideraton. The detailed fcrmulation of finite strip method for cylindrical shell is discussed later in this chapter.

3.2 Orientation of Strips

Cylindrical shell structures can be divided into a number of longitudinal strips (Figure 3.2), or curved shell strips (Figure 3.1), spanning in the transverse direction.

With the rectangular strip, the cylindrical shell is assumed to be made of many sided polygon. The more the number of rectangular strips considered, the clcser it is to the original curved shape of the shell. This type of strip orientation embeds given boundary conditions alcng the ends of strips i.e. along the curved ends of the shell, in the

assumed displacement functions. The rectangular strip formulation can be conveniently used for cylindrical shells with or without longitudinal stiffeners. The longitudinal stiffener spanning the full length of a shell can make one or more such strips. If the longitudinal stiffener is eccentric to the main shell (as is usually the case), modified type of displacement functions are required to be used to take care of the discontinuity in centroidal surfaces. Any type of boundary conditions (clamped, hinged or simple support) along the curved supports of the shell can be preset by longitudinal flat strip. However, for the cylindrical shells that are fitted with curved stiffeners, the shell needs to be idealized by a number of curved or cylindrical shell strips (Figure 3.1).

Cylindrical (curved) strip orientation can take any boundary condition along the curved edges of the strip. The transverse stiffened shell portion can constitute one or more such strips.

3.3 Displacement Functions

The finite strip method can be considered as a special form of the finite element procedure using the displacement approach. Unlike the standard finite element method which uses polynomial displacement functions in all directions, the finite strip method calls for the use of simple polynomials in the strip width direction (X direction), and

continuously differentiable smooth series functions in the strip length direction (curved direction in present case), with the stipulation that such a series should satisfy 'a priori' the boundary conditions at the ends of the strips.

The assumed displacement patterns for membrane displacements (u & v) and lateral/radial displacement (w), are chosen in such a way that both force and displacement boundary conditions at the two ends of the strip (i.e. $\theta = 0, \alpha$) are satisfied in advance. Moreover, the displacement functions must satisfy the geometric admissibility conditions of the principle of minimum total potential energy. If these two conditions are met, convergent solutions are expected.

The general form of these displacement functions consists of following two parts:

1) Shape Function, which is a n'th order polynomial in the strip width direction.

2) Basic Function, which is a continuous differentiable function in the strip length direction.

This type of displacement function is the combination of displacement functions used in finite element approach and that used in the classical methods of plate analysis.

The following form of displacement functions are considered for the cylindrical shell strip:

$$u = \sum_{m=1}^{M} Pu^{(m)}(\eta)\ \phi_u^{(m)}(\theta)$$

$$v = \sum_{m=1}^{M} Pv^{(m)}(\eta)\ \phi_v^{(m)}(\theta), \quad \text{and} \qquad [3.1]$$

$$w = \sum_{m=1}^{M} Pw^{(m)}(\eta)\ \phi_w^{(m)}(\theta)$$

$Pu^{(m)}(\eta)$, $Pv^{(m)}(\eta)$ and $Pw^{(m)}(\eta)$ are the shape functions of n'th order depending on the type of accuracy desired, and $\phi_u^{(m)}(\theta)$, $\phi_v^{(m)}(\theta)$ and $\phi_w^{(m)}(\theta)$ are the basic series functions in the ϕ direction.

3.3.1 Shape Functions

The shape functions relate the undetermined displacement coefficients (or the degrees of freedom, DOF), $\{ d_j \}$, along the nodal lines of strip. For $Pu^{(m)}(\eta)$, $Pv^{(m)}(\eta)$ and $Pw^{(m)}(\eta)$, third order polynomials have been used which are of the following form:

$$Pu^{(m)}(\eta) = \sum_{j=1}^{2} [\ H_{oj}^{(1)}(\eta) \cdot u_{jm} + H_{1j}^{(1)}(\eta) \cdot ux_{jm}\ ]$$

$$Pv^{(m)}(\eta) = \sum_{j=1}^{2} [\ H_{oj}^{(1)}(\eta) \cdot v_{jm} + H_{1j}^{(1)}(\eta) \cdot vx_{jm}\ ] \qquad [3.2]$$

and

$$Pw^{(m)}(\eta) = \sum_{j=1}^{2} [\ H_{oj}^{(1)}(\eta) \cdot w_{jm} + H_{1j}^{(1)}(\eta) \cdot wx_{jm}\ ]$$

where $H^{N}_{ki}(\eta)$ is a Hermite interpolation polynomial such that,

- N = no. of derivatives that the polynomial can interpolate.
- η = argument (variable) of the function = x/b
- i = station or nodal line numbers

and,

- k = index ranging over the number of derivatives to be interpolated.

By going through the interpolation scheme, the following interpolation polynomials are obtained:

$$H^{(1)}_{01} = 1 - 3\eta^2 + 2\eta^3$$

$$H^{(1)}_{02} = 3\eta^2 - 2\eta^3 \qquad [3.3]$$

$$H^{(1)}_{11} = b\,(\eta - 2\eta^2 + \eta^3)$$

$$H^{(1)}_{12} = b\,(\eta^3 - \eta^2)$$

These interpolation polynomials are derived on the basis of four points. For example, u_1, ux_1, u_2 and ux_2 for u displacement, v_1, vx_1, v_2, and vx_2 for v displacement and w_1, wx_1, w_2 and wx_2 for w displacement. The first derivative of $Fu^{(m)}(\eta)$ with respect to x is quadratic therefore, the axial strain δx which is a function of first derivative of $Fu^{(m)}(\eta)$ has a parabolic variation over the strip width. Also, since $dH^{(1)}oj/dx$ has zero values at j=1 and j=2, the axial strain

has no discontinuity at a common nodal line of two strip elements. Similarly, the shearing strain ($\gamma_{x\theta}$) has no discontinuity at the common nodal line of two adjacent strips. The bending moment M_x is a function of second derivative of the shape function $Fw^{(m)}(\eta)$. In order to achieve a continuity in moment M_x in the X direction along the common nodal line, six point (w_1, wx_1, wxx_1, w_2, wx_2, and wxx_2) interpolation must be considered. However, in the corrugated soil-steel structure system, with the corrugation in the direction of strip, the capacity M_x is of secondary importance, and hence the accuracy in the continuity of M_x is not considered significantly important. Therefore, the third order or four point interpolation polynomial has been used for the shape function $Fw^{(m)}(\eta)$ also. The discontinuity induced in the marginal values of M_x due to the third order interpolation polynomial is not considered erroneous. However, this may not be acceptable in case of isotropic shell where, to achieve M_x continuity fifth order (or six point) interpolation polynomial has to be used.

3.3.2 Basic Functions

The basic functions for structural systems are derived such that force and displacement boundary conditions at the end of the strip are satisfied. These basic functions can usually be obtained by seeking the solution of the differential equation of a vibrating beam spanning the two ends of the structure [22]. The differential equation is given by,

$$Y^{IV}(y) - \frac{\lambda^4}{L^4} Y(y) = 0 \qquad [3.4]$$

where,

- L = the length of the beam between the two supports (ends)
- λ = A certain parameter connected with the natural frequency of a beam.
- Y(y) = represent the basic functions.

The general solution of the above homogeneous differential Eq. 3.4 is given as follows:

$$Y(y) = C_1 \sin\left(\frac{\lambda y}{L}\right) + C_2 \cos\left(\frac{\lambda y}{L}\right) + C_3 \sinh\left(\frac{\lambda y}{L}\right) + C_4 \cosh\left(\frac{\lambda y}{L}\right) \qquad [3.5]$$

Where C_1, C_2, C_3 and C_4 are arbitrary constants, which can be obtained by satisfying the force and displacement boundary conditions at both ends of the beams (or strip). The Eq. 3.4 and Eq. 3.5 are for straight beam (or strip). Similar to Eq. 3.5, the general form of basic function $\phi(\theta)$ for a cylindrical shell strip can be obtained by substituting $R\theta$ for y and $R\alpha$ for L in Eq. 3.5, which is written as follows;

$$\phi(\theta) = C_1 \sin\left(\frac{\lambda\theta}{\alpha}\right) + C_2 \cos\left(\frac{\lambda\theta}{\alpha}\right) + C_3 \sinh\left(\frac{\lambda\theta}{\alpha}\right) + C_4 \cosh\left(\frac{\lambda\theta}{\alpha}\right) \qquad [3.6]$$

Here also, the values of constants C_1, C_2, C_3 and C_4 can be obtained by imposing the specific force and displacement boundary conditions at $\theta=0$ and $\theta=\alpha$ ends.

Specific basic functions for u, v and w need to be derived for the cylindrical shell strip to represent two important life stages of soil-steel structure, namely (i) soil-steel structure during side filling and (ii) soil-steel structure under traffic loads. The basic functions for these two cases are discussed below.

3.3.2.1 Basic Functions For Structure During Side Filling

During side filling of the structure, a horizontal force is applied at the sides and at the thrust beam level (Figure 3.3). Due to this horizontal force, the shell segment between the thrust beams is considered having moved in the radial and tangential direction, as well as rotated at the ends. This structural system is idealized by a structure as shown in Figure 3.4. The tangential displacements are allowed to take place at the ends while no radial (w) displacements are allowed. The rotation at the ends is considered by assuming no moments at the ends. The following force and displacement boundary conditions for this case can be written.

$$\begin{matrix} u = 0 & M_\theta = 0 \\ w = 0 & N_\theta = 0 \end{matrix} \qquad \text{at } \theta = 0 \text{ and } \theta = \alpha \qquad [3.7]$$

The following basic functions satisfy these force and displacement boundary conditions:

$$\phi_u^{(m)}(\theta) = \sin\left(\frac{m\pi\theta}{\alpha}\right)$$

$$\phi_v^{(m)}(\theta) = \cos\left(\frac{m\pi\theta}{\alpha}\right) \qquad [3.8]$$

and

$$\phi_w^{(m)}(\theta) = \sin\left(\frac{m\pi\theta}{\alpha}\right)$$

By assuming no axial thrust at the ends, the external and internal $N\theta$ forces do not match at the ends. Therefore, a certain corrective force effect is required to be added in the displacement function v. This is considered in section 3.3.3 of this chapter.

These sets of basic functions are orthogonal in nature. The following integrals become non-zero only when m and n are equal.

$$\int_0^{\alpha} \phi_u^{(m)}(\theta)\, \phi_u^{(n)}(\theta)\, r\,d\theta = 0$$

$$\int_0^{\alpha} \phi_v^{(m)}(\theta)\, \phi_v^{(n)}(\theta)\, r\,d\theta = 0$$

$$\int_0^{\alpha} \phi_w^{(m)}(\theta)\, \phi_w^{(n)}(\theta)\, r\,d\theta = 0 \qquad \text{For } m \neq n \qquad [3.9]$$

$$\int_0^{\alpha} \phi_v^{(m)\prime}(\theta)\, \phi_w^{(n)}(\theta)\, r\,d\theta = 0$$

$$\int_0^{\alpha} \phi_u^{(m)\prime}(\theta)\, \phi_v^{(n)}(\theta)\, r\,d\theta = 0$$

This nature of orthogonality causes decoupling effects of $\{d^{(m)}\}$ and $\{d^{(n)}\}$ with each other. Therefore, for the above basic functions the resulting band width of the stiffness matrix is small.

3.3.2.2 Basic Functions For Structure Under Traffic Load

This case is modelled by a two hinged arch as shown in Figure 3.5. No displacements are allowed along the supports.

The force and displacement boundary conditions that needed to be satisfied are:

$$u = v = w = 0$$
$$\text{and} \qquad \text{at } \theta = 0, \alpha \qquad [3.10]$$
$$M_\theta = 0$$

To satisfy these boundary conditions the following types of basic functions are suggested:

$$\phi_u^{(m)}(\theta) = \sin\left(\frac{m\pi\theta}{\alpha}\right)$$
$$\phi_v^{(m)}(\theta) = \sin\left(\frac{m\pi\theta}{\alpha}\right) \qquad [3.11]$$
$$\phi_w^{(m)}(\theta) = \sin\left(\frac{m\pi\theta}{\alpha}\right)$$

For the cylindrical shell element, the membrane and lateral displacements are coupled because of the presence of curvature, unlike the case of a rectangular flat strip. It

is observed here that the coupling of basic function $\phi_v(\theta)$ and its derivatives with the derivatives of the remaining basic functions result in a high degree of non-orthogonality as shown below:

$$\int_0^{\alpha} \phi_u^{(m)*}(\theta)\, \phi_v^{(n)}(\theta)\, r\,d\theta \neq 0$$

$$\int_0^{\alpha} \phi_v^{(m)*}(\theta)\, \phi_w^{(n)}(\theta)\, r\,d\theta \neq 0 \qquad \text{for } m \neq n \qquad [3.12]$$

Because of the non-orthogonality nature of the basic functions (Eq. 3.11), coupling exists between $\{d^{(m)}\}$ and $\{d^{(n)}\}$. Therefore, in this case, the solution is obtained by considering all Fourier series terms together, unlike the orthogonal basic functions. Non-orthogonality has the effect of increasing the size and the bandwidth of stiffness matrix. It is observed that due to the high degree of non-orthogonality in basic functions of Eq. 3.11, a sufficiently high number of Fourier series terms need to be considered. This forfeits the main advantage of the finite strip in terms of time and storage reduction. Therefore, the basic function $\phi_v^{(m)}(\theta)$, for v displacement needs revision.

In order to reduce the non-orthogonality effect, one must use the cosine series function for $\phi_v^{(m)}(\theta)$ and some constants to impose the given displacement boundary condition as shown below.

Let the new $\phi_v^{(m)}(\theta)$ be given by the following expression.

$$\phi_v^{(m)}(\theta) = \cos\left(\frac{m\pi\theta}{\alpha}\right) - L_{1m}(\alpha-\theta) - L_{2m}(\theta) \qquad [3.13]$$

where (L_{1m}) and (L_{2m}) are the constants, to be determined by imposing a condition of zero tangential (v) displacement at the ends.

i.e. $v = 0$ at $\theta = 0, \alpha$ [3.14]

Imposing this condition on Eq. 3.13, the following form of basic function is obtained.

$$\phi_v^{(m)}(\theta) = \cos\left(\frac{m\pi\theta}{\alpha}\right) - 1 + \frac{\theta}{\alpha}\left(1 - (-1)^m\right) \qquad [3.15]$$

This new basic function for v is necessarily a modified sine series obtained by superposition of a linear polynomial on a cosine series in order to give zero end displacements.

The set of basic functions for the case under consideration are,

$$\phi_u^{(m)}(\theta) = \sin\left(\frac{m\pi\theta}{\alpha}\right)$$

$$\phi_v^{(m)}(\theta) = \cos\left(\frac{m\pi\theta}{\alpha}\right) - 1 + \frac{\theta}{\alpha}\left(1 - (-1)^m\right) \qquad [3.16]$$

$$\phi_w^{(m)}(\theta) = \sin\left(\frac{m\pi\theta}{\alpha}\right)$$

The modified basic function for v is still non-orthogonal with the remaining basic functions. However, the degree of

non-orthogonality is considerably reduced due to the presence of the cosine series term in $\phi_v^{(m)}(\theta)$. Yet the unknown displacement coefficients corresponding to each Fourier series cycle, m, cannot be independently solved. However, as will be shown in Appendix D, $\phi_v^{(m)}(\theta)$ and its derivatives are orthogonal with $\phi_u^{(m)}(\theta)$ and $\phi_w^{(m)}(\theta)$ when the values of m'th and n'th terms of the Fourier series are even and odd. Thus unknown displacement coefficients for odd values of m (=1, 3, 5 etc.) are coupled together, so also the displacement coefficients for even values of m. Therefore, the solution is obtained in two stages.

Although the non-orthogonality of basic functions has the effect of increasing the size of the strip matrix and the overall stiffness matrix of the structure, the resulting size is not alarming due to the existence of non-coupling of odd and even terms, and limited non-orthogonality due to the presence of cosine series in the basic function for v displacement.

3.3.3 Corrections in Displacement Functions

The displacement functions in Eq. 3.1 with basic functions as given in Eq. 3.8, do not give axial force equal to the tangential component of applied force at the supports. Therefore, a corrective displacement function must be added to Eq. 3.1. The corrective displacement functions are assumed as follows:

$$v_c = \frac{P_i R}{D_\theta} \sin(\alpha/2 - \theta') \qquad [3.17a]$$

and,

$$w_c = 0 \qquad [3.17b]$$

where,

- P = The horizontal force applied at supports per unit width of i'th strip.
- R = Radius of the shell strip.
- D_θ = Axial rigidity of i'th shell strip in the curved direction.
- θ' = Angle measured from the support.

Eq. 3.17a gives zero v displacement at $\theta' = \alpha/2$ and maximum v displacements at the supports (and are equal and opposite in nature). The axial force at the supports is given by:

$$(N_\theta)_{\theta'=0,\alpha} = (\varepsilon_\theta)_{\theta'=0,\alpha} \times D_\theta \qquad [3.17c]$$

$$= \left[\frac{1}{R} \frac{\partial v_c}{\partial \theta} - \frac{w_c}{R} \right] \times D = P \cos(\alpha/2) \qquad [3.17d]$$

which is same as the tangential component of applied horizontal force at the supports.

3.4 Displacement Functions For Eccentric Stiffeners

Usually the curved stiffeners are provided either on the underside or outside of the shell surface. This causes an eccentricity in the centroidal surface of the stiffened portion of the shell with respect to the centroidal surface of the main shell as shown in Figure 3.6. The displacement functions given in section 3.3 are based on the displacement coefficients $\{d_i^{(m)}\}$ along the surface 1-1. The centroidal surface of the stiffened portion is 2-2. Thus there is a shift in the surface by an amount P. In order to specify the displacement functions along the surface of the stiffened element, the displacements along the surfaces 1-1 and 2-2 must be correlated. This is shown in Figure 3.7 and Figure 3.8.

Let 'P' be the eccentricity of the centroidal surface 2-2 with respect to 1-1. P is considered positive if the stiffener is installed on the outer surface of the shell.

From the shell deformation geometries shown in Figure 3.7 and Figure 3.8, the displacements u_s, v_s and w_s for the stiffened element at surface 2-2 can be expressed in the following form:

$$u_s = u + F\frac{\partial w}{\partial x}$$

$$v_s = v - F\frac{\partial w}{\partial y}, \quad \text{or}$$

$$v_s = v - \frac{F}{R'}\frac{\partial w}{\partial \theta}, \quad \text{and} \qquad [3.18]$$

$$w_s = w$$

Where u, v and w are the displacements at the surface 1-1 of the main shell, which are given by Eq. 3.1. In this study, the effect of eccentricity on the displacement u_s is considered negligible. On substituting the expressions for u, v and w in Eqs. 3.18, the following expressions are obtained for displacement functions for eccentric stiffener.

$$u_s = \sum_{m=1}^{M}\sum_{j=1}^{2}\phi_u^{(m)}(\theta)\left[H_{oj}^{(1)}(\eta)\,u_{jm} + H_{1j}^{(1)}(\eta)\,ux_{jm}\right] \qquad [3.19a]$$

$$v_s = \sum_{m=1}^{M}\sum_{j=1}^{2}\left\{\phi_v^{(m)}(\theta)\left[H_{oj}^{(1)}(\eta)\,v_{jm} + H_{1j}^{(1)}(\eta)\,vx_{jm}\right]\right.$$

$$\left. - \frac{F}{R'}\frac{\partial \phi_w^{(m)}(\theta)}{\partial\theta}\left[H_{oj}^{(1)}(\eta)\,w_{jm} + H_{1j}^{(1)}(\eta)\,wx_{jm}\right]\right\} \qquad [3.19b]$$

and

$$w_s = \sum_{m=1}^{M}\sum_{j=1}^{2}\phi_w^{(m)}(\theta)\left[H_{oj}^{(1)}(\eta)\,w_{jm} + H_{1j}^{(1)}(\eta)\,wx_{jm}\right] \qquad [3.19c]$$

Where $H^N_{ki}(\eta)$ are as defined in Eq. 3.3 and the basic functions as defined in Eq. 3.8 or Eq. 3.15 depending on the problem at hand.

3.5 Strain-Displacement Relations

Any point on the middle surface of the shell element will undergo displacements u, v and w in the directions of X, ϕ and Z respectively. The strains (ε_x, ε_θ and $\gamma_{x\theta}$) have been expressed in terms of the displacements u, v, w and their derivatives by several investigators [31,38,78]. The accuracies of these different formulations and the factors affecting their degrees of approximation have been examined by Marzouk and Abdel-Sayed [58] and they have proposed the following linear strain-displacement relations.

$$\varepsilon_x = \frac{\partial u}{\partial x}$$

$$\varepsilon_\theta = \frac{1}{R'} * \frac{\partial v}{\partial \theta} - \frac{w}{R'} \qquad [3.20]$$

$$\gamma_{x\theta} = \frac{1}{R'} * \frac{\partial u}{\partial \theta} + \frac{\partial v}{\partial x}$$

Where, u, v and w are as defined by Eq. 3.1. From the above equations, it is observed that the in-plane and out-of-plane displacements are coupled together (unlike for the flat plates) even for small deformations due to the presence of the curvature. The strain-displacement relations for the

stiffener are obtained by substituting the displacement functions u_s, v_s and w_s (Eq. 3.19), in the above expressions instead of u, v and w.

3.6 Curvature-Displacement relations.

Similar to the strain-displacement relations, the curvature-displacement relations as proposed by Marzouk and Abdel-Sayed [58] are used in this study and are given below.

$$\chi_x = - \frac{\partial^2 w}{\partial x^2}$$

$$\chi_\theta = - \frac{1}{R'^2} \left(w + \frac{\partial^2 w}{\partial \theta^2} \right) \qquad [3.21]$$

$$\chi_{x\theta} = - \frac{1}{R'} * \frac{\partial^2 w}{\partial x \partial \theta}$$

3.7 Internal Force Components

For the case of an ideal orthotropic shell, the material has three planes of symmetry with respect to its elastic properties. These planes are the co-ordinate planes X, ϕ and Z. The relations between the internal force components, i.e., axial forces (Nx, Nθ), shear force (Nxθ), bending moments (Mx, Mθ) and torsional moment (Mxθ), in terms of strain components, for the case of plane stress in the X and ϕ planes can be represented by the following expressions.

$$\begin{Bmatrix} Nx \\ Ne \\ Nxe \end{Bmatrix} = \begin{bmatrix} Dx & D1 & 0 \\ D1 & De & 0 \\ 0 & 0 & Dxe \end{bmatrix} \begin{Bmatrix} \varepsilon x \\ \varepsilon e \\ \gamma_{xe} \end{Bmatrix} \qquad [3.22]$$

or,

$$\{ N \} = [Dp] \{ \varepsilon \} \qquad [3.23]$$

and

$$\begin{Bmatrix} Mx \\ Me \\ Mxe \end{Bmatrix} = \begin{bmatrix} Bx & B1 & 0 \\ B1 & Be & 0 \\ 0 & 0 & Bxe \end{bmatrix} \begin{Bmatrix} \chi_x \\ \chi_e \\ \chi_{xe} \end{Bmatrix} \qquad [3.24]$$

or,

$$\{ M \} = [Db] \{ \chi \} \qquad [3.25]$$

Where,

{ N } array of axial forces (axial and shear)

{ M } array of moments (bending and torsional)

Dx, De and Dxe are the extentional and shear rigidities.

Bx, Be and Bxe are the bending and torsional rigidities.

$D_1 = \nu Dx$

$B_1 = \nu Bx$

[Dp] axial rigidity matrix.

[Db] bending rigidity matrix.

Substituting Eq. 3.20 and Eq. 3.21 for strains and curvatures, into Eq. 3.23 and Eq. 3.25, the internal force.

components can be written in terms of the displacement components and their derivatives. Thus, if the state of displacements is known, the internal force components can be calculated.

Eq. 3.23 and Eq. 3.25 can be written in combined form as shown below:

$$\begin{Bmatrix} \{ N \} \\ \{ M \} \end{Bmatrix} = \begin{bmatrix} [Dp] & [0] \\ [0] & [Db] \end{bmatrix} \begin{Bmatrix} \{ \varepsilon \} \\ \{ \chi \} \end{Bmatrix} \qquad [3.26]$$

3.8 Mechanical Properties of Corrugated Sheets.

Cylindrical shells made of corrugated sheets can be treated as being made of elastic orthotropic material in which the mechanical properties are equal to the average properties of the sheet. This approach was proved to be valid and to adequately consider the main features of response of the shell [3,35]. The determination of the appropriate elastic properties is an important part of any analysis in which an essentially open profile is replaced by a planar orthotropic material. The inplane and bending rigidities used in this study are those for a standard sinusoidal (arc and tangent) profile as shown in Figure 3.9 and may be expressed in terms of the profile dimensions as follows [3]:

$$Dx = \frac{E}{6(1-\nu^2)} \left(\frac{t}{I} \right)^2 t$$

$$D\theta = \frac{1}{C} t E$$

$$Dx\theta = \rho \frac{Et}{2(1+\nu)} \frac{C}{1} \qquad [3.27]$$

$$Bx = \frac{C}{1} \frac{Et^3}{12(1-\nu^2)}$$

$$B\theta = 0.522 E f^2 t , \quad \text{and}$$

$$Bx\theta = \frac{1}{C} \frac{E t^3}{12(1+\nu)}$$

In the above equations Dx and Dθ are the in-plane rigidities in the directions of the axis of the shell co-ordinate system, and Dxθ is the in-plane shear stiffness. Bx, Bθ and Bxθ are the corresponding bending rigidities. The profile dimensions c, l, f and t are as defined in Figure 3.9, and ρ represents a reduction factor to allow for slip in the sheet to sheet and sheet to frame connections. A value of ρ = 0.75 has been used in this study.

For corrugated sheet, values of D1 and B1 (Eq. 3.23 and 3.24) are assumed to be negligible, because of the fact that the stretching or bending in one direction does not cause significant change in the forces in the perpendicular direction of the corrugation profile.

3.9 Development Of Element Stiffness Matrix.

3.9.1 General

The element stiffness matrix is obtained by invoking the principle of minimum potential energy. The substitution of the properly chosen displacement functions into the appropriate strain energy expressions (U) and the potential of applied loads expression (W) and integrating over the entire reference surface area of the strip results in the total discretized potential energy (Πp) of the i'th strip element. Thus the total potential energy (Πp)i of each element is given by,

$$\Pi_{pi} = Ui - Wi \qquad [3.28]$$

The potential energy Πpi is a function of the undetermined displacement coefficients along the nodal lines of the strip under consideration. The total potential energy of the entire shell is then simply the addition of individual potential energy of each strip. Since the potential energy is a scalar quantity, its magnitude remains independent of the co-ordinate system chosen. Thus the following expression can be written for Πp,

$$\Pi_p = \sum_{i=1}^{N} \Pi_{pi} = \sum_{i=1}^{N} Ui - \sum_{i=1}^{N} Wi \qquad [3.29]$$

In an exact solution, the total potential energy will always be truly minimum. Since the displacement functions will, in

general, only model the true situation approximately, Π_p will not have the true minimum value and an approximate solution is obtained by minimizing Π_p with respect to the variations in the values of the displacement coefficients in the assumed displacement functions. This operation results in a number of simultaneous algebraic equations equal to the total number of displacement coefficients for the entire shell structure which is equal to the number of degrees of freedom (NDF).

The alternate procedure for obtaining the simultaneous algebraic euations for the entire structural system is that instead of minimizing the total Π_p, individual Π_{pi} is minimized with respect to the variations in displacement coefficients for the i'th element, resulting in a number of equations equal to the number of unknown displacement coefficients for the i'th strip element (say n_i). Thus we have the total number of equations equal to n_i times the number of elements (N). Noting the fact that there are common nodal lines for adjacent strip elements, the total number of equations for entire structural system are reduced to the required number of equations equal to the total independent displacement coefficients for the entire structure by achieving geometric admissibility conditions between the adjacent strip elements by means of variable correlation technique. These final sets of equations are solved simultaneously by standard mathematical methods, such

as Gauss Elimination Method, for displacement coefficients. Once these coefficients are known, the state of displacements and forces at any point on the shell is known. In the following sections this procedure is demonstrated.

3.9.2 Strain Energy Of Each Strip

The strain energy of the strip is given by the following expression.

$$Ui = \frac{1}{2} \int_V \{ \delta_T \}^T \{ \sigma \} \, d \, (vol) \qquad [3.30a]$$

Where,

$$\{ \delta_T \} = \text{strain array} = \begin{Bmatrix} \delta \\ \chi \end{Bmatrix} = [B] \{ d \} \qquad [3.30b]$$

$[B]$ = strain matrix

$$\{ \sigma \} = \text{stress resultants} = \begin{Bmatrix} N \\ M \end{Bmatrix} = [D] \{ \delta_T \} \qquad [3.30c]$$

$$= [D] [B] \{ d \}$$

$$[D] = \text{property matrix} = \begin{bmatrix} [0] & [Db] \\ [Dp] & [0] \end{bmatrix} \qquad [3.30d]$$

Substituting the values of $\{\delta_T\}$ and $\{ \sigma \}$ in the Eq. 3.30a, the following expression for internal strain energy in the strip is obtained.

$$Ui = \frac{1}{2} \int_V \{ d \}^T [B]^T [D] [B] \{ d \} d(vol) \quad [3.31]$$

3.9.3 Simulation Of Surrounding Soil

Soil plays an important role in the behavior of soil-steel structures after the backfilling. Many investigators have come up with a procedure of idealization of the surrounding soil by means of extensional radial and tangential springs, thereby avoiding complexities involved in the behavior of the surrounding soil [49,61,66]. The mixed type of shell strip with such springs is shown in Figure 3.10.

Recent studies by Okeagu and Abdel-Sayed in 1984 [66], find the normal coefficients of soil reaction (Kn), to depend on the type and depth of soil, span of the conduit, as well as on the direction of displacement of conduit wall, and are given by the following expressions:

$$Kn = \gamma B C_d C_\theta \left(\frac{h}{D} \right)^{1/2} \quad [3.32]$$

In which,

$$C_d = 4.25 - \frac{0.75 D}{100} \quad [3.33]$$

$$C_\theta = 0.25 \left(1 + 5.4 \frac{\theta}{\pi} \right) \quad [3.34]$$

B = 1.0 for dense compacted granular fill

or

$$= 0.45 + \frac{D}{200}\left(\frac{\theta}{\pi} - 0.5\right)^2 \qquad [3.35]$$

where,

- h = depth of fill at the point where Kn is computed
- D = span of the conduit in inches.
- γ = unit weight of soil in lb./in^3.
- θ = angular co-ordinate in radians (see Figure 3.11)

The tangential coefficient of soil reaction, Ks, is assumed to be constant around the conduit surface and is about 20% of the coefficient Kn at the invert of the conduit.

The evaluation of the equivalent axial stiffness of radial and tangential springs, in terms of Kn, Ks and the spacing of springs is illustrated in Appendix D.

3.9.3.1 Strain Energy Due To Normal (Radial) Springs

As seen before, the assumed radial deflection of the strip is given by:

$$w = \sum_{m=1}^{M} \phi_w^{(m)}(\theta)\left[H_{o1}^{(1)}(\eta)\, w_{1m} + H_{11}^{(1)}(\eta)\, wx_{1m} + H_{o2}^{(1)}(\eta)\, w_{2m} + H_{12}^{(1)}(\eta)\, wx_{2m} \right] \qquad [3.36]$$

Since the springs are attached to the shell strip, the axial deformation of the i'th spring at θ_i radians from the supports is given by,

$$w_i = \sum_{m=1}^{M} \phi_w^{(m)}(\theta_i) \left[H_{01}(\eta) \overset{(1)}{w}_{1m} + H_{11}(\eta) \overset{(1)}{wx}_{1m} + H_{o2}(\eta) \overset{(1)}{w}_{2m} + H_{12}(\eta) \overset{(1)}{wx}_{2m} \right] \quad [3.37]$$

where,

$\eta_i = \frac{\tilde{x}_i}{b}$ and η has the following values,

$= \frac{1}{6} b, \frac{1}{2} b$ and $\frac{5}{6} b$ (Figure 3.10)

The axial strain in i'th normal/radial spring is given by,

$$\varepsilon_i = \frac{w_i}{l_i} \quad [3.38]$$

Where l is the length of i'th spring. Therefore,

$$\varepsilon_i = \sum_{m=1}^{M} \frac{\phi_w^{(m)}(\theta i)}{l} \left[H_{o1}^{(1)}(\eta_i) \; H_{11}^{(1)}(\eta_i) \; H_{o2}^{(1)}(\eta_i) \; H_{12}^{(1)}(\eta_i) \right] \begin{Bmatrix} w_{1m} \\ wx_{1m} \\ w_{2m} \\ wx_{2m} \end{Bmatrix} \quad [3.39]$$

or

$$\varepsilon_i = [B_i] \{w_i\} \quad [3.40]$$

The stress in i'th spring is

$$\sigma_i = (E A)_i \, \delta_i \qquad [3.41]$$

Where $(EA)_i$ is the equivalent axial rigidity of the i'th spring. (see Appendix D)

The strain energy in the i'th spring is given by,

$$U_i^{sn} = \frac{1}{2} \int_0^{l_i} \{\delta_i\}^T \{\sigma_i\} \, dl_i \qquad [3.42a]$$

or

$$U_i^{sn} = \frac{1}{2} \int_0^{l_i} \{w_i\}^T [B_i]^T (EA)_i \{w_i\} \, dl_i \qquad [3.42b]$$

3.9.3.2 Strain Energy Due To Tangential Spring

As seen before, the assumed tangential displacement of the strip is given by the following general form:

$$v = \sum_{m=1}^{M} \phi_v^{(m)}(\theta) \left[H_{o1}^{(1)}(\eta) \, v_{1m} + H_{11}^{(1)}(\eta) \, vx_{1m} + H_{02}^{(1)}(\eta) \, v_{2m} \right.$$

$$\left. + H_{12}^{(1)}(\eta) \, vx_{2x} \right] - \frac{P}{R} \sum_{m=1}^{M} \frac{\partial \phi_w^{(m)}(\theta)}{\partial \theta} \left[H_{o1}^{(1)}(\eta) \, w_{1m} \right. \qquad [3.43]$$

$$\left. + H_{11}^{(1)}(\eta) \, wx_{1m} + H_{o2}^{(1)}(\eta) \, w_{2m} + H_{12}^{(1)}(\eta) \, wx_{2x} \right]$$

The axial strain in the i'th tangential spring is given by,

$$\delta_i = \frac{v_i}{l_i} \qquad [3.44]$$

Following the same procedure, as given for normal spring, the strain energy for i'th tangential spring can be expressed in terms of displacement coefficients, strain matrix and equivalent stiffness $(EA)_i$, of spring.

3.9.4 Potential Of Applied Loads

The potential of the applied loads is generated using a work equivalent load approach. The external work expression for the i'th strip can be expressed as follows:

$$W = R\int_0^b\int_0^\alpha q_x(x,\theta)\cdot u(x,\theta)\cdot dx\,d\theta + R\int_0^b\int_0^\alpha q_\theta(x,\theta)\cdot v(x,\theta)\cdot dx\,d\theta + R\int_0^b\int_0^\alpha q_w(x,\theta)\cdot w(x,\theta)\cdot dx\,d\theta \qquad [3.45]$$

where, $q_u(x,\theta)$, $q_v(x,\theta)$ and $q_w(x,\theta)$ are the surface loads at a given point (x,θ) on the strip and $u(x,\theta)$, $v(x,\theta)$ and $w(x,\theta)$ are the displacements of the strip at (x,θ) point.

The work equivalent loads for the i'th strip are calculated by substituting the assumed displacement patterns into the expression of the potential of the applied loads (Eq. 3.45) and then performing the indicated integrations. The work done by the applied loads can be expressed as,

$$W = \{P_s^{(m)}\}^T \{d_i^{(m)}\} \qquad [3.46]$$

where $\{P_s^{(m)}\}$ consists of the equivalent load vectors in the directions of undetermined displacement coefficients $\{d_i^{(m)}\}$.

The use of Eq. 3.45 in deriving the consistent load matrix is demonstrated in Appendix E for the case of uniform load. The evaluation of equivalent load vectors for the case of uniform vertical load is demonstrated in Appendix F.

3.9.5 Discretized Potential Energy

The discretized potential energy of the i'th strip is given by Eq. 3.28. As mentioned before, in the case of orthogonal basic functions (Eq. 3.8), the resulting stiffness matrix is uncoupled. Therefore, the solution can be obtained by determining the degrees of freedom corresponding to each Fourier series term independently, and the final solution is the sum of the solutions of all terms of the Fourier series considered. For such systems, the discretized potential energy for the m'th term of the Fourier series can be written as,

$$\Pi_{pi}^{(m)} = U_i^{(m)} - W_i^{(m)} \qquad [3.47]$$

Or,

$$\Pi_{pi}^{(m)} = \frac{1}{2}\int \{d^{(m)}\}^T [B^{(m)}]^T [D] [B^{(m)}] \{d^{(m)}\} d(vol) - \{P_s^{(m)}\}^T \{d^{(m)}\} \qquad [3.48]$$

or,

$$\Pi_{pi}^{(m)} = \frac{1}{2}\int \{d^{(m)}\}^T [S^{(m,m)}] \{d^{(m)}\} \, d(vol) - \{P_s^{(m)}\} \{d^{(m)}\} \quad [3.49]$$

where,

- $[S^{(m,m)}]$ is the strip stiffness matrix.
- $\{P_s^{(m)}\}$ contains the work equivalent loads associated with each degree of freedom $\{d^{(m)}\}$

However, in the case of non-orthogonal basic functions (Eq. 3.16), the resulting stiffness matrices are coupled with each other. Therefore, in the solution, all appropriate number of Fourier series terms (M) are required to be considered together. For such a system, the discretized potential energy can be written as,

$$\Pi_{pi} = \frac{1}{2}\sum_{m=1}^{M}\sum_{n=1}^{M} \{d^{(n)}\}^T [S^{(m,n)}] \{d^{(m)}\} - \sum_{m=1}^{M}\sum_{n=1}^{M} \{P_s^{(m)}\}^T \{d^{(n)}\} \quad [3.50]$$

where $[S^{(m,n)}]$ is coupled stiffness matrix and is given by,

$$[S^{(m,n)}] = \int [B^{(m)}]^T [D] [B^{(n)}] \, d(vol) \quad [3.51]$$

By virtue of the principle of minimum total potential energy, the equilibrium positions are associated with the displacement states for which Π_p is minimum. This is achieved by the partial differentiation of the total

potential energy with respect to each displacement coefficient. This minimization procedure leads to the following sets of equations.

$$[S] \{ d \} - \{ P \} = 0 \qquad [3.52]$$

In which,

$$[S] = \int [B^{(m)}]^T [D] [B^{(m)}] \, d(vol) \qquad [3.53]$$

for orthogonal basic functions.

$$[S] = \int [B^{(m)}]^T [D] [B^{(n)}] \, d(vol) \qquad [3.54]$$

for non-orthogonal basic functions.

The evaluation of [S] is shown in Appendix E.

3.10 Equivalent Angular Span Of Full Conduit

The assumed displacement functions (Eq. 3.16) are compatible to the cylindrical shell strip with hinged supports. The use of full alfa (=360°) in these displacement functions will not represent the true behavior of the closed shaped conduit. The bending moment and displacements in the lower portion of the conduit are usually negligible. The bending moment diagram for soil-steel structures, Figure 3.12, indicates two points of contraflexure in the bottom half of the structure. These two points can be treated as two hinges in the equivalent conduit. The bottom portion beyond these two points of contraflexure can be neglected, since the movement of the conduit and bending moments below

these points are not significant. The angle between these two points in the upper zone of the conduit can be regarded as an equivalent angle alfa, in the displacement basic functions. The point of contraflexure in the upper zone of the conduit is located approximately at an angle θ_o from the vertical axis of the conduit [1]. The central equivalent angle alfa, between the lower contraflexure points, is assumed to be proportional to the angle θ_o. By observation, the equivalent angle can be given in terms of θ_o as follows,

$$\frac{1}{2}\alpha_{eq} = 2.25\ \theta_o \quad \text{radians} \qquad [3.55]$$

where,

$$\theta_o = 1.6 + 0.2 \log_{10}\left(\frac{E\ I}{E'R^3}\right) \quad \text{rad.} \qquad [3.56]$$

Therefore,

$$\alpha_{eq} = 7.2 + 0.9 \log_{10}\left(\frac{E\ I}{E'R^3}\right) \quad \text{rad.} \qquad [3.57]$$

As seen from the above expression, the equivalent angular span is considered dependent on the relative stiffness of conduit wall with respect to the stiffness of the surrounding soil. In the case of conduit with high bending rigidity (EI) and poor soil stiffness ($E'R^3$), the equivalent angle has higher magnitude. On the other hand, lower value of equivalent angle is considered for very flexible conduit with good surrounding soil media. The equivalent angular span alfa of closed conduit is in the range of 230° to 270°

depending on the relative stiffness of conduit wall with respect to soil stiffness.

3.11 Load Transfer Simulation In Top Soil

In the analysis, the soil-steel interaction is simulated by means of tangential and radial equivalent springs attached to the cylindrical shell at a number of points. Both radial and tangential springs are considered active on the sides and bottom portion of the conduit where the movement of the conduit is towards the soil. Only tangential springs are considered to be active in the top portion of the conduit in which the movement of the conduit is away from the soil. The part of the vertical load applied at the embankment level is shared by the top soil, by means of shear action as shown in Figure 3.13. Therefore, the axial thrust at the crown level is smaller than that at the shoulders. This action of load sharing has not been accounted for by the radial or tangential springs. In order to take this action into account, the shear force T_o, which is assumed to vary sinusoidally over the projected load area on one side of the crown, is applied at the conduit top. T_o is resolved into two components, tangential (q_θ) and normal (q_w) to the surface, the load vectors of which are calculated by the work equivalent approach (section 3.9.4). By doing this the axial thrust in the conduit is redistributed giving maximum thrust at the shoulders. The

derivation of the normal and the tangential components of T_o is as follows.

Total horizontal force at the crown level is

$$Ph = k_o \, q_c \, H_c \qquad [3.58]$$

where,

- k_o = coefficient of earth pressure at rest ranging from 0.85 to 0.95 (as seen from Figure 3.14)
- q_c = load intensity at the crown level.
- H_c = depth of soil cover over the crown.

Let T_o be the shearing force varying sinusoidally, given by

$$T_o = F_s \sin \left(\frac{\pi \theta}{\theta_1} \right) \qquad [3.59]$$

$$\text{Total shear force at depth } H_c = \int_0^{\theta_1} T_o \, R \, d\theta \qquad [3.60]$$

or,

$$k_o \, q_c \, H_c = \int_0^{\theta_1} T_o \, R \, d\theta \qquad [3.61]$$

This gives, on simplification, an expression for F_s as follows:

$$F_s = \frac{1}{2} k_o \, q_c \, \frac{\pi}{R\theta_1} h \qquad [3.62]$$

and, radial and tangential components of this shear force are given by the following expressions:

$$q_w = T_0 \sin(\theta_1 - \theta) \qquad [3.63]$$

$$q_\theta = T_0 \cos(\theta_1 - \theta) \qquad [3.64]$$

or,

$$q_w = F_s \sin\left(\frac{\pi\theta}{\theta_1}\right) \sin(\theta_1 - \theta) \qquad [3.65]$$

$$q_\theta = F_s \sin\left(\frac{\pi\theta}{\theta_1}\right) \cos(\theta_1 - \theta) \qquad [3.66]$$

3.12 Some Comments On The Developed Computer Program

The computer programs for a soil-steel structure with or without curved eccentric stiffeners have been developed based on a finite strip method of analysis as discussed in all the above sections of this chapter. The flow charts for these programs are given in Appendix G. The following are some of the features of the programs.

3.12.1 Division Of Structure Domain

A structure is required to be divided into a number of cylindrical shell strips. The number of such strips for a given structure depends on the number of stiffeners and the type of loading. A structure without stiffeners subjected to constant horizontal load or uniform vertical load needs to be divided into a minimum number of strips since the internal force component variations is gradual and smooth. Near the stiffener section the internal force variations are steep. In such a case the structure needs to be divided into

a large number of strips near the stiffeners. The finite strip idealizations of White Ash Creek structure and Cheese Factory Bridge structure are shown in Figure 3.15 and Figure 3.16, respectively.

3.12.2 Iteration Procedure

3.12.2.1 Shell Subjected to Lateral Load

To begin with, the approximate horizontal force along the support of each strip is calculated from the known applied displacement, by using Castigliano's theorem as follows;

$$P = \frac{2d_o}{\int \frac{y^2 ds}{Be_i}} \qquad [3.67]$$

where,

- d_o = applied horizontal displacement along both supports.
- y = perpendicular distance from support line to the crown.
- Be_i = bending rigidity of individual strip.

The equivalent load vectors due to these approximate horizontal forces are calculated by the work done approach. After the first cycle of analysis, the horizontal components of the tangential displacement at the end of each strip (d_{hi}), are not equal to the applied displacement (d_o). Therefore, the horizontal forces are corrected by the following expression;

$$P_{corrected} = P_i \times \frac{d_o}{d_{hi}} \qquad [3.68]$$

This procedure of correcting the applied horizontal forces is carried out until the ratio of d_o to d_{hi} becomes approximately equal to unity for all individual strips.

3.12.2.2 Soil-Steel Structure Under Traffic Loads

In order to activate or delete certain springs on the shell surface, the deflection profile must be known. To begin with all springs are considered to be active during the first cycle of analysis. The results of the first cycle of the analysis then become the basis for the deletion or activation of the springs. If the radial deflection of the conduit wall at the i'th spring location is away from the soil-fill, the i'th normal (or radial) spring experiences tension and is deleted in the following cycle of analysis. The normal springs which are located in the passive pressure zone, are considered in the subsequent cycle of analysis. The tangential springs are considered active even in the region where the conduit wall moves away from the fill (i.e. active pressure zone), since no physical separation of soil and the conduit wall takes place. This procedure of deletion and activation of normal springs is pursued until the deflection profile of conduit does not change in the subsequent iterations. It is observed that not more than

three iterations are required in order to get a fairly constant deflection profile.

3.12.3 Validation Of Computer Program

The results obtained from the developed computer program have been verified directly as well as indirectly. The direct verification by experimental results will be discussed in the next chapter on Experimental Verification. Another computer program, called SHELLPL, based on rectangular flat strip (Figure 3.2) was developed. The example problem of folded plate structure given at the end of the reference [21], was analysed by SHELLPL program and the results were compared with those given at the end of the same reference. The results of SHELLPL matched upto the fifth decimal point. Thus having gained confidence in SHELLPL, a cylindrical shell structure was approximated by many sided polygon, made of a number of rectangular flat strips as shown in Figure 3.2. The shell structure with unit uniform snow load was then analysed by SHELLPL, as well as by the developed computer program based on cylindrical shell strip formulation. These results along with the results of the theory of orthotropic shells [35], were compared as shown in Figure 3.17. The percentage difference between the results of the two solutions is about 14%. This demonstrated validity of the computer program that has been developed in this study.

3.12.4 Convergence Of Results

The convergence of the results (e.g. internal force components and deflections) depends on the type of loading and the number of derivatives of the displacement functions required for a particular result. If the structure is subjected to a point load, a large number of Fourier series terms (M) are required to be considered, because of the concentration of stresses below the point load. On the other hand, fewer number of Fourier series terms are required for a structure with uniform load. The results that are dependent on the higher derivatives of the displacement function need more number of Fourier series terms to achieve convergence. The deflection, axial thrust and bending moment results in a structure during and after backfilling under uniform loads (horizontal and vertical) by considering different values of M, are tabulated in Table 3.1 and Table 3.2 respectively. The deflection results converge very fast, while axial thrust and bending moment converge slowly, since they are derived by taking first and second derivatives of the displacement functions. However, practically acceptable accuracy in these results has been achieved with M=3 terms.

3.12.5 Merits And Demerits Of Developed Program

The computer program 'NEWSHELL' can analyse stiffened or non-stiffened shell subjected to horizontal soil compaction forces at the thrust beam level and can predict the state of stresses in the stiffeners and the main shell.

The computer program 'NEWSOIL' can analyse stiffened or non-stiffened soil-steel structure with varying depth of soil cover over the crown level, subjected to live load at the embankment level. It is capable of three dimensional analysis of such structures. The curved stiffeners can be on the outer side or the under side of the shell. The soil-steel structures are often made of two or more radii of curvature, or full closed shape. These types of structures can also be analysed with certain modifications. For a structure with more than one radius of curvature, the top arch portion of the structure is considered for analysis. Closed shape conduit is replaced by means of equivalent open shell arch with hinged supports, as discussed in section 3.10.

The developed computer program embeds in it all the advantages and disadvantages of the finite strip method of structural analysis. The time and computer storage required for this program is thought to be considerably less than that required for any other comparable method. Force and structural properties variation in the length direction can be handled conveniently. Varying depth of soil cover in the longitudinal direction (as required for road profile) can also be handled. The number of cycles of analysis required to define passive and active zones in the structure is not more than three.

However, there are certain shortcomings embedded in this program. Due to the presence of non-orthogonality in the basic functions, the stiffness matrices are coupled and their size is dependent on the number of Fourier series terms. Load dispersion pattern through the soil media has to be assumed. The state of stress and strain in the surrounding soil media cannot be predicted by this program.

Chapter IV

EXPERIMENTAL VERIFICATION

4.1 General

The results obtained from the developed computer programs are compared with the test results of a laboratory scale model, as well as with the full scale existing soil-steel bridges. The Ontario Ministry of Transportation and Communications recently conducted several prototype tests [13] out of which the White Ash Creek Structure test results have been used to demonstrate the validity of the developed computer program. Several laboratory scale model tests are also carried out to represent the soil-steel structures during and after backfilling. The model, prototype, instrumentation, test procedures and the comparison of the results are described in the following text.

4.2 Prototype Tests

The prototype structure, the White Ash Creek Bridge, is located in Thamesville, Ontario. It has been in service for quite a few years. The White Ash creek structure is free from special features such as longitudinal thrust beams, transverse stiffening ribs etc..

The White Ash Creek structure has a circular cross section, 25 feet (7.62m) in diameter and is made of 6x2 in. (152x51 mm) standard arc and tangent corrugations with a thickness of 0.184 in. (4.67 mm). The maximum height of soil cover is 4 ft. 1 in. (1.25m) above the crown level. The details of this structure are shown in Figure 4.1.

4.2.1 Instrumentation

Strains in the structure walls were monitored by means of uniaxial electrical resistance strain gages. All the strain gages were of constantan alloy formulated for temperature self-correction on the steel surfaces. The gages were polyimide backed for adhesive attachment. In order to increase the sensitivity and reduce the influence of lead wire resistance, 350 ohm gages were used in conjunction with 18 gage copper wire.

Two control sections were established, one near the longitudinal centre of the structure and the other 4 feet (1.22 m) west of this section. At each control section six monitoring points were located around the circumference as shown in Figure 4.2. At every location three strain gages were installed as shown in Figure 4.3.

Displacement transducers were used to measure the vertical deflection of the crown and the relative horizontal movements of the spring lines at each control section.

The strain gages and the displacement trarsducers were connected to a computer based data acquisition system. The

instrumentation employed was capable of independent balance and calibration of each gage. Both digital and hardcopy readouts of strain and displacement data were possible.

Two testing vehicles were used to apply the live load on the White Ash Creek structure. Their axle weights were regulated by means of concrete blocks. For each vehicle, two levels of weights were used. The axle spacings and wheel reactions corresponding to these load levels are shown in Figure 4.4 for one of the OHBDC testing vehicles. The other testing vehicle has the same dimensions and similar weights.

4.2.2 Testing Procedure And Analysis Of Test Data

The testing procedure and the analysis of experimental data for White Ash Creek structure are reported in the reference [43]. Therefore, the detailed test procedure and the analysis of strain raw data are not discussed here.

Since only two control sections were established for the White Ash Creek structure, the deflection profile in the longitudinal direction was obtained by employing Maxwell's principle of reciprocal deflections. The crown deflections in the longitudinal direction due to the central one truck load (second level) are tabulated in Table 4.1. The same procedure has been used to obtain an axial thrust variation in the longitudinal direction of the White Ash Creek structure due to one truck loading (second level) and are tabulated in the same table. Similar deflection and thrust variation profile was impossible to be established in the

two truck loading case because fewer exchangeable readings were available.

The measured wall thrusts and bending moments are presented below and compared with analytical results computed using the developed computer program.

In the case of White Ash Creek structure, only the case of symmetric loading (second level) with one and two trucks is considered for the comparison.

4.2.3 White Ash Creek Structure Results Comparison

Experimentally obtained thrusts, moments and deflections under the effect of live loads are compared with analytical results.

4.2.3.1 Axial Thrust Variation

Live load thrust variations at the central section due to one and two second level truck loads over the central section are shown in Figure 4.5 and Figure 4.6 respectively. The conduit wall thrust computed from the measured strains and those obtained by the proposed finite strip method of analysis are plotted. The results of finite element plane analysis by Hafez [43] are also plotted in the same figure. In the case of central one truck loading the maximum values of axial thrust by measurement, proposed method and plane analysis are 294, 285 and 350 lb/in. respectively. The corresponding thrust values under two truck loading are 382, 360 and 420 lb/in.. In the finite

strip method of analysis, the closed shape conduit has been replaced by an equivalent open two hinged shell arch with a 235° intersection angle (Section 3.10).

In general, good agreement is found between the experimental and analytical thrust values. It is observed that generally the plane finite element analysis results [43] (neglecting the shell action of the structure) are higher than the measured as well as the finite strip results. The average percentage difference between the measured and the propcsed finite strip values and between the measured and plane analysis values are 5% and 12% respectively. A large discrepancy between finite strip and finite element results is found at the crown section where no field measurements were recorded.

Figure 4.7 shows the axial thrust distribution in the longitudinal direction at the haunch level of the structure due to the central second level one truck loading. Experimentally measured and analytically obtained results are compared. The spread of the assumed uniform load at the crown level is about 6 ft. (1.83 m) beyond the central section. However, both experimental and analytical results show that the axial thrust diminishes beyond a distance of 12 ft. (3.66 m) from the centre, indicating very poor shell action of the shell. In general, the analytical results are close to the measured results. In the central portion of the conduit, the analytical thrust is more or less constant,

while actual thrust gradually drops. This is attributed to the assumption of uniform loading in analytical approach which is not true in reality.

Figure 4.8 shows the axial thrust variation at the west section, 4 ft. (1.22 m) away from the central section, due to two truck second level central loading. Here also, the measured and analytical performances are in good agreement.

Both experimental and analytical results show that the live load thrust is far from being uniform around the conduit as assumed in the Ring Compression theory. The thrust is maximum at the haunches of the upper half of the conduit. It diminishes quickly in the lower half because of the effect of dispersion of the applied embankment loading.

4.2.3.2 Bending Moment

Figure 4.9 through Figure 4.12 show the comparison of the analytical and the measured bending moments at two central sections of White Ash Creek structure due to one and two truck second level loading. The bending moments are very small in magnitude. Analytically maximum moment occurs at the crown where no measurements were recorded. In general, most of the moment values at strain gage locations are in reasonably good agreement with the analytical values. However, at few locations the measured moment values are very large compared to the analytical results. The measured large values of moments are considered to be erroneous, since for a case of symmetric loading, the measured moment response has to be approximately symmetric.

4.2.3.3 Relative Vertical Deflections

A comparison of measured relative vertical deflections, between the crown and bottom line of White Ash Creek structure is shown in Table 4.2. In the same table, the deflections by finite element plane analysis [43] are also shown. The analytical values of deflections are larger than the measured values. The values of deflections by the finite strip method of analysis are in between the measured values and those calculated by the finite element plane analysis. The measured values seem to be erroneous due to the exceptionally long connecting transducer flexible wires. Table 4.1 shows deflections along the crown due to one truck loading. Those are compared to the analytical values in Figure 4.13. The measured and analytical deflections become negligible at about 12 ft. (3.66 m) away from the central section, indicating poor shell action of the White Ash Creek structure.

4.3 Laboratory Model Tests

A small scale shell structure with the central angle equal to 83.75° was used to represent a structure between the thrust beams of soil-steel structure during and after backfilling. This model (with and without stiffeners) was tested under horizontal displacements at the support with no surrounding soil. This situation represents a construction stage, wherein the compaction forces induce horizontal

displacements at the ends of the upper arch of the structure. Similarly a model (with and without corrugated stiffeners) under 9 in. (229 mm) height of soil cover was tested under various loads. The details of these tests are briefly presented in the following sections and the test results are compared with the results obtained from the developed formulation.

4.3.1 Description Of Models

The models to represent soil-steel structure, during and after backfilling, were made of 2-11/16 in. x 1/2 in. (68mm x 13mm) standard arc and tangent corrugated 24 in. (610mm) wide curved steel sheets having a radius of 34-3/8 in. (873mm) and a thickness of 0.052 in. (1.32mm). These curved sheets were jointed together by means of bolts and nuts, 3/8 in. (9.5mm) in diameter and 1/2 in. (13mm) long. The bolt holes were 7/16 in. (11mm) in diameter. In order to avoid any possible slippage at the joints, lock washers were used and the nuts were tightened by applying a constant amount of torque by means of a torque wrench. Along the straight ends of the model, 4x3x1/4 in. (100x75x6.3mm) angles were used as buttress or thrust beams.

4.3.1.1 Model to Simulate the Upper Zone During Side Filling

The model is simply supported, with a hinge support at one end and a roller support at the other as shown in Figure 4.14. Two types of stiffeners were used. The corrugated stiffeners were made of 2-11/16x1/2 in. (68x13mm) standard arc and tangent curved sheets having a thickness of 0.052 in. (1.32mm) and a width of 7 in. (178mm). The tee stiffening ribs were made from 4 in. (101mm) wide, 2-1/8 in. (54mm) deep and 0.125 in. (3.18mm) thick structural steel plates. Four aircraft cables were used to connect the ends of the shell. These cables were anchored on one side of the shell and bolted on the other. Horizontal displacement along the support was applied by tension force in the cables by screwing the bolts (Figure 4.15). Pre-calibrated ring load cells, Figure 4.16, were installed on the cables in order to measure the magnitude of the tension force due to applied amount of horizontal displacement.

4.3.1.2 Model to Simulate Soil-Steel Structure Under Live Load

The structure under traffic load is modelled as a cylindrical shell with hinged supports. The model was fitted with 7 in. (178mm) wide standard 2-11/16in.x1/2in. (68mm x13m) corrugation profile curved stiffners. The soil used in this test was clean, dry sand from Lake Erie. In order to study the interaction of soil and the structure a test model

was built. The test cell was made of 3/4 in. (19mm) thick plywood, 3/4 in. (19mm) thick plexiglass and structural angles of various sizes. The test cell was of 8' long, 4'-1" wide and 4' high. The model was securely placed on a bed in the test cell, Figure 4.17. On the sides of the model in the test cell, the soil was compacted manually leading to a soil density of 120 pcf. (1920 kg/m³). Thereafter, two layers of soil were placed on the crown level, compacting each time to a specified density. The compacted layer of 9 in. (229mm) was achieved over the crown of the model. The ends of the model were wrapped with foam rubber to seal the gap between the model ends and the test cell walls to avoid soil leakage, Figure 4.18. This sealing of the model end gaps did not prevent the free movement of the ends in the vertical direction.

4.3.2 Instrumentation

To monitor the strains at various locations, uniaxial electrical resistance strain gages were used. These gages were of constantan alloy and had matching temperature compensation for steel surface. The strain gages were of the type N11-FA-10-120-11 with a gage factor of 2.12 ±1.0% at 11° C. In order to reduce the influence of 18 gage connecting electrical wires, the length of such wires was kept to the minimum required length. Thirty nine gages were used for each model in this project. Figure 4.19 and Figure 4.20 show the strain gage layouts of the scale model.

Each gage was connected in 3-wire, quarter bridge configuration in order to negate the temperature effects in lead wires. The third wire was connected to a dummy resistor resident in the instrumentation module. The instrumentation module (Figure 4.21) was capable of independent balance and calibration of each gage. Automatic scanning of the gages was possible at the rate of about one gage per second. Both digital and hardcopy readouts were produced directly in micro strains.

All the strain gages were aligned in the circumferential direction to measure the circumferential strains only. No attempt was made to measure the strains in the longitudinal (perpendicular to corrugations) direction, since the mechanics of orthotropic corrugated plates suggests that while extreme fibre longitudinal strains might appear significant, they are in fact manifestations of longitudinal flexural stresses caused by accordian-like deformation. These flexural stresses on the crests of the corrugations are hundreds of times greater than the average longitudinal stress. Clearly, accordian action would commence before any significant average longitudinal stress would develop.

Mechanical dial gages were used to record the radial and horizontal deflections along different control sections in the model (Figure 4.22 and Figure 4.23).

Pre-calibrated ring load cells (Figure 4.16), were used to measure the horizontal force (or tension in the cables).

Two strain gages were installed on each ring load cell and were connected in half bridge circuit.

A hydraulic jack was used to apply the vertical load on the loading plates on the soil surface. A pre-calibrated flat universal load cell, placed between the hydraulic jack and the loading plates (Figure 4.24), was used to measure the magnitude of the applied load. The maximum capacity of the load cell was 25 kip. (110 kN). A portable strain indicator, by which the load cell was calibrated, was used to record the load readings in equivalent micro strains.

4.3.3 Testing Procedure

4.3.3.1 Model to Represent Structure During Side Filling

A horizontal displacement $2d_o$ was applied along one support of the model by creating tension in the aircraft cables. The tension force in the cables was created by screwing the bolts at one end of the cable resting against the angle. Four mechanical deflection gages were installed at the locations of the cables in order to monitor and ensure constant displacement along the model support. All strain gages were zeroed before the application of horizontal displacement. The tension force in the cables was recorded by pre-calibrated ring load cells. Also the strains in micro units were recorded by an automatic digital strain indicator module. The radial deflections along the control sections were recorded by means of mechanical dial

gages, (Figure 4.15). After the completion of the data recording, the horizontal diplacement along the support was increased and once again all the measurements were recorded. This procedure was followed for both unstiffened model and stiffened model (with tee and corrugated sheet stiffeners).

4.3.3.2 Model Under Live Load

Two models, with and without corrugated stiffener, were tested under uniform, strip/line and patch (localized) loads. After adequate compaction of the top layer of soil, the loading system was placed at the central section of the model (Figure 4.24). Three different types of loading plate sizes were used, as shown in Figure 4.25. On the top of the loading system a pre-calibrated and zero adjusted load cell was placed. The vertical load was applied on this load cell in increments of 500 lbs. (2224 N). The load was held approximately constant until all the measurements (strains and deflections) were recorded. The nature of the loading was changed by changing the loading plate size. At the beginning of each load type all the instrumentations were set to zero. The loading was stopped when the deflections started increasing rapidly. Once again the instrumentation readings were recorded at the end of each test. This procedure was followed for both stiffened and non-stiffened models.

4.3.3.3 Failure Test

Model failure test was carried under the localized patch load (Figure 4.26). The unstiffened model was loaded in increments of 500 lbs. (2224 N) of patch load until the model deflections started becoming very large at no further increase in the load. This was considered to be the elastic buckling failure of the non-stiffened model. Similarly the stiffened model (with corrugated stiffeners) was loaded in increments of 500 lbs. (2224 N) of patch load until the failure of the model took place. At each incremental load the strains and deflections were monitored and recorded.

4.3.4 Raw Data Analysis

Since the strain gages were installed on the hills and valleys from the inside of the shell, the outer fibre strains needed to be corrected as shown in Figure 4.27. If ε_1 and ε_2 are the measured strains at hill and valley from the inside, the strain at the outer fibre ε_2' is calculated by the following expression:

$$\varepsilon_2' = \varepsilon_1 + \left(\frac{\varepsilon_2 - \varepsilon_1}{d}\right) \times (d + t) \qquad [4.1]$$

or,

$$\varepsilon_2' = \varepsilon_2 + \frac{t}{d} (\varepsilon_2 - \varepsilon_1) \qquad [4.2]$$

where,

- d = depth of corrugations (Figure 3.9)
- t = thickness of corrugated sheets (Figure 3.9)

For the unstiffened model the bending moment and axial thrust were calculated by the following expressions:

$$T = \frac{1}{2} E A (\delta_2 + \delta_1) \quad \text{lb/in.} \qquad [4.3]$$

and,

$$M = \frac{1}{2} \frac{E I}{c} (\delta_2 - \delta_1) \quad \text{lb.in/in} \qquad [4.4]$$

where,

- E = modulus of elasticity = 29 x 10^6 psi.
- A = area of cross section per unit width (in^2/in)
- I = moment of inertia per unit width (in^4/in)
- c = extreme fibre distance from neutral axis

The strain results of the stiffened model were not decomposed into axial thrust and bending moment values since the values of c, A and I in Eq. 4.3 and Eq. 4.4 are not known for the stiffened shell because of partial interaction of the stiffeners with the rest of the shell. Therefore, for the stiffened models the strains were converted into stress values by the following expression:

$$\sigma = E \cdot \delta \qquad [4.5]$$

and these stresses were compared with the theoretical stresses obtained by the developed computer program.

The symmetric radial deflections in a model subjected to equal displacements along both supports were obtained by the superposition of deflections due to actual loading case and the rigid body motion by d_o as shown in Figure 4.28.

$$(w)_{\text{case I}} = (w)_{\text{case II}} + (w)_{\text{case III}} \qquad [4.6]$$

or

$$(w)_{\text{corrected}} = (w)_{\text{measured}} - d_o \sin\left(\frac{\alpha}{2} - \theta\right) \qquad [4.7]$$

where, θ is measured from the support along which the total displacement has been applied.

4.3.5 Comparison of Results

The analytical results are compared with the test results of the laboratory scale model.

4.3.5.1 Model with Applied Horizontal Displacement

The axial thrust, bending moment and the radial deflections along the central control section of non-stiffened shell model subjected to horizontal displacement of 0.05 in. along both supports are compared with the analytical results in Table 4.3. These experimental results generally confirm the analytically predicted results. However, the measured axial thrust at few strain

gage locations do not agree well with the analytical ones. The measured thrust variation is not symmetric, which indicates an error in the measured values of thrust. Since, in a model subjected to horizontal loads along supports, the axial thrust is of secondary importance compared to the bending moment, the mismatch in the thrust values is not considered significantly important. The analytical and measured bottom fibre stresses along the central section are also compared in the same table. The maximum deviation between the measured and the analytical stress is 9.5%.

For the stiffened models, the measured stresses are compared (as explained in section 4.3.4) with the analytically predicted stresses. Table 4.4 shows the comparison of the stresses at strain gage locations (Figure 4.19) between measured and analytical values. The maximum difference in these stresses is found to be ±12%, which is considered acceptable. Similarly the extreme fibre stress variations along the crown of the stiffened shell (with corrugated and Tee-section stiffeners) are plotted in Figure 4.29 and Figure 4.30. In general, the measured stress variation confirms the analytical stress variation.

4.3.5.2 Soil-Steel Model Under Live Load

Figure 4.31, Figure 4.32 and Figure 4.33 show the measured and analytical stress variations along the crown and haunch section of the model due to vertical load of 500 lbs. acting through the different sizes of the loading

plates. Although the stresses were measured at very few locations, the experimental stress variation reasonably confirms the analytical results.

The analytical and measured crown deflections are compared in Table 4.5. The measured deflections do not agree very well with the analytical ones. However, the trend of deflections is similar. The measured deflection values are larger than the analytical values. This could be due to the assumed values of coefficient of soil reactions, Kn and Ks, which are basically applicable for the field size structures. Secondly it could be due to the fact that the measured deflections are not corrected for the final zero load deflections (deflections on unloading). Moreover, the deflections are too small to be measured accurately by ordinary mechanical deflection dial gages.

Thus the experimental program, in general, confirms the validity of the analytical approach.

Chapter V

OBSERVATIONS AND DISCUSSION OF RESULTS

5.1 General

The proposed formulation based on finite strip method of analysis and the developed computer programs have been verified by the laboratory model tests as well as by the test results of full scale prototype structure under the service conditions as described in the previous chapter. These tests confirm the validity of the proposed analytical procedure for corrugated soil-steel structures. Thus, having gained confidence in the developed computer program, a parametric study of the soil-steel structures, both during and after backfilling, has been undertaken. Particular emphasis has been given to the behavior of the radial stiffener with respect to the main shell with and without the surrounding soil media. Stiffeners made from corrugated plates and hot rolled sections have been studied.

The previously outlined analytical and experimental studies are directed to examine and develop a rational procedure to determine the effect of stifferers on the behavior and load carrying capacity of soil-steel structures. They address these two effects at two main stages in the life of the soil-steel structures, namely, during construction and under dead and traffic loads.

5.2 Stffened Soil-Steel Structure During Side Filling

Field experience has revealed that with the increase in size of the soil-steel structure and with very low flexibility of the walls, excessive peaking and thereby yielding at the conduit crown could take place. This problem has been overcome by improved construction techniques (Figure 1.3), and also by increasing the flexural rigidity of the upper zone of the conduit by providing curved stiffeners of various cross sections (Figure 1.4 and Figure 3.6). The bending rigidity of the stiffened zone controls the crown deflection under side filling, as well as the corresponding stresses induced at the crown zone.

5.2.1 Effective Width of Shell

To evaluate the bending rigidity or stresses induced in a stiffened shell, the equivalent or effective width approach has been followed. Herein, an imaginary width of the shell is considered effective with the stiffener so that:

a) The stress calculated by the effective width concept is equal to the stress obtained by the three dimensional analysis, or

b) The rigidity ratios calculated by the effective width concept are equal to the rigidity ratios obtained by the three dimensional analysis.

This effective width could be dependent on several parameters such as width of stiffener, w, eccentricity of the centroidal surface of stiffened portion with respect to

the centroidal surface of main shell, F, spacing of the stiffeners, S, radius of shell, R, central angular span of shell, α, the bending rigidity of unstiffened portion of shell, EI, the bending rigidity of stiffened portion of shell, EI_s, and the longitudinal length of shell, L.

$$\text{i.e} \quad We = F(W, F, S, R, \alpha, EI, EI_s, L) \qquad [5.1]$$

$$\text{or} \quad We = K\, W^a\, F^b\, S^c\, R^d\, \alpha^e\, EI^g\, EI_s^h\, L^i \qquad [5.2]$$

To study the effect of each parameter, three dimensional analysis has been conducted for two hinged shells with sizes ranging from a model to the actual field size, subjected to horizontal loading. The eccentricity 'F', between the centroidal surfaces of stiffener and main shell, (Figure 3.6), varied from 0.25" to 5.0" (6.35mm-127mm). In practice, the maximum value of 'F' used is not more than 6" (150 mm) (e.g. Cheese Factory Bridge, County of Wellington, Ont.). The lower range of F (=0.25" or 6.3mm) corresponds to that of the laboratory model. The width of stiffeners considered ranges from 7" to 24" (178-610 mm), which represents the width of all types of commonly used stiffeners. Stiffener spacing considered ranges from 27" to 109" (686-2740 mm). The lower limit is that for laboratory model and the upper limit is the practical range for field stiffeners. The range of the radius of the shell is chosen from 34" (864 mm) to a maximum of 405" (10287 mm). The central angular span (α)

considered for the study ranges from 30° to 120°. Usually the angle included between the thrust beams (Figure 3.3), or the central angle of top arch of the structure is between the range of 30° to 120°. Finally, the bending rigidities of selected available corrugation profiles and the stiffening elements that are widely used in the field are considered. The range for the longitudinal-length of structure was chosen arbitrarily. The author believes that the range of values considered for all of the above parameters for the study is truly representative of the field soil-steel structures.

A total of 102 data sets have been analysed under a given magnitude of horizontal displacements along the supports, using the developed computer program NEWSHELL.

5.2.1.1 Effective Width Based on Stresses

The effective width, We, was evaluated in each data set so that the bottom fibre stress calculated by the effective width concept is equal to the stress obtained from the three dimensional analysis. The effective widths are tabulated in Table 5.1 for few structures. It is observed that the effective width is inversely proportional to the intersection angle, α, and the stiffener spacing S, while it is directly proportional to the magnitude of eccentricity, (F), and the width of stiffener (W). The exact nature of variation of effective width (We) with respect to all other parameters is difficult to detect merely by inspection of

the above table. A statistical analysis of all 102 data sets, has been carried out using a standard statistical package program called Linear Regression [44]. Eq. 5.2 is in the exponential form and cannot be used directly, in its original form to do a linear regression. Therefore, it is reduced to a simple polynomial form by taking logarithms of both sides and rewriting in the following form,

$$W_1 = K_1 + a.W_S + b.P_1 + c.S_1 + d.R_1 + e.\alpha_1 + g.EI_1 + h.EI_2 + i.L_1 \qquad [5.3]$$

where,

$$\begin{aligned} W_1 &= \text{Log}(We), & K_1 &= \text{Log}(K) \\ W_S &= \text{Log}(W), & P_1 &= \text{Log}(P) \\ S_1 &= \text{Log}(S), & R_1 &= \text{Log}(R) \\ \alpha_1 &= \text{Log}(\alpha), & EI_1 &= \text{Log}(EI) \\ EI_2 &= \text{Log}(EI_S), \text{ and} & L_1 &= \text{Log}(L) \end{aligned} \qquad [5.4]$$

Also, various combinations of two or more parameters have been considered to create a new parameter, for example, $R\alpha/S$, EI/EI_S, $\text{Sin}(\alpha/2)/(\alpha/2)$ etc.. After reducing the unknown correlation equation into the polynomials in terms of new parameters and unknown multiplying constants a, b, c, ... etc. (similar to Eq. 5.3), a linear regression statistics has been employed to develop a correlation between the dependent variable (We) and the independent variables (W, P, S, R, α, EI, EI_S, L, or any other

combination of these variables). During the process of this analysis, any variable that had very little or no effect on 'We' was discarded. This was identified by the probability factor and a very small correlation coefficient. In this way the parameters EI, EI_s and L were found to have very little or no effect on the value of 'We'. The following expression for the effective width has been developed by the statistical analysis,

$$We = 12.85 \times \left(W \right)^{0.37} \times \left(F \right)^{0.72} \times \left(\frac{l_1}{S} \right)^{0.28} \times \left(\frac{\sin(\alpha/2)}{\alpha/2} \right)^{1.67}$$

or

$$We = S \quad \text{whichever is smaller} \qquad [5.5]$$

where,

- W = actual width of stiffeners, in.
- F = the eccentricity between the stiffener and the shell, in.
- $l_1 = R\alpha$, arc length of the arch, in.
- S = spacing between the stiffeners, in.

and,

- $\alpha/2$= half the intersection angle of the arch, rad.

Table 5.2 shows the comparison of theoretically derived effective width values and predicted 'We' values by Eq. 5.5, for the selected type of corrugation profiles and stiffener combinations. The predicted values of effective width are within ±12% of their theoretically calculated values.

Therefore, in the absence of three dimensional shell analysis, the proposed Eq. 5.5 is considered acceptable for practical purposes to predict the effective width of stiffened shell.

In the development of Eq. 5.5, no slippage between the stiffener and main shell is assumed. No slippage is ensured by providing an adequate number of bolts and nuts, securely tightened along the stiffener. If partial or full slippage takes place, the stiffener is not considered to be fully acting together with main shell and therefore, Eq. 5.5 is not valid.

On examining Eq. 5.5 and the results outlined in Table 5.2, it is seen that the effective width is affected mainly by the eccentricity, F. It can also be noticed that the magnitude of the effective width, We, is relatively small when compared with the spacing between the stiffeners or with the effective width of stiffened plane panels. This fact falls in line with the characteristics of curved beams in which the curvature of the flange leads to a reduction in their effective area and the total bending rigidity of curved beams [67]. These results point also at the poor shell effect, which is attributed to its low axial rigidity Dx, in the longitudinal direction.

5.2.1.2 Effective Width Based on Rigidity

Eq. 5.5 is based on the extreme-fibre stress due to the combined action of thrust and bending. The ratios of moments of inertias of stiffened and non-stiffened shells (I_s and I_o) are also calculated as the ratio of the analytically obtained horizontal forces Ps and P_o for stiffened and non-stiffened shells respectively, when subjected to equal horizontal displacements. This ratio of horizontal forces (P_s/P_o) represents the ratio between the bending rigidities of the different shells. This can be understood, since the displacement is attributed mainly to the bending moment. In order to match these rigidity ratios, Eq. 5.5 has been modified as follows:

$$We = 8.00 \times \left(\frac{W}{F}\right)^{0.37} \times \left(\frac{l_1}{S}\right)^{0.72} \times \left(\frac{\sin(\alpha/2)}{\alpha/2}\right)^{0.28} \cdot 2$$

or

$$We = S \quad \text{whichever is smaller} \qquad [5.6]$$

Table 5.3 shows the rigidity ratios (I_s/I_o) calculated by various methods.

5.2.2 The Effect of Stiffeners on Distribution and Magnitude of Stresses

Since the bending rigidity of the shell is increased due to the addition of stiffeners, the stiffened portion of the shell attracts large bending moment while the bending moment on unstiffened zone remains the same as that of unstiffened

shell subjected to the same magnitude of horizontal displacements along the supports.

Figure 5.1 shows the comparison of bottom fibre stress (obtained by experiment, theory and effective width concept Eq. 5.5) along the crown of a model (α=83.75°, R=34.375 in.), with corrugated stiffeners subjected to horizontal displacement of 0.05" (1.3mm). Also, Figure 5.2 shows the comparison of stresses for the same model with tee-section stiffeners under similar loading. It is observed that the predicted stress variation is within an acceptable accuracy of the actual stress variation.

Figure 5.3 shows the maximum stresses induced in the bottom fibres of stiffened and non-stiffened shell models (α=83.75° and R=34.375 in.), subjected to the same magnitude of horizontal forces. The corrugated sheet stiffeners, which account for a 19% increase in the shell material, reduce the maximum fibre stress by 20% in the stiffened zone. Similarly, the tee-section stiffeners, which account for a 35% increase in the shell material, reduce the maximum bottom fibre stresses by only 21% in the stiffened zone. This indicates the stress reduction in this particular structure is not substantial compared to the stiffener material added.

The effect of spacing on the stress distribution in the upper zone of the full scale structure is shown in Table 5.4 and Table 5.5, under the same magnitude of the total applied

horizontal load along the supports (for a structure with and without thrust beams respectively), the stiffener eccentricity, P, as well as the cross sectional area and the moment of inertia per unit length of structure are kept constant. Since the crown of the structure is subjected to maximum bending forces under the action of the horizontal load, the stresses and the deflections are studied at the crown level only. The state of stress and the deflection at the crown level is the same for a structure with and without thrust beams subjected to the same magnitude of total horizontal force. The changes in the forces and deflections are localized near the supports. The combined stresses in the non-stiffened zone are reduced substantially (82 to 87%). The reduction of these stresses under the stiffeners at spacings of 9 ft. (2.75m), 6 ft. (1.83m) and 3 ft. (1.0m) are 44%, 55% and 65% respectively. This indicates that the spacing of the stiffeners has a more pronounced effect on stress reduction under the stiffener than the type of the stiffener and its total material.

5.2.3 The Rigidity Effect of Stiffeners

Table 5.6 shows the experimental ratio of bending rigidities of shell with and without stiffeners. It is observed that the magnitudes of these experimental rigidity ratios lie in between $(I_S/I_0)_{sum}$ and $(I_S/I_0)_{comb}$. This suggests the limited participation of the shell with the stiffeners. The corrugated stiffener has an effective width

of 8.51 in. (216mm) which is greater than the width of the stiffener itself. However, in the case of tee-section stiffener, a shell width equal to only the width of stiffener, is acting with the stiffener. The tee-section had higher value of eccentricity, F, compared to that of the corrugated stiffener. Therefore, a larger effective width of tee-section stiffener was anticipated. The error introduced is attributed to the fact that the curved lengths of the shell and the stiffeners were not the same. The weaker section beyond the stiffener curved ends deformed more, thereby, giving small value of Ps for the given magnitude of horizontal displacement.

The actual P_s/P_o ratios, (Table 5.6), suggest that there is very limited interaction between the stiffeners and the shell. The fact that the stiffener is not much effective with the shell is also seen from the deflection along the crown level (Table 5.7). This deflection pattern shows the limited interaction between the stiffened and the unstiffened zones of the shell.

5.2.4 Deflection Control

In order to study the exact beneficial action of the stiffener in terms of deflection reduction, one has to study the deflection variation in both shells with and without stiffeners, under the action of same magnitude of horizontal force.

Table 5.7 shows the decrease in the crown deflection of the stiffened shells under equal applied load and equal applied displacements. The crown deflection has been reduced almost 50% in the shell with corrugated stiffeners, while the same has been reduced by almost 70% in the shell with tee stiffeners having the same spacing of stiffeners in both cases. This means that the stiffeners are more useful in controlling the upward deflection of the crown during construction, rather than improving the bending moment capacity. However, if the stiffeners are closely spaced (say at 3' c/c), both the deflection control and the bending moment capacity are improved (Table 5.4 and Table 5.5).

5.2.5 Analysis Procedure

As mentioned in chapter I, currently there exist two methods of estimating the effective bending rigidity of the stiffened shell. The first one assumes absolutely no interaction of the stiffener with the rest of the shell (i.e. We=0), and the effective bending rigidity is calculated by the addition of individual rigidities of the stiffener and the rest of the shell. The second method assumes full interaction of the stiffener with the shell (i.e. We=S), and the effective bending rigidity is calculated as if the entire shell section, including the stiffeners, is acting as one section. Of the two methods, the former one is conservative in nature. It estimates higher stresses at the stiffener, while the second method

underestimates the stresses on stiffeners. The exact method of estimating bending rigidity falls between these two methods (i.e. W<We<S). This fact is demonstrated by the concept of the effective width of the shell as suggested by Eq. 5.5 and Eq. 5.6. The stresses calculated by these three approaches are plotted and compared with the actual analytical stress variation in the Figure 5.4. The procedure of calculation for the stresses by each approach is explained below.

Let P_t be the total horizontal force applied along the longitudinal support lines of the structure with stiffeners. The horizontal force shared by stiffened (P_s) and non-stiffened (P) portions are proportional to their bending rigidities; and are calculated as follows.

$$P_t = P + P_s \qquad [5.7]$$

where,

$$P = \frac{I}{I_t} \times P_t \qquad [5.8]$$

$$P_s = \frac{I_s}{I_t} \times P_t \qquad [5.9]$$

and

- I = Total moment of inertia of unstiffened zone of the structure

It is given by,

$$I = (L - n\ We)\ I' \qquad [5.10]$$

- I_s = Total moment of inertia of the stiffened zone (with effective width We) of the structure.

And is given by,

$$I_s = n\ We\ I'_s \qquad [5.11]$$

- n = number of stiffeners on the structure.
- L = longitudinal length of the structure.
- I' = unit moment of inertia of nonstiffened zone.
- I_s' = unit moment of inertia of the stiffened zone.

Therefore, horizontal force (P') per unit width of the unstiffened zone of the shell is calculated by,

$$P' = \frac{P}{(L - n\ We)} \qquad [5.12]$$

And the horizontal force per unit width of stiffened portion of the shell (with effective width We) is calculated by,

$$P'_s = \frac{P_s}{(n\ We)} \qquad [5.13]$$

Let 'A_t' be the summation of the cross sectional area of the stiffened (A_s) and non-stiffened (A) zones of the structure.

$$A_t = A + A_s \qquad [5.14]$$

Further A and As are given by,

$$A = A' (L - n W_e) \qquad [5.15]$$

and,

$$A_s = A_s' (n W_e) \qquad [5.16]$$

where,

A' and A_s' are the unit areas of non-stiffened and stiffened zones respectively.

The values of I', I_s', A' and A_s' are calculated by assuming full, partial and zero interaction of the stiffeners as discussed before.

The stresses in the unstiffened portion of the structure are now calculated by,

$$\sigma = - \frac{P'}{A'} \pm \frac{P' y c}{I'} \qquad [5.17]$$

And the stresses in the stiffened zone of the structure are given by,

$$\sigma = -\frac{P'_s}{A'_s} \pm \frac{P'_s \, y_s \, c_s}{I'_s} \qquad [5.18]$$

Where c and c_s are the extreme fibre distances from the centroid of non-stiffened and stiffened zones respectively. y and y_s are the vertical distances from the support line of the structure to the centroidal surface of non-stiffened and stiffened zones respectively.

5.2.6 Limiting Horizontal Deflection During Construction

Usually the total horizontal force P_t (Eq. 5.7) is difficult to determine in the soil-steel structure during construction. It can be calculated from the horizontal displacement at the thrust beam level using Castigliano's energy principle as shown below.

$$d_p = \int \frac{M}{EI_t} \cdot \frac{dM}{dP_t} \cdot ds \qquad [5.19]$$

where,

$$M = P_t \cdot y \qquad [5.20]$$

and,

- d_p = total horizontal displacement along supports.

The horizontal displacement, Δ, must be restricted during construction, in order to avoid the yielding of the conduit at the crown level. The limiting value of horizontal displacement can be obtained by substituting the value of bending moment (M), in Eq. 5.19 that will induce the maximum bending stress equal to the yield stress (F_y) of the conduit material. By performing the indicated integration, the following expression for the limiting deflection is obtained.

$$\Delta = \frac{R^2}{d} \left(\frac{F_y}{E}\right) K_I \qquad [5.21]$$

where,

- d = depth of corrugation profile
- K_I = the non-dimensional parameter given in Figure 5.5

The OHBDC [64], clause 12.8 specifies similar limiting deflection at the crown during construction. If the deformations exceed the specified limit (Eq.5.21), measures should be taken to contain them.

5.3 Soil-Steel Structure Under Traffic Loads

At the present time, all methods developed to analyse and design the composite soil-steel structures are based on considering a slice of a unit width of the conduit and the surrounding soil. This approach is valid for the analysis and stability problems of conduits with no radial stiffeners and subjected to uniform loads. It is also accepted by

engineers for the analysis of non-stiffened conduits subjected to loading, which could have variable intensity in the longitudinal direction. Herein, it is assumed that the conduit shell has negligible ability to transfer the loading in the longitudinal direction, i.e. no interaction takes place between the different slices (shell strips) in the non-stiffened conduit. However, a stiffened conduit is composed of strips of different rigidities, and therefore, concentration of thrust and bending moment takes place at and near the stiffeners.

This study is mainly confined to the behavior of the stiffened shell surrounded by engineered soil. The action of engineered fill has been simulated by a number of extensional (normal and tangential) springs.

The influence of frictional force on the distribution of axial thrust and bending moment in a soil-steel structure does not seem to be significant, as shown in Figure 5.6. The results of the analysis neglecting the effect of frictional forces (i.e. neglecting the tangential springs), are close to those obtained by considering the tangential springs. Although, not many cases of backfill heights and structure sizes have been studied to draw a firm conclusion on the effect of frictional forces on the structural behavior, the author believes, it is safe to neglect its effect. However, the frictional forces have been considered in the analysis that follows.

It is assumed that the soil failure does not take place and no attempts were made to know the stresses in the soil media, which is not within the scope of this study.

The live load dispersion through the soil media has been applied as suggested by OHBDC [64], over the conduit crown. Herein, the distributed load at the crown level is obtained by positioning the wheel load centrally above the crown at the embankment level, distributing load through fill at a slope of one vertically to one horizontally in the transverse (or span) direction of the conduit and a slope of two vertically to one horizontally in the longitudinal direction, and assuming that the dispersed load at crown level is uniformly distributed over a rectangular area that is subtended by the extremities of individual areas. OHBDC load dispersion is shown in Figure 5.7. Although, there may be a discrepancy in the OHBDC load dispersion and actual load dispersion, the analytical results seem to be in reasonably good agreement with the field performance results.

The effect of horizontal load transfer in the top soil as discussed in section 3.11 is shown in Figure 5.8. Without considering the load transfer, the maximum thrust by the developed formulation, occurs at the crown level. However, on considering the load transfer in the top soil, the maximum thrust occurs at the shoulder level of the structure, which is a commonly observed nature of the thrust variation in the soil-steel structures.

The distribution of the thrust and bending can be obtained through the three dimensional analysis of the stiffened conduit. Since the design of conduits is based on either the criterion of thrust [61] or bending moment [33], the effect of the stiffeners on these two design criteria is examined in the following.

5.3.1 Distribution of Thrust

The design of soil-steel structure is usually based on the ultimate thrust capacity of the conduit wall (stability and yield criteria under axial loading). By the addition of stiffeners to the conduit wall, the thrust is redistributed with some concentration at the stiffeners, i.e. at the strips of increased inertia which possess increased load carrying capacity against thrust. The actual effect of stiffeners on the design of conduits can be determined by comparing the variation of the thrust, as well as the load carrying capacity of the different strips. This is expected to vary according to the type of stiffeners, spacing, etc.

Figure 4.7 shows the comparison between measured and analytical axial thrust and its distribution in the longitudinal direction of White Ash Creek structure (which is without stiffeners) when subjected to one truck, second level loading at the central section. This type of loading on a structure with shallow soil cover represents a localized patch load. The thrust variation indicates that the White Ash Creek structure has poor shell action because

of very low axial rigidity in the longitudinal direction compared to that in the curved direction.

Figure 5.9 and Figure 5.10 show the axial thrust variation in shell model (R=873mm and α=83.75°), with and without corrugated sheet stiffeners with spacing S=27 in. (686mm) under the uniform load (1.565 kN/m^2). As expected, the axial thrust is constant over the length of the shell without stiffeners. However, the axial thrust in the stiffener has increased by 40% compared to that of the non-stiffened shell. This increase in the axial thrust in the stiffener is accompanied by increase in the thrust carrying capacity of the stiffened zone. The increase in axial thrust at the haunch level of stiffened zone is not significant. The tension developed in the bottom (flange) plate of the stiffener extends over the shell for a short distance beyond the stiffener edge. This tension diminishes quickly and becomes compressive, attaining a peak at A, Figure 5.9, and thereafter, the thrust in the rest of the shell becomes approximately equal to the average thrust at the crown level of the unstiffened shell. The localized peaking of axial thrust that takes place near the stiffeners, is not considered to cause an additional stability problem, since the stiffener is in its vicinity and the stiffened zone has a higher thrust carrying capacity. It should be noted that the maximum axial thrust occurs at haunch level of the structure. On addition of

stiffeners, this maximum thrust at the unstiffened zone is reduced by 14% (Figure 5.10).

Figure 5.11 shows the comparison of axial thrust variation in the curved direction of the same shell at various locations, under the same loading. As seen before, the thrust variation at the central section and the stiffener section are more or less the same in both stiffened and non-stiffened shells. However, there is a shift in the thrust variation near the stiffener edge.

Figure 5.12 and Figure 5.13 show the thrust variation along the crown and haunch of stiffened and non-stiffened shell models (R=873mm, α =83.75°) under the line/strip loading (3.95 kN/m²) on the central non-stiffened zone. In both stiffened and non-stiffened shells, the axial thrust is mainly distributed in the area of load application. Here also, a peak in thrust is observed near the stiffener. Herein also, it should be noted that the maximum axial thrust occurs at the haunch level of the unstiffened model and is reduced by about 13% on addition of the stiffeners.

Figure 5.14 and Figure 5.15 show the comparison of axial thrust variation in the same shell models (R=873mm), with and without corrugated sheet stiffeners along the crown and haunch level due to the localized patch loading of 135 lb/ft² (6.47 kN/m²) over the central non-stiffened zone (between the stiffeners). Herein also, the axial thrust is mainly distributed in an area of load application. Very

little load dispersion is observed beyond the loaded area. A peak in axial thrust is observed near the stiffener at the crown level. This rise in thrust is not considered to create a stability problem, since a stiffener is present in its vicinity. Maximum axial thrust in the shell without stiffeners occurs at the haunch level of the central section and its variation in the longitudinal direction is gradual and smooth, unlike that at the crown level. This indicates that the shell action is more pronounced at a distance away from the load. On addition of the stiffeners, however, the magnitude of maximum thrust at the haunch of central non-stiffened zone has reduced by 20%, which indicates an improvement in the load carrying capacity of the non-stiffened zone.

All the above comparisons, so far, have been made for the model with a spacing of 27 in. (686mm) between the stiffeners. It is of interest to study the thrust distribution in a structure with different stiffener spacing and equal cross sectional area and the moment of inertia of stiffeners per unit length of the structure. Figure 5.16 shows the comparison of axial thrust variation along the shoulder of a full scale structure (R=185 in. or 4700mm and 152mmX52mm corrugation profile) with different spacing of stiffeners due to the central patch load of 400 lb/ft^2 (19.15 kN/m^2) over an area of 102 ft^2 (9.48 m^2). The axial thrust at the non-stiffened zone has dropped by 2.2%, 12.7%

and 20.9% in the case of stiffener spacing of 9' (2.75m), 6' (1.83m) and 3' (1.0m) respectively (Table 5.8). This indicates that the closer the spacing of the stiffeners, the more the reduction in axial thrust in the non-stiffened zone. The stiffener spacing of 9' (2.75m) or more, do not cause substantial reduction of axial thrust at the non-stiffened zone. The deflection of the central non-stiffened zone under the action of localized patch load is reduced by 2.2%, 11.3% and 18.26% for stiffener spacing of 9', 6' and 3' c/c (2.75m, 1.83m and 1.0m) respectively. Since the deflection of the central non-stiffered zone of a structure with stiffener spacing greater than 9' (2.75m) c/c is approximately equal to that of the structure without stiffeners under similar conditions of patch loading, it can be said that the local buckling strength of the non-stiffened zone is not improved under localized load if the spacing is more than 9 ft. (2.75m) c/c.

5.3.2 Combined Stress Variation

Figure 5.17 through Figure 5.19 show the bending moment variation along the crown and the haunch level of the stiffened and unstiffened soil-steel models (B=873mm, α=83.75°) under various types of loads (uniform, line/strip and patch loads). It is observed that the summation of bending moments in stiffened model (along crown and haunch level) has increased by about 10 to 14% over that in non-stiffened models under similar conditions of loading.

Moreover, the bending moments in non-stiffened strips of stiffened model have significantly reduced compared to the bending moments in the corresponding strips of unstiffened model. This indicates that the stiffener's strips attract most of the bending moments. Therefore, it is necessary to examine the combined stresses due to the bending moments and the axial thrust in the stiffened and non-stiffened zones.

In order to evaluate the effect of the stiffeners on the extreme fibre stress, conduits with and without stiffeners are examined when subjected to similar loading conditions. It should be noted that such comparison is affected by the type of stiffener, spacing and all other geometric parameters of the conduit.

The results obtained from the analysis of the model (R=873mm) with corrugated sheet stiffeners under three cases of loading, as well as a full scale structure (R=4700mm, α=80°) with different stiffener spacing under the patch load are presented below.

Under the action of uniform load, which simulates the condition of conduit under deep fills, the maximum tensile stress in a model without stiffeners occurs at the crown and its magnitude is 410 psi., while the maximum compressive stress in the same shell occurs at the haunch level with a magnitude of 620 psi. With the stiffener added (S=686mm), the maximum stresses at the crown and haunch locations are reduced by 42% and 27% respectively (Figure 5.20). Inspite

of the increase in the moment on the stiffener, the net bottom fibre stress at the crown and haunch levels have reduced considerably. If the maximum stress is the criterion for design, the stiffeners are useful in reducing the extreme fibre stresses.

Similarly, under the action of strip loading of 82.5 lb/ft² (3.95 kN/m²) over the central non-stiffened zone of the model, the maximum tensile and compressive stresses in non-stiffened shell are 1000 psi. and 1600 psi., respectively (Figure 5.21). On addition of stiffeners (S=873mm), these extreme fibre stresses are reduced by 48% and 25% at the crown and haunch level of central non-stiffened zone, respectively. The stresses under the stiffener are also decreased.

The localized patch loading of 135 lb/ft² (6.465 kN/m²) over the non-stiffened zone produces maximum stresses of 2450 psi. at crown and 3110 psi. at the haunch of non-stiffened shell. On addition of stifferers, these stresses at central crown and haunch section of unstiffened zone are reduced by 32% and 24%, respectively (Figure 5.22). Also, the stresses under the stiffener are less than the stresses in a shell without stiffener, at the same locations.

Figure 5.23 shows the combined stress variation at the shoulder level of the full scale structure (R=4700mm), with different stiffener spacing (S=∞, 2.75m, 1.83m and 1.0m c/c) and constant amount of total cross sectional area and

total moment of inertia of stiffeners, under the patch loading of 400 lb/sqft. (19.15kN/m²). Here also, the closer the spacing of the stiffeners, the more the reduction in the combined stresses at non-stiffened zone (Table 5.8).

In general, it can be concluded that the combined stresses due to axial thrust and bending in the stiffened shell are smaller than those in unstiffened shell under the similar conditions of loading.

5.3.3 Crown Deflection Variation

Figure 4.13 shows the comparison of measured and analytical deflection along the crown of White Ash Creek structure (without stiffeners) due to second level, one truck loading at the central section. Deflections are negligible beyond a distance of 10 ft. (3m) from the central section. This indicates the poor shell action of the White Ash Creek structure.

The variation of deflection at the crown of the conduit with corrugated stiffeners due to the three cases of loading are shown in Figure 5.24. In all cases the deflection of the crown has reduced due to the addition of stiffener.

Figure 5.25 shows that under comparable treatment of the soil, the live load deflection at the crown of the model is only slightly reduced as a result of the addition of stiffeners. This can be understood, since the resistance to the deflection in the conduit is attributed partially to the wall rigidity and partially to the soil rigidity (Spangler

Formula, Eq. 2.1). Also, that the soil resistance is usually the major contribution. This observation is further emphasized when examining Figure 5.26. Herein, the different treatment of the soil had a substantial effect on the deflection and the wall rigidity parameters.

5.3.4 Effect of S/R Ratio

The observations made so far regarding the variations of forces and the deflections are based on the results of particular cases of structures. The study of the effect of non-dimensional parameter S/R on the distribution of forces and deflections is essential in order to make the general conclusions. Therefore, a few more cases of full scale structures (R=150" and 120") having standard arc and tangent corrugation profile of 152mmX52mm and different spacings of stiffeners (S=1.0m, 1.83m, 2.75m and ∞) under the soil cover of 3 feet (0.92m) subjected to patch loading, have been analysed. The forces and deflections obtained for structures with stiffeners are divided by the respective forces and deflections in a structure without stiffeners under similar conditions and are tabulated in Table 5.9. It is observed that the reduction in forces and deflections is inversely proportional to the S/R ratio. In order to correlate the reduction in forces and the S/R ratio, a Statistical Linear Regression [44] has been carried out for the limited number of analysed cases. During the process of linear regression, it was observed that the relationship

between the dependent variable, the reduction factor Kc, and the independent variable, S/R ratio, can best be represented by a quadratic equation as given below:

$$Kc = a + b\left(\frac{S}{R}\right) + c\left(\frac{S}{R}\right)^2 \qquad [5.22]$$

The coefficients a, b and c are evaluated from the limited data and Eq. 5.22 takes the following form.

$$Kc = 0.37 + 1.51\left(\frac{S}{R}\right) - 0.9\left(\frac{S}{R}\right)^2 \qquad [5.23]$$

It is to be noted that Eq. 5.23 is valid for the range $0.15<S/R<1.0$. Eq. 5.23 is plotted in Figure 5.27, which indicates that for S/R ratio greater than 0.6, the reduction in forces and deflections is not significant. If the S/R ratio is extremely small (say $S/R\leq 0.2$), the reduction in the forces at the unstiffered zone is about 30% (i.e. Kc=0.7). The plot of Kc versus S/R can be divided into three regions A, B and C. The region C indicates that the stiffeners are not useful in reducing the forces and deflections of the shell portion between the stiffeners. The region B is the transition zone which indicates the partial interaction of stiffeners and the shell. In the region A, the stiffeners have full participation and therefore, the stiffeners can be regarded as an integral part of the entire shell.

5.3.5 Analysis Procedure

Usually soil-steel structures are analysed by considering a unit transverse slice of the steel structure and the surrounding soil. In the absence of three dimensional analysis, the unstiffened zone and the stiffened zone can be analysed separately as a plane stress problem if the effect of stiffeners is accounted for by the use of Eq. 5.23. The following text outlines this procedure in three regions of S/R values.

5.3.5.1 Case I $S/R \geq 0.6$

If the S/R ratio is greater than 0.6 (Region C), the stiffeners do not participate in reducing the forces and deflections of non-stiffened zone under the traffic loads. In such a case the stiffened and non-stiffened unit slices of the structure could be analysed separately with actual loading on them.

5.3.5.2 Case II $0.2 < S/R < 0.6$

If the S/R ratio lies between 0.2 and 0.6 (i.e. Region B), the stiffeners are useful in carrying the part of load on non-stiffened zone. Therefore, in such a case the unit slice of non-stiffened zone could be analysed with a reduced loading q_1 on it as follows.

$$q_1 = Kc\ q \qquad [5.24]$$

And the unit slice of stiffened zone could be analysed with increased load q_2 given by the following equation.

$$q_2 = q \left[1 + \frac{(S-W)\ (1-Kc)}{W} \right] \qquad [5.25]$$

where, q is the distributed load per unit area, W is the width of stiffeners and Kc is the reduction factor obtained by Eq. 5.23.

5.3.5.3 Case III $S/R \leq 0.2$

This situation results when the stiffeners are closely spaced. In this range of S/R ratios, the stiffeners are considered to be a fully integral part of the entire shell. Therefore, the combined section of the shell and the stiffeners should be considered for plane analysis with actual loading on it.

5.3.6 Test to Determine Failure Load of Conduit

To study the nature of failure and the failure load of the soil-steel structure, the models with and without corrugated sheet stiffeners were tested under localized patch load (Figure 4.26). The model without stiffeners was loaded until large crown deflections started to occur. The model was unloaded without actually failing it. However, the trend of the load-deflection curve for unstiffened model (Figure 5.28), shows that the unstiffened model almost reached failure load at 2200 lb. (9.8 kN). The extreme fibre

stresses measured at this load level were well below the yield stress. Similarly, the shell with corrugated stiffeners (S/R=0.79), was tested under similar conditions of loading. This conduit also had an almost similar load-deflection curve upto 2200 lb. Initiation of local buckling was observed at 2200 lb. load level (Figure 5.29). The deflections at stiffener's crown are substantially smaller than that of the central non-stiffened zone. This indicated that the stiffener was not very much helpful in carrying the central localized load. In this case also, the measured stresses at a load level of 2200 lb. were well below the conduit material yield stress. The stiffened model failed locally at 3800 lb. (16.9 kN) with the stiffeners intact (Figure 5.30). This revealed that the stiffened shell had considerable post buckling strength (73% greater than the local buckling strength). However, the post buckling strength is at the cost of large crown deflection. For this particular model, the stiffened shell had failed in local buckling at the same load level (2200 lb.) as non-stiffened model. The post buckling failure was due to the yielding of stretched central corrugations. The patch loading plates (Figure 4.25) were sized in such a way that the projected load area on the conduit crown level as per CHBDC [64], spread only over the central non-stiffened zone. Similar results are anticipated in the case of conduit of normal spacing of stiffeners (9 ft. or 3m or S/R≥0.6). This

leads to the conclusion that the stiffeners have considerable effect on the overall buckling of the conduit but little effect on the local buckling in the zone between the stiffeners especially when localized live load is applied on the central non-stiffened zone.

Chapter VI

SUMMARY AND CONCLUSIONS

6.1 Summary

The method of finite strip is modified and applied to the three dimensional analysis of the soil-steel structure with radial rib stiffeners. The assumed displacement patterns for a particular strip are approximated in terms of the sum of products of one-dimensional third order interpolation polynomials relating undetermined displacement coefficients along the two curved edges of the strip and the basic function series which describe the variation of the displacement coefficients along the entire length of the strip and satisfy the force and displacement boundary conditions at the two ends of the strip. Modified displacement functions have been presented to incorporate the eccentricity between the centroidal surfaces of the main shell and the stiffener so that the continuity of the shell is satisfied between the strips. The displacement functions developed can represent a soil-steel structure both during side filling and under the traffic loads.

The effect of soil interaction has been acccunted for by representing the surrounding soil media by extensional (radial and tangential) springs with coefficierts dependent

on the depth and density of the soil, as well as the radial direction at the contact surface between the conduit wall and the soil.

The following cases were analysed:

1) Cylindrical shells subjected to horizontal forces acting lateral to the longitudinal edges and,
2) Cylindrical shells supported along two hinged edges and subjected to radial or gravity load. Herein, the analysis was conducted with the presence of soil, as well as for the cases of loading (uniform or variable) in the direction of the axis of the conduit.

All cases of loading were analysed with no stiffeners, as well as with stiffeners, in order to determine the effect of the stiffeners on the following:

1) the bending rigidity of the stiffened zone of the shell and the corresponding load carrying capacity.
2) the shell effect under local live load and the effect of stiffeners on the load dispersion in the shell.

The method of analysis has been verified experimentally and leads to the following conclusions:

6.2 Conclusions

1) The Finite Strip Method is a powerful approach for predicting the three dimensional response of stiffened soil-steel structure and it is most ideally suited for systems where orthogonal basic functions can be chosen.

The basic functions which are highly non-orthogonal in nature forfeit the main advantages of the finite strip method. The basic functions with limited non-orthogonality yield convergent solutions within three terms of Fourier series.

The displacement functions for stiffeners are capable of considering the eccentricity in the centroidal surfaces at the common nodal line of the unstiffened and stiffened strips.

2) Closed conduits can also be analysed by the formulation of the two hinged shell embedded in soil by cosidering an intersection angle in the range of 230° to 270° which depends on the relative stiffness of the conduit wall and the surrounding soil.

3) The cylindrical shell finite strip offers excellent tool for three-dimensional analysis of soil-steel structures, although the existence of coupling between the in-plane and out-of-plane displacements due to the curvature of strip complicates the mathematical formulation.

Complex behavior of the surrounding soil can be simplified in the three dimensional analysis by the tangential and radial extensional springs with the coefficients suggested by Okeagu and Abdel-Sayed.

4) Formulas have been developed to determine the effective width of the conduit shell which can be

considered in the calculation of the section properties of the stiffened zone of the conduit. Equation based on the stresses is to be applied for proper evaluation of the stresses induced in the stiffened section, while equation based on rigidity is to be applied for the proper evaluation of the rigidity, i.e. for the calculations of deflections and/or the overall buckling of the stiffened zone. It is also noticed that the magnitude of the effective width, We, is relatively small when compared with the spacing between the stiffeners or with the effective width of the stiffened flat panels.

5) The provision of stiffeners in the upper zone of the conduits has a considerable effect in reducing the conduit deformation during construction. If the spacing of the stiffeners is more than 9' (2.75m) c/c, the bending load carrying capacity of the stiffened upper zone is increased but slightly when compared with the capacity of non-stiffened conduits. However, the closely spaced stiffeners (say 3' or 1.0m c/c) improve both deflection reduction and the bending moment capacity significantly.

6) The horizontal deflection during construction stage should always be limited in order to avoid yielding at the crown level.

7) The stiffener spacing of 3' (1.0m) c/c reduces bending moment, axial thrust and combined stresses in a non-stiffened zone of soil-steel structure under traffic load by 20%, whereas, the spacing of 9' (2.75m) c/c or more has no effect on reducing these forces. This shows that the spacing of the stiffeners is the major factor affecting the distribution of thrust and bending moment over the length of the conduit.

8) In general, the shell action of corrugated soil-steel structure is ineffective with regard to the load transfer in the longitudinal direction. This is attributed to the very low rigidities of the corrugated sheets in the longitudinal direction (perpendicular to corrugations). There is some improvement in shell action at a distance (say shoulders of structure) away from the patch load application area.

9) The practice of analysing the conduit as a plane structure by neglecting the presence of stiffeners is found to be approximately valid when S/R ratio is greater than or equal to 0.6.

If the S/R ratio is less than or equal to 0.2, the stiffened soil-steel structure under traffic load can be analysed by considering a combined section of the shell and the stiffeners.

If the S/R ratio has value between 0.2 and 0.6, the plane analysis of non-stiffened zone and the stiffened zone can be carried out separately provided the loads on these sections are modified.

10) For conduits with S/R greater than or equal to 0.6, the stiffeners have considerable effect on the overall buckling of the conduit but little effect on the local buckling in the zone between stiffeners especially when localized live load is acting.

11) The influence of frictional force on the distribution of axial thrust and the bending moment in the curved direction is not significant.

12) The degree of compaction of the surrounding soil has a more substantial effect on the deflection and the wall rigidity parameters of the soil-steel structure than the addition of stiffeners.

Appendix A

BIBLIOGRAPHY

1. Abdel-Sayed, G., "Stability of Flexible Conduits Embedded in Soil." Canadian Journal of Civil Engineering, v-5, 1978, pp 324-366

2. Abdel-Sayed, "Progress Report on Live Load Effects in Soil-steel Structures", Ontario Ministry of Transportation and Communication, University of Windsor, Ont., Canada, March 1982.

3. Abdel-Sayed, George, "Critical Shear Loading of Curved Panels of Corrugated Sheets." ASCE Journal of Engineering Mechanics Div., v-96, n-EM6, Dec. 1970, pp 895-912

4. Abdel-Sayed, George, "Effective Width of Steel Deck-Plate in Bridges." Journal of Struct. Div., ASCE, v-95, n-ST7, July 1969, pp 1459-1474

5. Abdel-Sayed, G., and Bakht, B., "Soil-Steel Structure Design by the Ontario Code, Part 2, Structural considerations," Canadian Journal of Civil Engineering, v-8, n-3, Sept. 1981.

6. Abdel-Sayed, G., and Ekhande, Shantaram G., "Cold Formed Steel Barrel Shells", A paper presented at the International Association for Shell and Spatial Structures, Moscow, Sept. 1985.

7. Abdel-Sayed, G., and Ekhande, Shantaram G., "Effect of Stiffeners on the Behavior of Soil-Steel Structures," A Final Research Report (IRI 17-10). For Ontario Ministry of Transportation and Communications Toronto, Ontario, November 7, 1985.

8. Abel, J. F., Mark, R., and Richards, B., "Stresses Around Flexible Elliptical Pipe," Journal of the soil mechanics and foundations div. ASCE, Vol. 99, no. SM7, July 1973.

9. AISI, "Handbook of Steel Drainage and Highway Construction Products," American Iron and Steel Institution, Washington, D.C., 1971.

10. Allgood, J. R., and Ciani, J. B., "The Influence of Soil Modulus on the Behaviour of Cylinders in Sand," Highway Research Record No. 249, Highway Research Board, National Academy of Sciences, Washington, D.C., 1968.

11. Allgood, J. R. and Takahashi, S. K., "Balanced Design and Finite Element Analysis of Culverts," Hwy. Res. Rec. 413, Washington D. C., 1972.

12. Bakht, Baider., "Soil-Steel Structure Response to Live loads", ASCE Journal of Geotech. Eng. Div., v-107 (GT6) June 1981, pp 779-799

13. Bakht, B., "Live Load Testing of Soil-Steel Structures." Structural Research Report 80-SRR-4, Ontario Ministry of Transportaion and Communications, Downsview, Ontario, Canada, Nov. 1980.

14. Beal, David B., "Field Tests of Long-Span Aluminium Culvert" , Journal of Geotech. Eng. Div., ASCE, v-108, n-GT6, June 1982, pp 873-890

15. Booy, C., "Flexible Conduit Studies," Prairie Farm Rehabilitation Administration, Canada, Department of Agriculture, Saskatoon, 1957.

16. Bowles, J. E., "Foundation Analysis and Design", McGraw-Hill Book Co., Second Edition, 1977.

17. Brown, C. B., Green, D. R., and Pawsey, S., "Flexible Culverts Under High Fills," Journal of Structural Division, ASCE, vol. 94, no. ST4, April 1968.

18. Burns, J. Q., "Analysis of Circular Cylindrical Shells Embedded in Elastic Media," Ph.D Thesis, University of Arizona, Tucson, Arizona, 1965.

19. Chandrashekhara, K., and Chandrashekara, S., "Analysis of clamped circular cylindrical shells using basic functions", Bull. Int. Assoc. for Shell Structures, v-49, pp 43-57, 1972.

20. Chang, C. S., Espinoza, J. M., and Selig, E. T., "Computer Analysis of Newtown Creek Culvert", Journal of Geotech. Eng. Div., ASCE, v-106, n-GT5, May 1980, pp 531-556

21. Cheung, Y. K., "Finite Strip Method in Structural Analysis", Pergamon Press, 1976.

22. Cheung, Y. K.,"Finite-Strip Method of Analysis of Elastic Slabs", Proc. of the ASCE, Eng. Mech. Div., EM6, pp 1365-1378 Dec. 1968.

23. Cheung, Y. K., "Folded Plate Structures by Finite Strip Method," Journal of Structural Division, ASCE, vol. 95, no. ST12, Dec. 1969, pp 2963-2979.

24. Cheung, M. S., and Cheung, Y. K.,"Analysis of curved box girder bridges by Finite Strip Method", Publications, International Association of Bridges and Structural Engineering, v-31-I, pp 1-20, 1971.

25. CSPI,"Soil-Steel Bridge Structures", Corrugated Steel Pipe Institute, Mississauga, 1978.

26. CSPI,"CSP Technical Manual", Corrugated Steel Pipe Institute, Mississauga, Ont. 1972.

27. CSPI,"Composite Design of Soil-Steel Structures", Corrugated Steel Pipe Institute, Mississauga, Ont., 1972.

28. Dally, James W., and Riley, William F.,"Experimental Stress Analysis", McGraw-Hill Book Company, Second Edition, 1978.

29. Davis, R. E., and Bacher, A. E.,"California's Culvert Research Program: Description, Current Status and Peripheral Pressures", Highway Research Record No. 249, 1968, pp 14-23

30. Dessouki, A. K., "Stability of Soil-Steel Structures," Ph.D. Thesis, Department of Civil Engineering, University of Windsor, Windsor, Ontario, 1985.

31. Donnell, L. H., "Stability of Thin Walled Tubes Under Torsion", Technical Report No. 479, National Advisory Committee for Aeronautics, 1933.

32. Drawsky, R., "An Accurate Design Method for Buried Flexible Conduit Structures," HRB Circ. 34, July 1966.

33. Duncan, J. M.,"Behavior and Design of Long-Span Metal Culvert Structure", Paper presented at the technical session on soil-structure interaction for shallow foundations and buried structures, ASCE, San Francisco, Oct. 1977.

34. Ekhande, Shantaram G.,"Effect of Live Load on the Soil-Steel Structure Under Shallow Cover", M.A.Sc. Thesis, Dept. of Civil Engineering, University of Windsor, Windsor, Ontaria, 1981.

35. El-Atrouzy, Mohamed N., and Abdel-Sayed, G., "Prebuckling Analysis of Orthotropic Barrel-Shells", ASCE journal of Struct. Div., v-104, n-ST11, Nov. 1978, pp 1775-1786

36. Fan, S. C., and Cheung, Y. K., "Analysis of Shallow Shells by Spline Finite Strip Method", Eng. Struct., Oct. 1983, v-5, pp 255-263

37. Fitzhardinge, C., "Economical Highway Bridge Designs Using Earth and Steel.", Paper presented at IRF International Road Federation, Australian Road Conference, Melbourne, April 1978.

38. Flugge, W., "Stresses in Shells", Springer-Verlag, New York, 1973

39. Ghobrial, M., and Abdel-Sayed, G., "Analytical Study of inelastic buckling of soil-steel structures", TRB, National Research Council, Washington D.C., 1985, pp. 7-14

40. Graves-Smith, T. R., and Sridharan, S., "A finite Strip Method for the Buckling of Plate Structures under Arbitrary Loading", Int. J. Mech. Sci., v-20, n-10, 1978, pp 685-693.

41. Graves-Smith, T. R., and Sridharan, S., "A Finite Strip Method for the Post-Local Buckled Analysis of Plate Structures", Int. Mech. Sci., v-20, n-12, pp 833-842, 1978.

42. Hafez, H. H., and Abdel-Sayed, G., "Long Span Soil-Steel Structures, An Economical Alternative to Short Span Bridges." Proceedings, AMSE Annual convention, Plainfield, Indiana, Sept. 1981

43. Hafez, H. H., "Stability of Flexible Conduits Under Shallow Cover", Ph.D. Thesis, Dept. of Civil Eng., University of Windsor, Windsor, Ontario, 1981.

44. Helwig, Jane T., "SAS Introductory Guide," SAS Institute Inc., SAS Circle, Box 8000, Carry, North Carolina 27511, 1978.

45. Howard, A. K., "Modulus of Soil Reaction (E') values for buried flexible pipes", Journal of Geotech. Eng. Div., ASCE, v-103, n-GT1, Jan. 1977.

46. Ibrahim, Ibrahim M., and Mcnforton, Gerard R., "Finite Strip Laminated Sandwich Roof Analysis", Journal of the Struct. Div., ASCE, v-105, n-5, May 1979, pp 905-919

47. Kantorovich, L. V., and Krylov, V. I., "Approximate Method of Higher Analysis," Interscience Publishers, New York, 1958.

48. Katona, M. G., Smith, J. M., Odello, R. J., and Allgood, J. R., "CANDE: Engineering Manual- A Modern Approach for the Structural Design of Buried Culverts," FHWA/RD-77-5, Navy Civil Engineering Laboratory, Port Hueneme, California, Oct. 1976.

49. Kloppel, K., and Glock, D., "Theoretische and Experimentelle Untersuchungen Zu den Tranglast-Problemen Fiegeweicher in die Ende Eingebetter Rohre," No. 40 Publication, Institute fuor Statik und Stahlbau, T. H. Darmstadt, Germany, 1970.

50. Kay, J. N., and Krizek, R. J., "Spring Analog Model for Flexible Culvert Behavior", Highway Research Record No. 310, 1970, pp 29-39

51. Lautensleger, R. W., "SUPERSPAN", A report, ARMCO Inc., Middletown, Ohio 45043.

52. Leonards, G. A., "Foundation Engineering", McGraw-Hill Book Co., 1962.

53. Luscher, U., and Hoeg, K., "The beneficial Action of the Surrounding Soil on the load carrying capacity of Buried Tubes." Proc. of the Symposium on Soil-Steel Structure Interaction, University of Arizona, Tucson, Arizona, 1964.

54. Luscher, U., and Hoeg, K., "The action of soil around buried tubes", Proc. of the 6th International Conference on Soil Mechanics and Foundations Engineering, Montreal, Canada, Vol. II, 1965.

55. Luster, U., "Buckling of Soil-Surrounded Tubes," Journal of Soil Mechanics & Foundations, Div., ASCE, Vol. 92, No. SM6, November 1966.

56. Madsen, J. H., "Development of Super Span Design", Paper presented at the 32nd Canadian Geotechnical Conference, Quebec, Quebec, Sept. 1979.

57. Marston, A., "The Theory of Loads on Closed Conduits in the Light of the Latest Experiments," Proc. HRB vol. 9, pp 139-170, 1930.

58. Marzouk, Osman A., and Abdel-Sayed, G., "Linear Theory of Orthotropic Cylindrical Shells", ASCE Journal of Struct. Div., v-99, n-ST11, Nov. 1973, pp 2287-2306.

59. Marzouk, Osman A., and Abdel-Sayed, G., "Stability of Half-Barrel Orthotropic Shells", ASCE journal of Struct. Div., v-101, n-ST7, July 1975, pp 1517-1530

60. McVay, Michael C., and Selig, E. T., "Perfcrmance and Analysis of Long-Span Culvert", Transportation Research Record 878, 1982, pp 23-29

61. Meyerhof, G . G., and Baikie, L. D., "Strength of Steel Culvert Sheets Bearing Against Compacted Sand Backfill," Hwy. Res. Bec. 30, Washington D. C., 1963.

62. Mirza, C., and Porter, W. A.,"Construction Considerations and Controls for Soil-Steel Bridge Structures." Canadian Journal of Civil Eng., v-8, 1981, pp 519-533

63. Monforton, G. R., "Structural Analysis by Finite Element Method" Class notes, University of Windsor, Windsor, Ont., 1982.

64. OHBDC,"Ontario Highway Bridge Design Code." Ontario Ministry of Transportation and Communicatcns, Downsview, Ontaric, Canada, 2nd Edition, 1983.

65. Okeagu, E. N.,"Analysis and Stability of Large Span Flexible Conduits." Ph.D. Thesis, Dept. of Civil Eng., Michigan State University, East Lansing, 1982

66. Okeagu, E. N., and Abdel-Sayed, G., "Coefficient of Soil Reaction for Buried Flexible Conduits", ASCE Journal of Geotech. Eng., v-110 n-7 July 1984, pp 908-922

67. Seely, Fred B., and Smith, James O,"Advanced Mechanics of Materials," 2nd Edition, John Wiley and Sons, Inc., New York, 1967.

68. Selig, E. T., Abel, J. F., Kulhawy, F. H., and Palby, W. E., "Long Span Buried Structures, Design and Construction." Journal of Geotech. Eng. Div., ASCE, v-104, n-GT7, July 1978

69. Selig, E. T., Abel, J. F., Kulhawy, F. H., and Palby, W. E., "Review of the Design and Construction of Long-Span Corrugated Metal, Buried Conduits.", FHWA/RD-77-131, Federal Highway Administration, Washington, D.C., August 1977.

70. Selig, E. T.,"Instrumentation of Large Buried Culverts", Performance Monitoring for Geotechnical Construction, ASTM STP 584, Philadelphia, PA., August 1975.

71. Selig, E. T., and Calabrese, S. J.,"Performance of Large Corrugated Steel Culvert", Transportaion Research Record No. 548, Washington, D.C., 1975.

72. Selig, E. T., Lockhart, C. E., and Lautensleger, E. W., "Measured Performance of Newtown Culvert", J. Geotech. Eng. Div., ASCE, v-105, n-GT9, pp 1067-1087, Sept. 1979.

73. Spangler, M. G.,"The Structural Design of Flexible Pipe Culverts", Iowa State College, Engineering Experimental Station, Bulletin No. 153, 1941.

74. Sridharan, S., and Graves-Smith, T. R.,"Post buckling Analyses with Finite Strips", Journal of the Engineering Mechanics Div., ASCE, v-107,n-EM5, pp 869-888, Oct. 1981.

75. Sridharan, S.,"A finite Strip Analysis of locally buckled plate structures subject to non-uniform compression", Eng. Struct., v-4, pp 249-255, Oct. 1982.

76. Timoshenko, S., and Woinowsky-Krieger, S.,"Theory of Plates and Shells", 2nd edition, McGraw-Hill Book Company, Inc., New York, 1959.

77. Van Leeuwen, H. J.,"A Product Designer Looks at Highway Overpasses", EIC-68, BRxSTR G, AGM preprint, Halifax, N.S., May 28-31, 1968

78. Vlasov, H. L., "General Theory of Shells and its Applications in Engineering," NASA Technical Translation, NASA-TTF-99, Washington D. C., April 1964, pp 601-617 and 698-714.

79. Watkins, R. K., and Musser, Samuel C.,"Structural performance of Ribbed Long-Span Corrugated Steel Culverts", A report, SYRO Steel Company, January 1984.

80. Watkins, R. K.,"Response of Corrugated Steel Pipe to External Soil Pressures", Highway Research Record No. 373, 1971, pp 86-96

81. Watkins, R. K.,"Failure Conditions of Flexible Culverts Embedded in Soil," Highway Research Board, Vol. 39, National Academy of Sciences, Washington, D. C., 1960

82. White, H. L.,"Largest Metal Culvert Designed by Ring Compression Theory", Civil Engineering, ASCE, vol. 31, no. 1, January 1961.

83. White, H. L., and Layer, J. P., "Corrugated Metal Conduit as a Compressible Ring," Proc. Highway Research Board No. 39, pp 389-397, 1960.

Appendix B

FIGURES

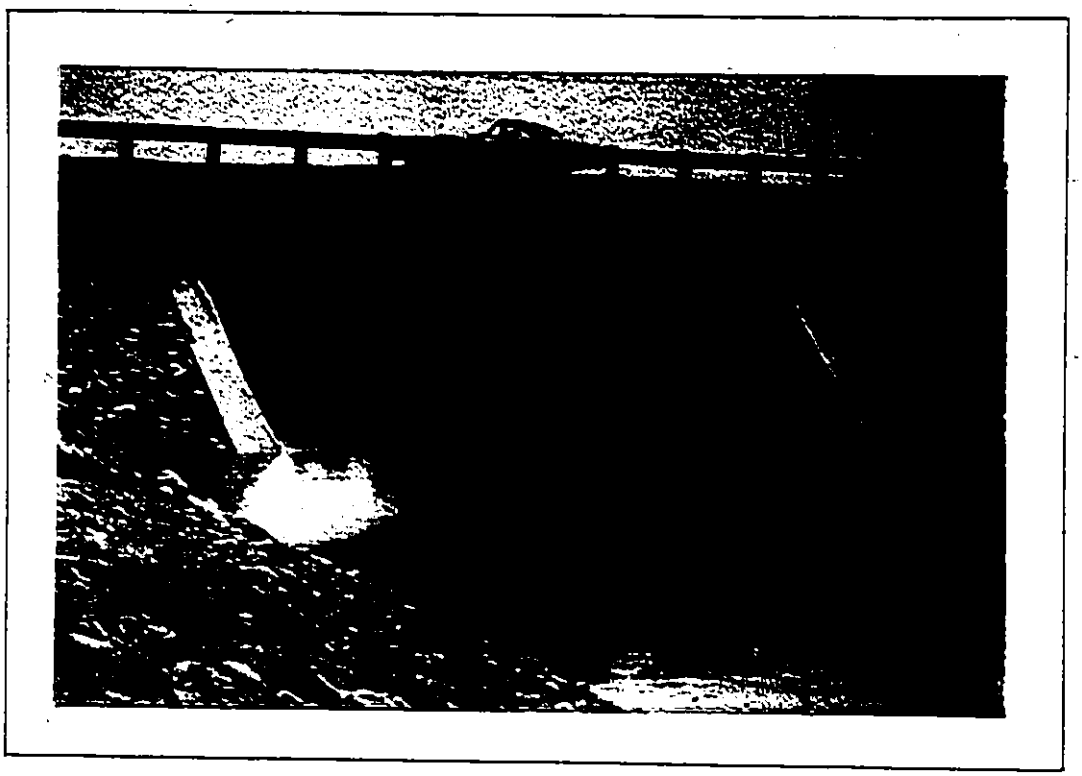

Figure 1.1: Typical Soil-Steel Structure

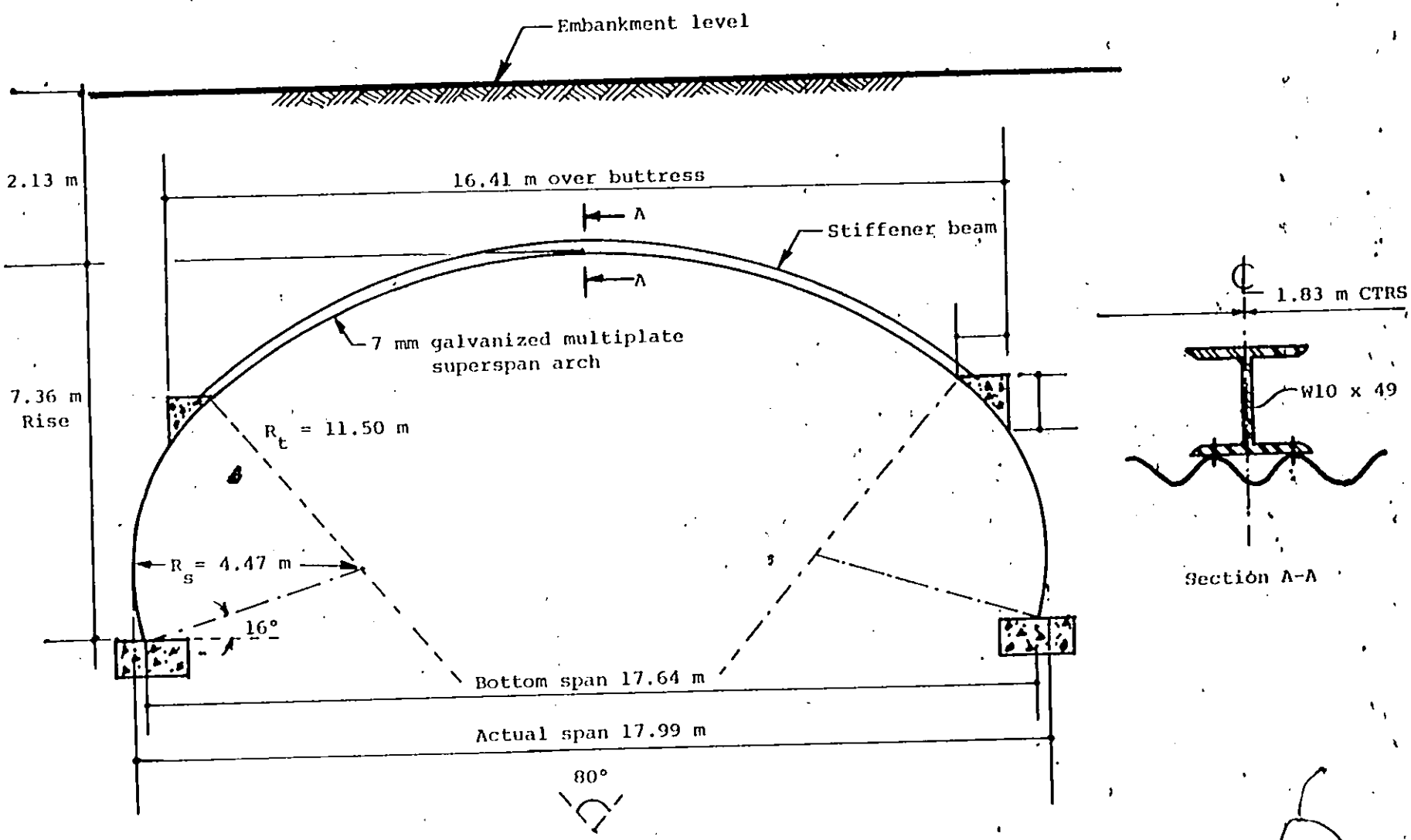

Figure 1.2: Cross-Sectional Details of Cheese Factory Bridge Structure

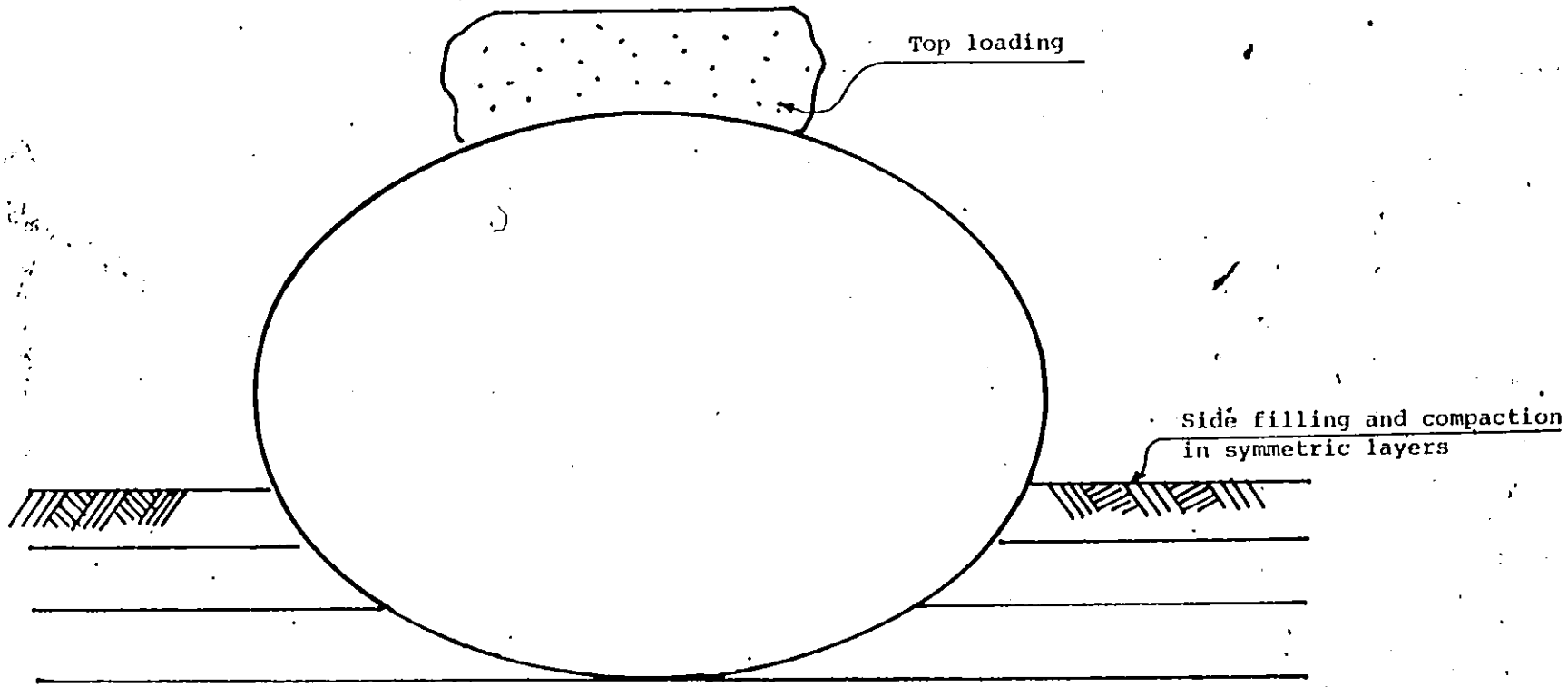

Figure 1.3: Top Loading to Limit Upward Deflection During Side Filling

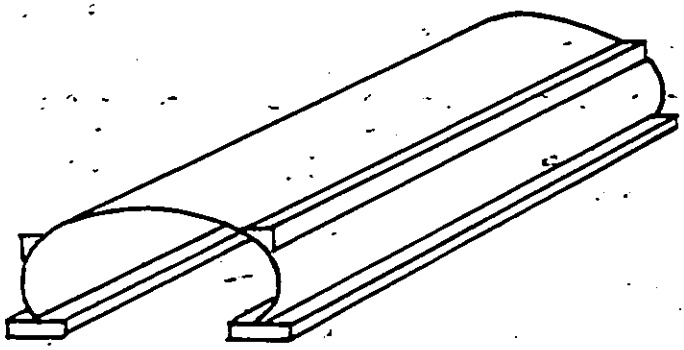

a) Longitudinal Beams at Shoulders

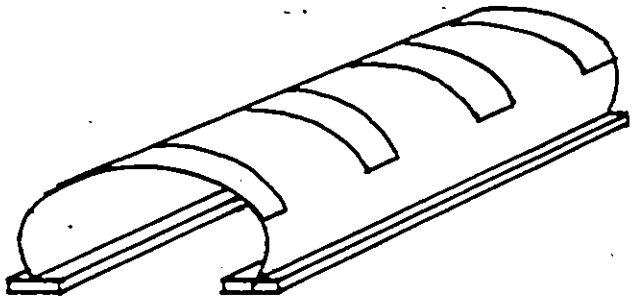

b) Transverse Stiffeners

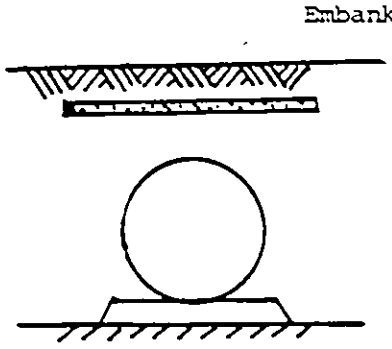

c) Relieving slab

Figure 1.4: Special Techniques to Improve Soil-Steel Structure Interaction

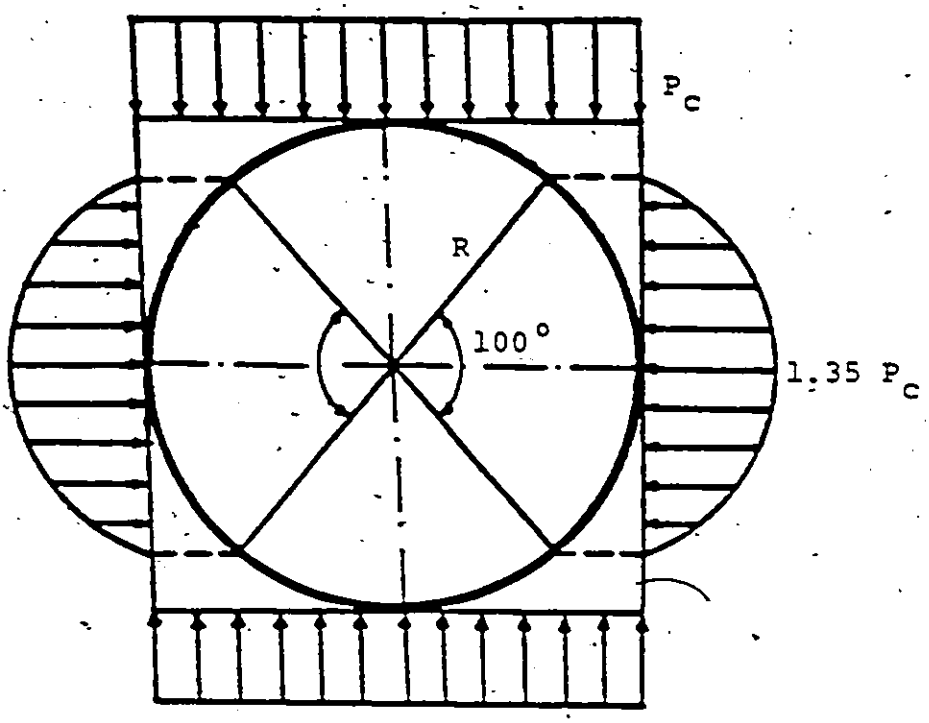

a) Pressure Distribution

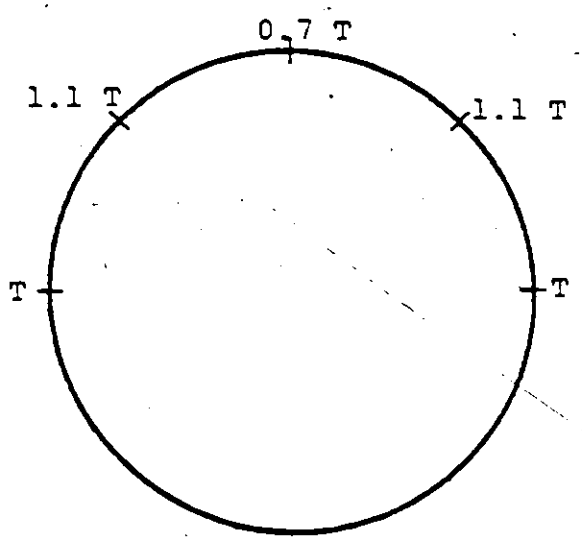

$T = P_c \cdot R$

b) Thrust Distribution

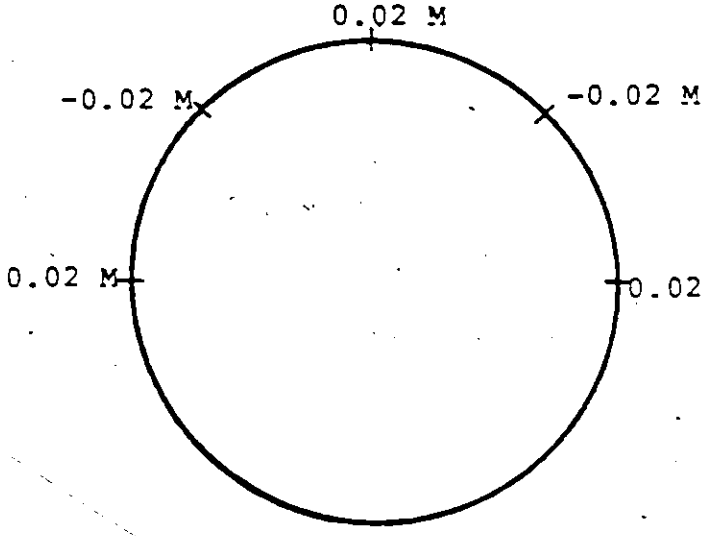

$M = P_c \cdot R^2$

c) Moment Distribution

Figure 2.1: Pressure, Thrust and Moment Distribution Assumed in the Marston-Spangler Method

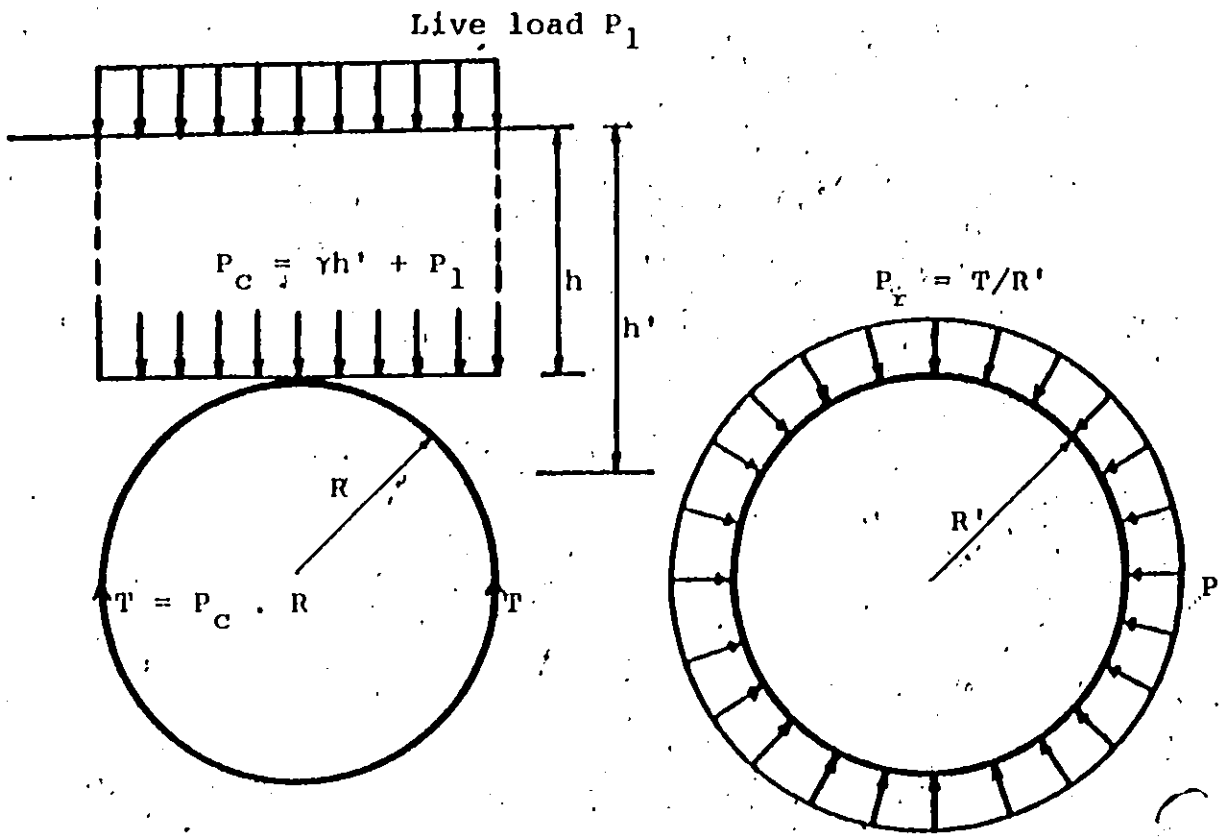

Figure 2.2: Pressure Distribution Assumed in Ring Compression Theory For Circular Cross Section

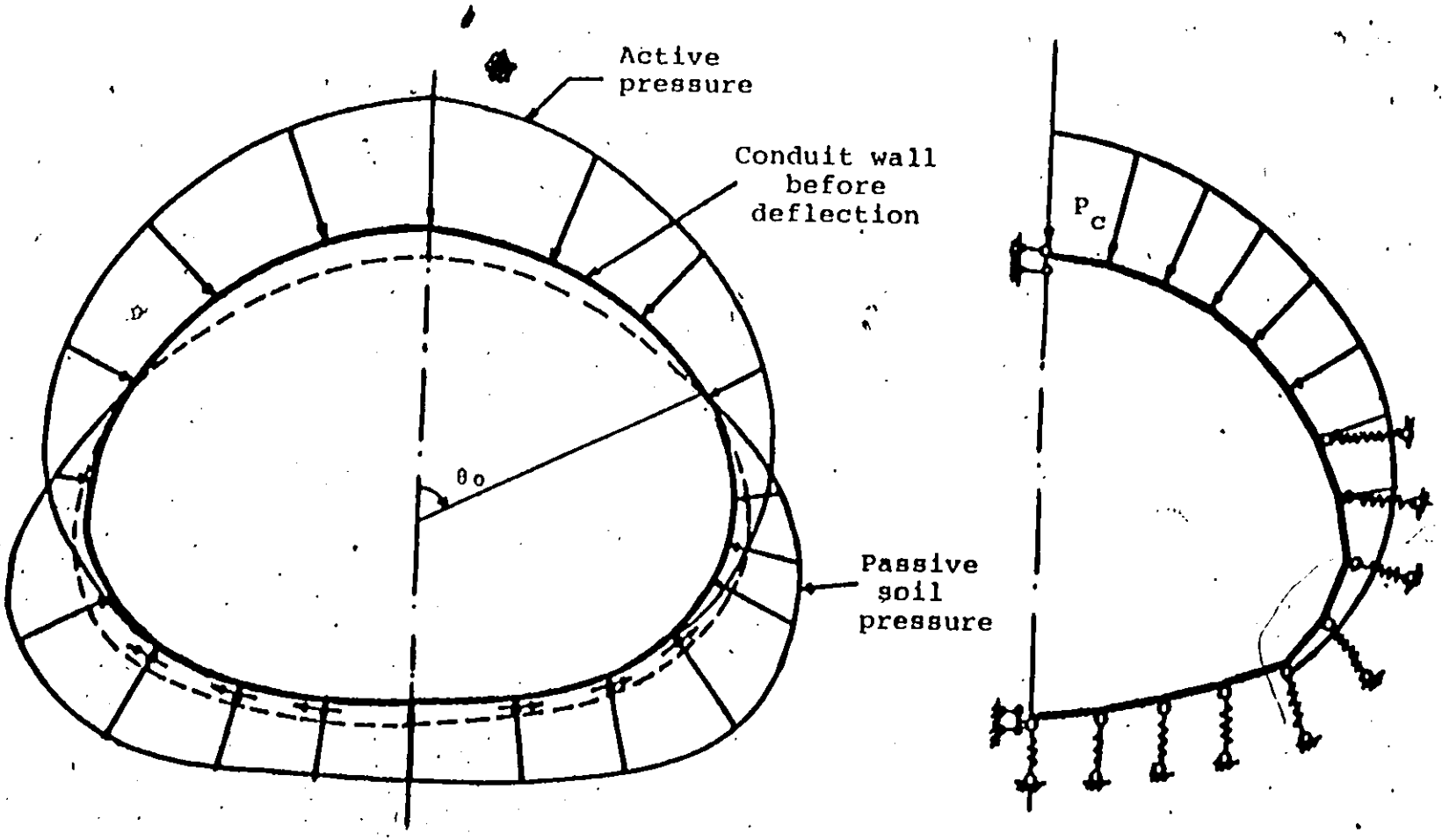

Figure 2.3: Structural System and Loading Assumed by Kloppel and Glock

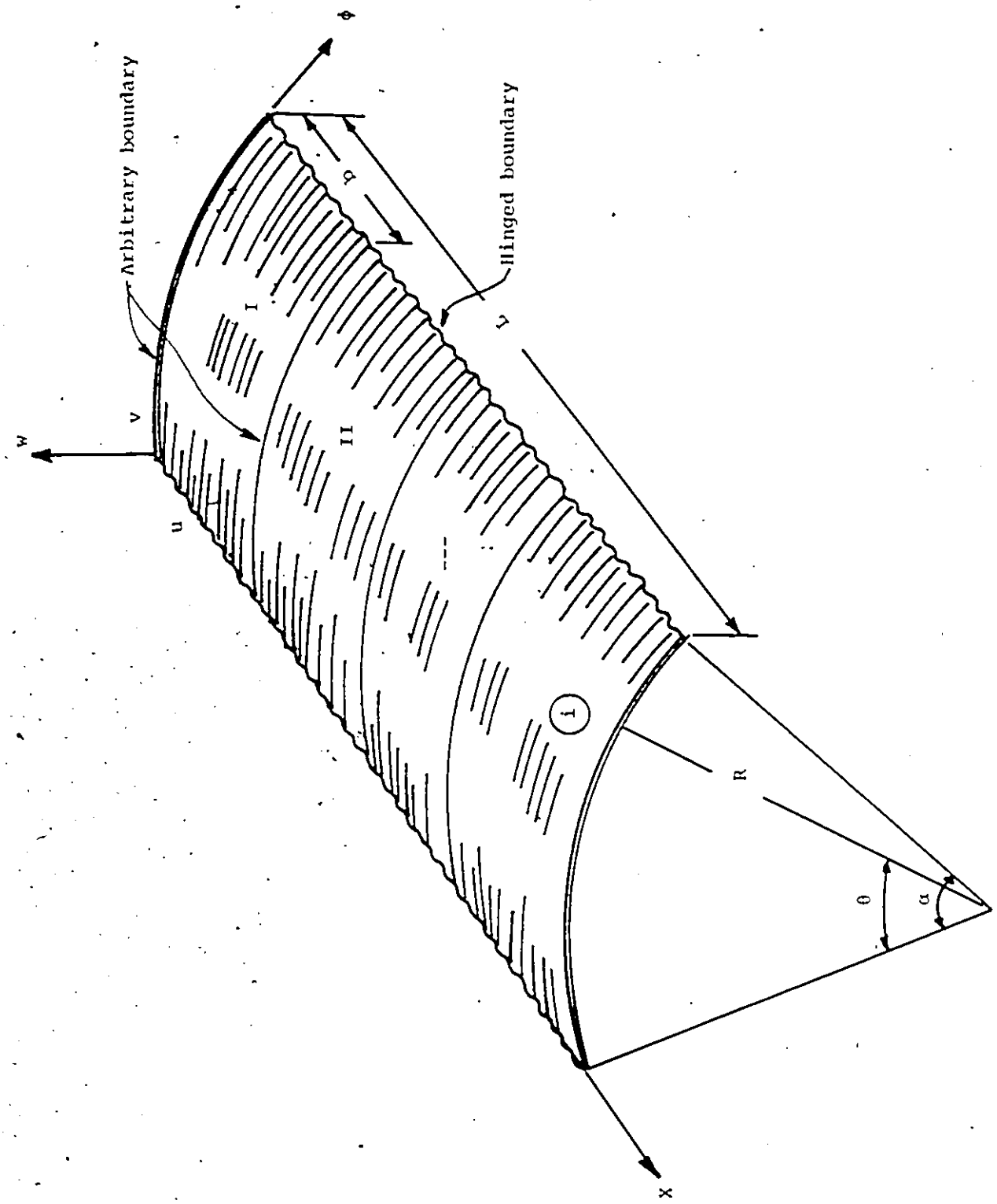

Figure 3.1: Cylindrical Shell Strip

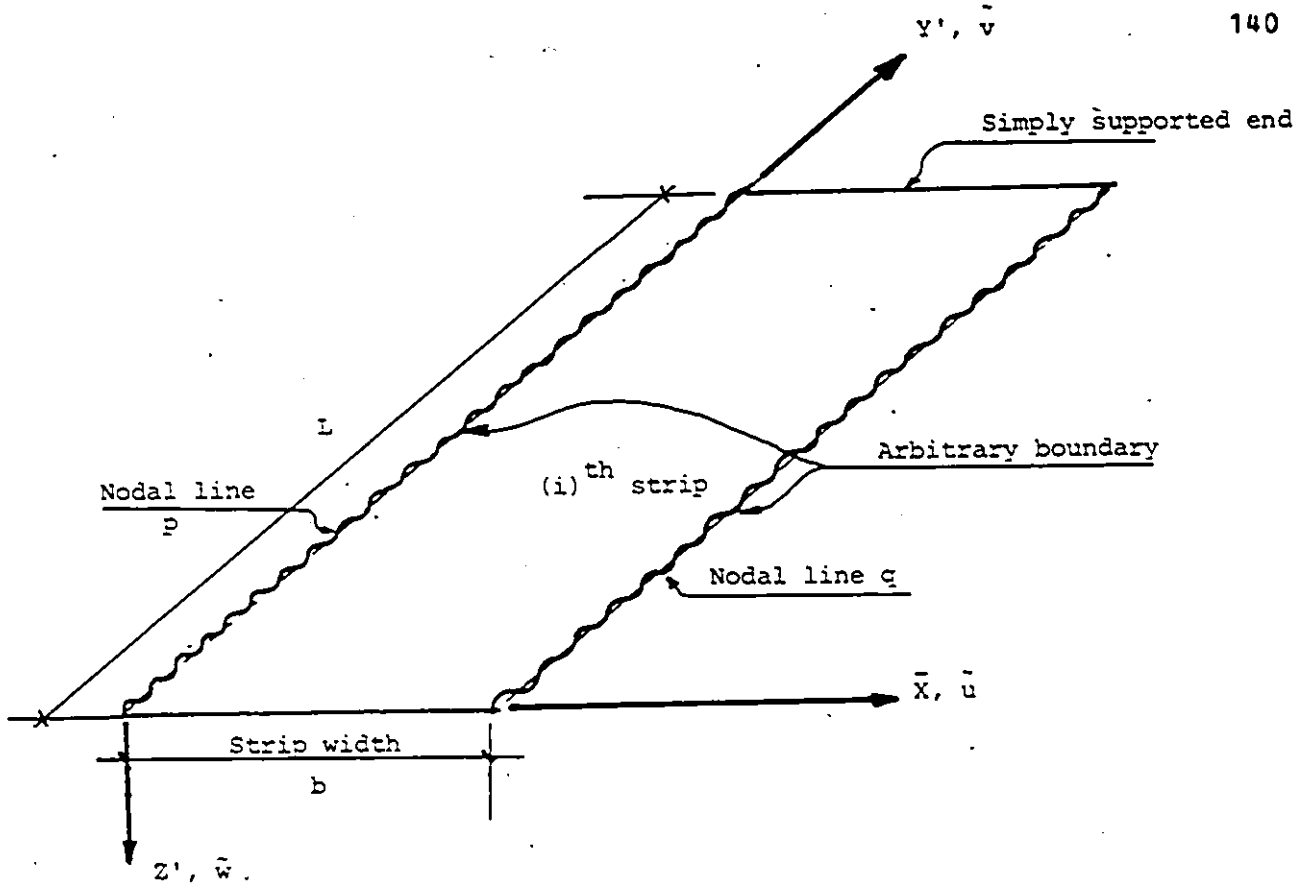

a) Typical Rectangular Flat Strip

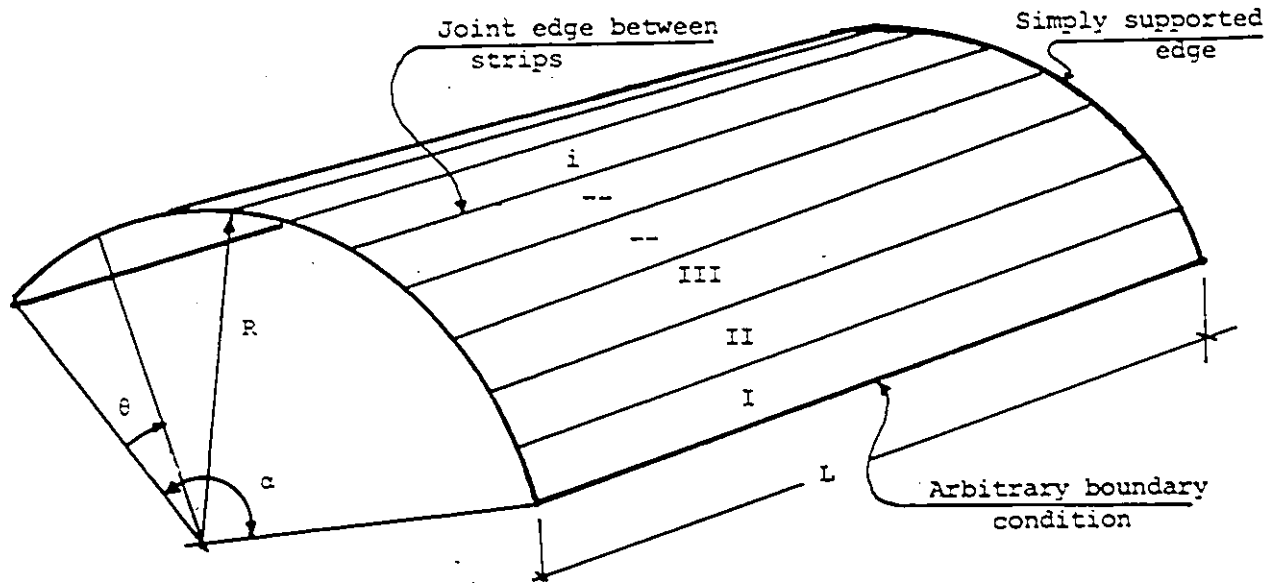

b) Shell With or Without Longitudinal Stiffeners

Figure 3.2: Rectangular Finite Strip Idealization of Shell

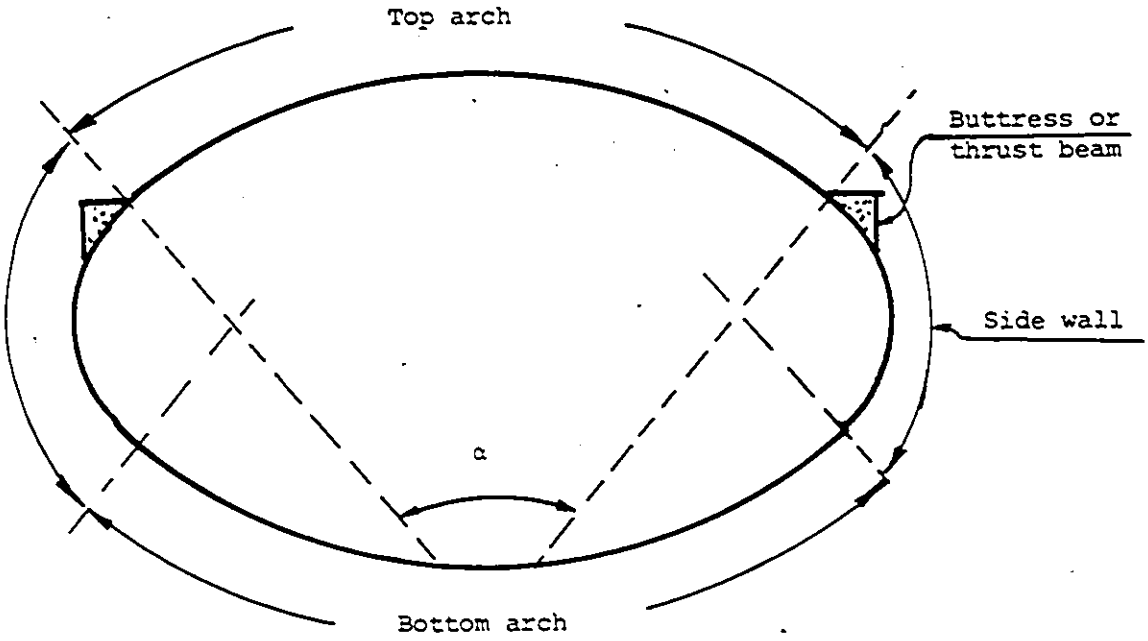

a) Practical conduit

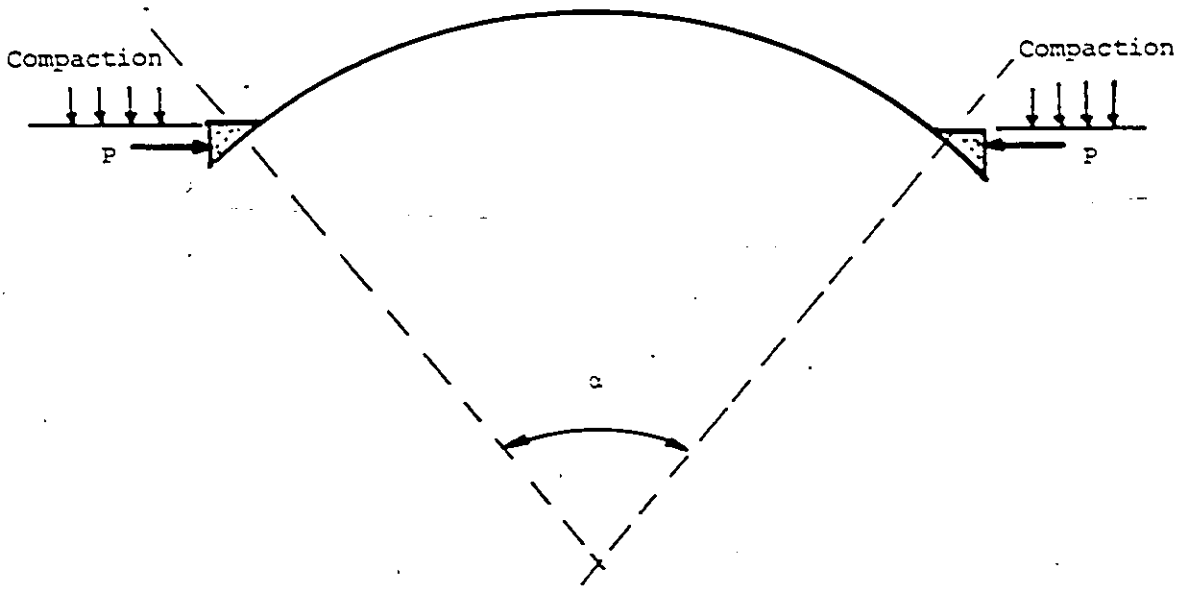

b) Equivalent Arch with Thrust Beam

Figure 3.3: Simulation of Practical Conduit During Side Filling

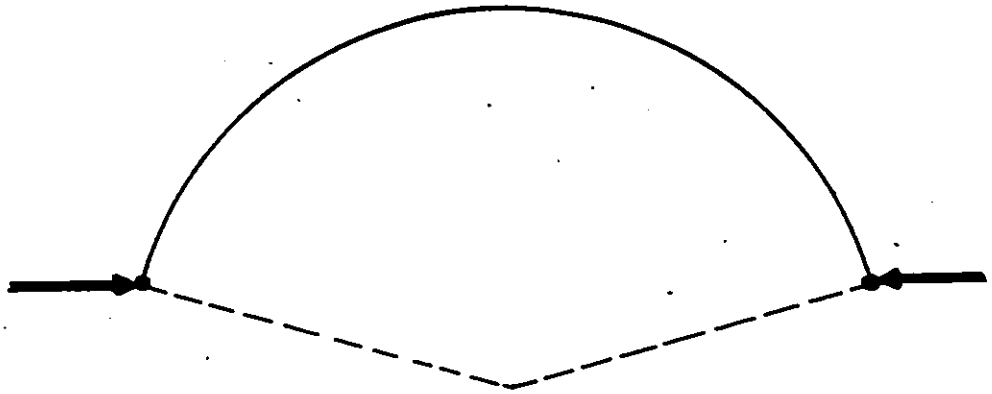

Figure 3.4: Model to Simulate the Structure During Side Filling

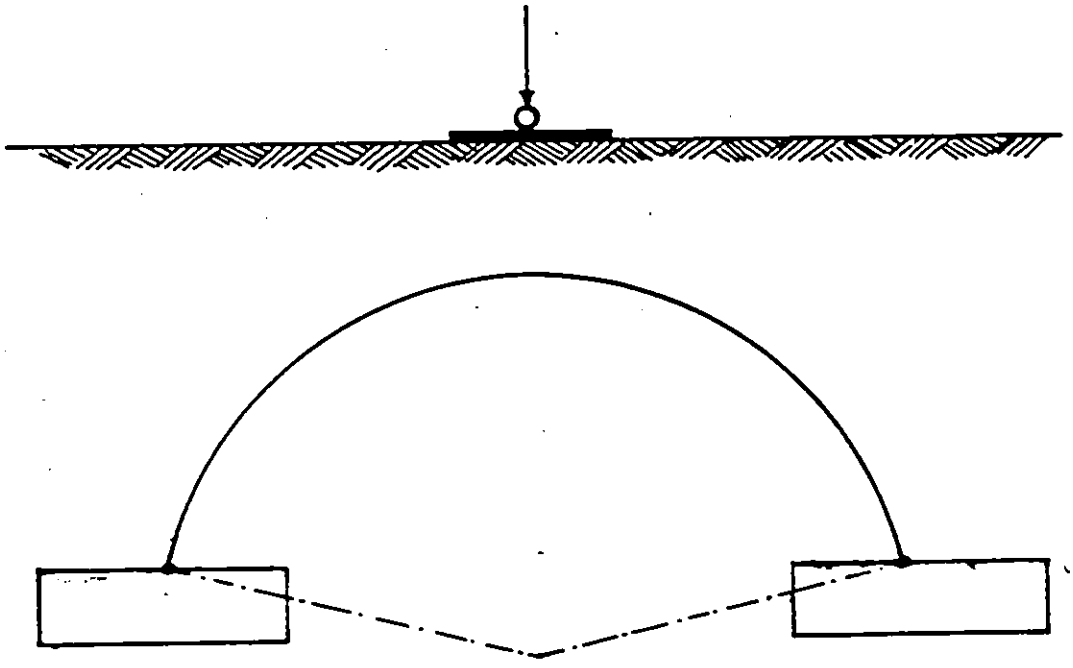

Figure 3.5: Model to Simulate the Structure Under Traffic Load

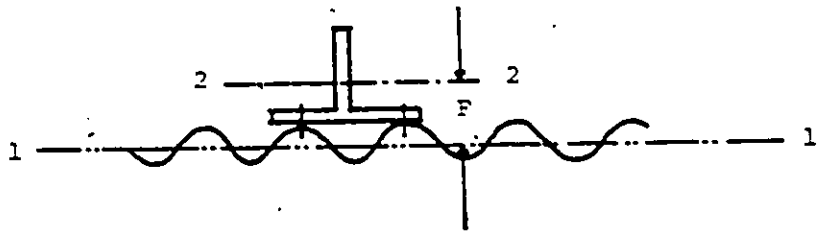

a) Tee Stiffener

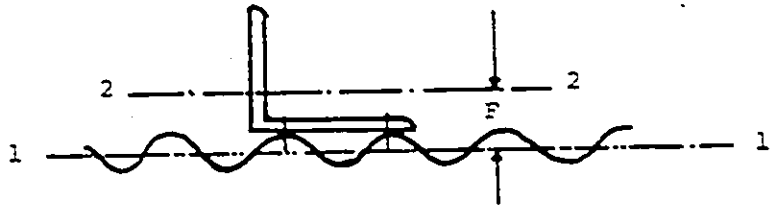

b) Angle Stiffener

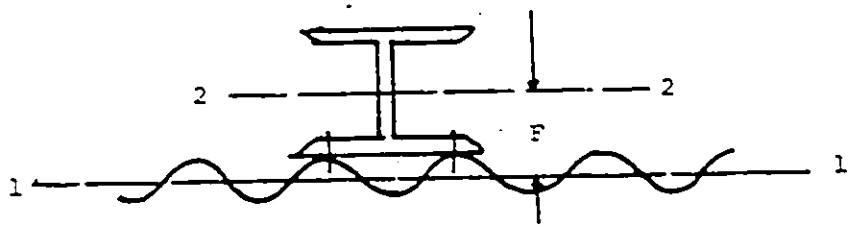

c) I-beam Stiffener

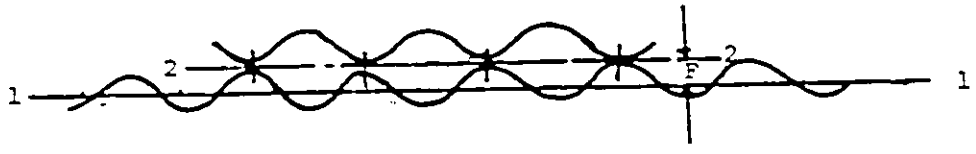

d) Corrugated Sheet Stiffener

1-1 Reference surface of the shell

2-2 Centroidal surface of stiffened element

Figure 3.6: Type of Stiffeners

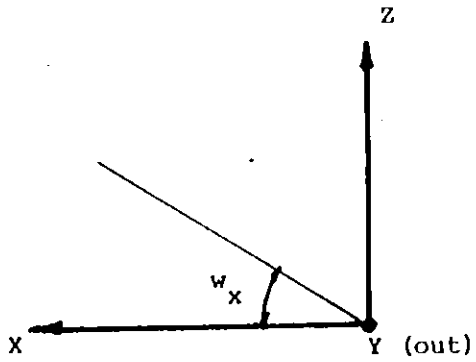

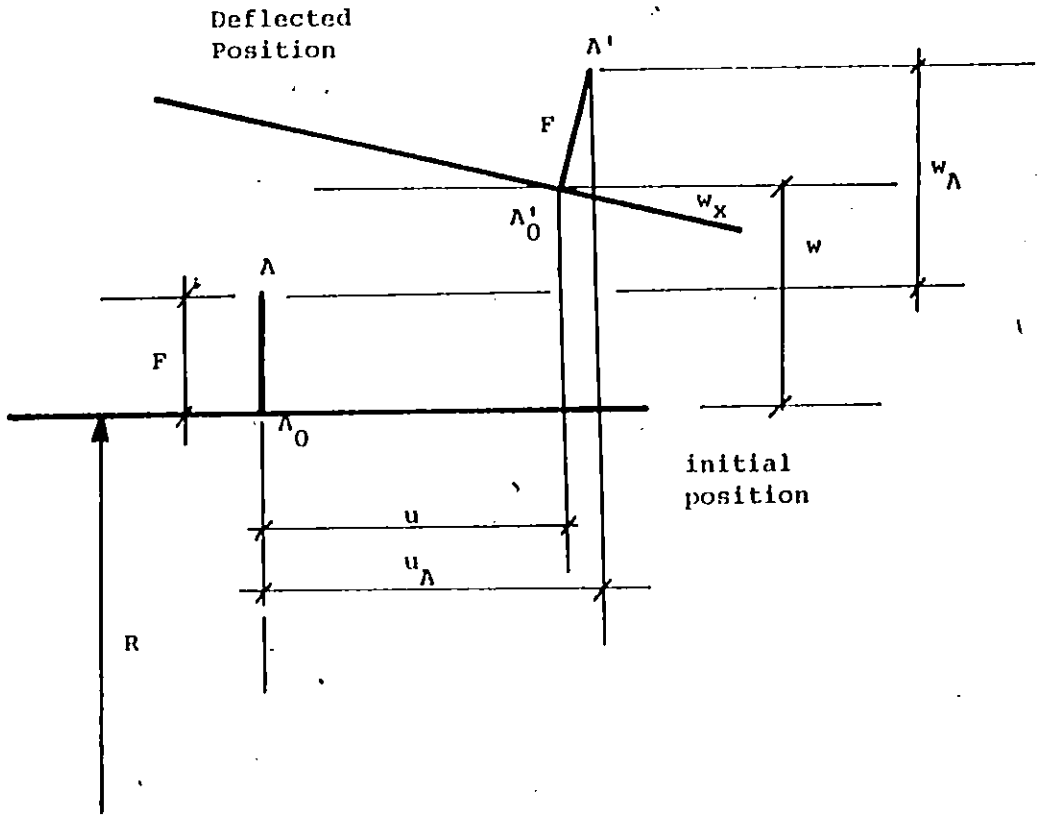

$$u_A = u + F \cdot w_x$$

or

$$u_A = u + F \frac{\partial w}{\partial x}$$

Figure 3.7: Shell Deformation in u Direction

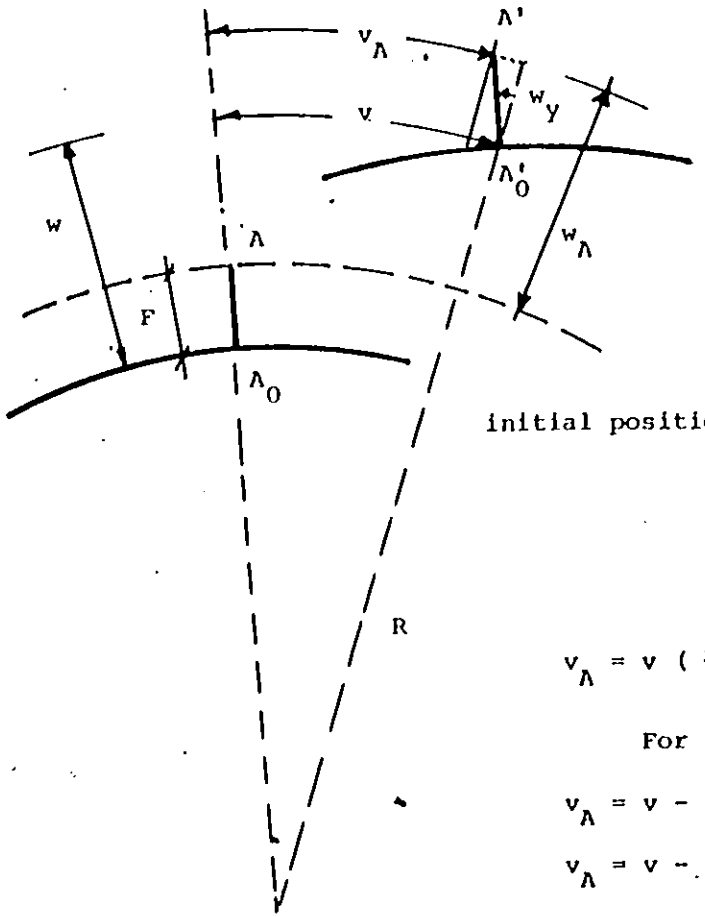

Deflected position

initial position

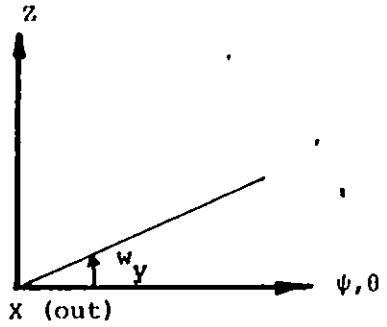

$$v_\Lambda = v\left(\frac{R+F}{R}\right) - F \cdot w_y$$

For $R >> F$ $\quad R + F \simeq R$

$$v_\Lambda = v - F \cdot w_y$$

$$v_\Lambda = v - F\frac{\partial w}{\partial y} \quad \text{in rectangular co-ordinates}$$

$$v_\Lambda = v - \frac{F}{R}\frac{\partial w}{\partial \theta} \quad \text{in cylindrical co-ordinates}$$

Figure 3.8: Shell Deformation in v Direction

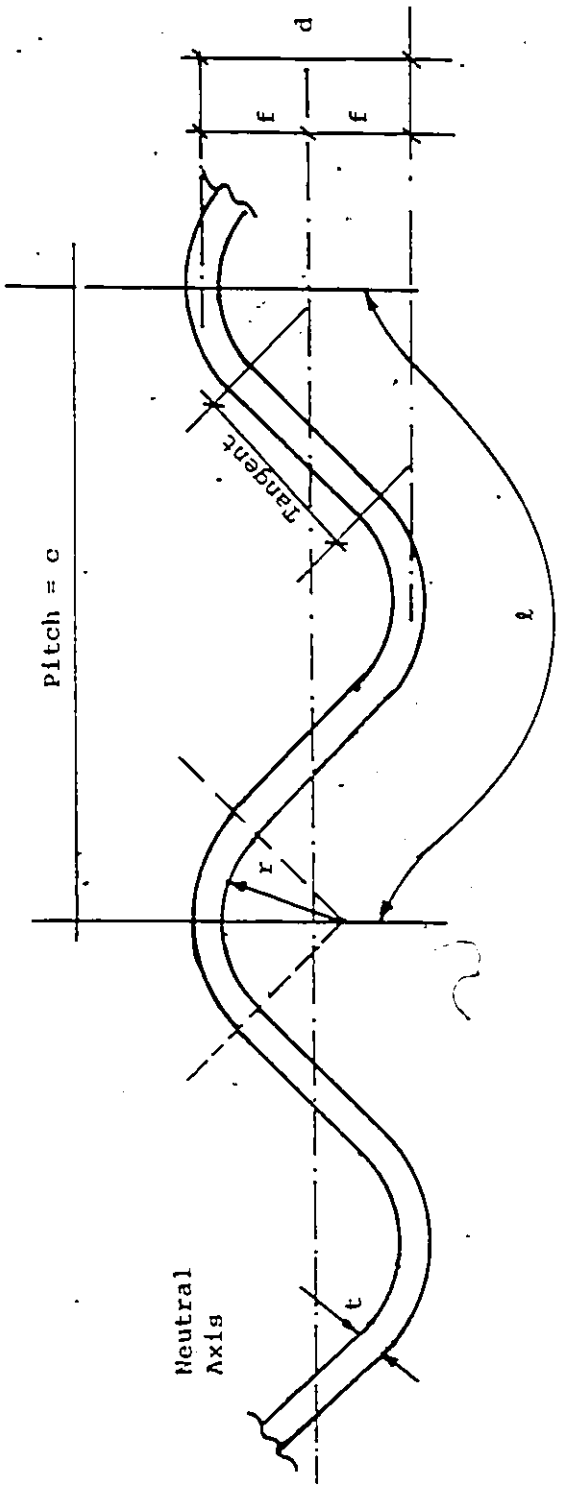

Figure 3.2: Standard Arc and Tangent Corrugation Profile

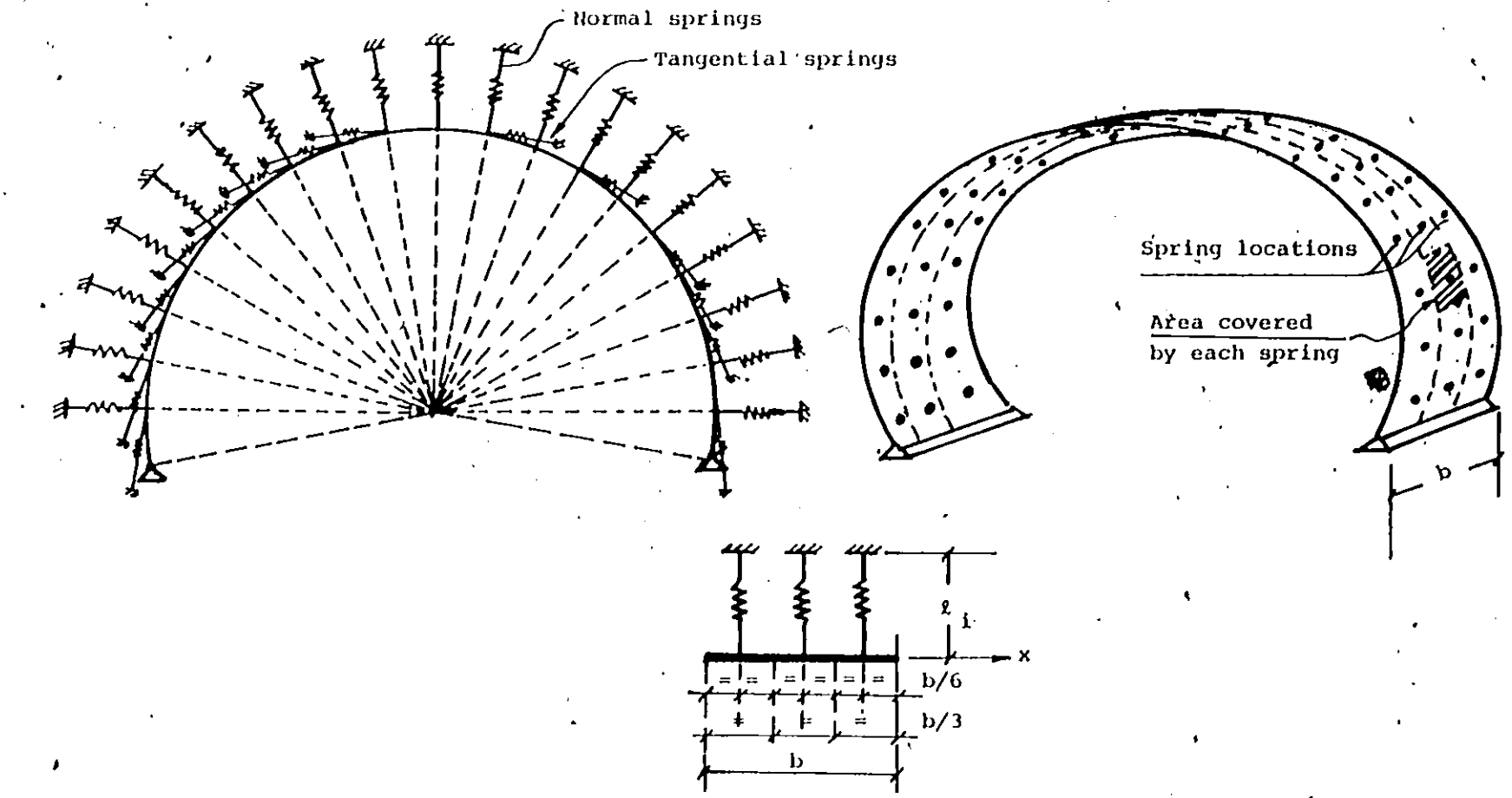

Figure 3.10: Shell Strip with Normal and Tangential Springs

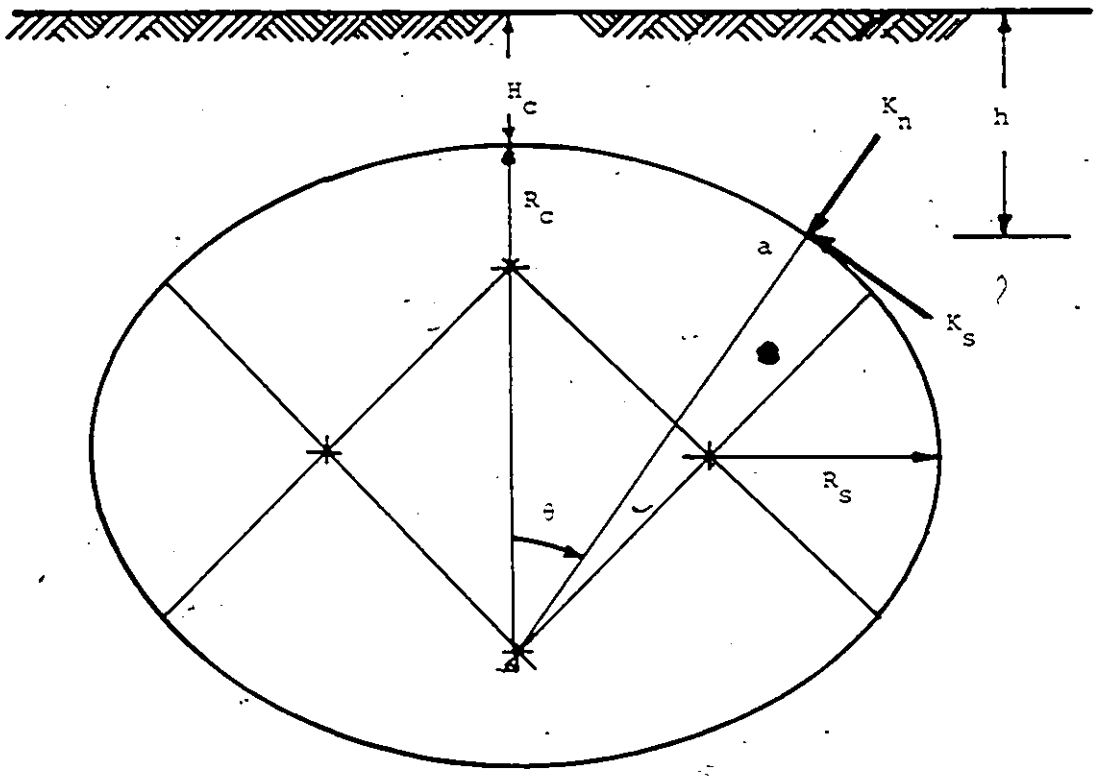

Figure 3.11: Geometry of Practical Conduit and Angular Co-ordinates

$$\theta_o = 1.6 + 0.2 \log_{10}\left(\frac{EI}{E'R^3}\right) \text{ rad.}$$

$$\alpha_{eq} = 4.5\ \theta_o$$

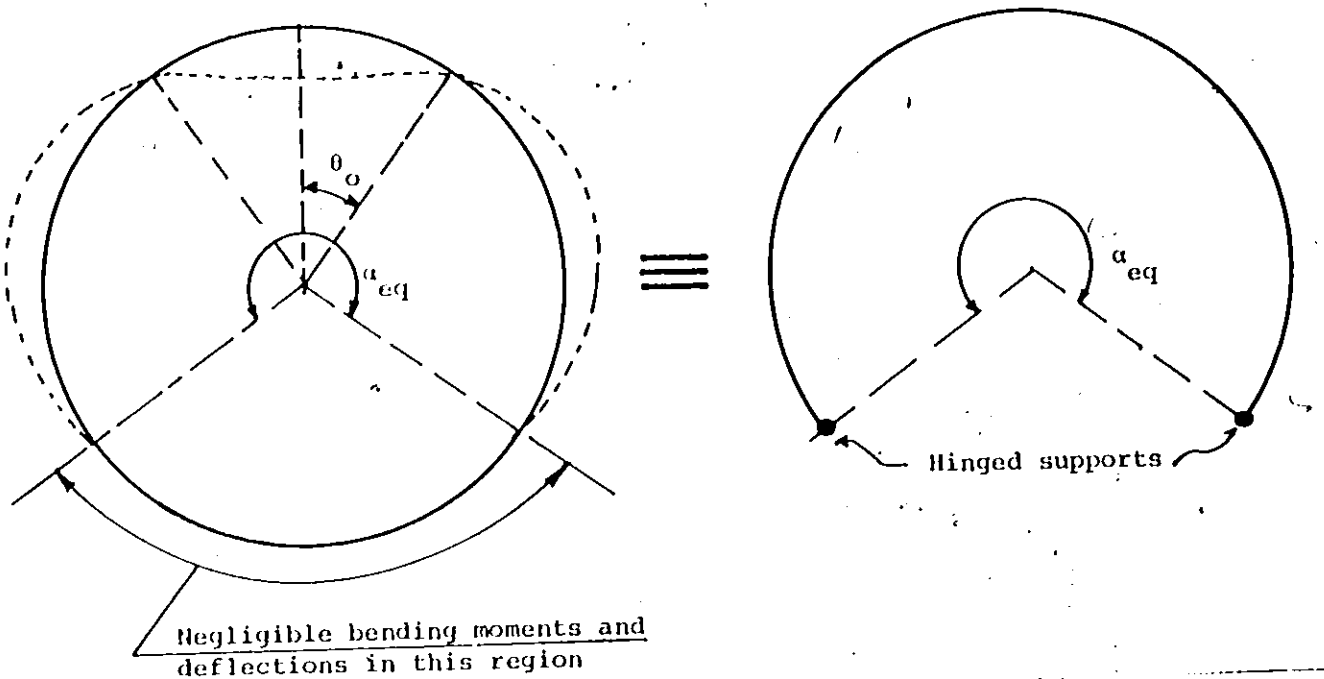

Figure 3.12: Equivalent Angular Span of Closed Shape Conduit

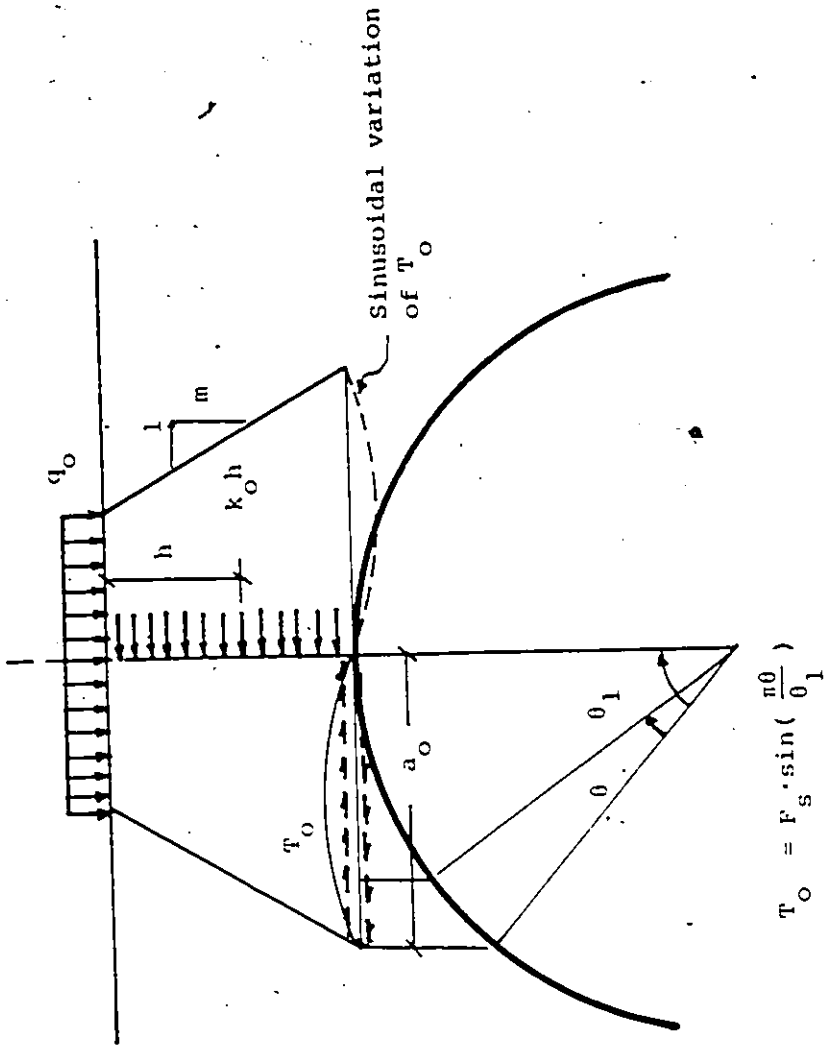

Figure 3.13: Load Transfer in Top Soil

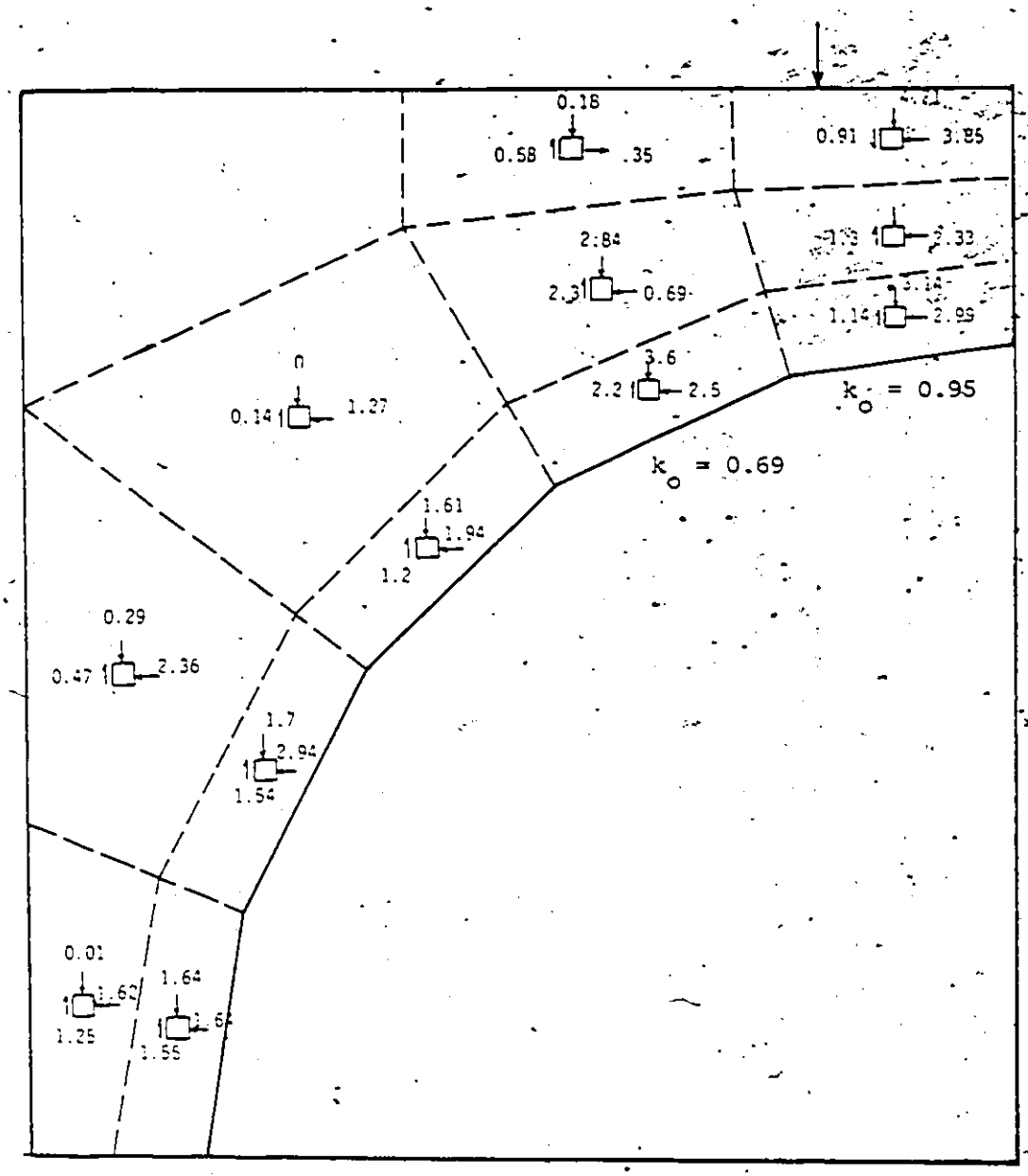

Figure 3.14: Stresses in Soil Elements Under Live Load (ref. 2)

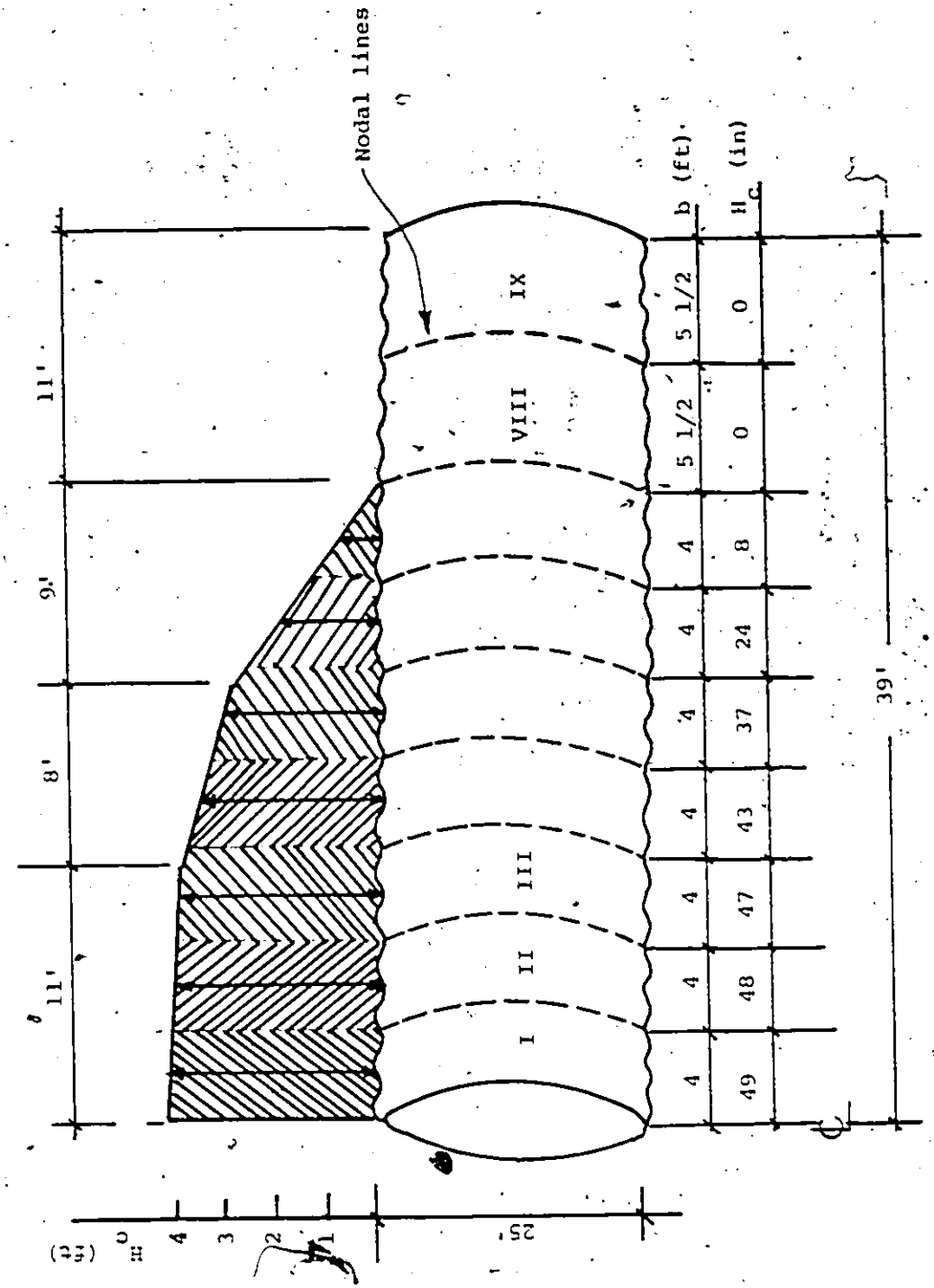

Figure 3.15: Finite Strip Idealization of White Ash Creek Structure

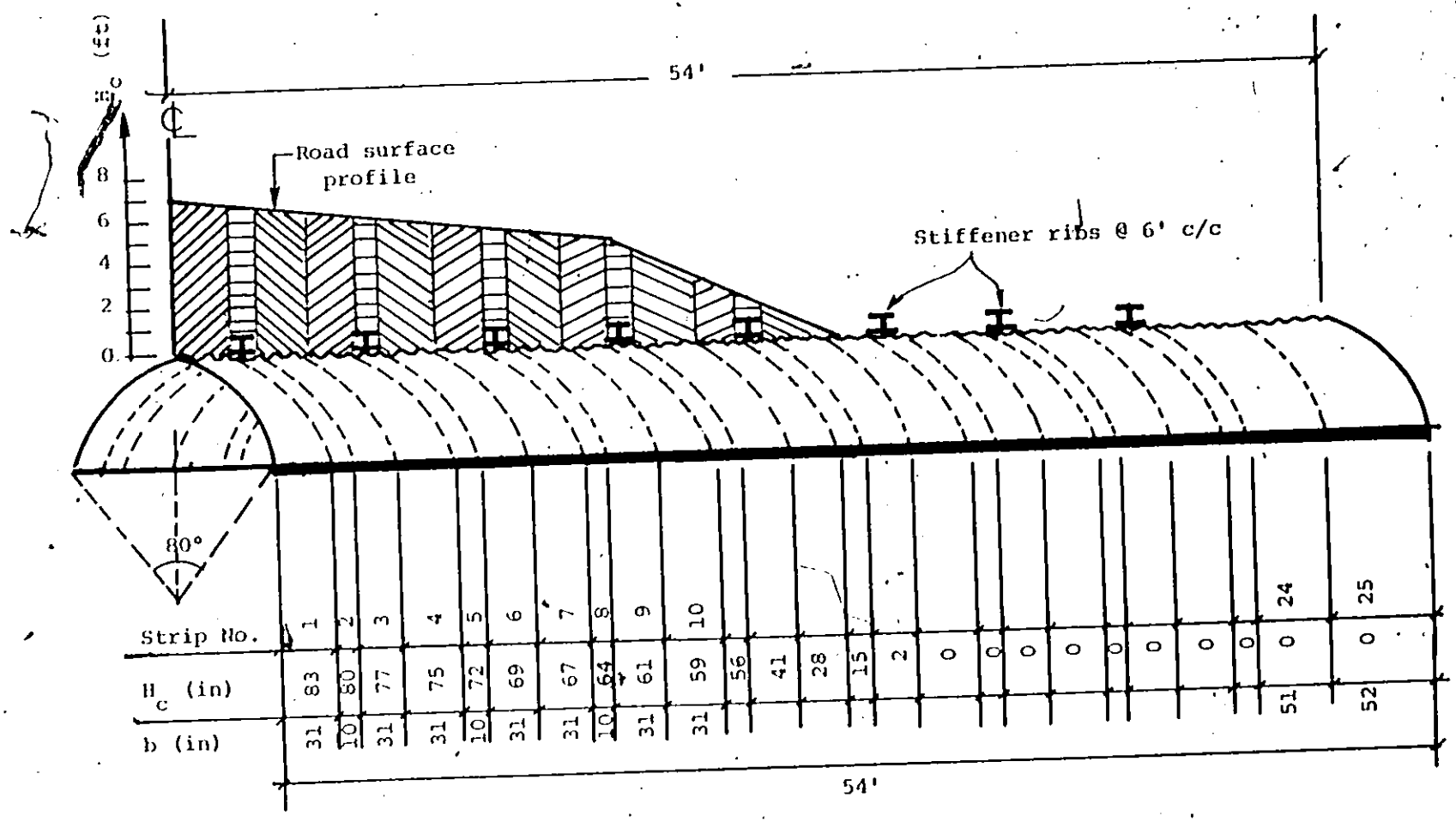

Figure 3.16: Finite Strip Idealization of Cheese Factory Bridge Structure

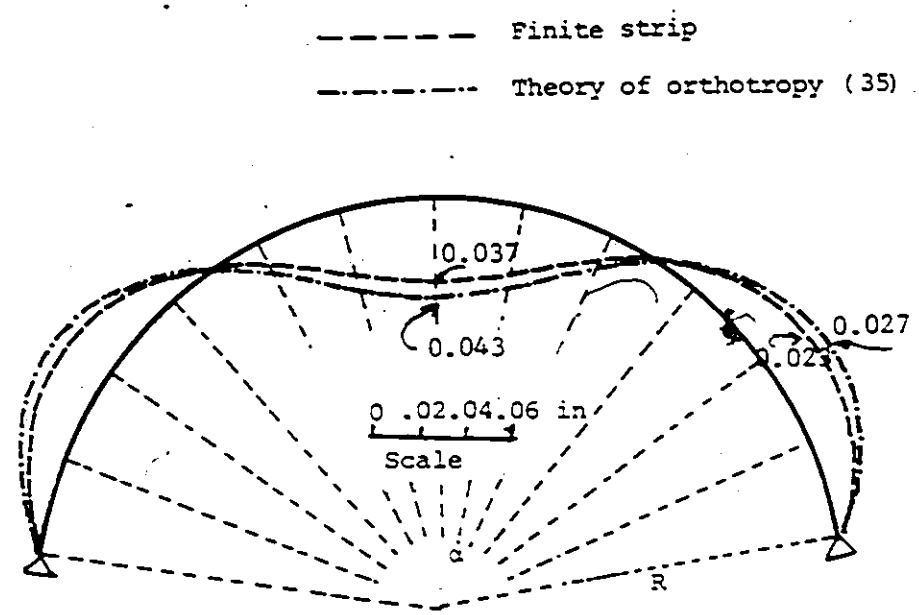

a) Radial Deflection w at Central Section

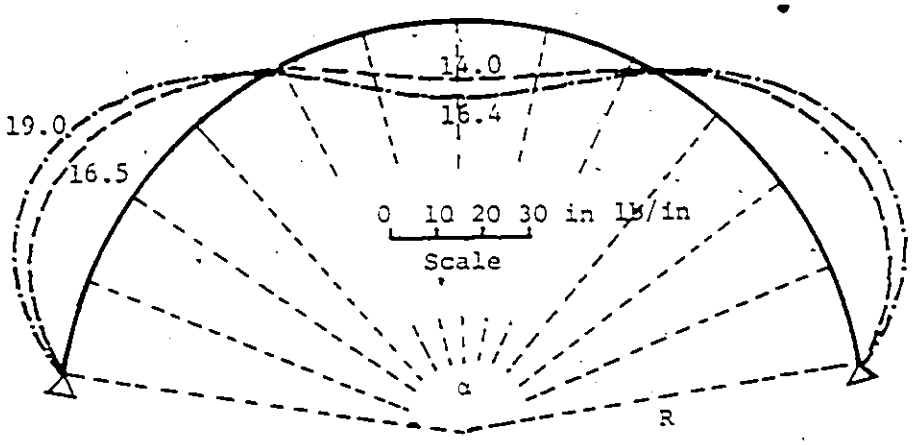

b) Bending Moment Variation at Central Section

Figure 3.17: Comparision of Finite Strip and Theory of Orthotropy Solutions

R = 210" α = 162° L = 700 in

Vertical Load = 1 lb/sqft.

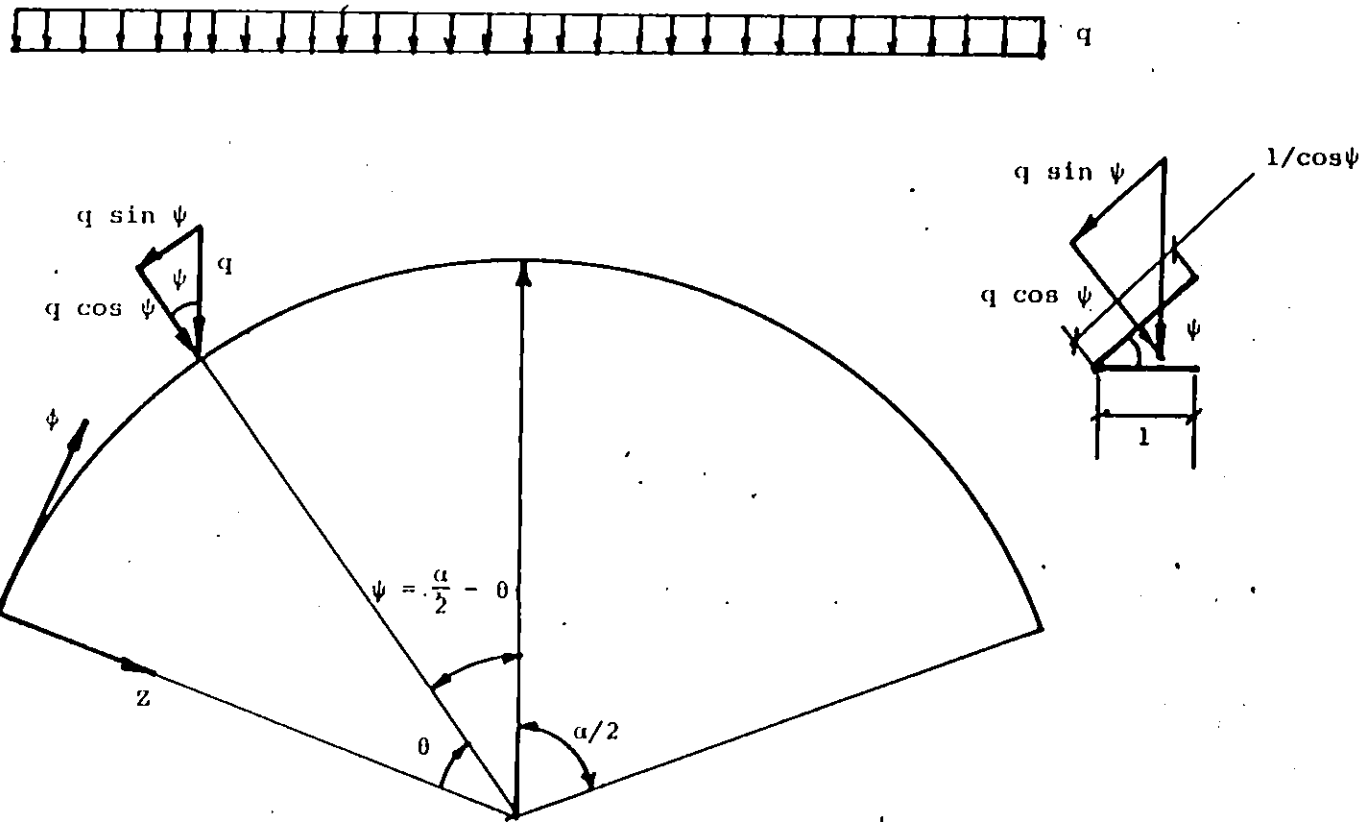

q = uniform load per unit horizontal area

$q_0 = q \sin \psi/(1/\cos\psi) = q \sin \psi \cdot \cos \psi = q \sin (\frac{\alpha}{2} - \theta)\cos(\frac{\alpha}{2} - \theta)$

$q_w = q \cos \psi/(1/\cos\psi) = q \cos^2\psi = q \cos^2 (\frac{\alpha}{2} - \theta)$

Figure 3.19: Radial and Tangential Components of Uniform Vertical Load q.

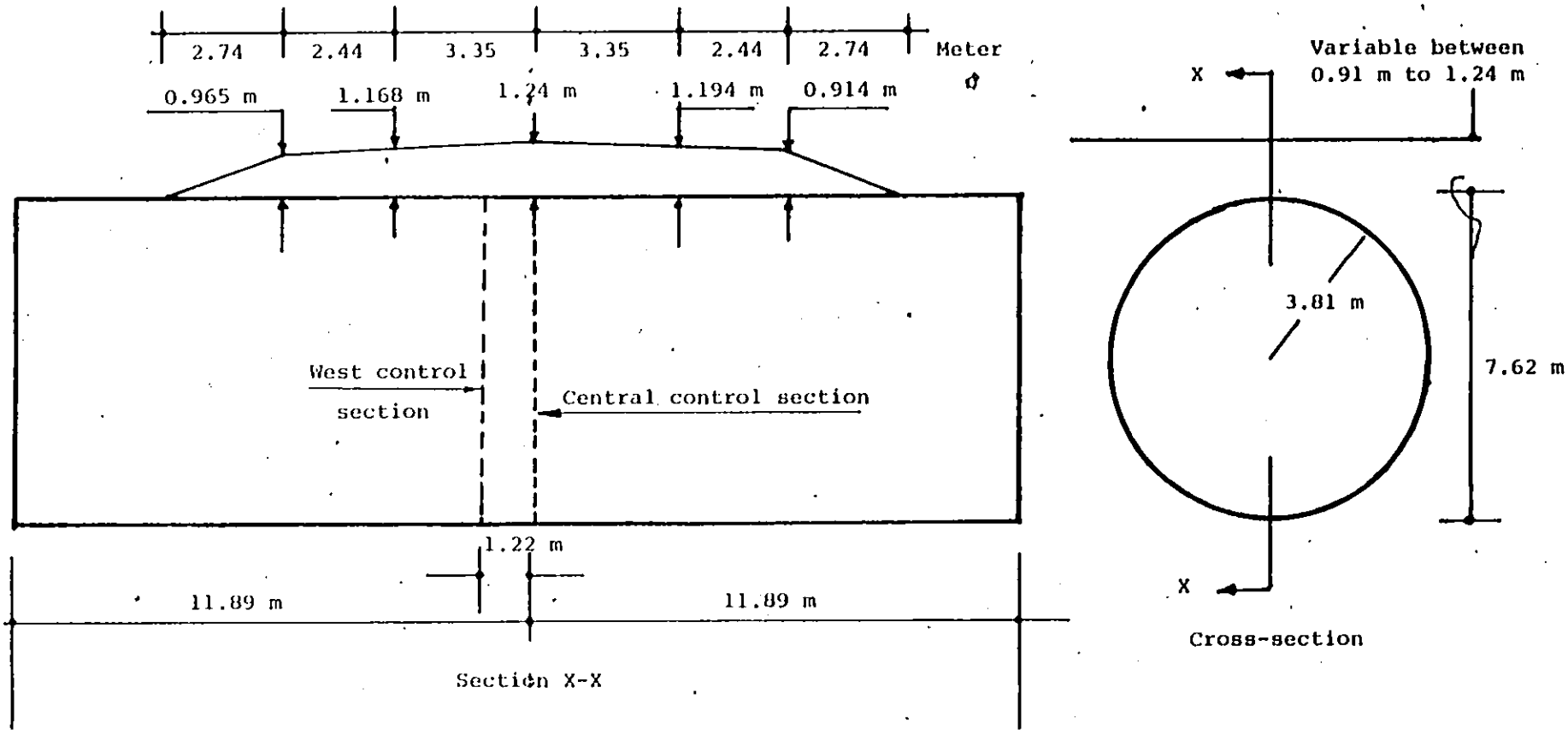

Figure 4.1: Details of White Ash Creek Soil-Steel Structure

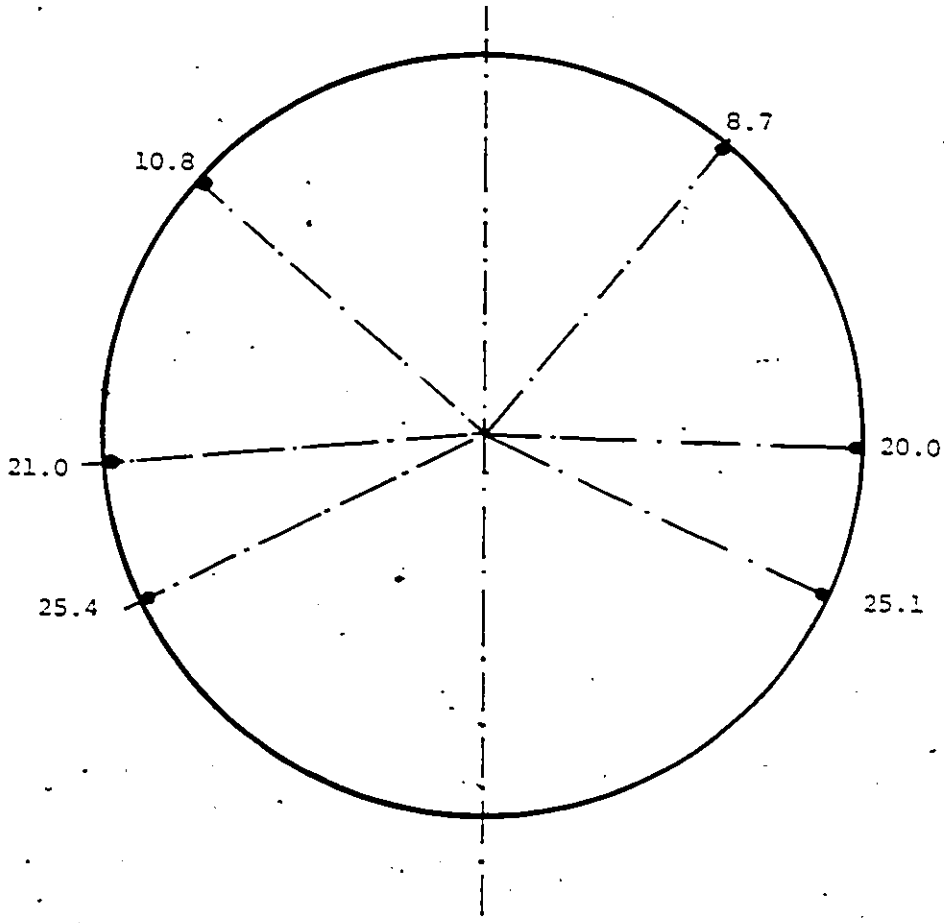

Figure 4.2: Instrumented Locations at the Central Cross Section of White Ash Creek Structure

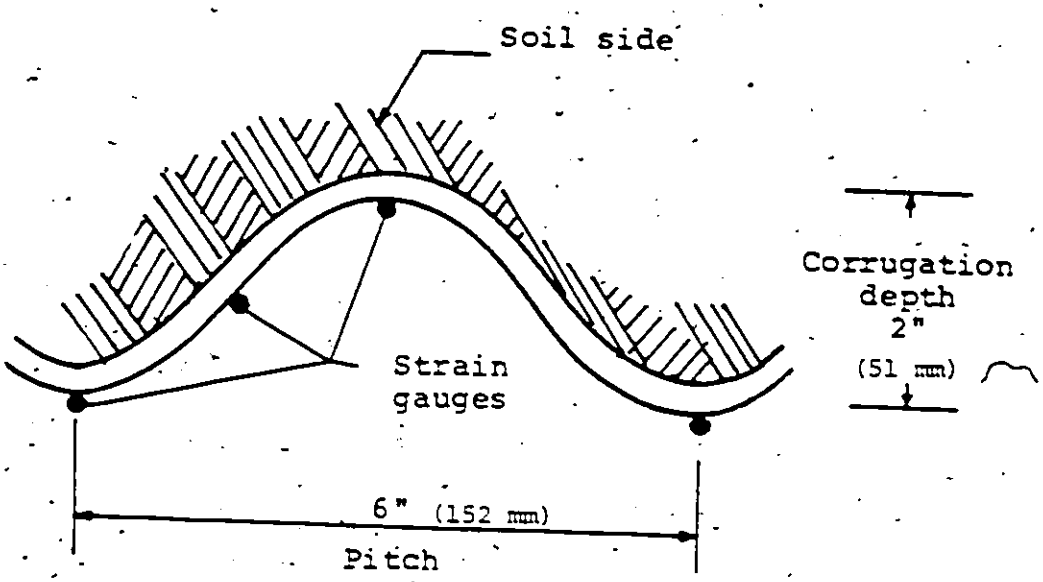

Figure 4.3: Typical Strain Gage Positions at One Location of White Ash Creek Structure

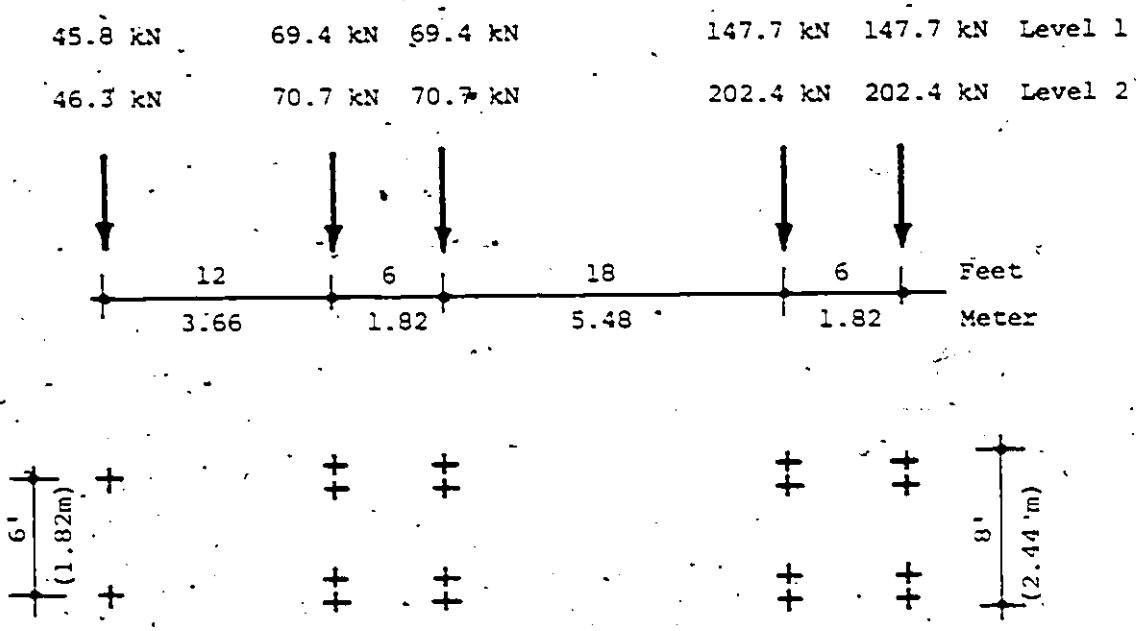

Figure 4.4: Details of One of the Testing Vehicles

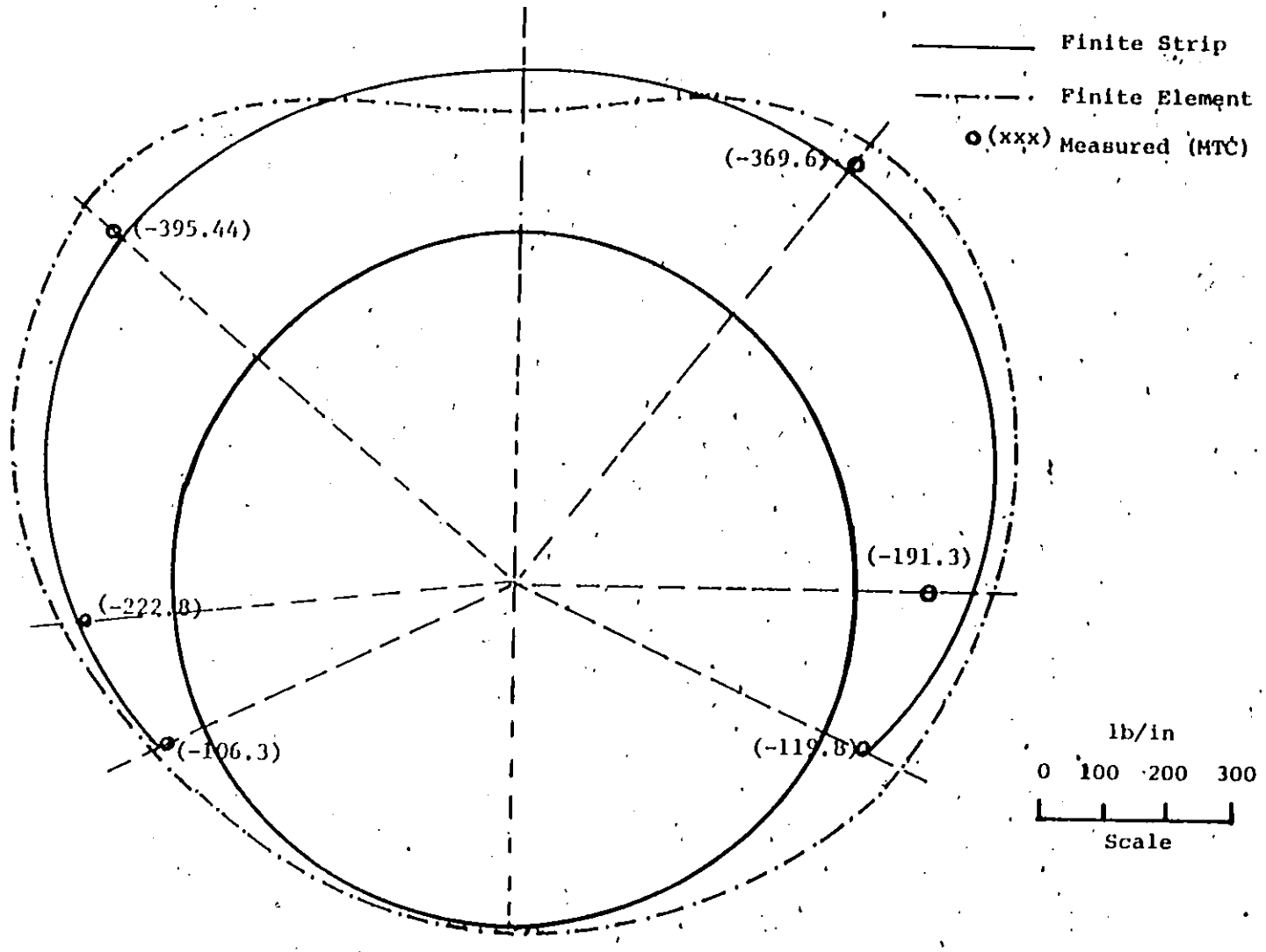

Figure 4.5: White Ash Creek Structure - Thrust Variation at the Central Section Due to One Truck Loading (Level 2)

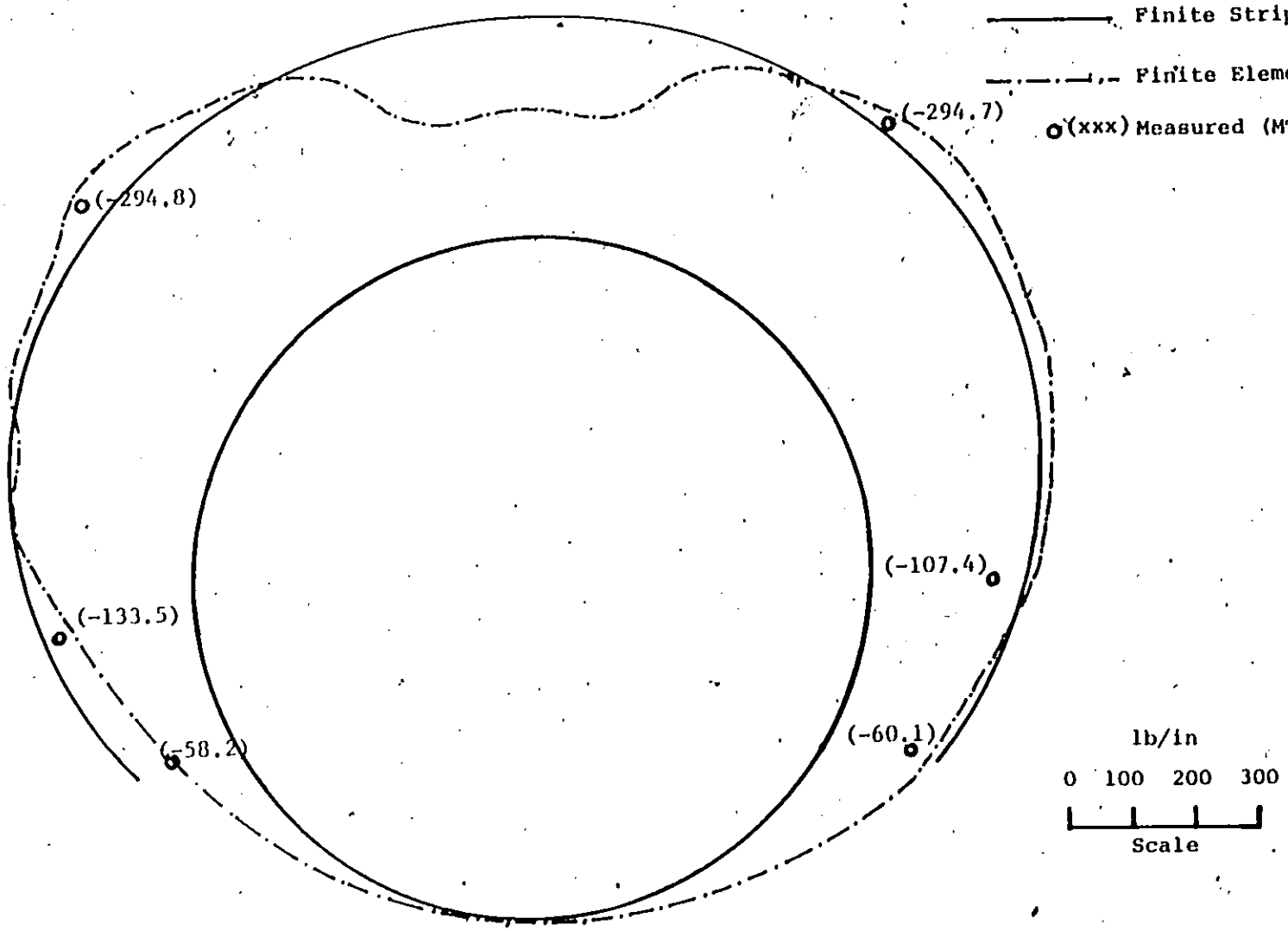

Figure 4.6: White Ash Creek Structure - Axial Thrust Variation at the Central Section Due to Central Two Truck Loading (Level 2)

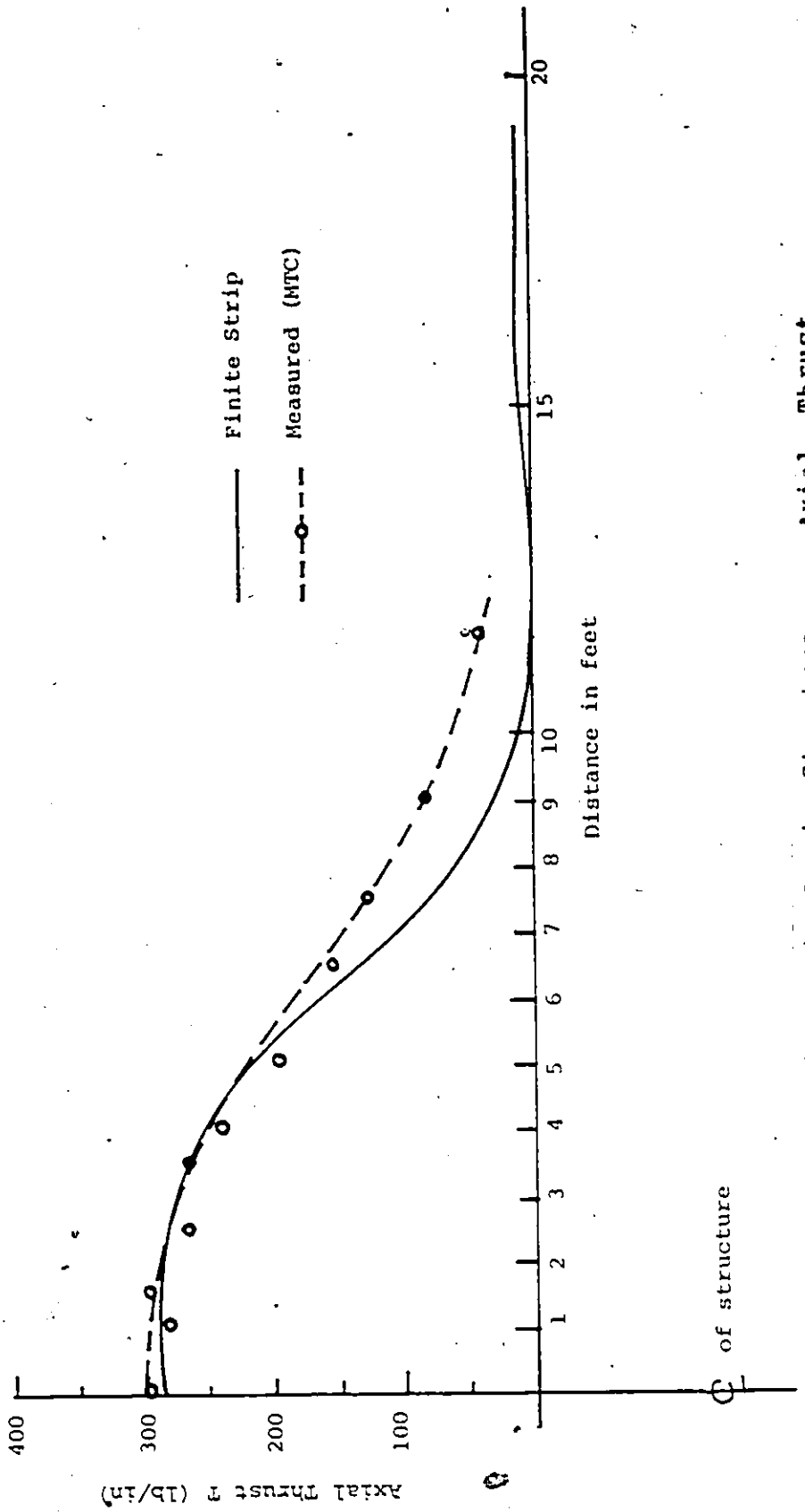

Figure 4.7: White Ash Creek Structure - Axial Thrust Variation Along the Length of Structure Due to Central One Truck Loading (Level 2)

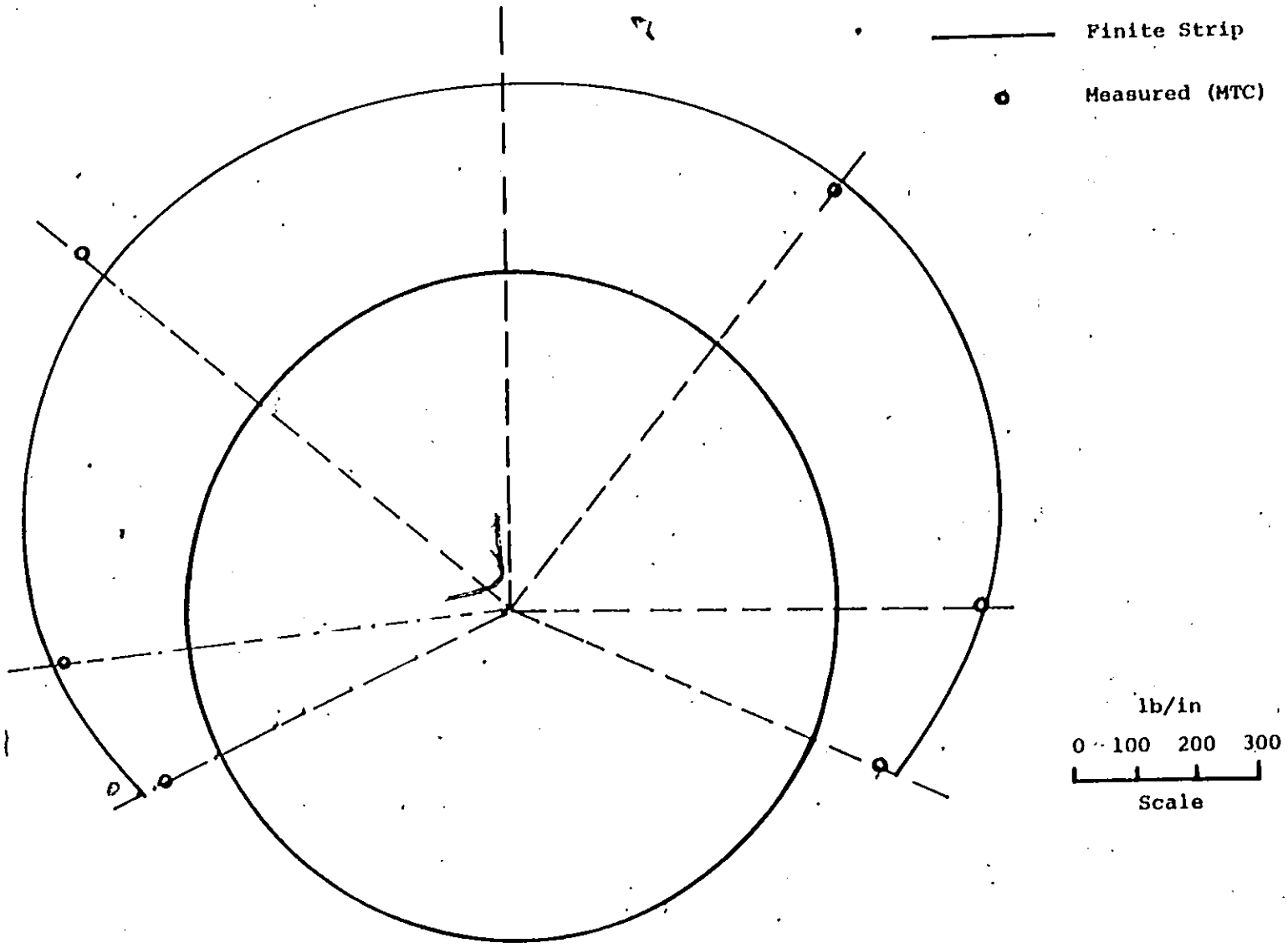

Figure 4.8: White Ash Creek Structure - Thrust Variation at West Section Due to Central Two Truck loading (Level 2)

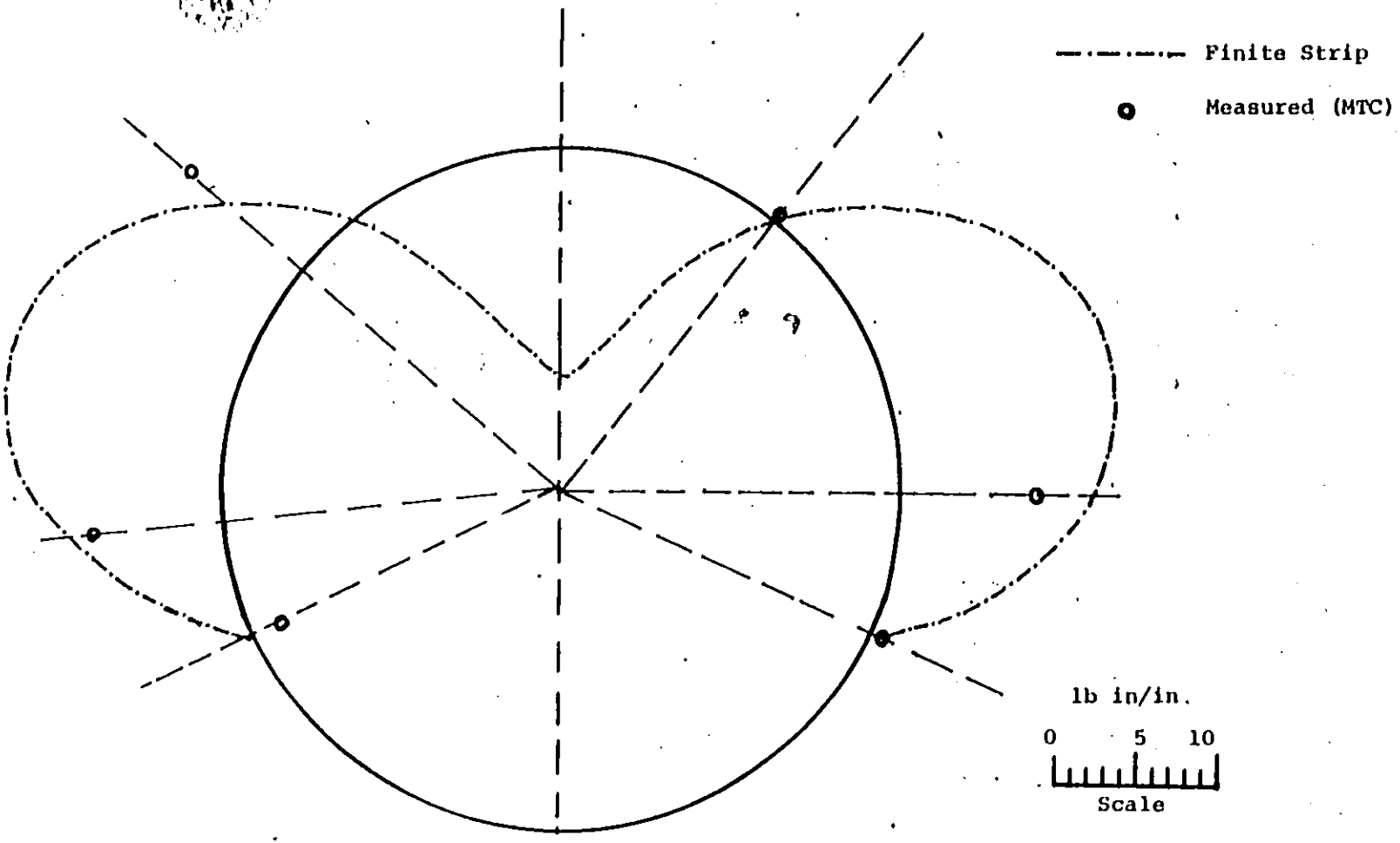

Figure 4.9: White Ash Creek Structure - Bending Moment Variation at the Central Section Due to Central One Truck Loading (Level 2)

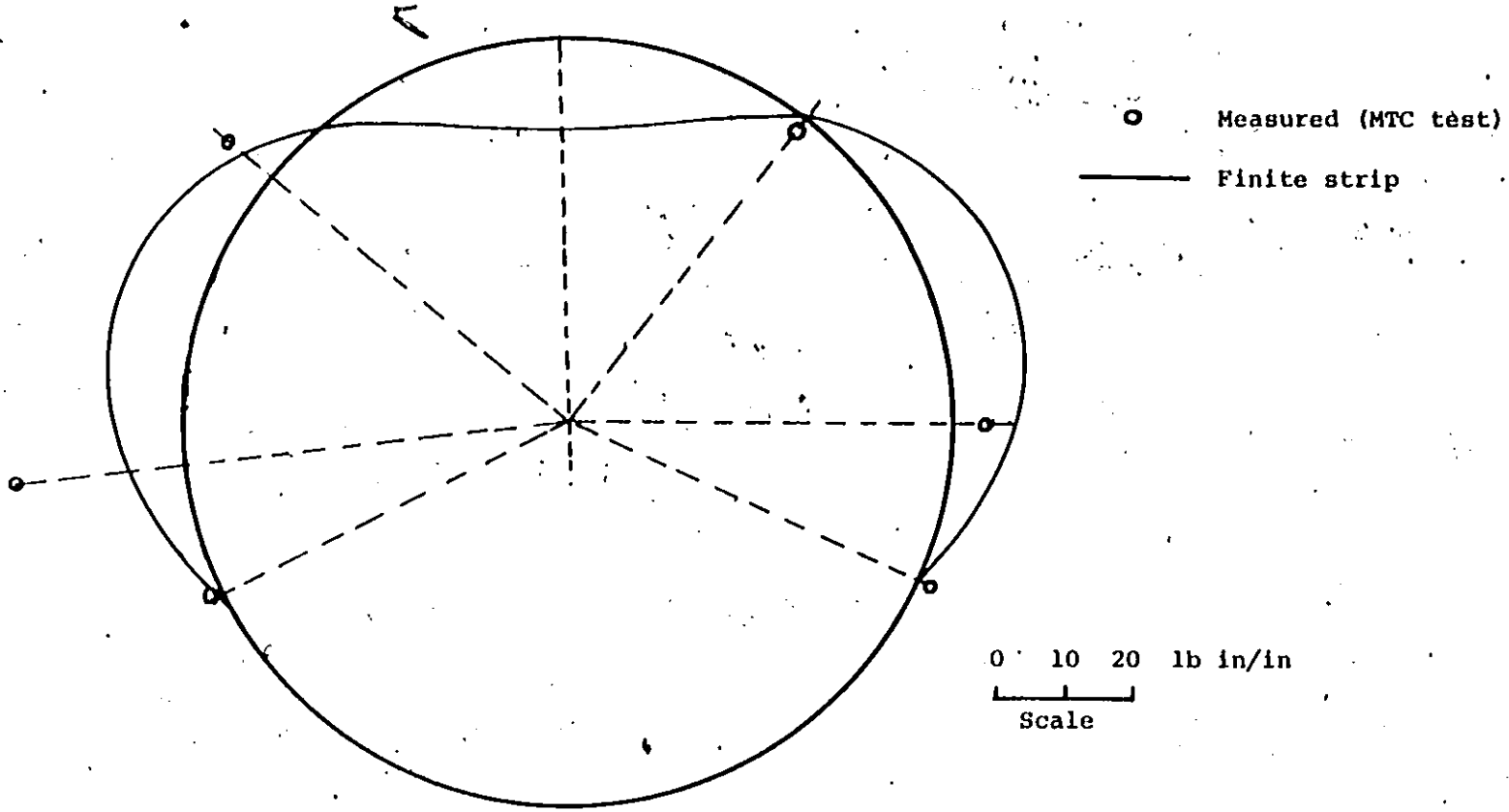

Figure 4.10: White Ash Creek Structure - Bending Moment Variation at West Section Due to Central One Truck Loading (Level 2)

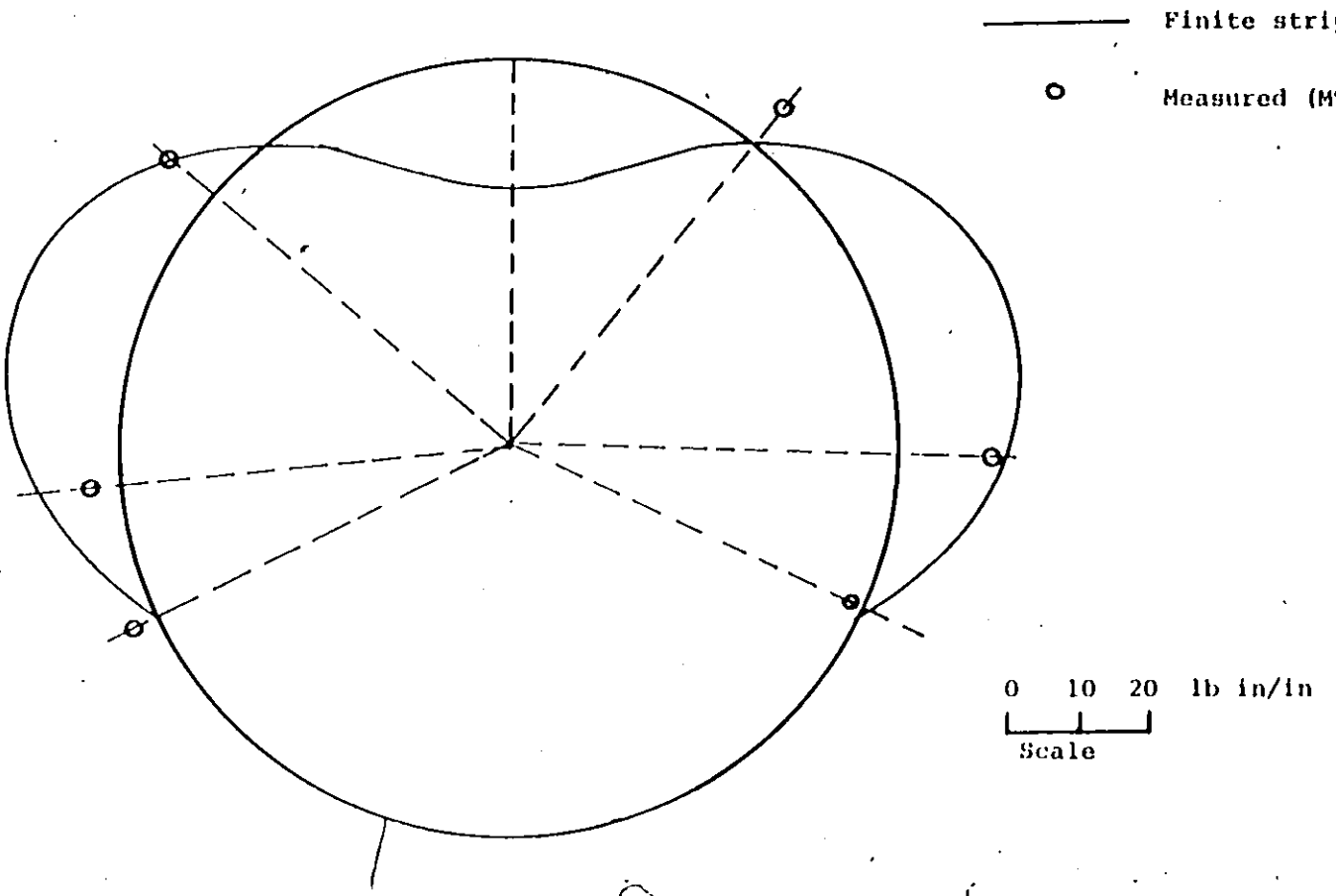

Figure 4.11: White Ash Creek Structure - Bending Moment Variation at Central Section Due to Central Two Truck Loading (Level 2)

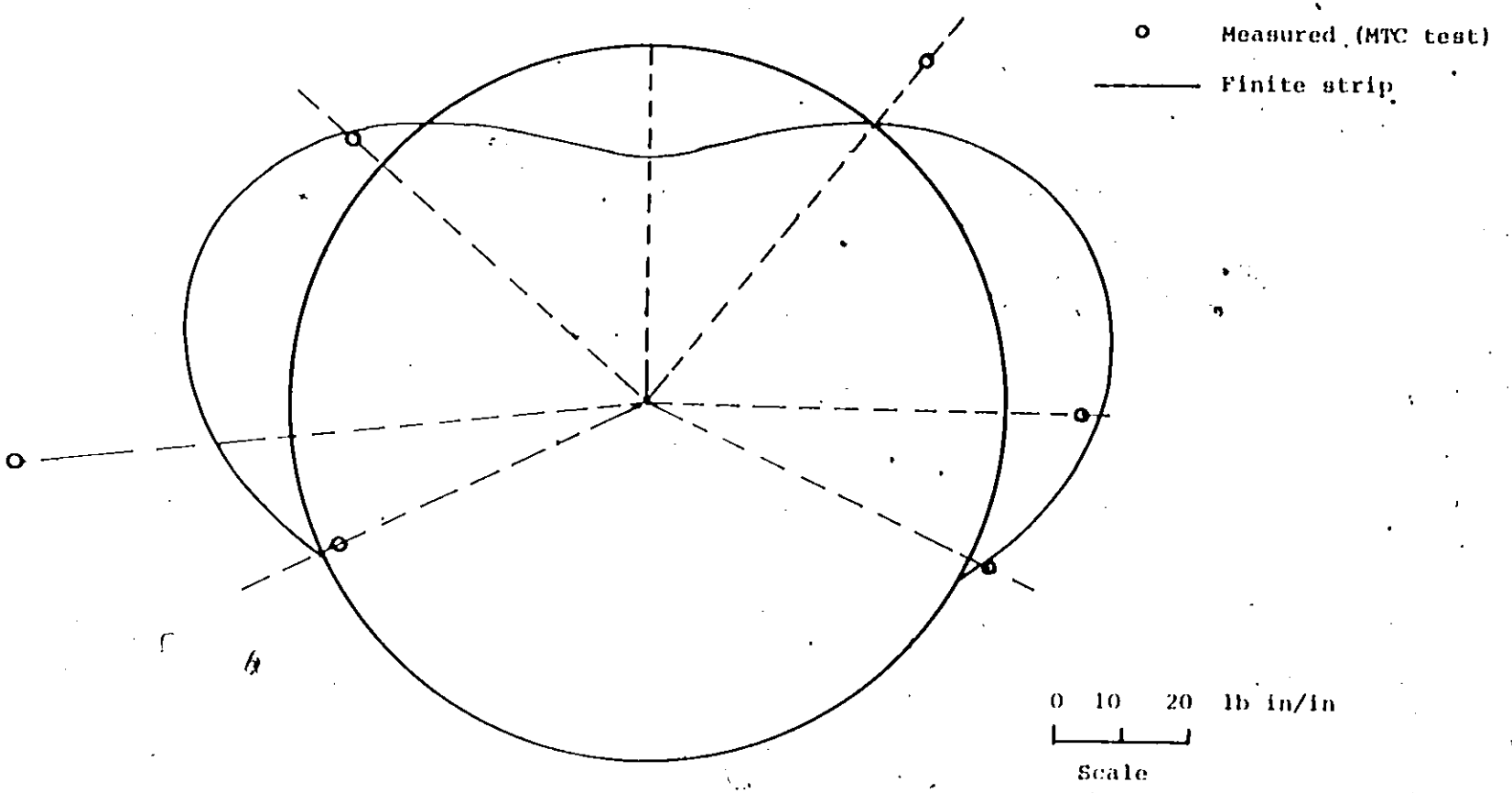

Figure 4.12: White Ash Creek Structure - Bending Moment Variation at West Section Due to Central Two Truck Loading (Level 2)

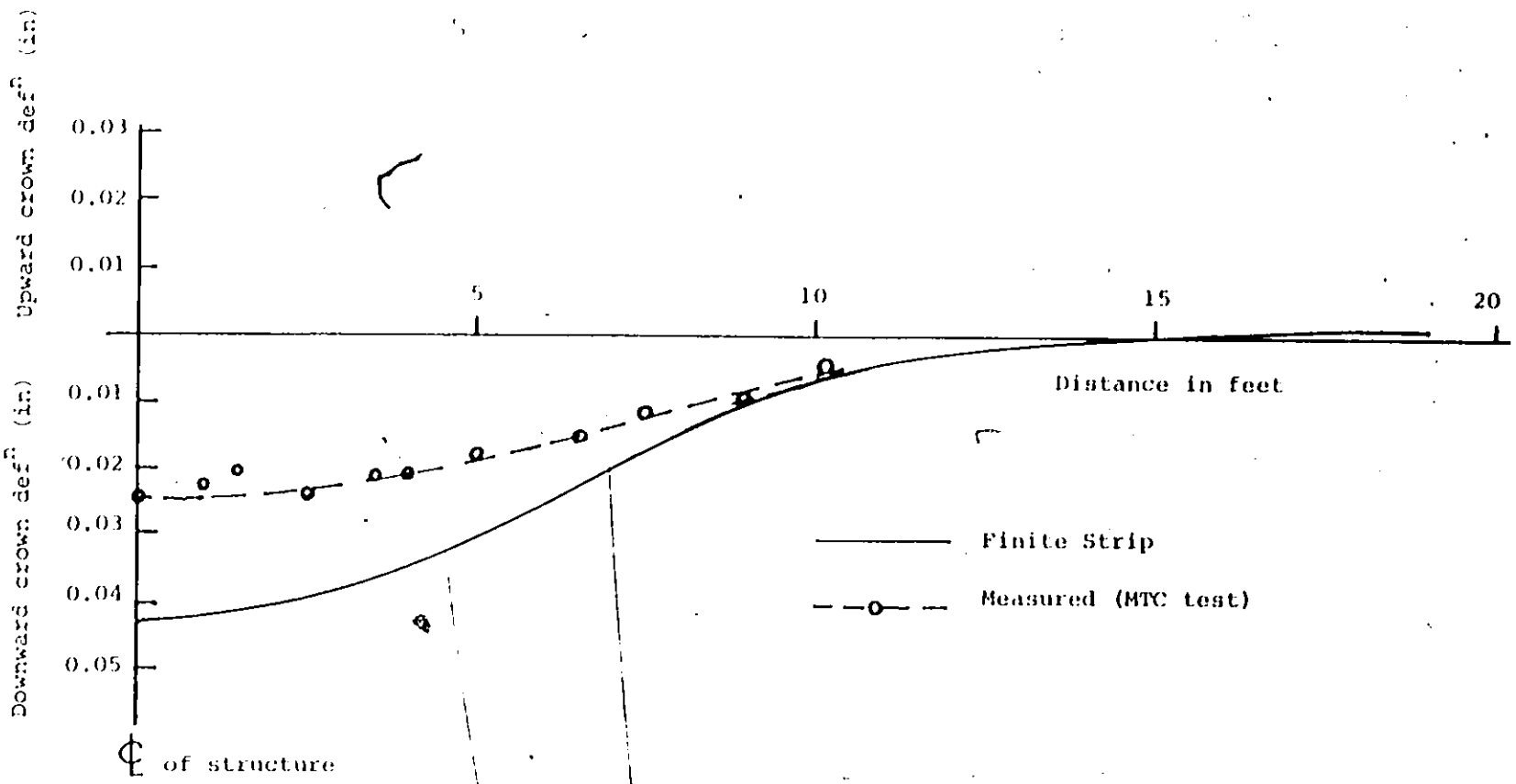

Figure 4.13: White Ash Creek Structure - Deflection Variation Along the Crown Due to Central On Truck Loading (Level 2)

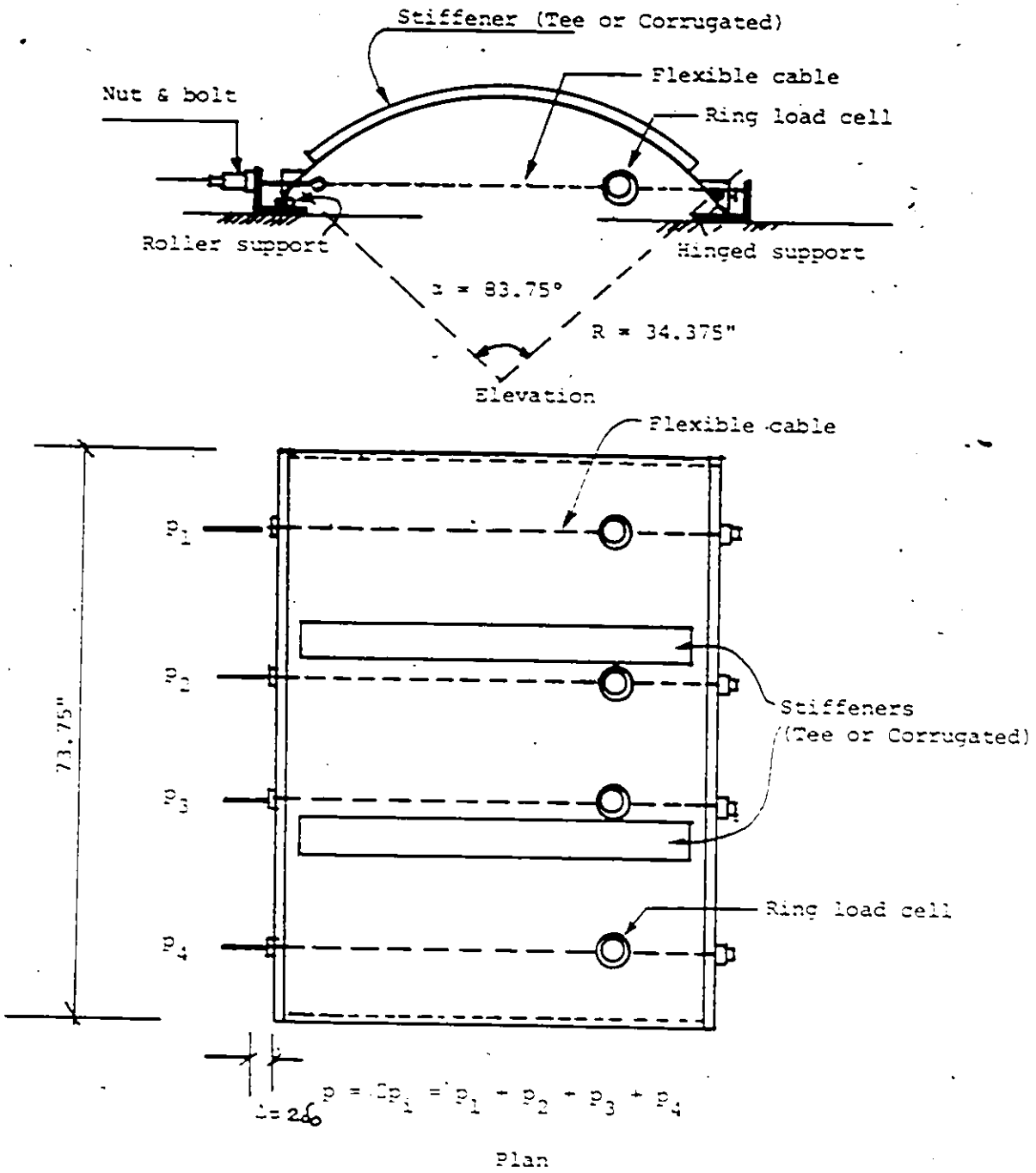

Figure 4.14: Details of Model and Loading for Structure During Side Filling

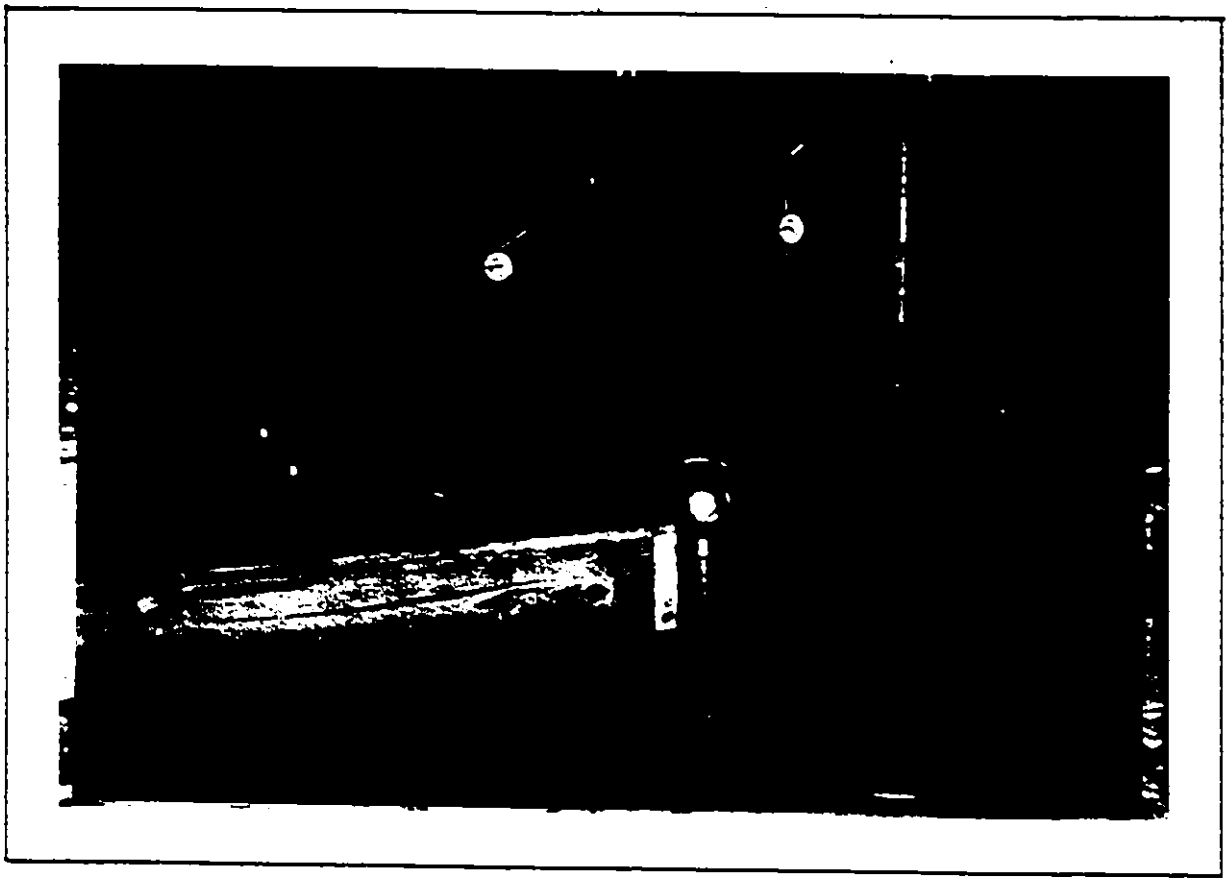

Figure 4.15: Method of Displacement Application at One end of Model

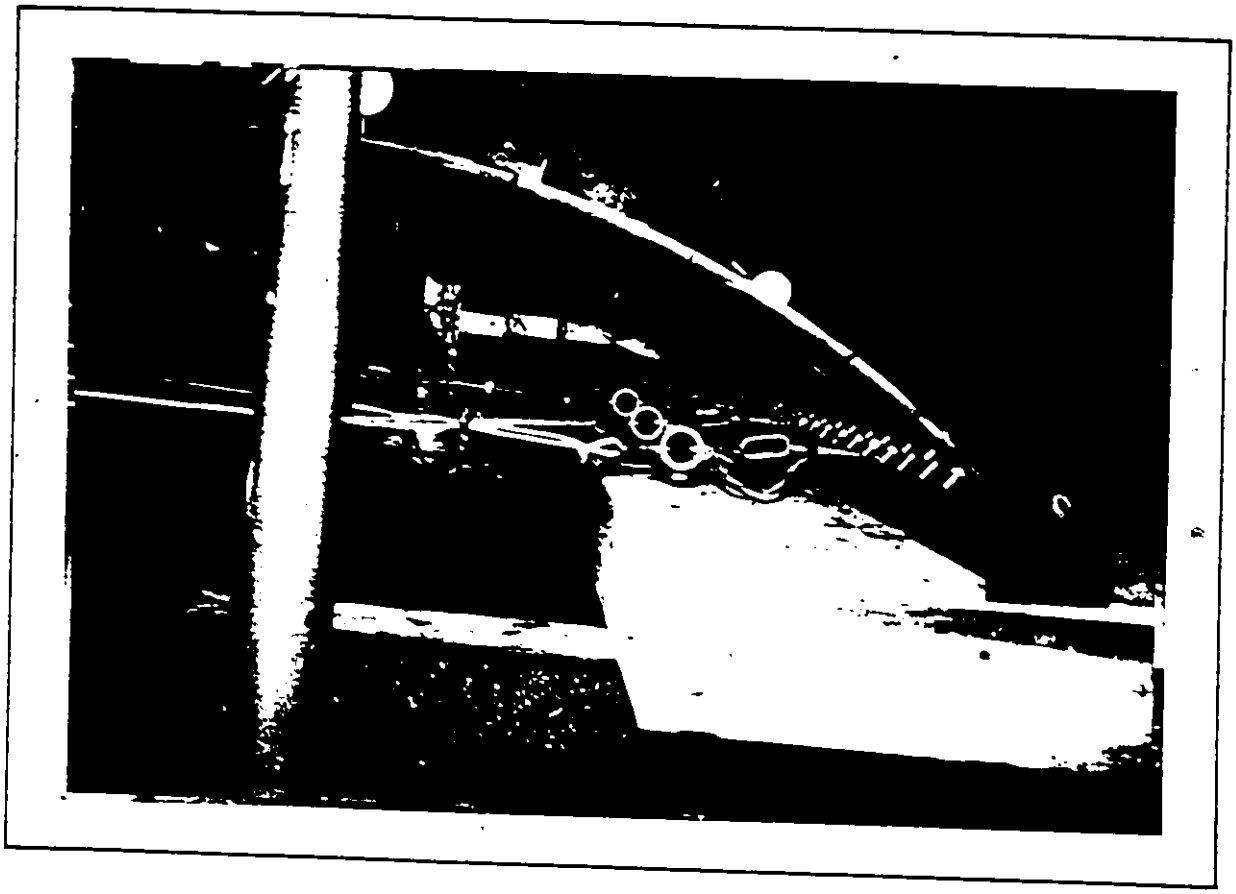

Figure 4.16: Ring Load Cells to Measure Tension in Cables

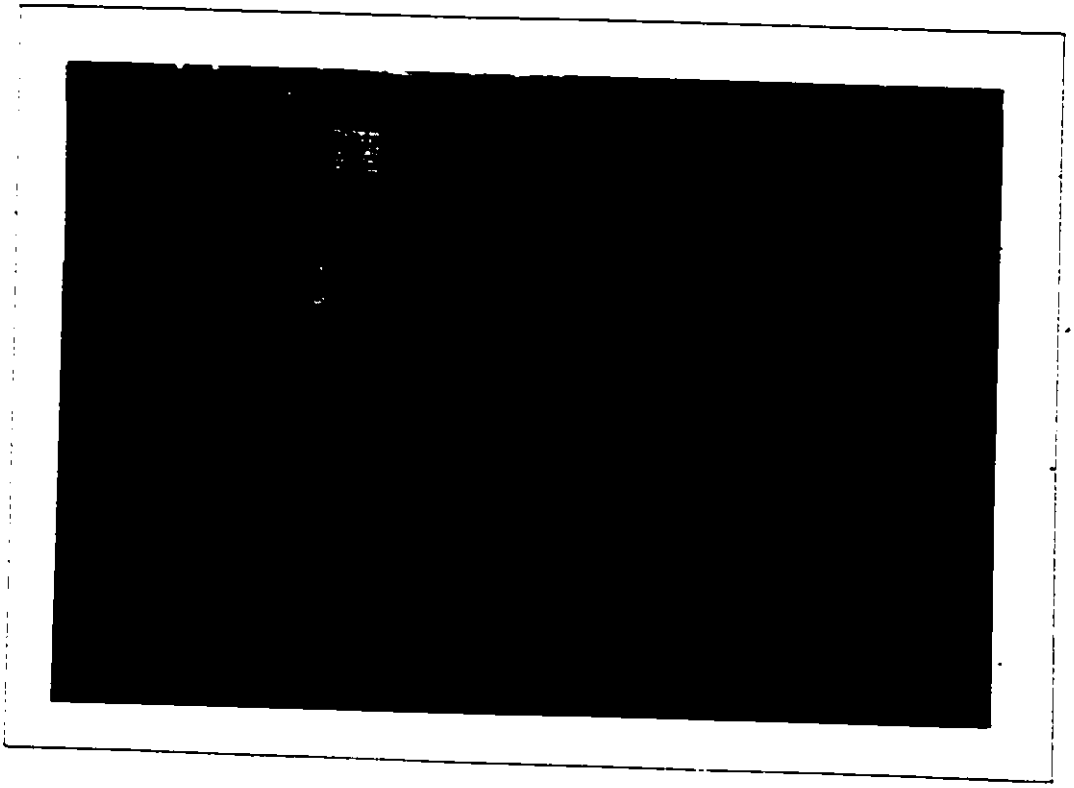

Figure 4.17: Model Before Filling of Soil

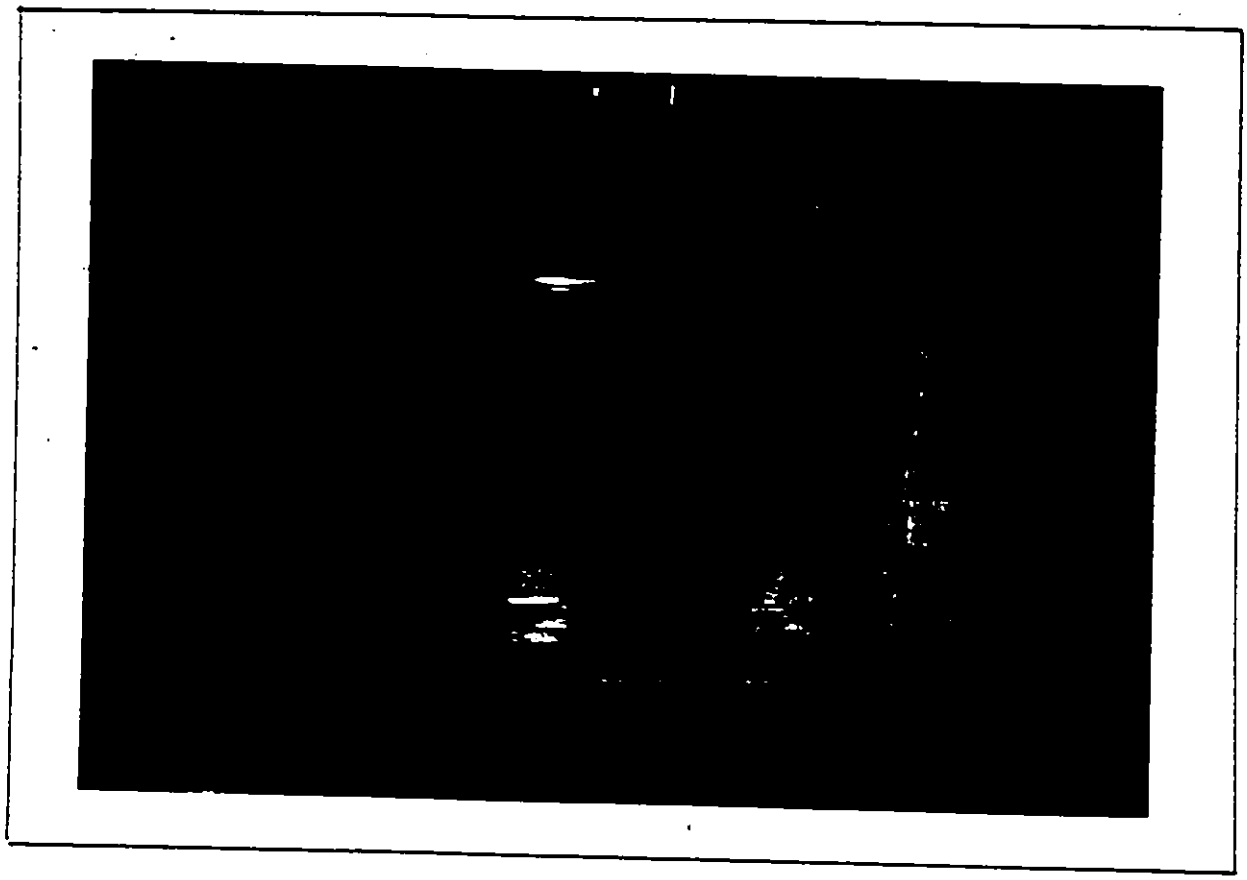

Figure 4.13: End Foam Wrapping of Model

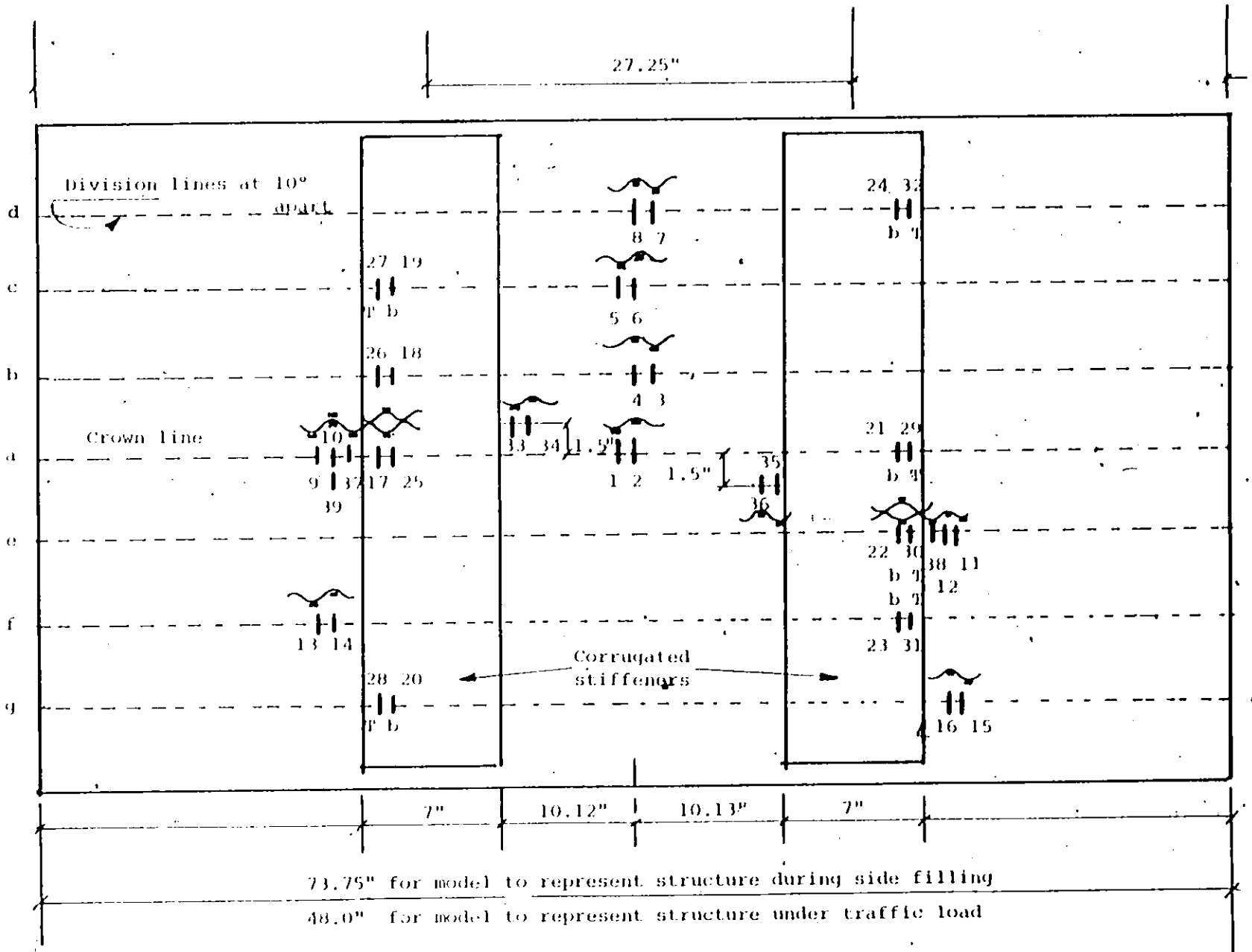

Figure 4.12: Test Model with Strain Gage Layout (Corrugated Stiffeners)

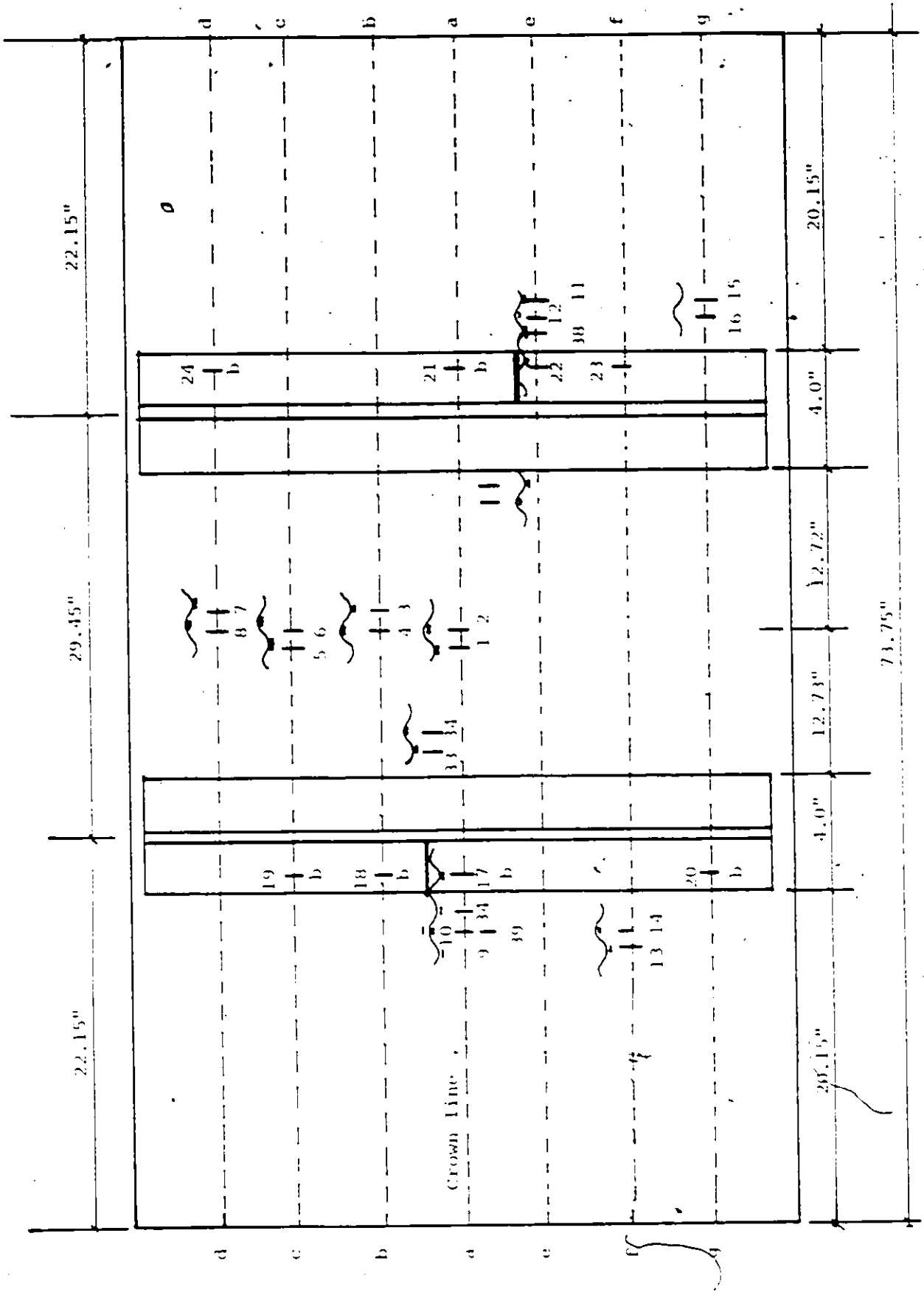

Figure 4.20: Test Model with Strain Gage Layout (Tee Stiffeners)

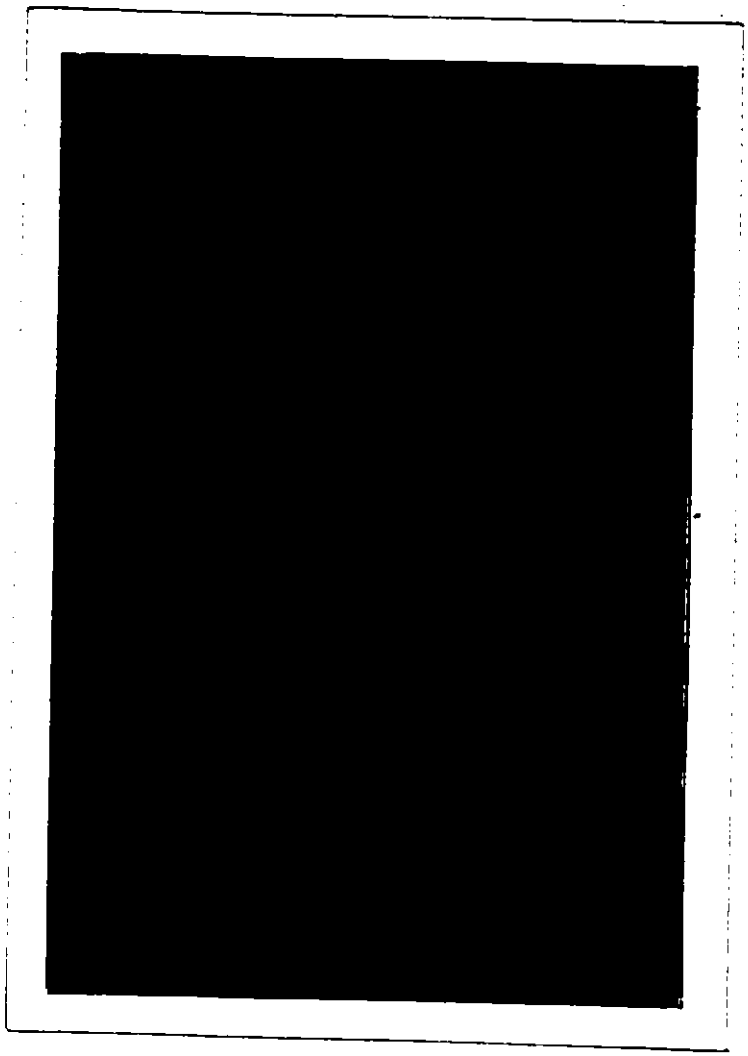

Figure 4.21: Automatic Scanning Digital Strain Indicator Module

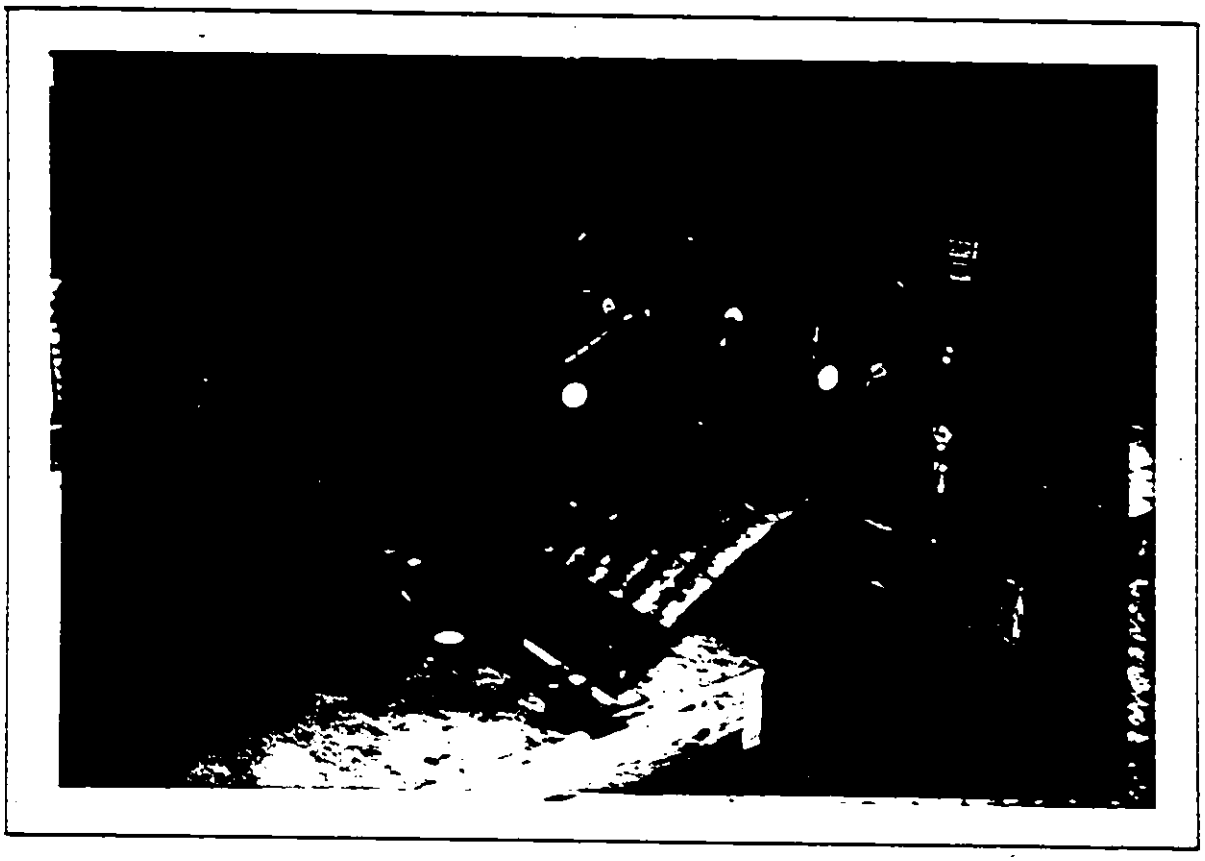

Figure 4.22: Experimental Set UP to Simulate Conduit During Side Filling

Figure 4.23: Deflection Gages to Record the Radial Deflection in Model

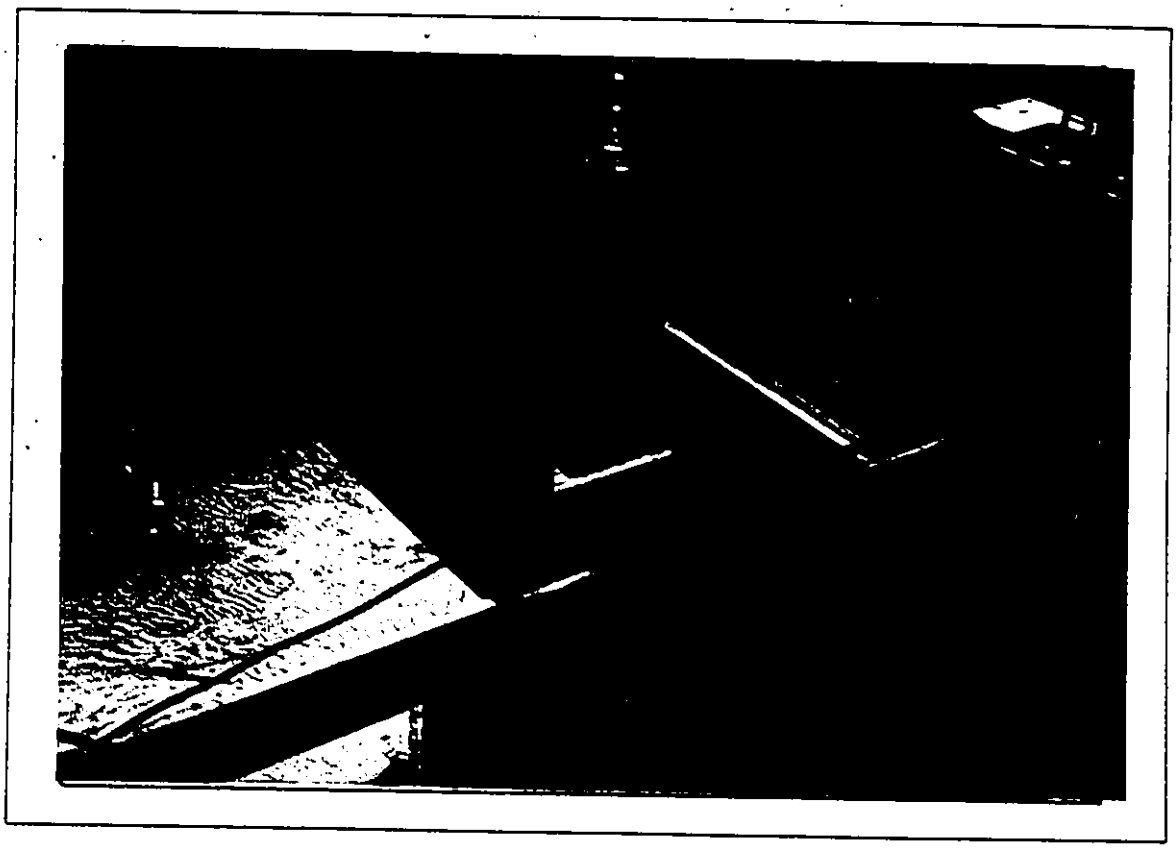

Figure 4.24: Flat Universal Load Cell and Patch Loading System

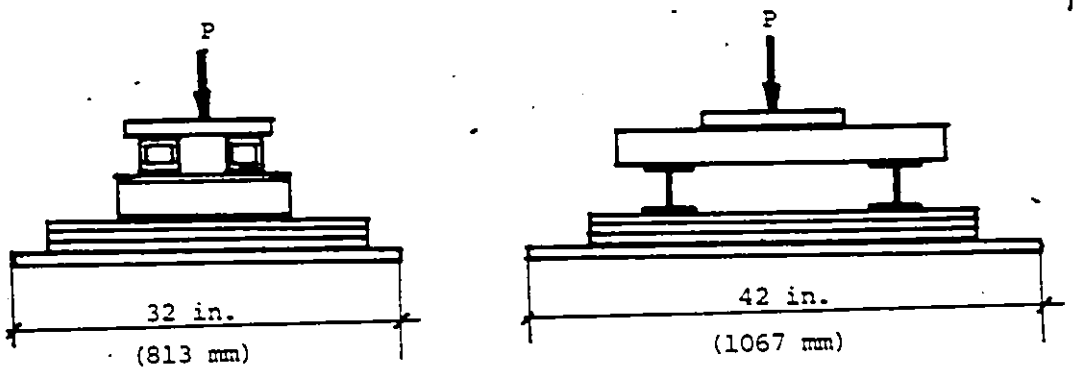

a) For Uniform Load

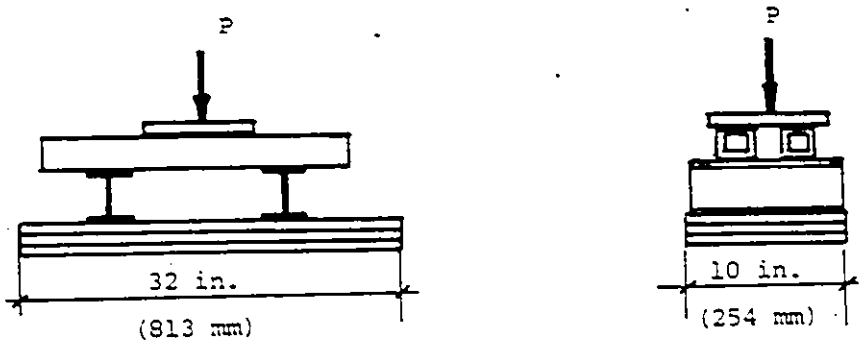

b) For Strip Load

c) For Patch Load

Figure 4.25: Loading System And Loading Plates

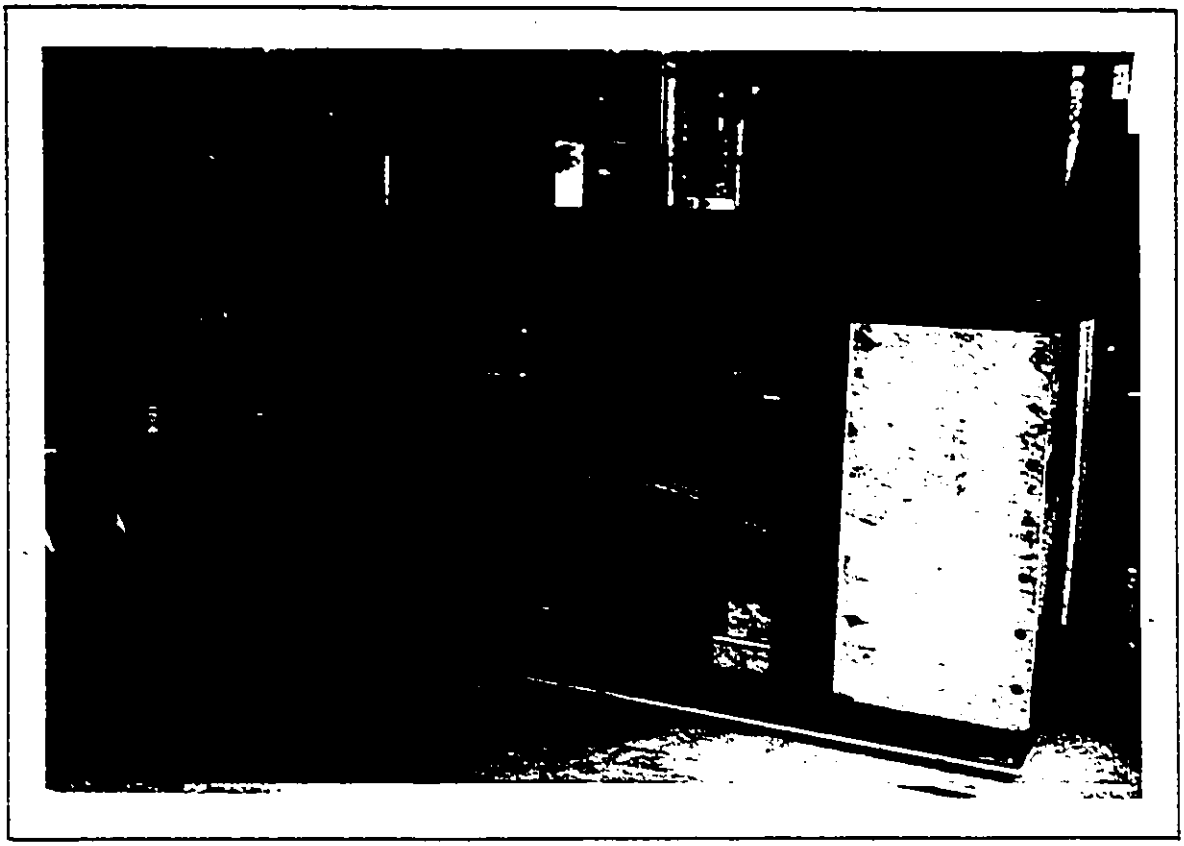

Figure 4.26: Soil-Steel Structure Model Under Localized Patch Loading

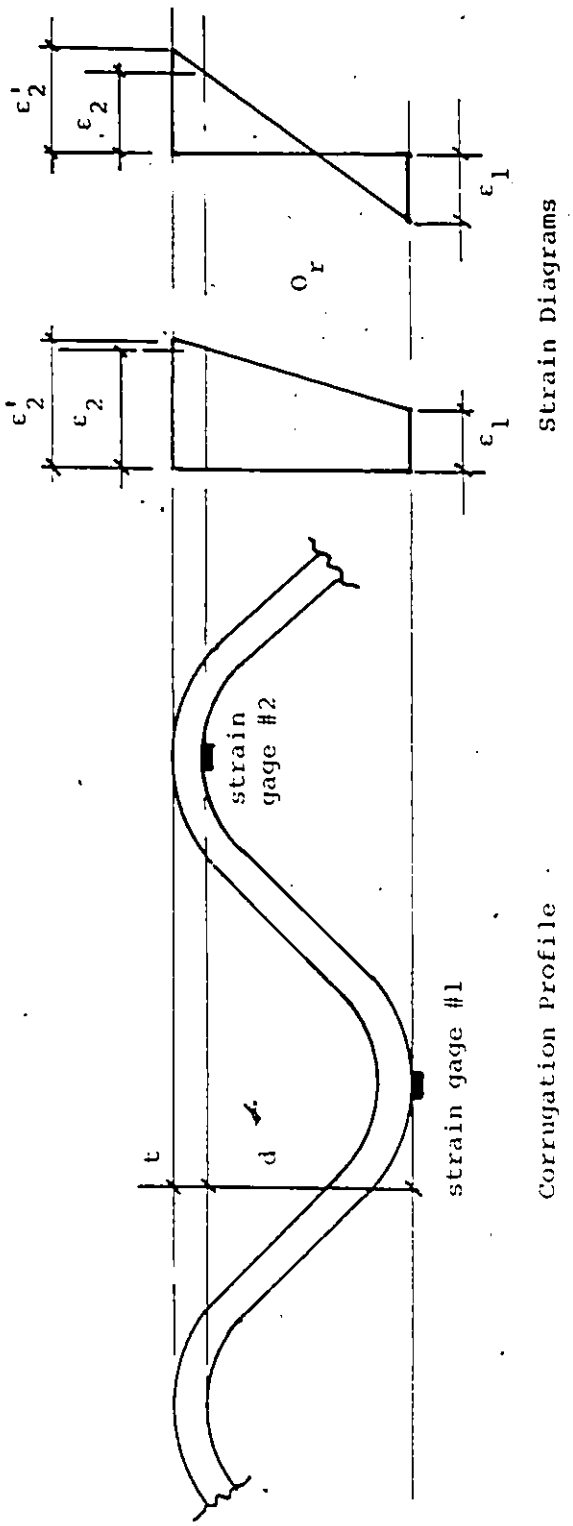

$$\varepsilon_2' = \varepsilon_2 + \frac{t}{d}(\varepsilon_2 - \varepsilon_1)$$

Figure 4.27: Strain Correction at Top Fibre

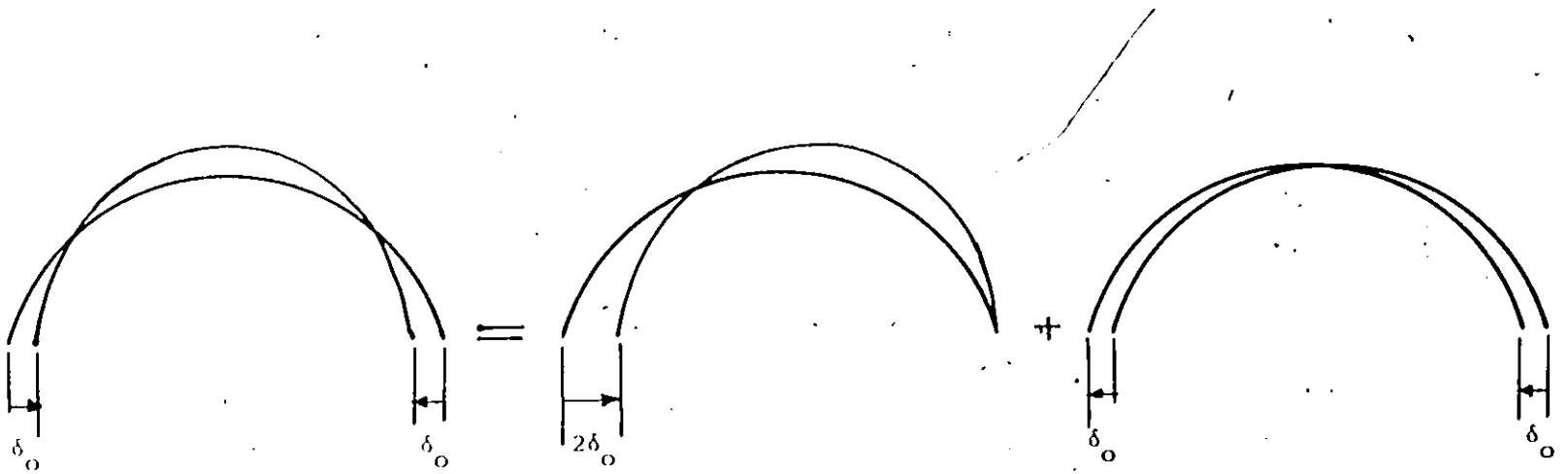

Required loading	=	Actual loading	+	Rigid body motion
Case I	=	Case II	+	Case III

Figure 4.28: Correction for Radial Deflections due to Horizontal Loading

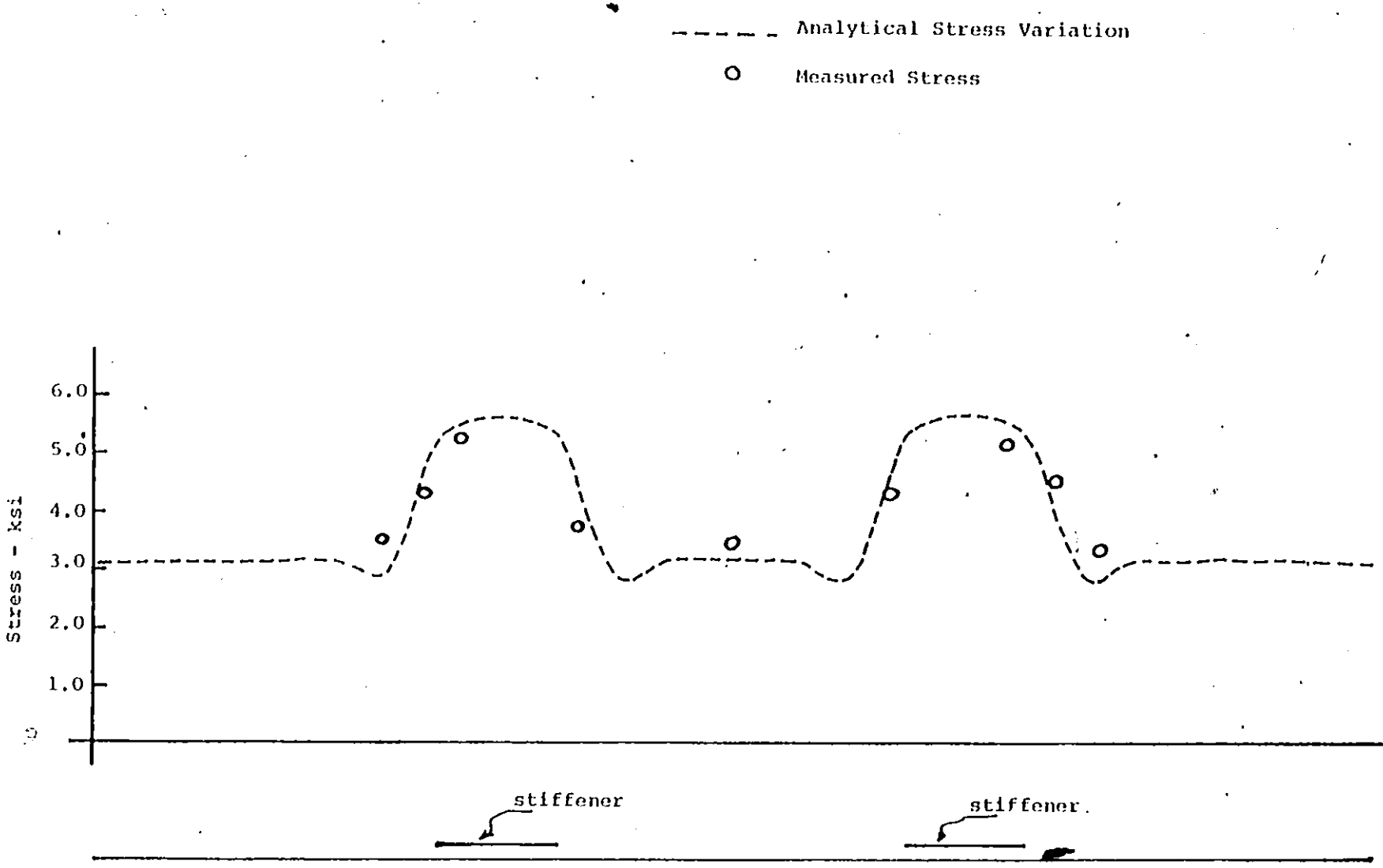

Figure 4.29: Measured and Analytical Stress Comparison in a Model with Corrugated Stiffeners Subjected to Horizontal Displacement d=0.05 in.

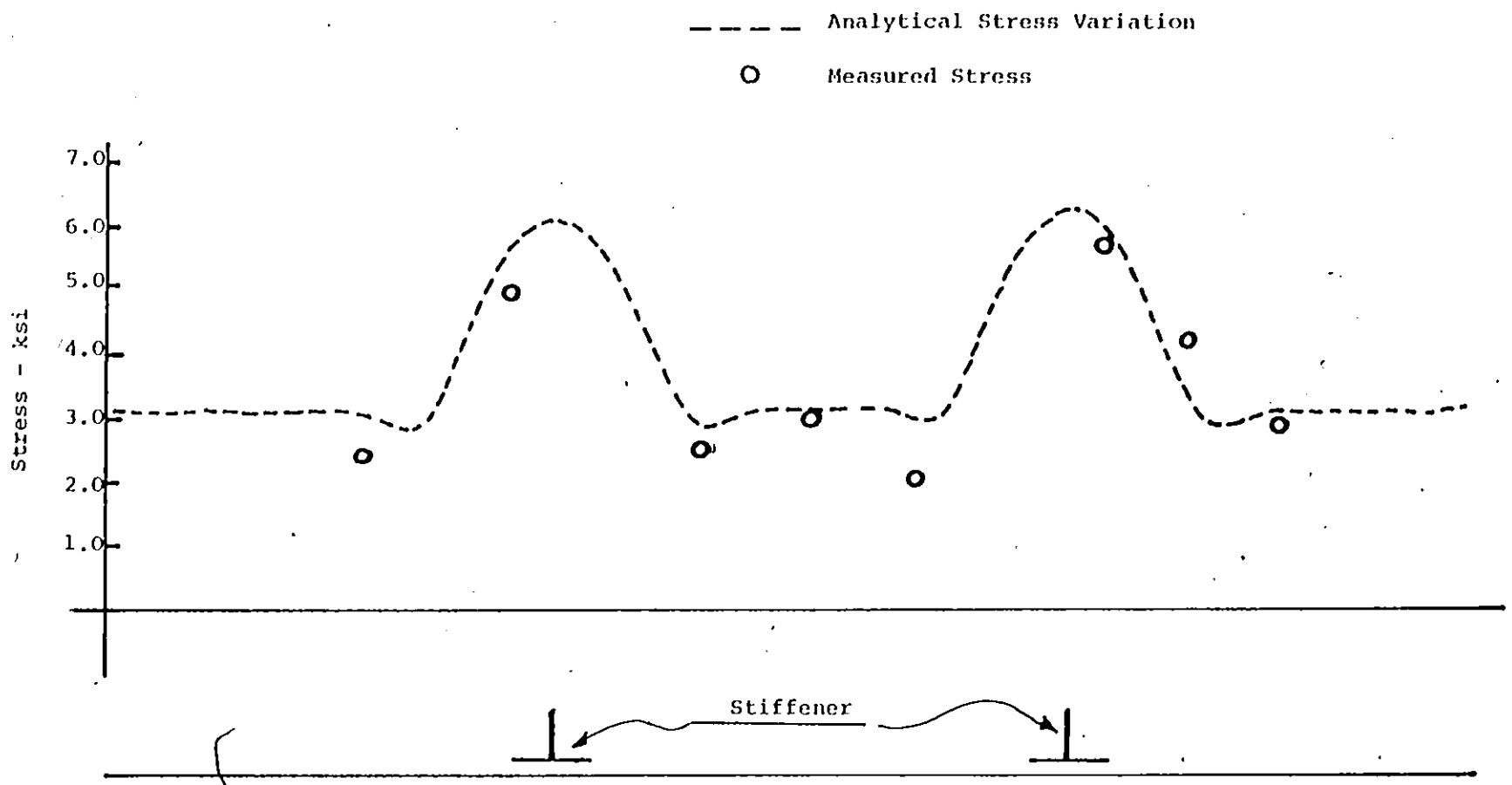

Figure 4.30: Measured and Analytical Stress Comparison in a Model with Tee-Section Stiffeners Subjected to Horizontal Displacement d=0.05 in.

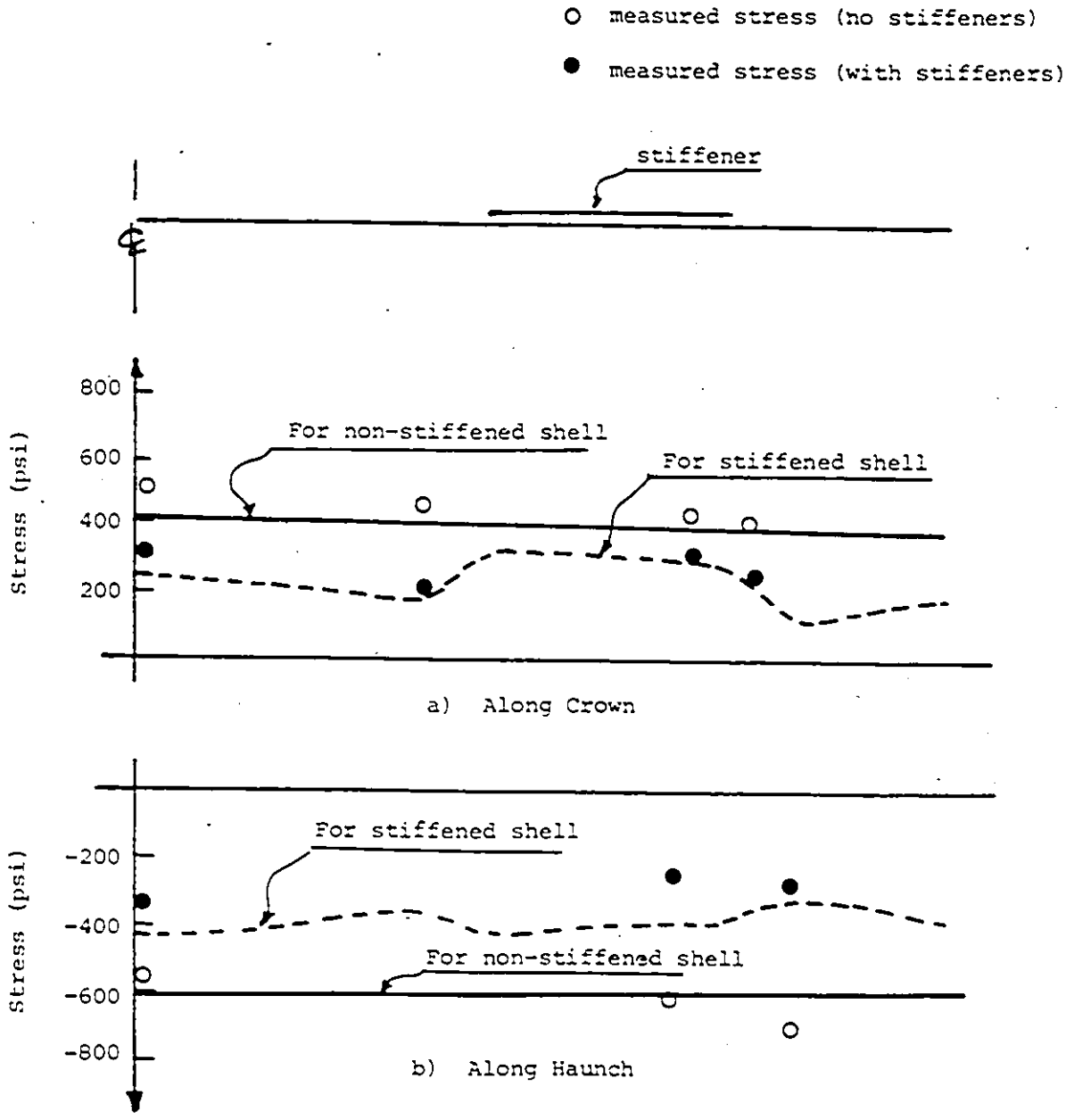

Figure 4.31: Measured and Analytical Stress Comparison in a Model with Corrugated Stiffeners Subjected to Uniform Load (P=500 lbs.)

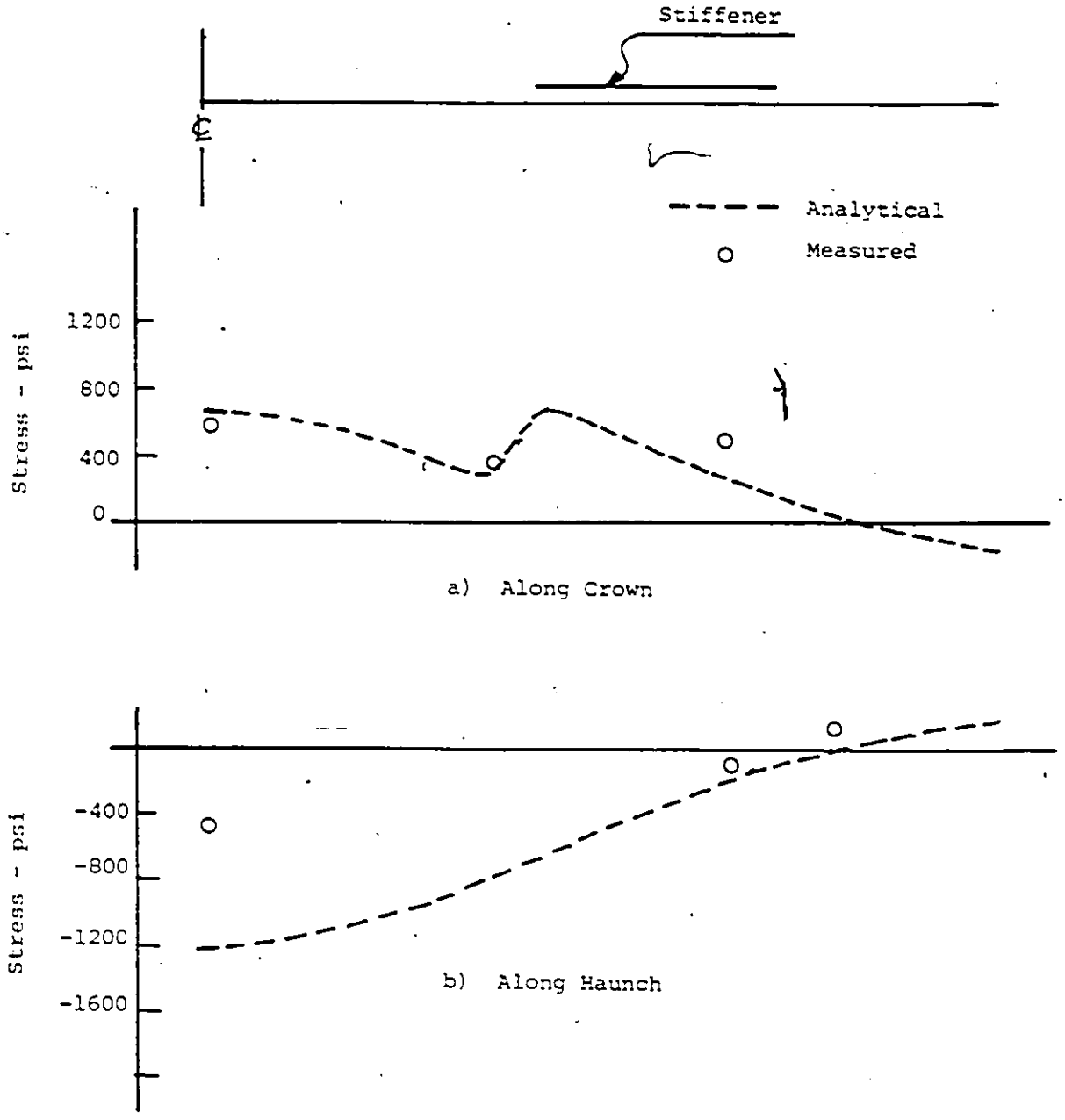

Figure 4.32: Measured and Analytical Stress Comparison in a Model with Corrugated Stiffeners Subjected to Strip load (P=500 lbs.)

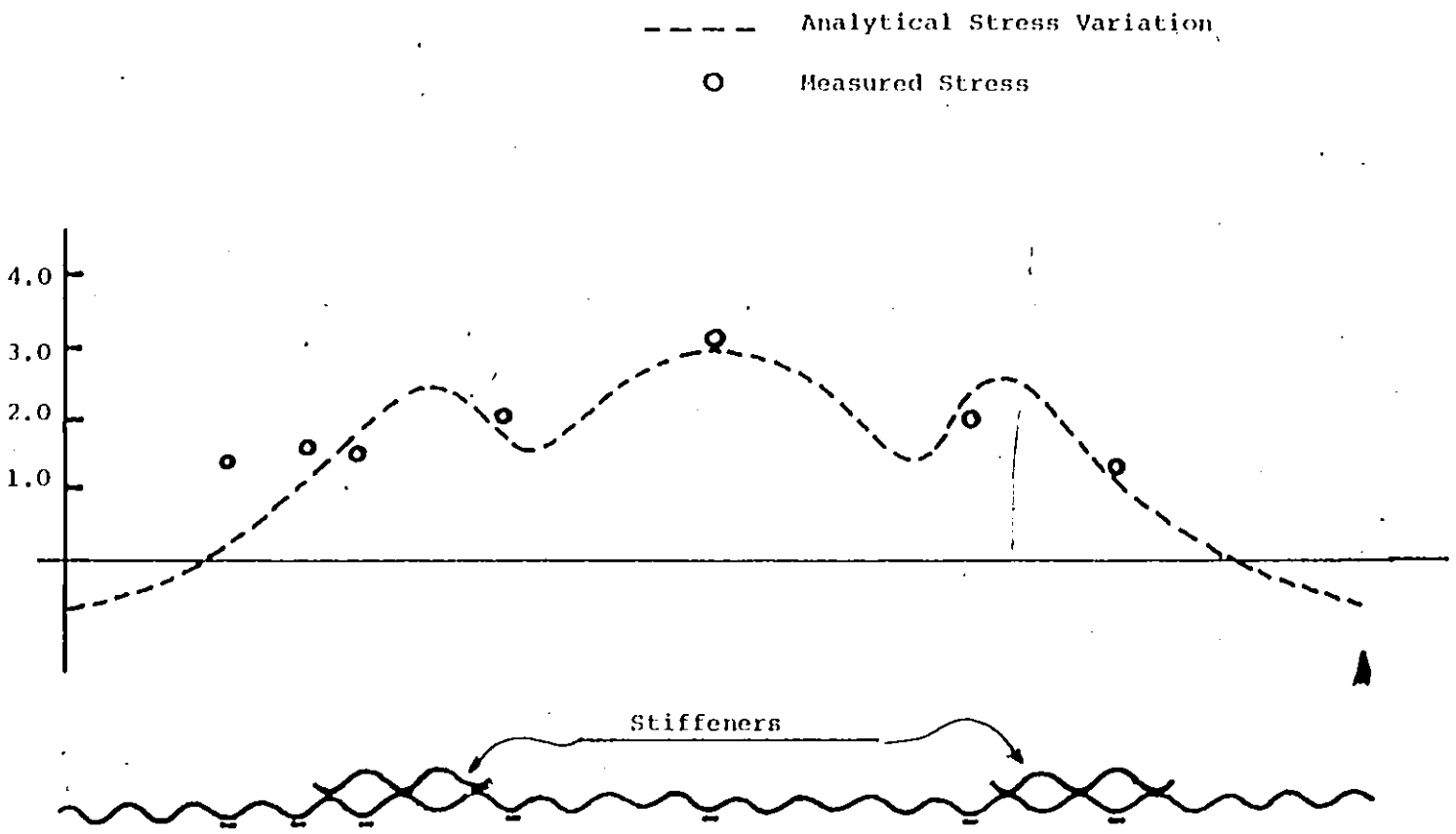

Figure 4.33: Measured and Analytical Stress Comparison in a Model with Corrugated Stiffeners Subjected to Localized Patch Load (P=500 lbs.)

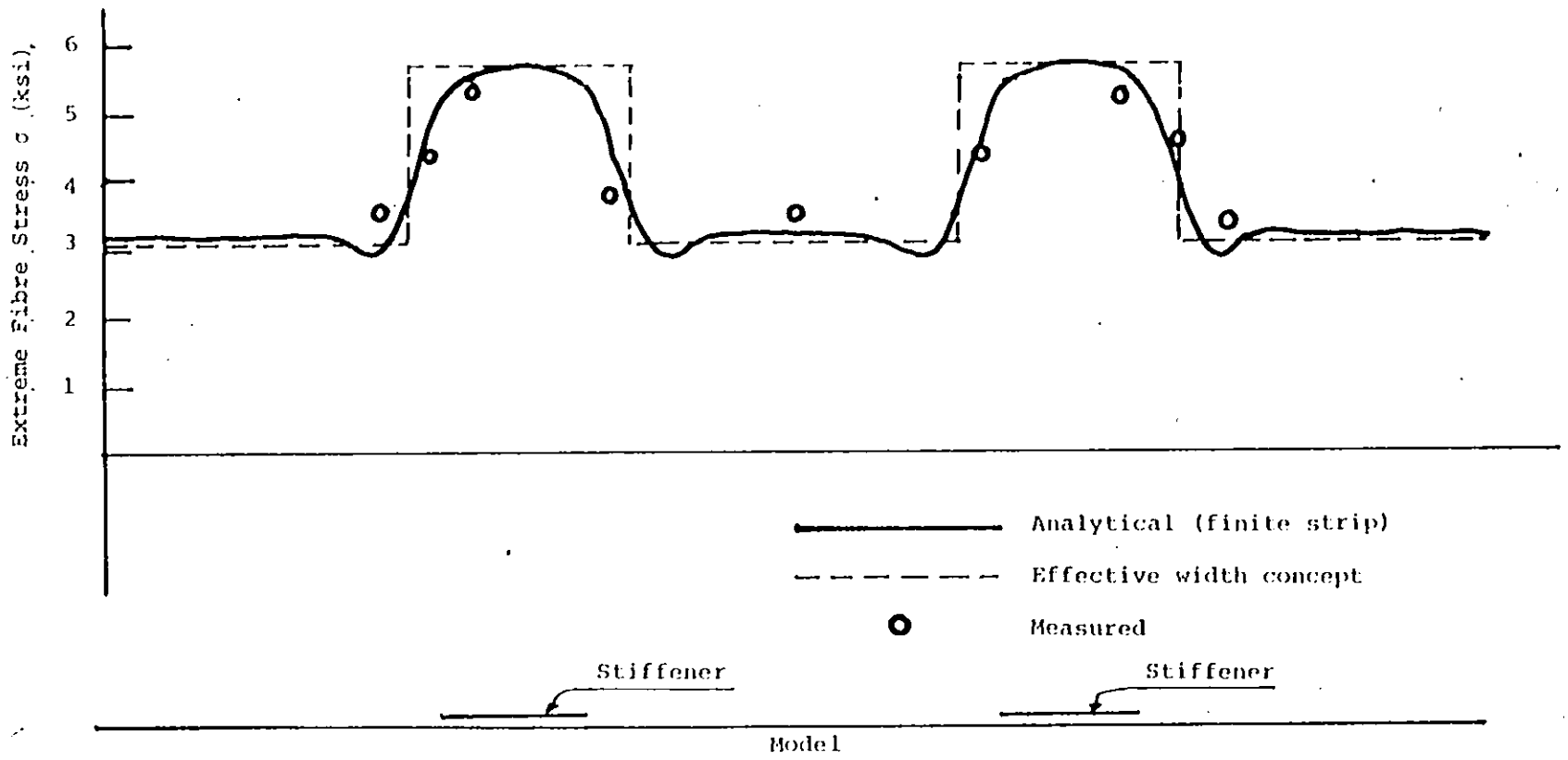

Figure 5.1: Bottom Fibre Stress Variation in a Model With Corrugated Stiffeners (d=0.05 in.)

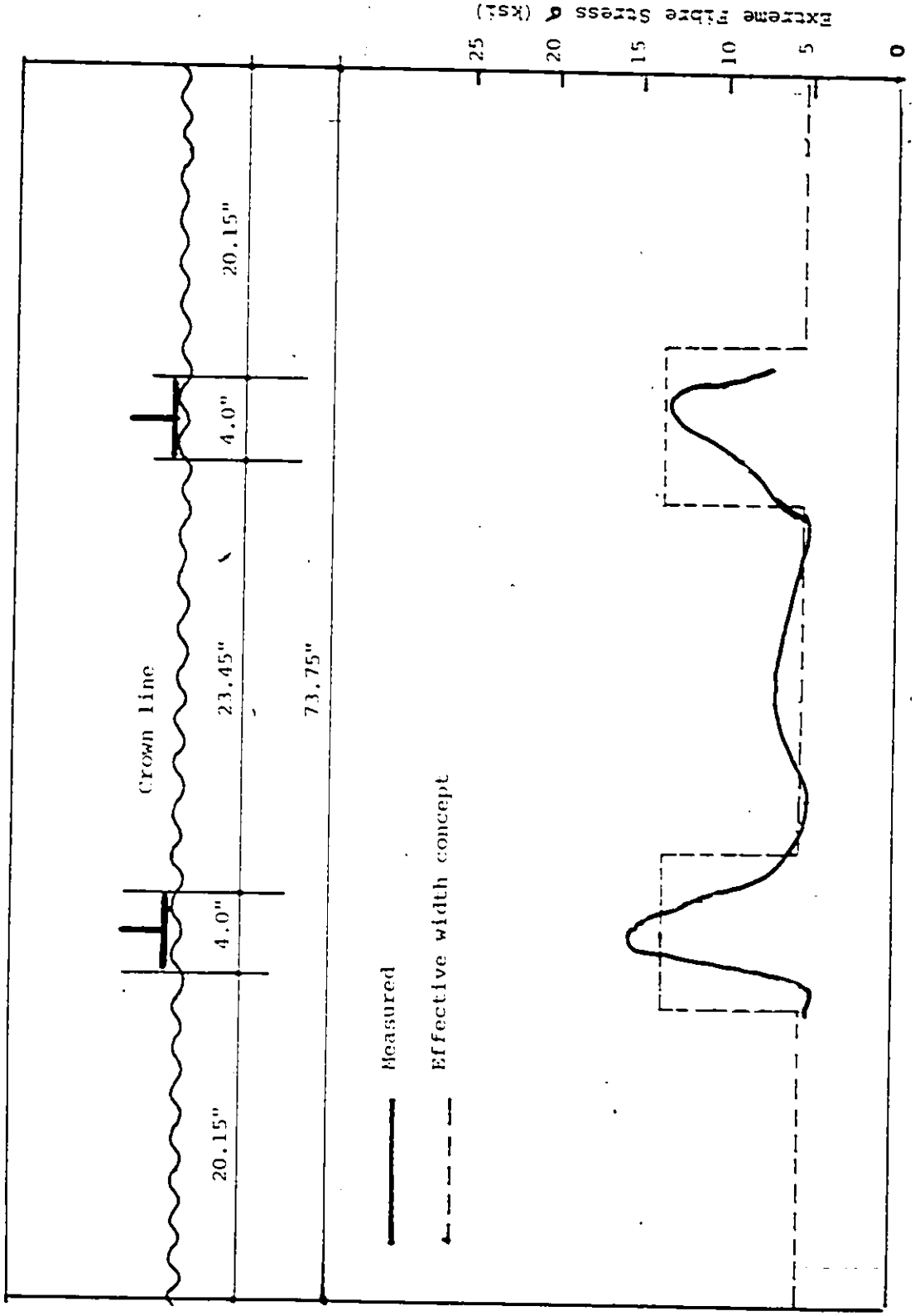

Figure 5.2: Bottom Fibre Stress Variation in a Model With Tee-Section Stiffener (d=0.5 in.).

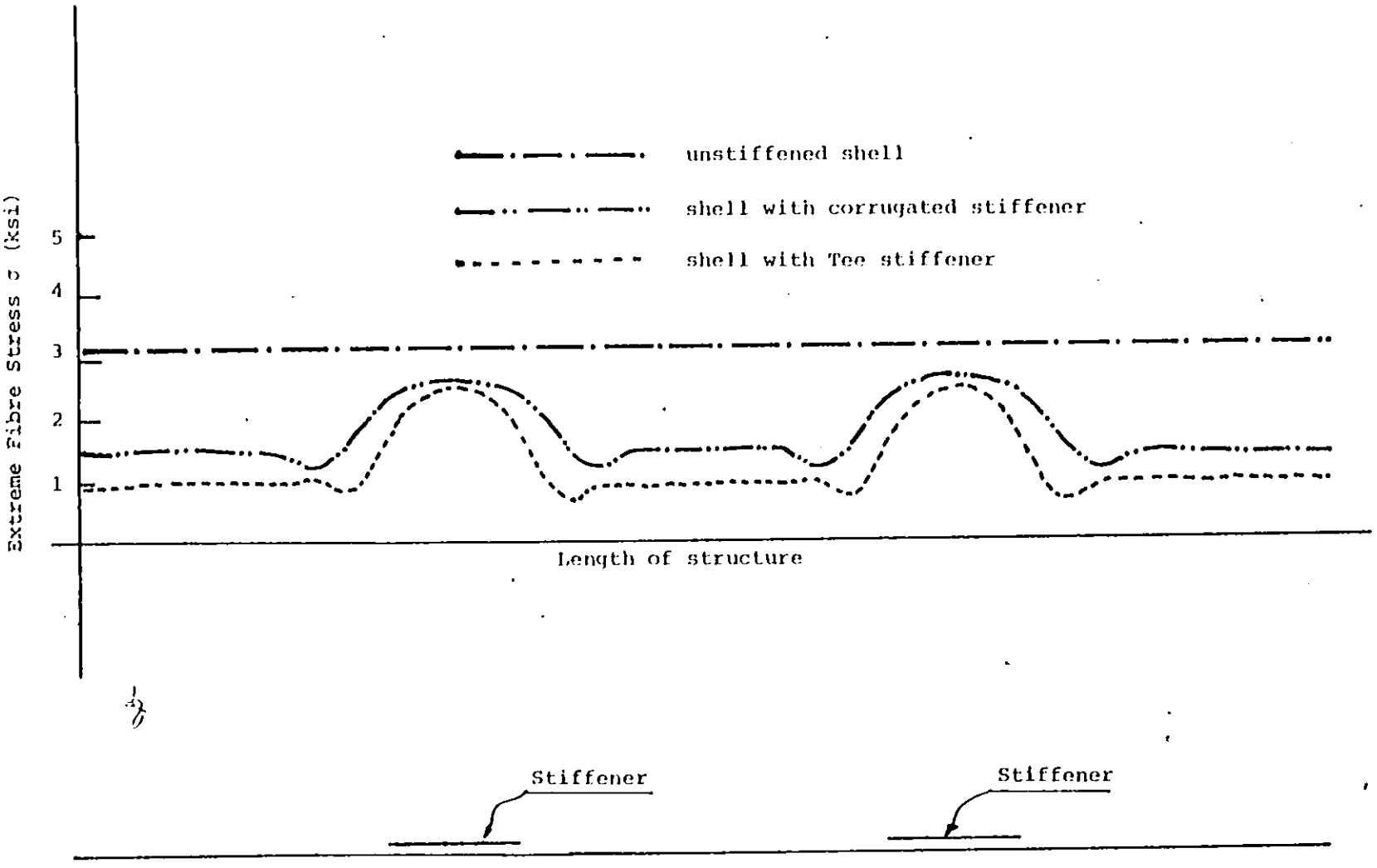

Figure 5.3: Extreme Fibre Stress Variation in Stiffened and Non-stiffened Shell Due to Same Magnitude of Horizontal Force P

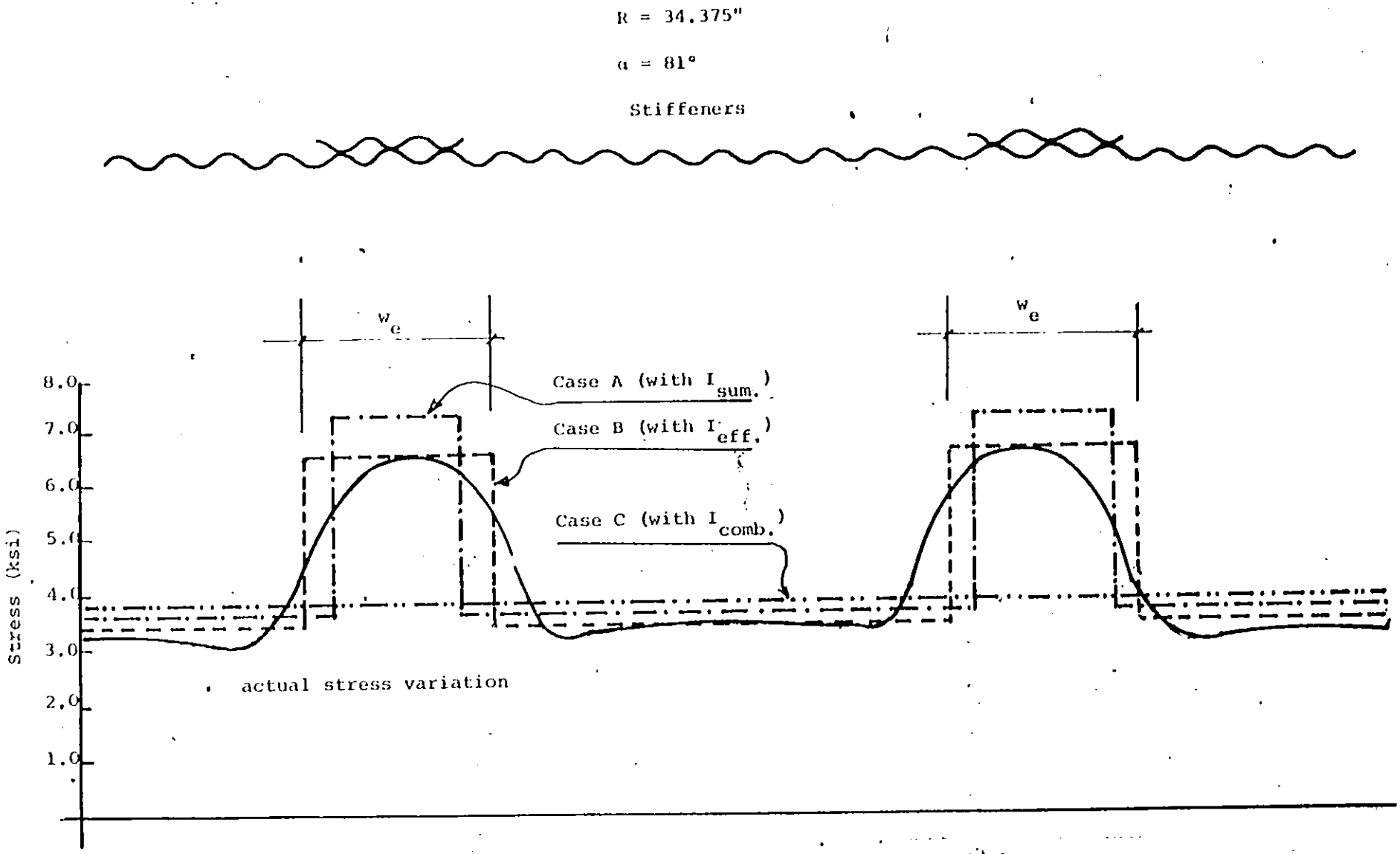

Figure 5.4: Stress Computation by Various Methods

Notes: 1) Bending moments at the sides are neglected in the derivation

2) α for non-stiffened conduits to be taken as an angle subtended by top arch from backfilling level

3) α for stiffened conduits to be taken as an angle of top stiffened arch

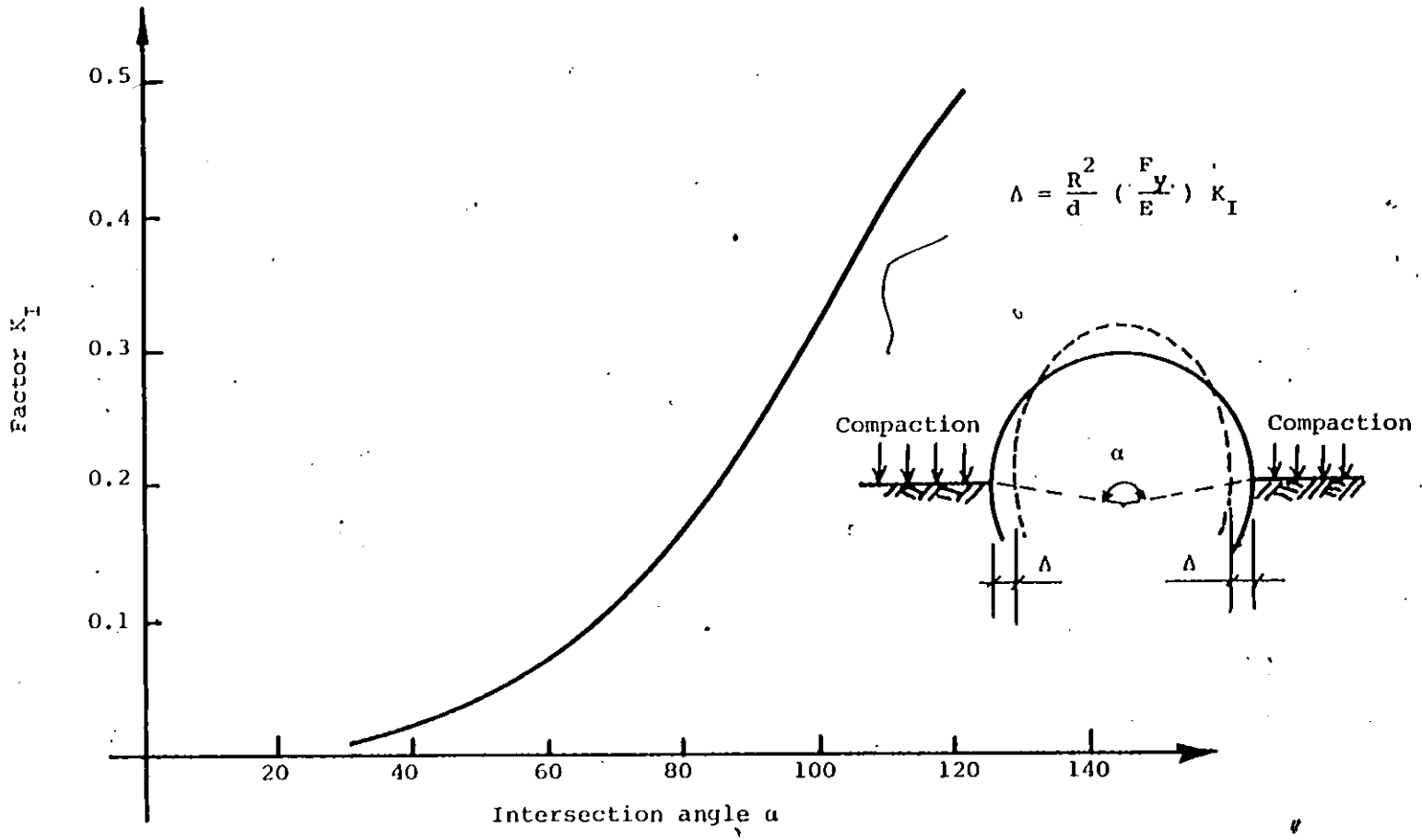

Figure 5.5: Variation of factor K_I with the intersection angle for a structure during side filling

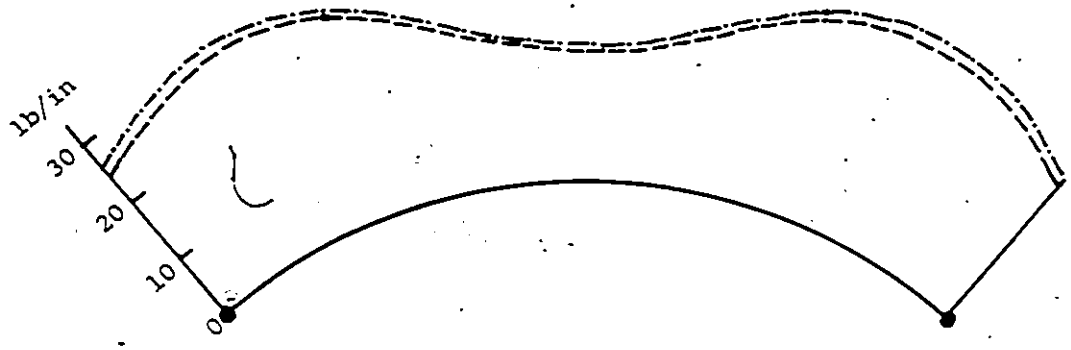

a) Axial Thrust

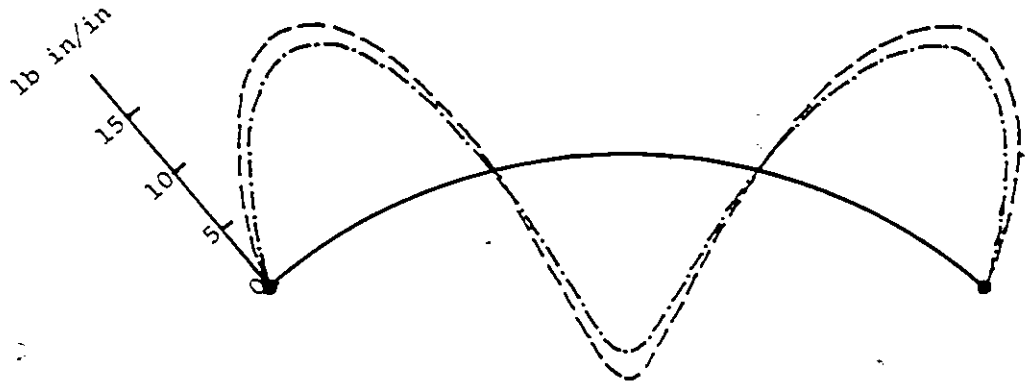

b) Bending Moment

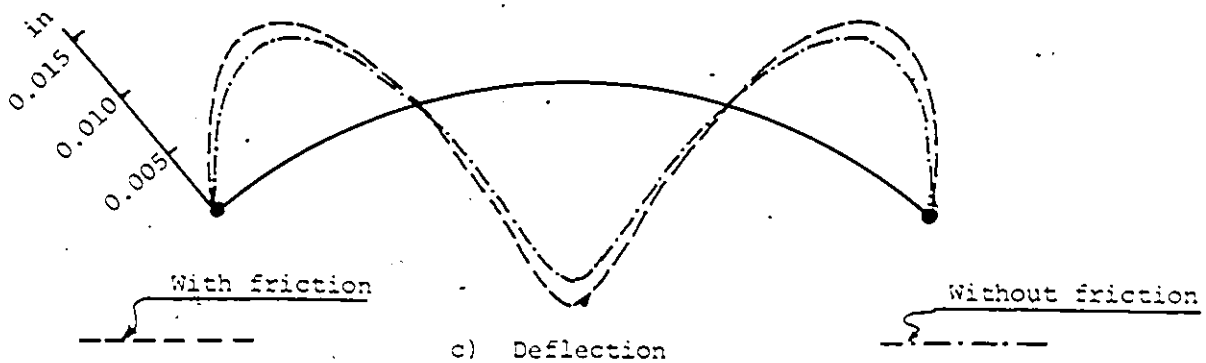

c) Deflection

Figure 5.6: Effect of Soil-friction Force on the Performance of Soil-Steel Structure

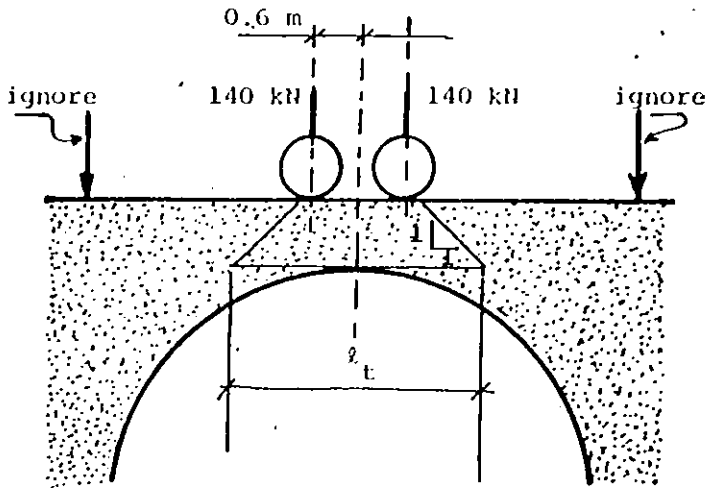

a) Load Dispersion in Transverse Direction

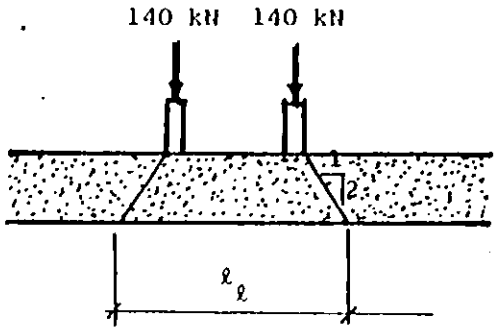

b) Load Dispersion in Longitudinal Direction

Figure 5.7: OHBDC Live Load Dispersion

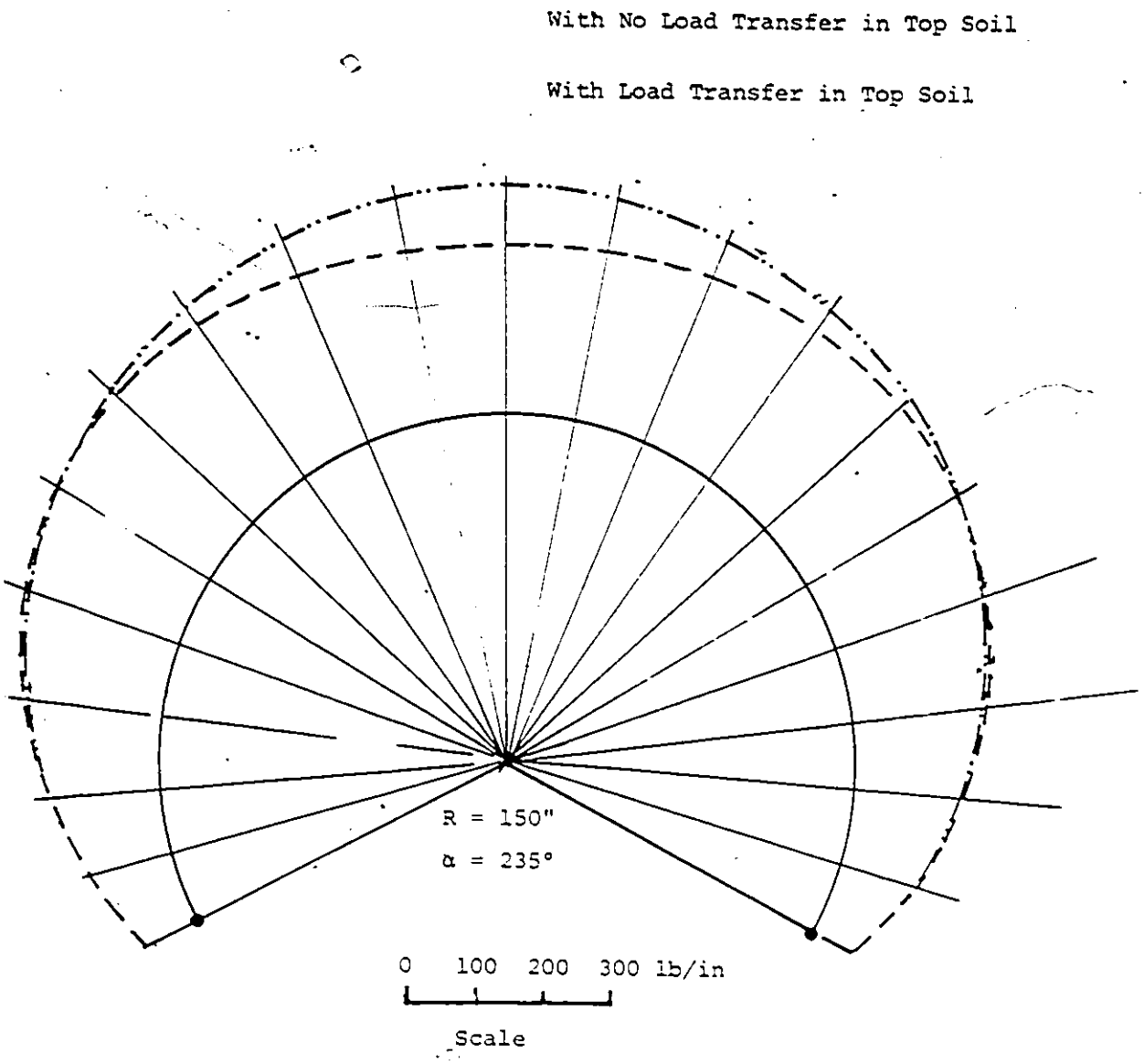

Figure 5.8: Axial Thrust Variation with and without Cosidering the Load Transfer in Top Soil

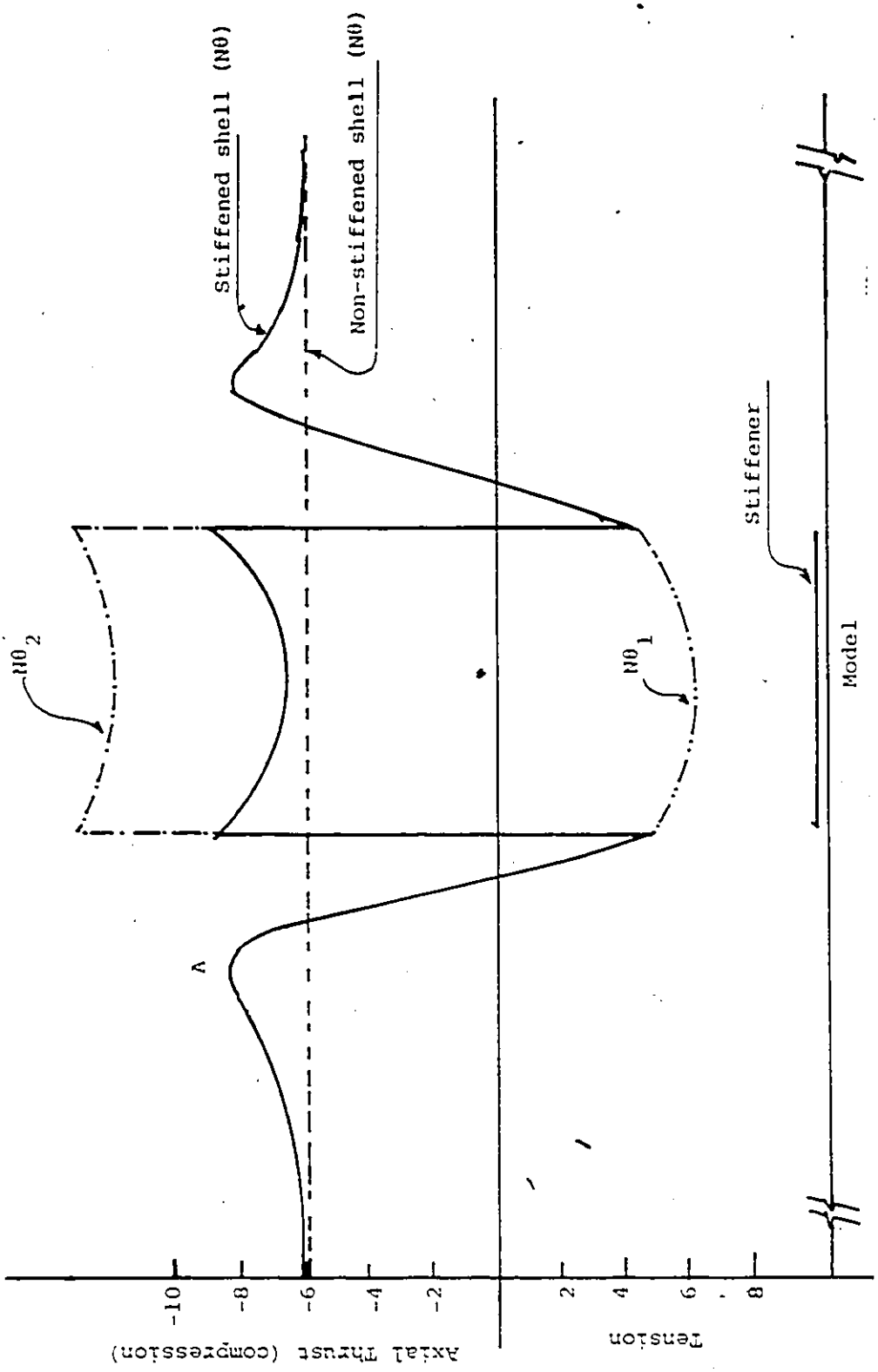

Figure 5.9: Axial Thrust Variation at Crown Due to Uniform Loading (p=500 lb.)

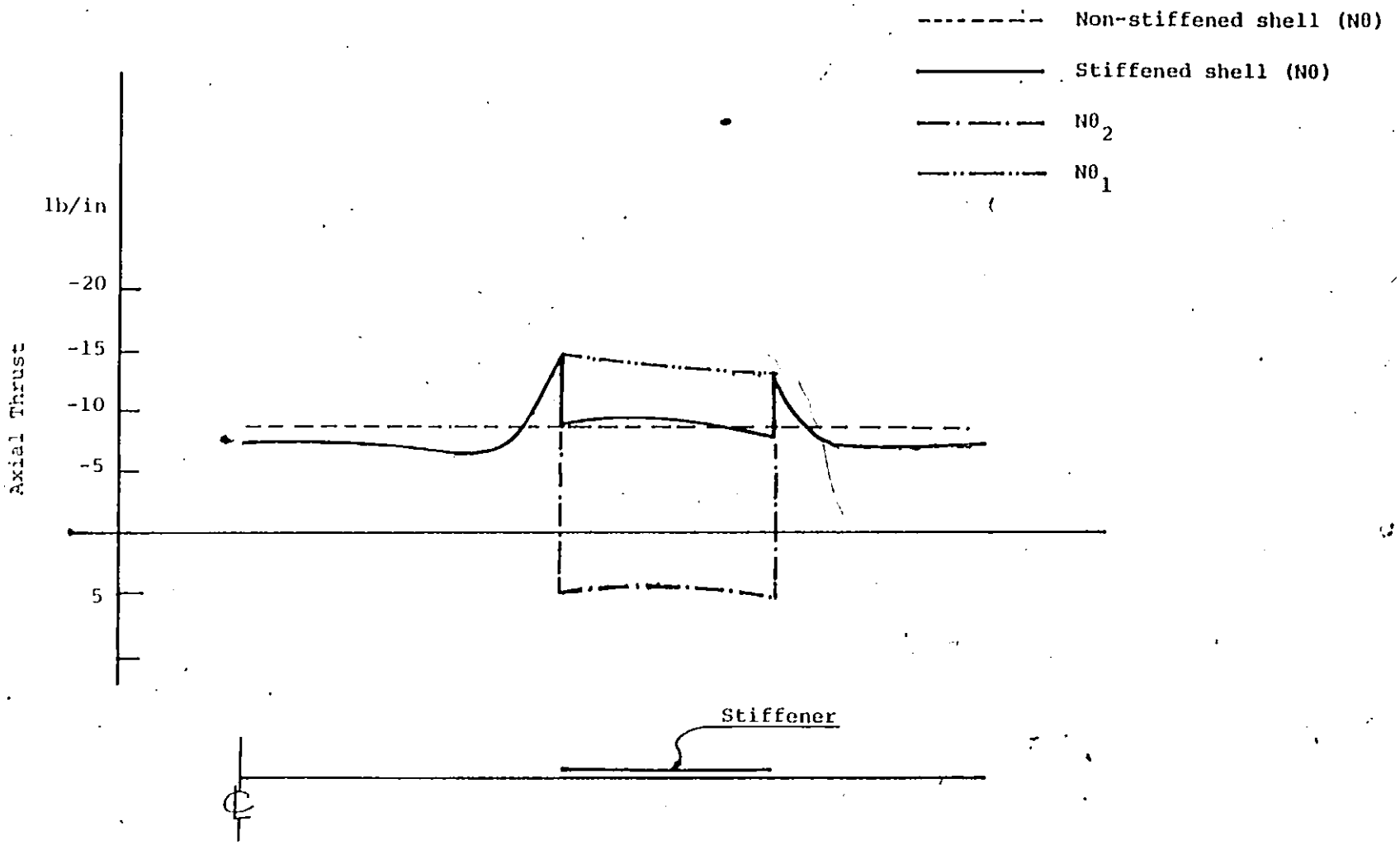

Figure 5.10: Axial Thrust Variation Along Haunch Due to Uniform Loading (P=500 lb.)

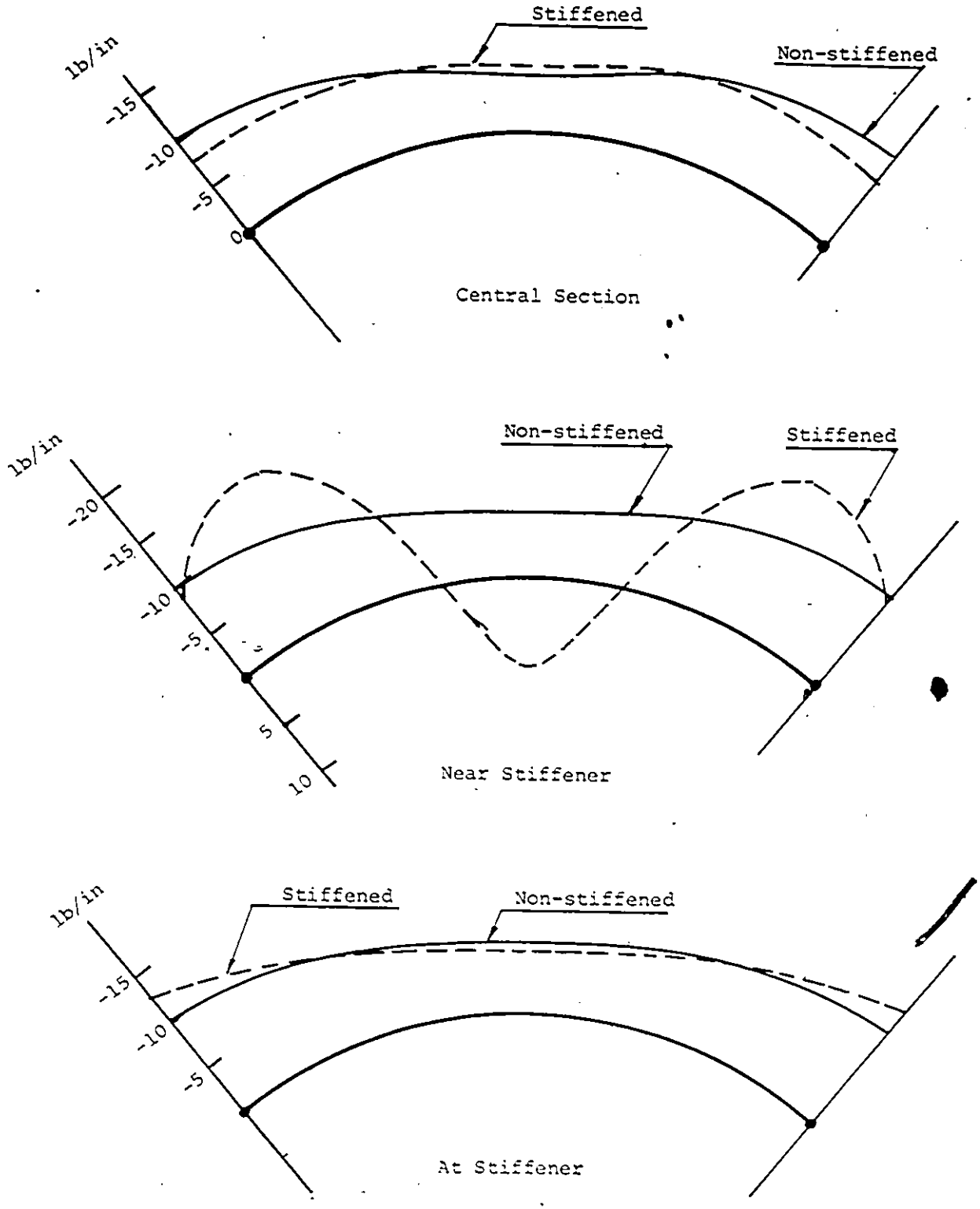

Figure 5.11: Axial Thrust Variation in Curved Direction Due to Uniform Loading (P=500 lb.)

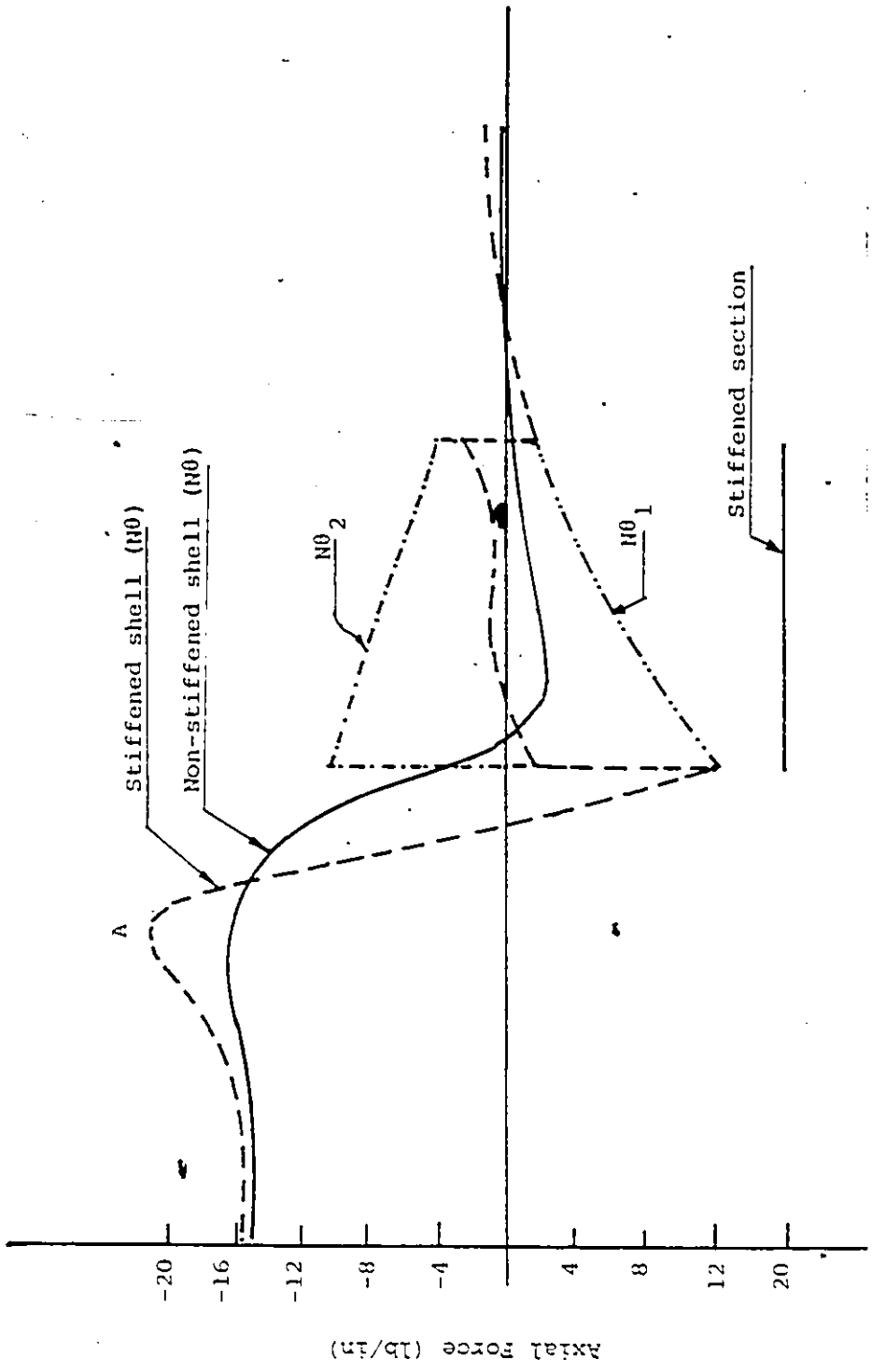

Figure 5.12: Axial Thrust Variation Along Crown Due to Strip/Line Loading (P=500 lb.)

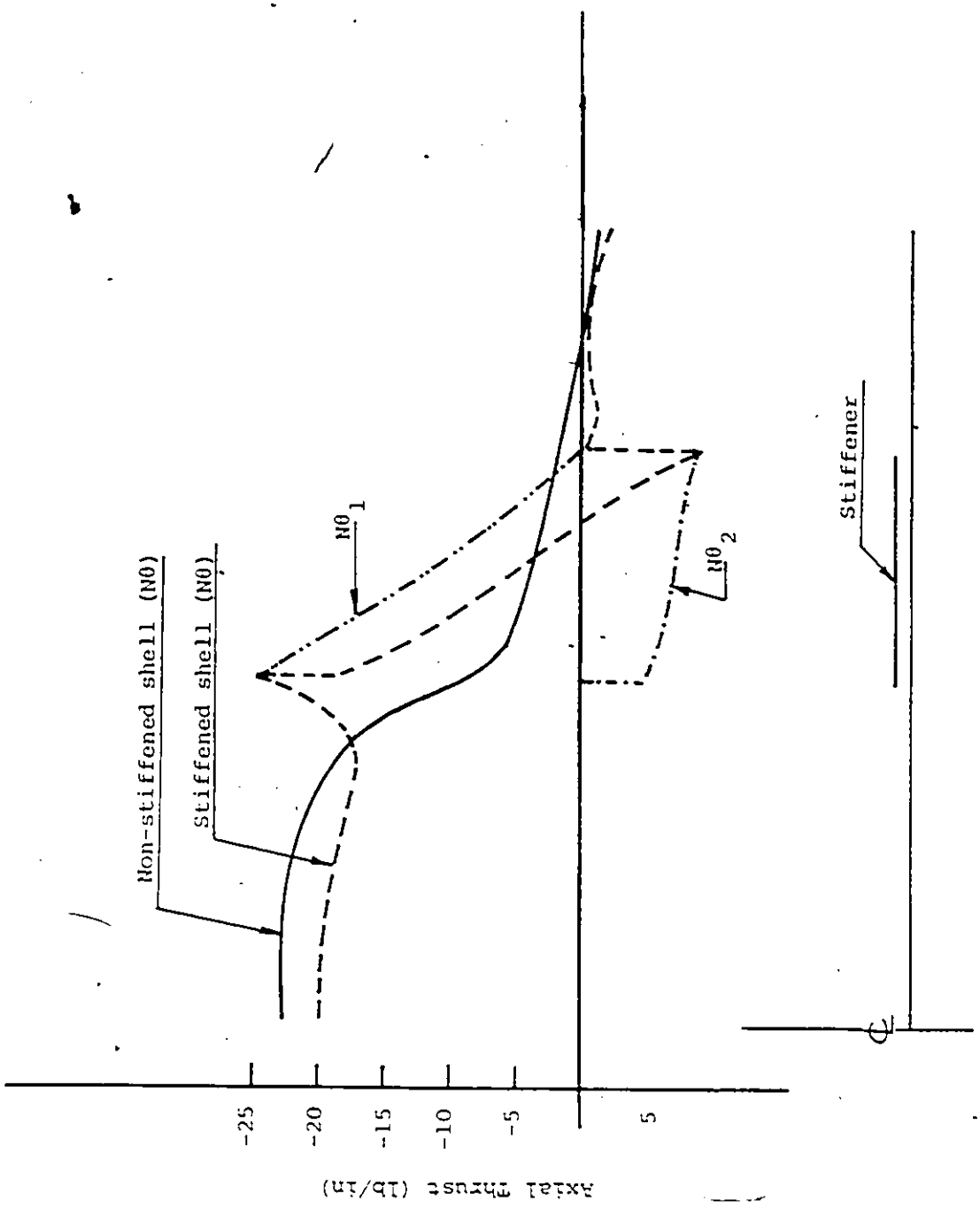

Figure 5.13: Axial Thrust Variation Along Haunch Due to Strip/Line Loading (P=500 lb.)

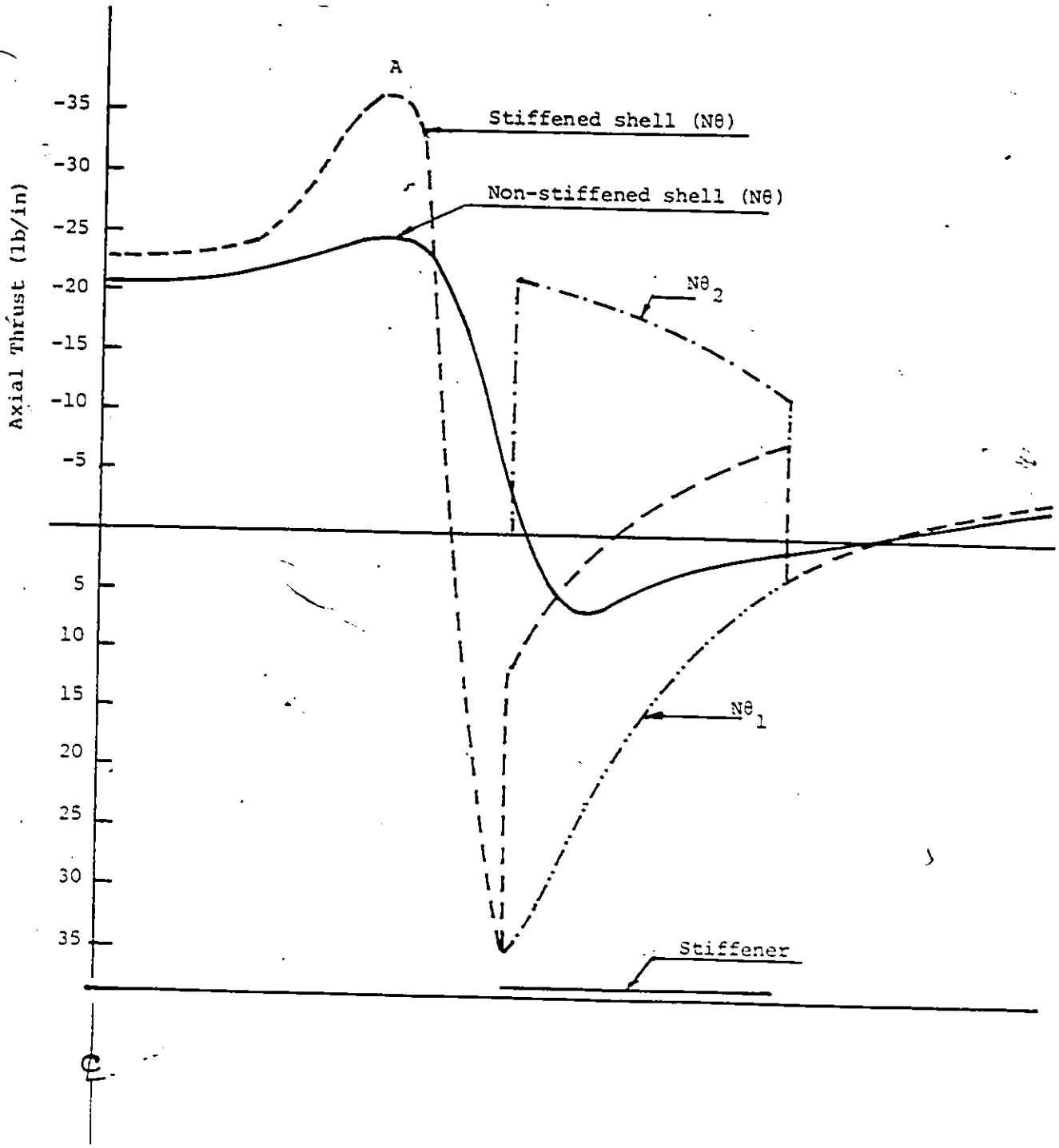

Figure 5.14: Axial Thrust Variation Along Crown Due to Patch Load (P=500 lb.)

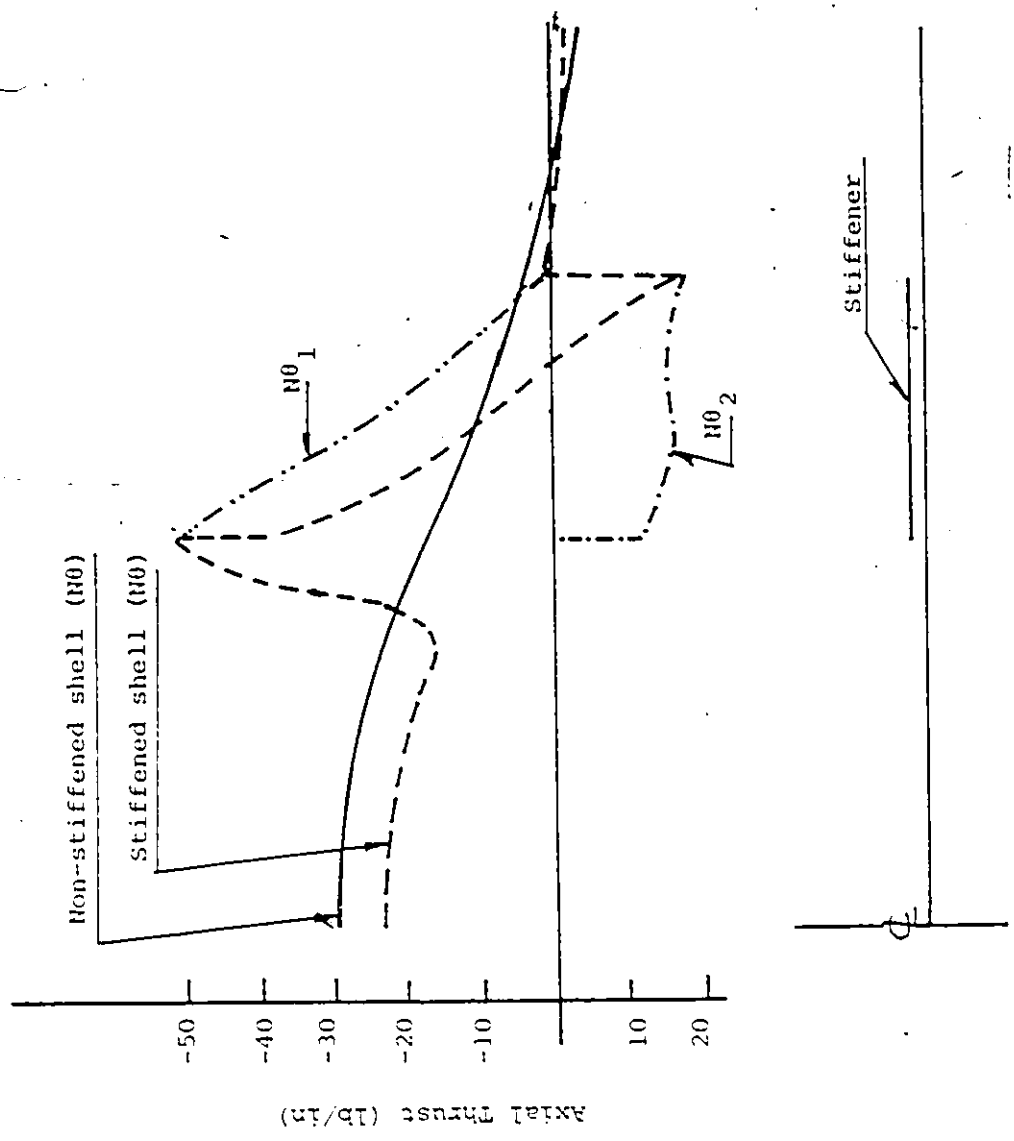

Figure 5.15: Axial Thrust Variation Along Haunch Due to Patch Loading (P=500 lb.)

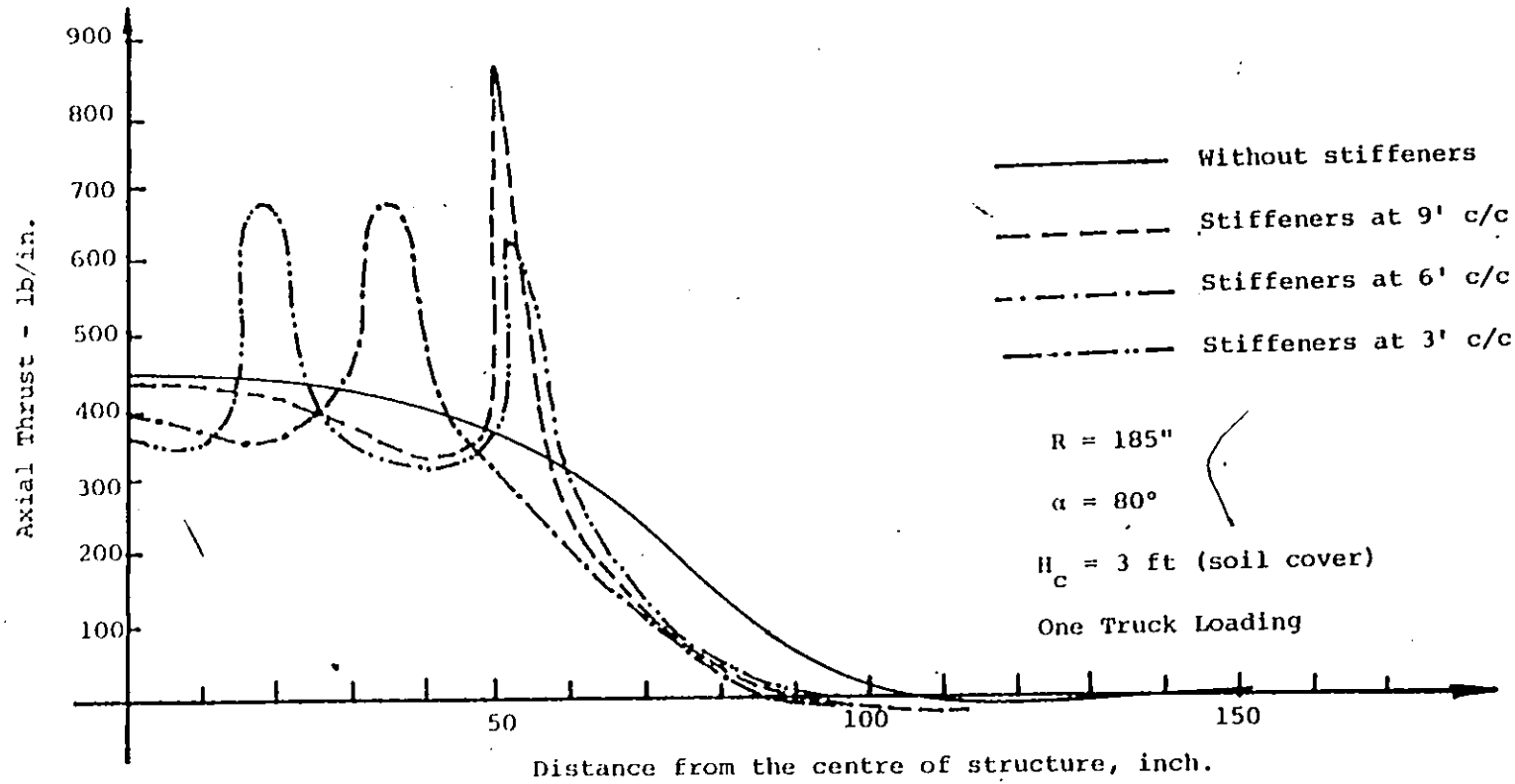

Figure 5.16: Effect of Stiffener Spacing on the Axial Thrust Variation along the haunch of full scale structure under patch loading

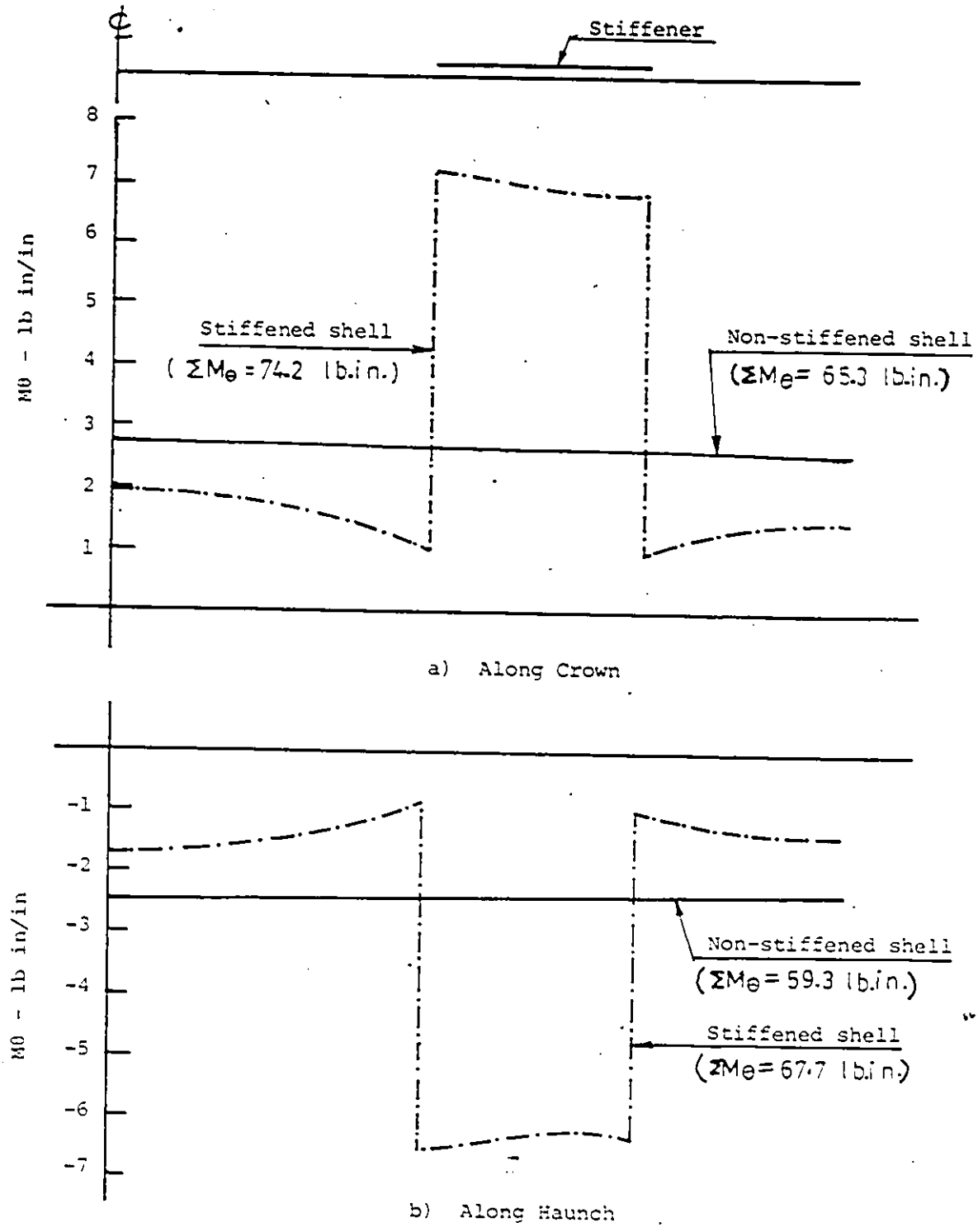

Figure 5.17: Bending Moment Distribution Due to Uniform Loading (P=500 lb)

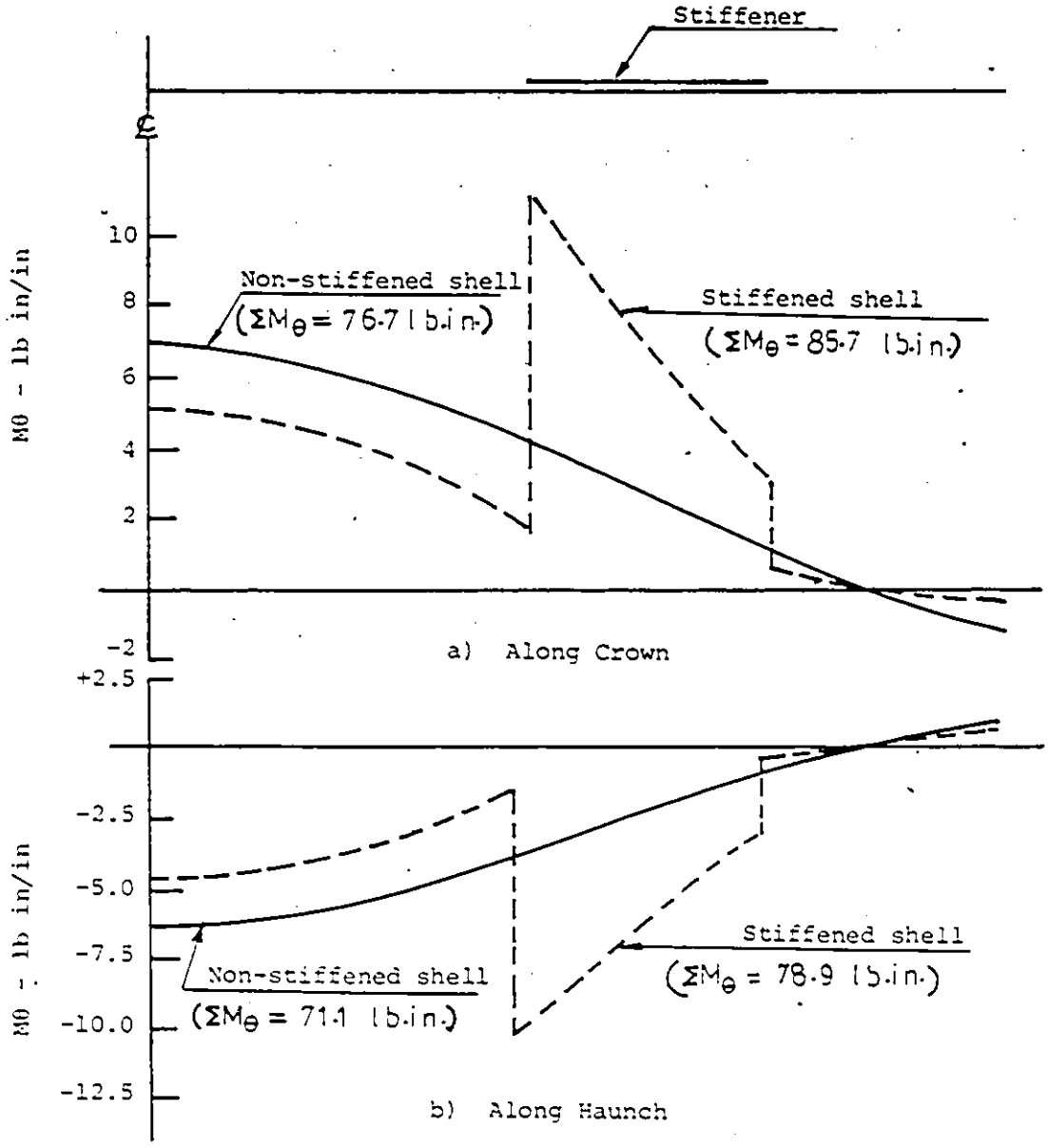

Figure 5.13: Bending Moment Variation Due to Strip/Line Loading (P=500 lb)

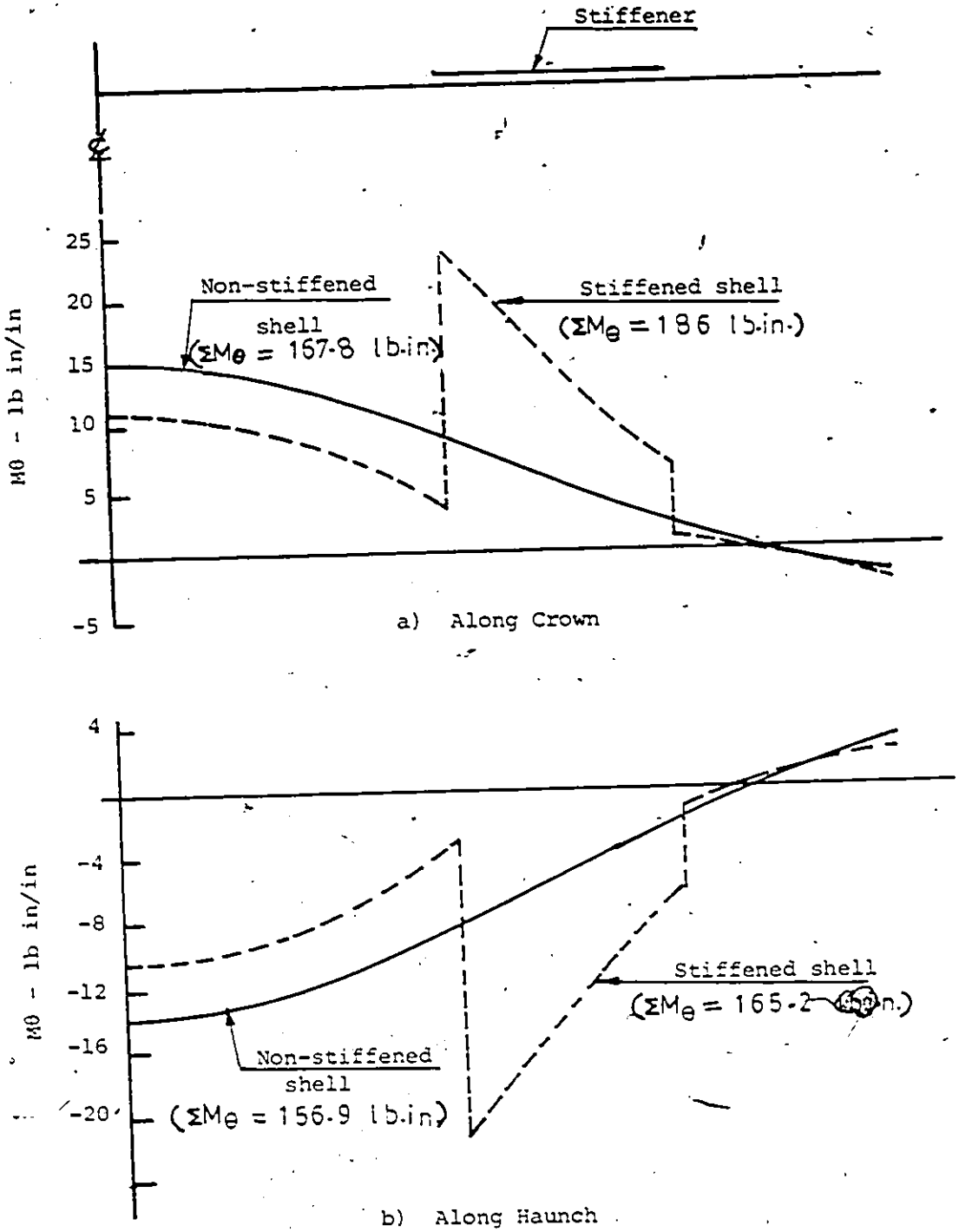

Figure 5.19: Bending Moment Variation Due to Patch Loading (P=500 lb)

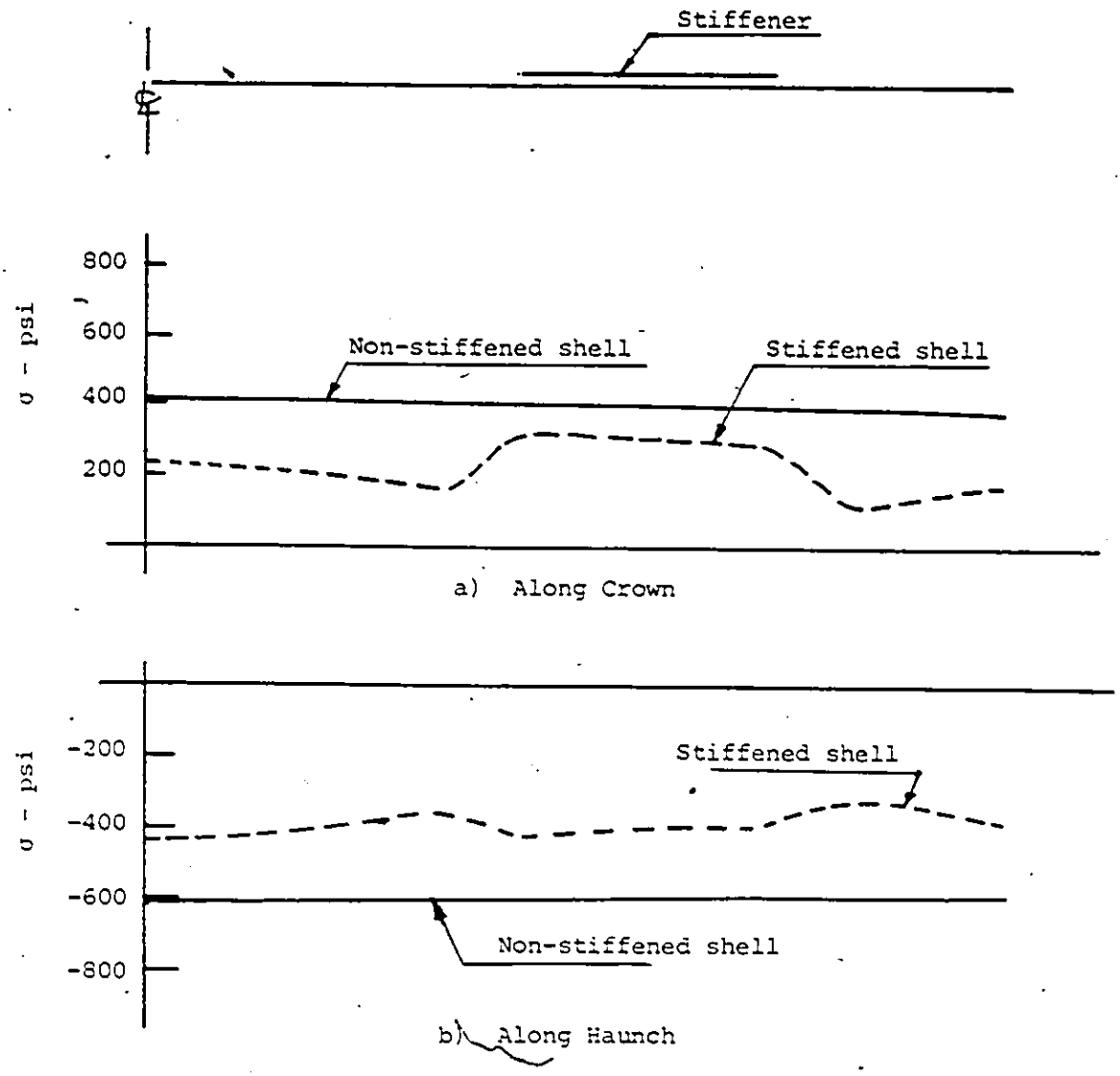

Figure 5.20: Extreme Fibre Stress Variation Due to Uniform Load (P=500 lb)

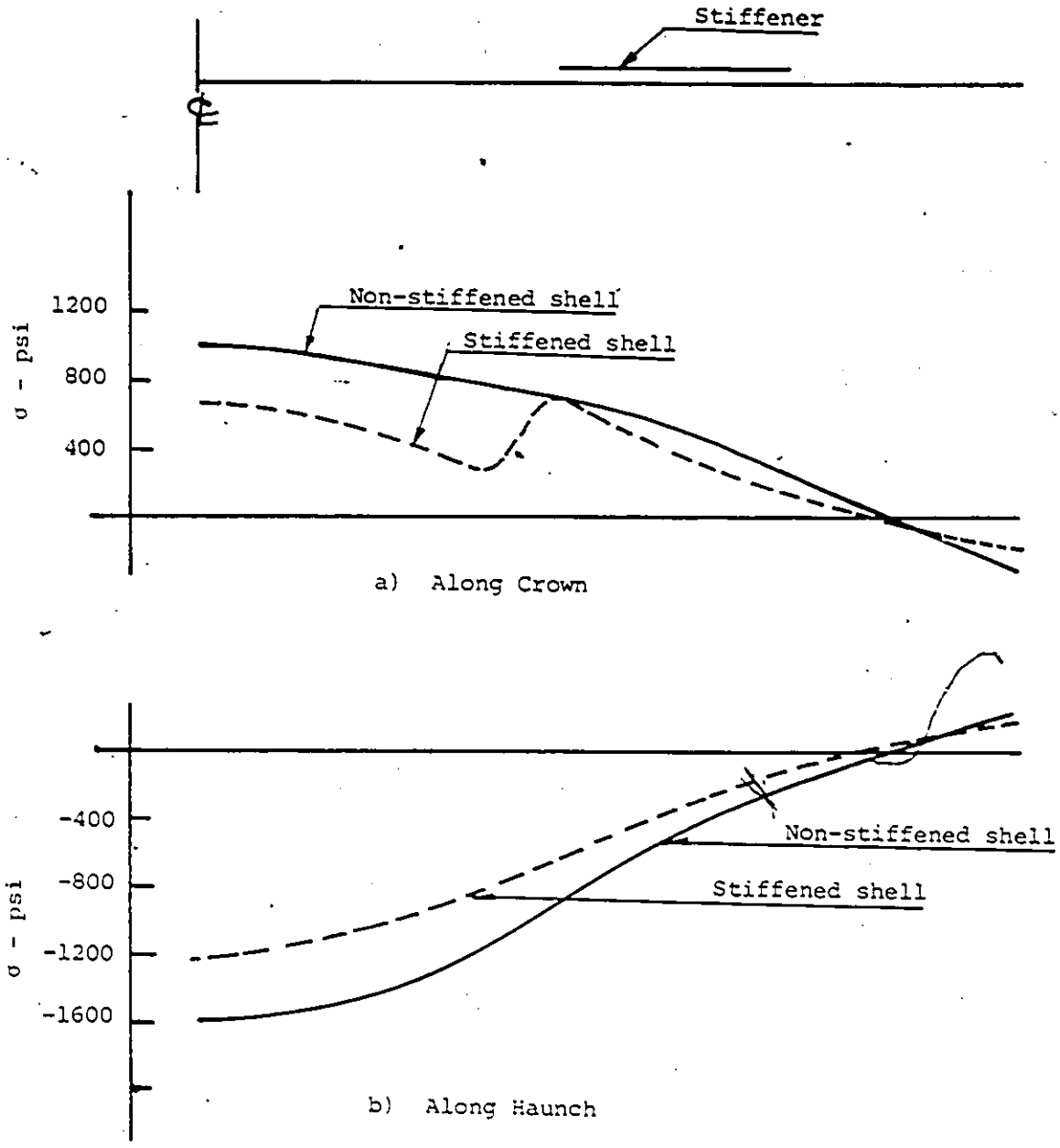

Figure 5.21: Extreme Fibre Stress Variation Due to Strip Loading (P=500 lb)

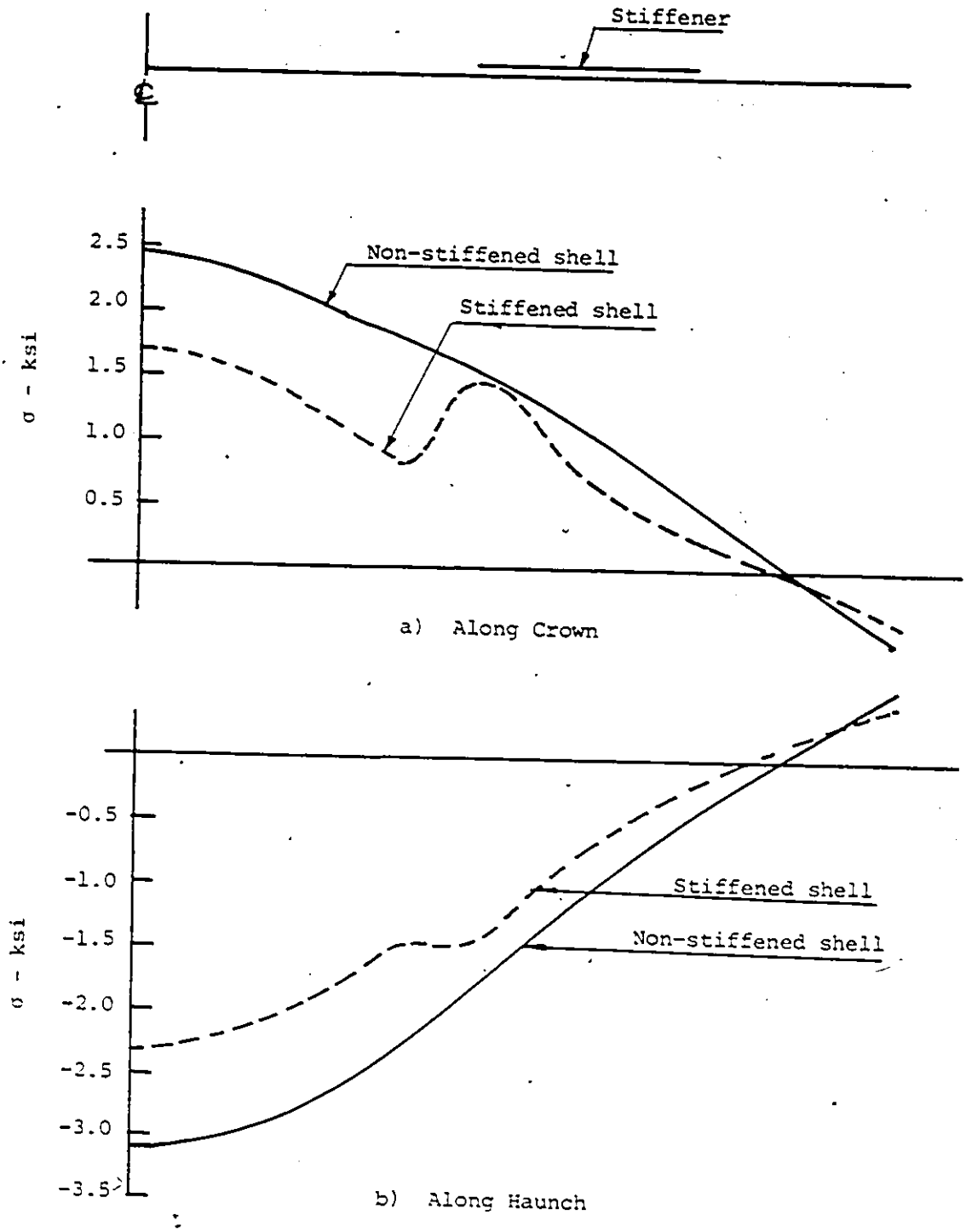

Figure 5.22: Extreme Fibre Stress Variation Due to Patch Loading (P=500 lb)

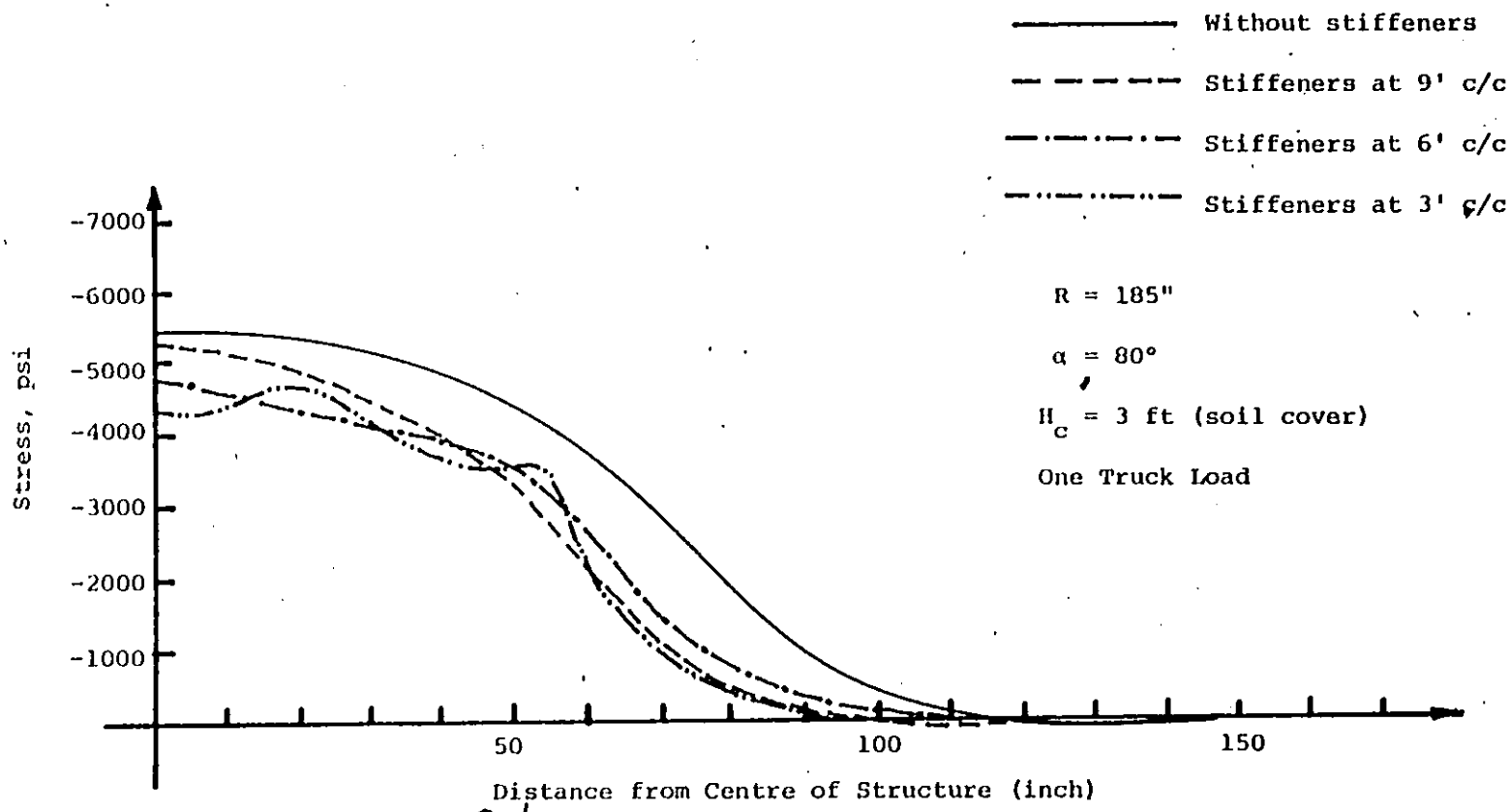

Figure 5.23: Effect of Stiffener Spacing on the Combined Stress Variation along the haunch of full scale structure under the patch loading

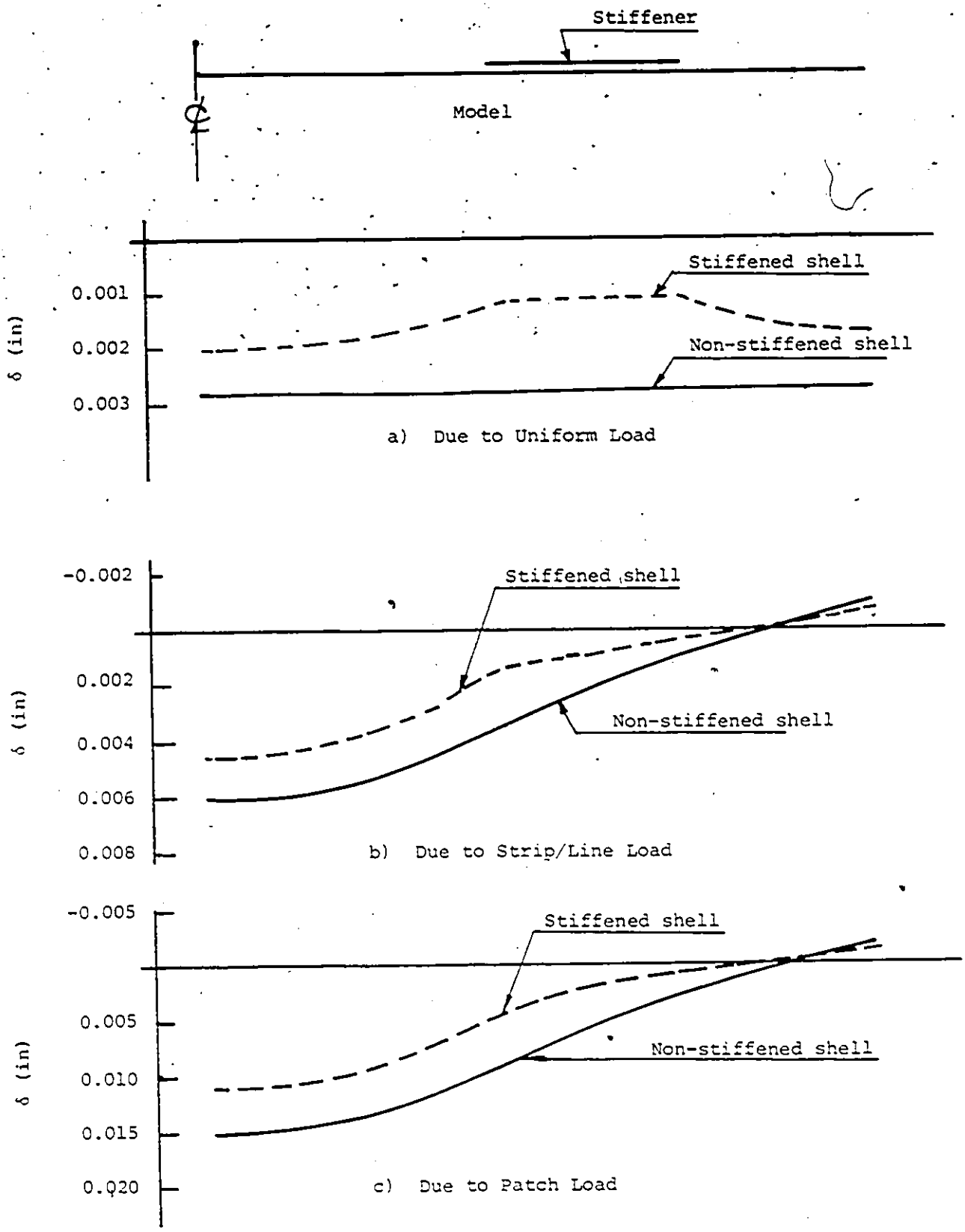

Figure 5.24: Crown Deflections of Model Under Various Loads (P=500 lb)

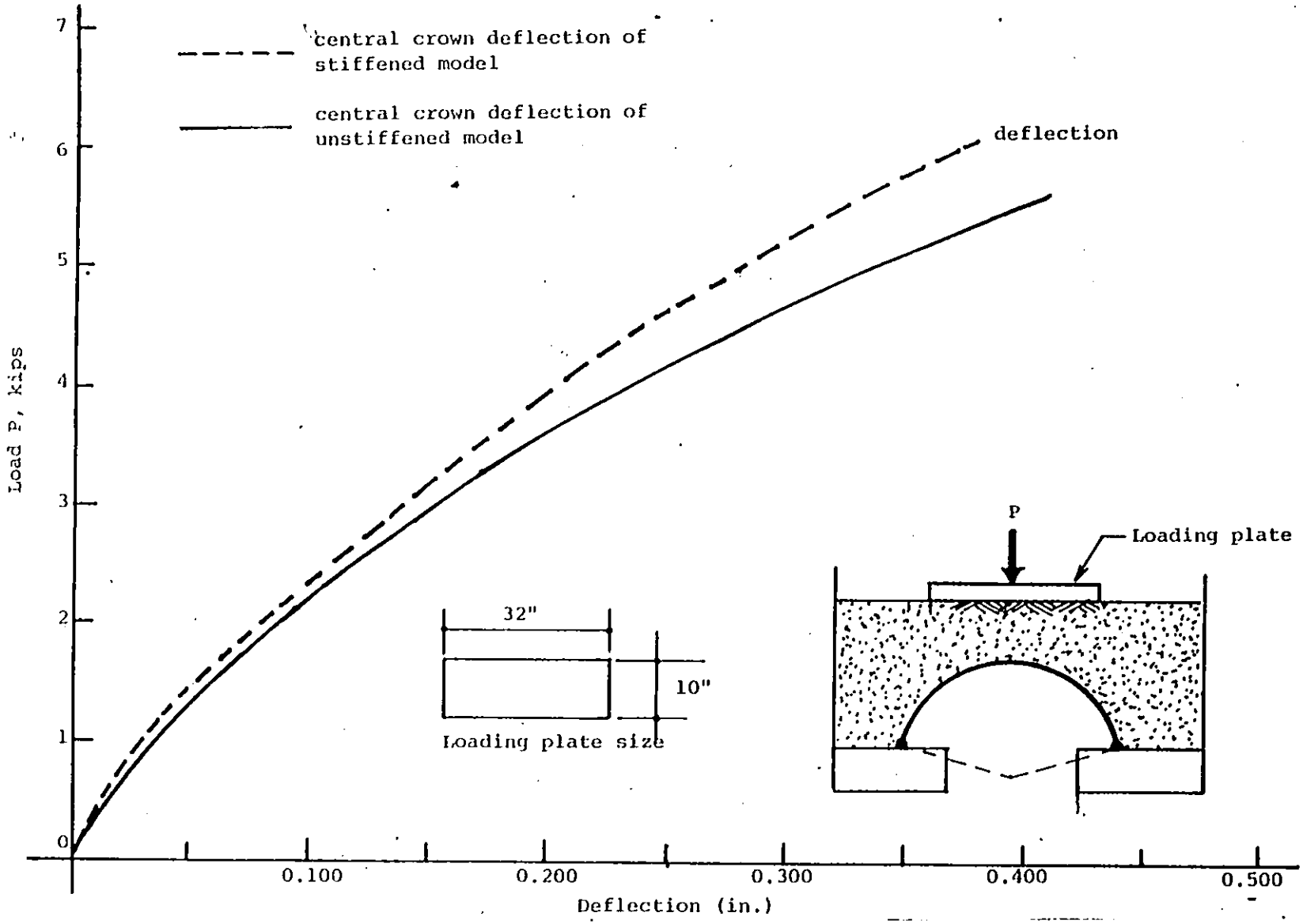

Figure 5.25: Load Deflection Curve for Stiffened and Non-stiffened Model Under Strip/Line Loading

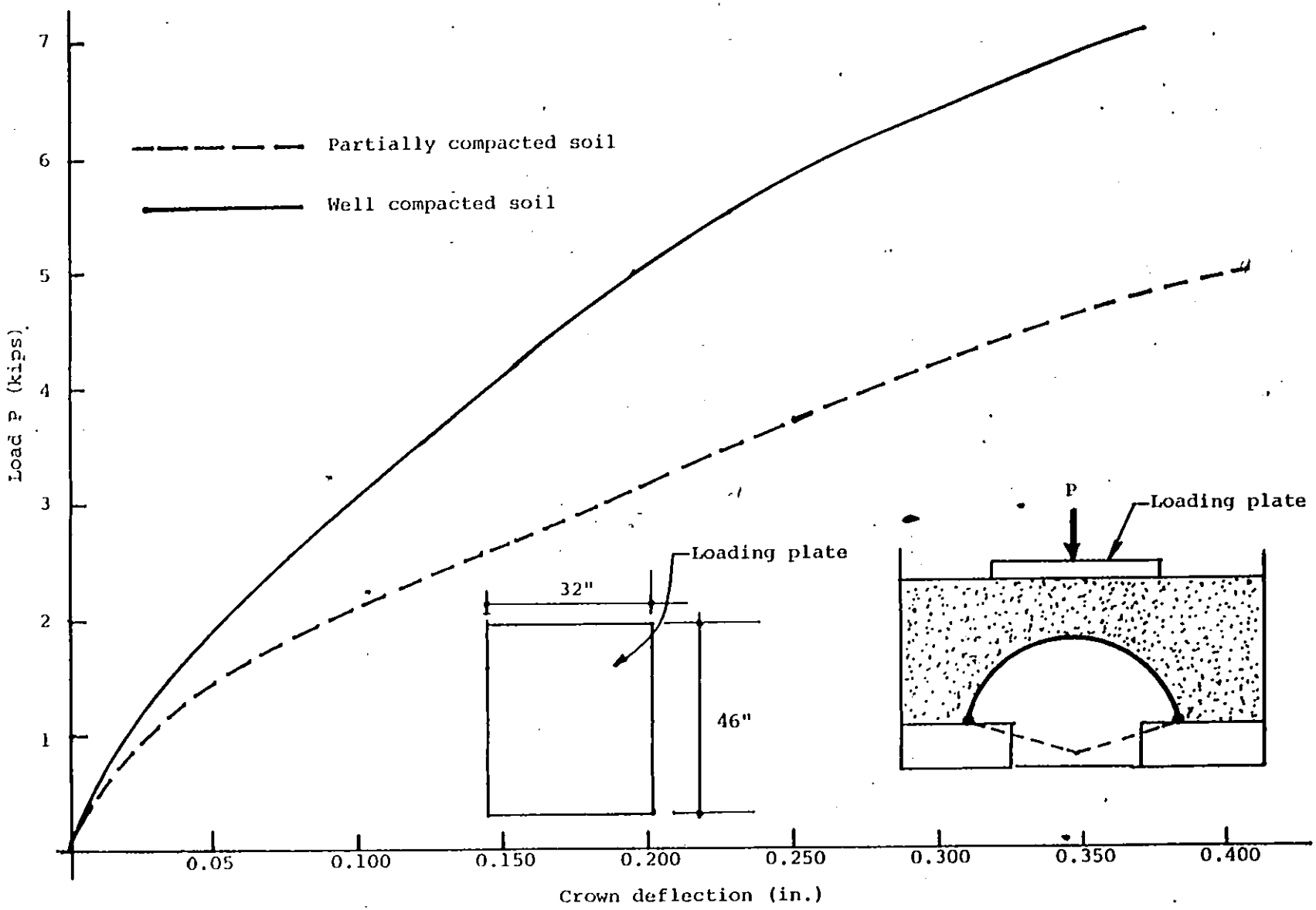

Figure 5.26: Load-Deflection Curve Under Different Treatment of Soil

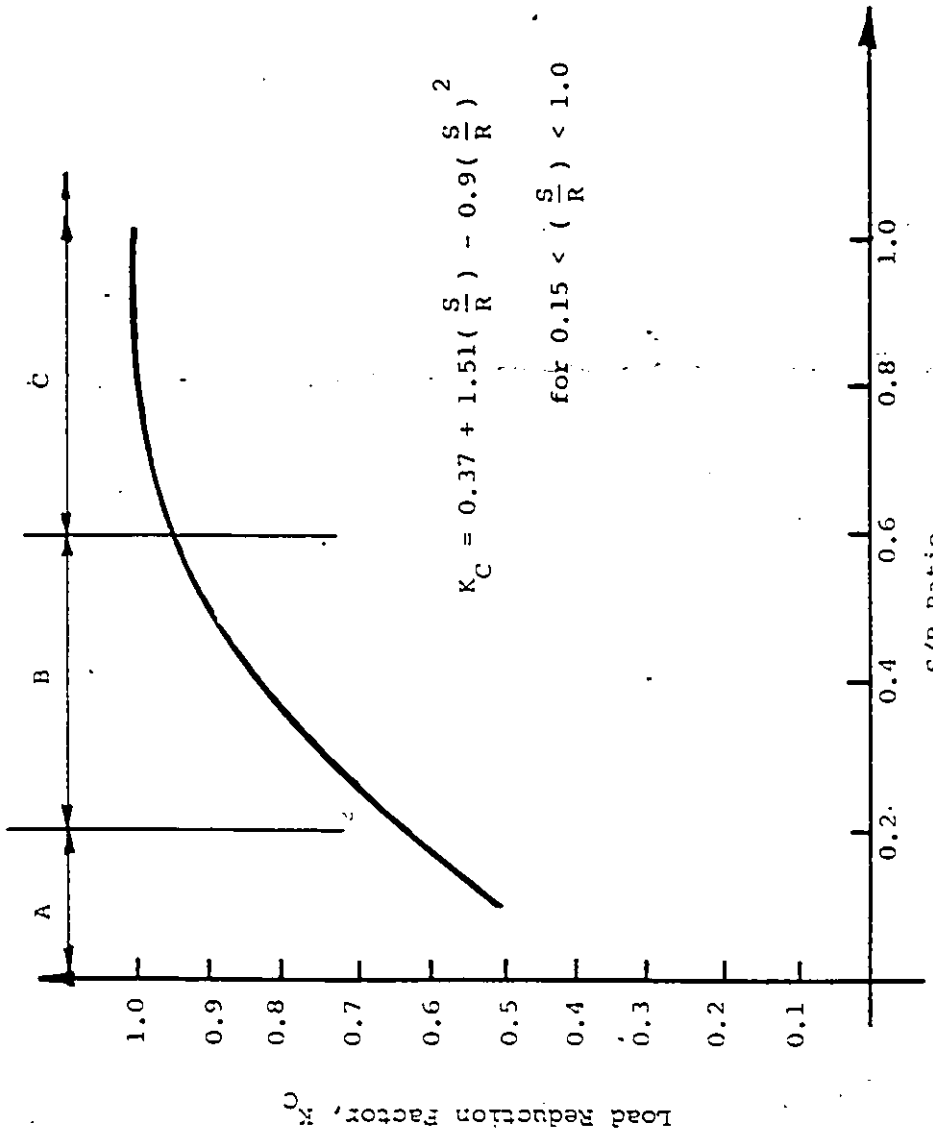

Figure 5.27: Variation of load reduction factor K_C with S/R ratio

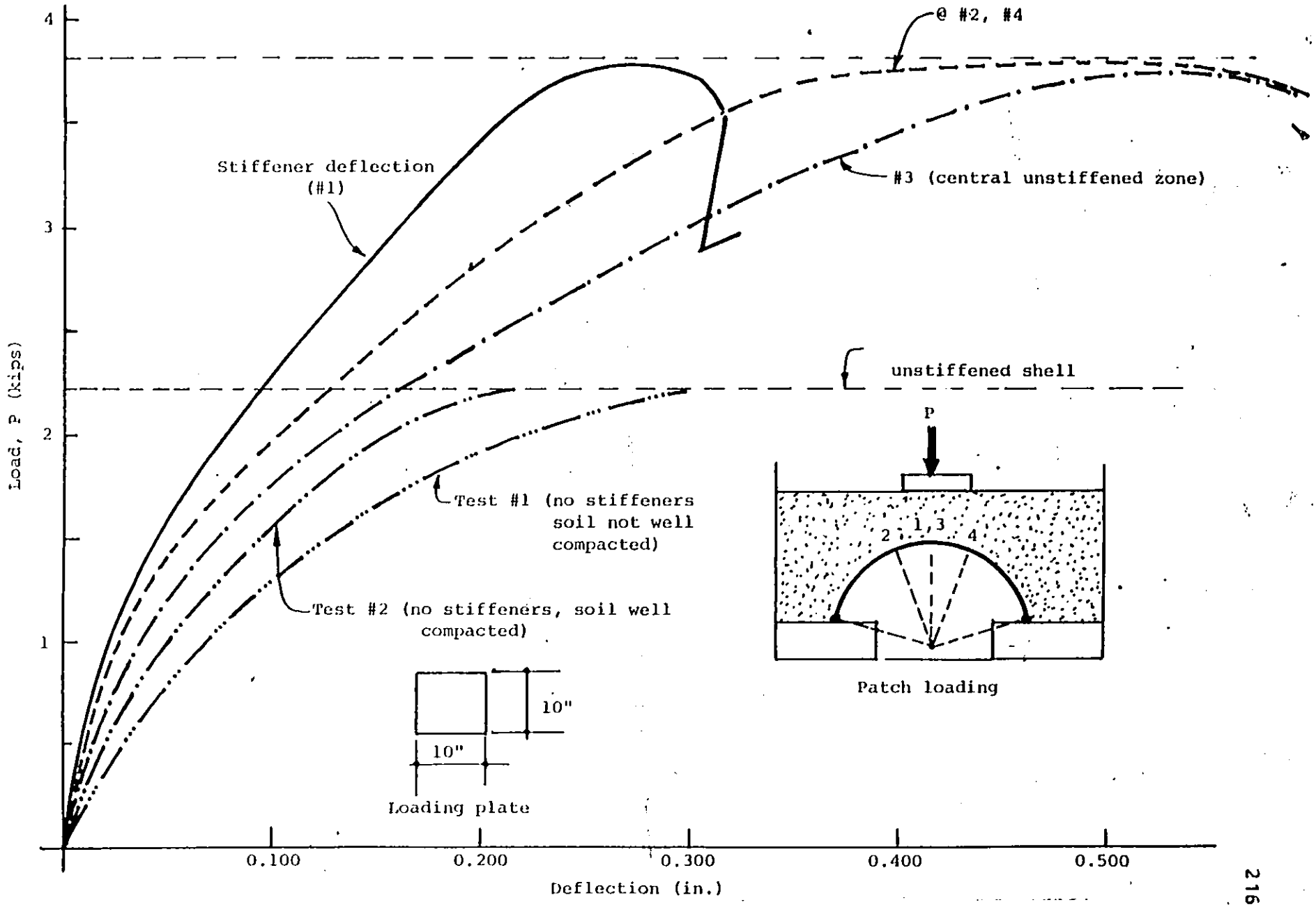

Figure 5.28: Load-Deflection Curve Under Localized Patch Loading

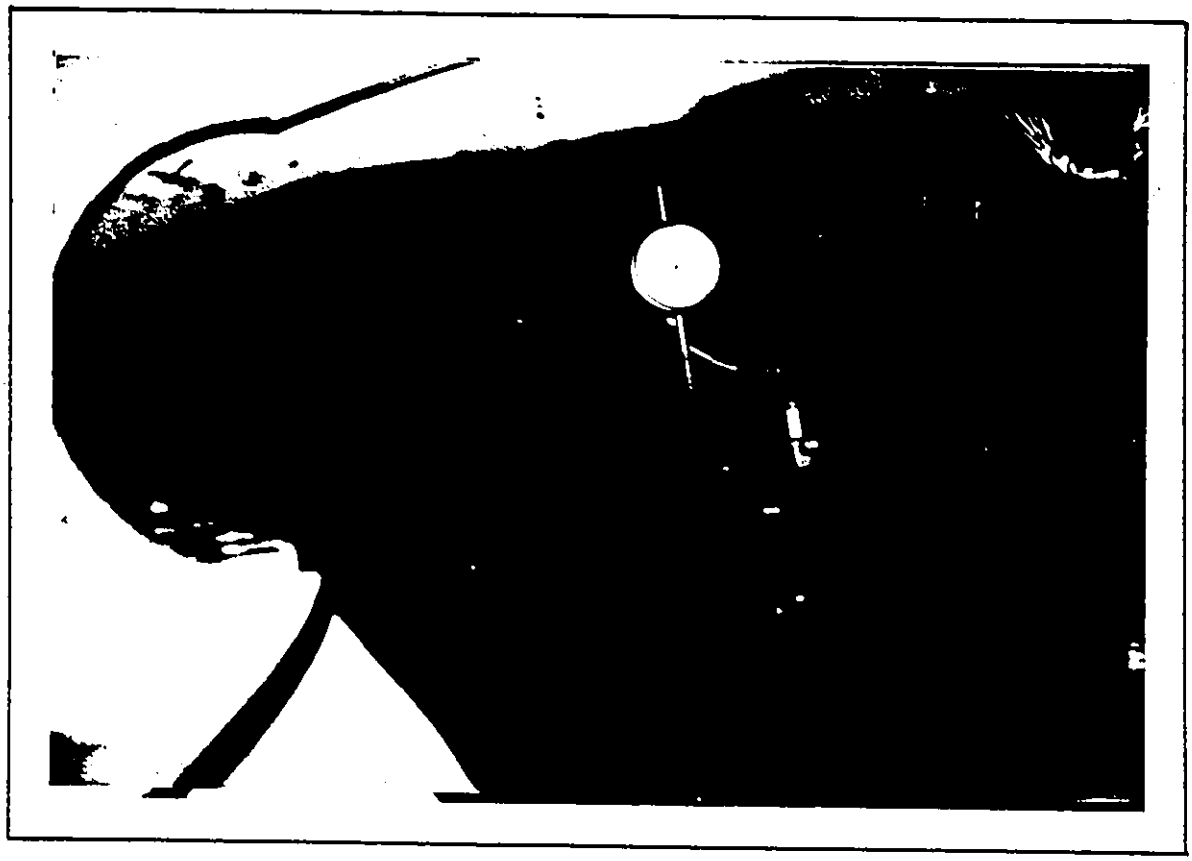

Figure 5.29: Initiation or Local Buckling of Central Non-stiffened Zone

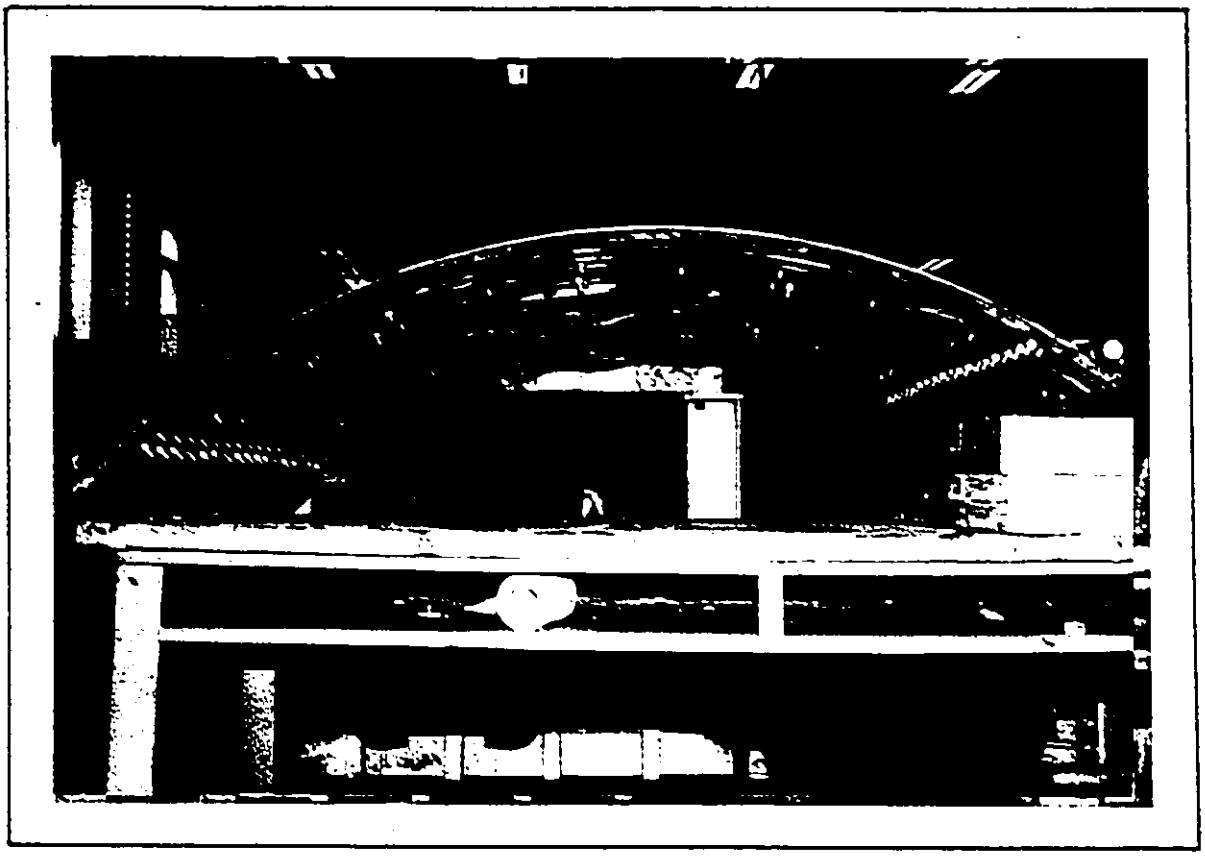

Figure 5.30: Post Buckling Failure of Stiffened Conduit

Appendix C

TABLES

Table 1.1: Ring Stiffness Factors For Various Installed Long Spans in the United States

Structure Location	Structure Type	Thickness of Shell in.	Stiffener and Spacing	Ring Stiffness *
Montrose County Colorado	31'-0"x10'-1" Low Profile Arch	0.218	31/2"x3"x5/16" @ 4'	0.5852
Sacramento County	23'-0"x14'-1" Horizontal Ellipse	0.138	3"x3"x1/4" @ 4'	1.0173
Willard Washington	33'-1"x12'-5" Low Profile Arch	0.218	3.5"x3.5"x5/16" @ 4'	0.5392
Mystic Creek Oregon	23'-9"x12'-1" High Profile Arch	0.280	3"x3"x1/4" @ 4'	1.1690
Tularosa New Mexico	22'-10"x14'-7" High Profile Arch	0.109	3.5"x3.5"x5/16" @ 4'	1.3977
Benton County Oregon	20'-10"x12'-2" Horizontal Ellipse	0.138	3"x3"x1/4" @ 4'	1.1037

* Ring Stiffness (EI/R^3) are based on considering full effectiveness of the stiffeners.

Table 3.1: Convergence Test -- Structure During Side Filling

Variable \ M	3	4	5	6	7
d_c	0.1457	0.1457	0.1457	0.1457	0.1457
$(N\theta)_c$	1.711	1.711	1.870	1.870	1.730
$(M\theta)_c$	18.63	18.63	18.76	18.76	18.71

Where,

d_c = crown deflection, in.

$(N\theta)_c$ = axial thrust at crown, lb/in.

$(M\theta)_c$ = bending moment at crown, lb.in/in.

Table 3.2: Convergence Test - Soil-Steel Structure Under Traffic Load

M / Variable	3	4	5	6	7
d_c	2.328E-3	2.328E-3	2.275E-3	2.275E-3	2.300E-3
d_s	-1.186E-3	-1.186E-3	-1.210E-3	-1.210E-3	-1.206E-3
T_c	- 5.455	- 5.455	- 5.484	- 5.484	- 5.467
T_s	- 8.747	- 8.747	- 8.773	- 8.773	- 8.771
M_c	2.207	2.207	2.001	2.001	2.149
M_s	- 2.035	- 2.031	- 2.160	- 2.161	- 2.137

Where,

d_c and d_s are deflections at crown and shoulder resply., in.

T_c and T_s are axial thrusts at crown and shoulder resply., lb/in.

M_c and M_s are moments at crown and shoulder resply., lb.in/in.

Table 4.1: White Ash Creek Structure - Measured Deflections and Axial Thrust Variation in the Conduit Axis Direction

No	Distance (ft) from central section	Deflection in.	Axial Thrust at the Shoulder		
			at #3 *	at #4 *	average
1	0.0	0.024	-294.87	-294.66	-294.76
2	1.0	0.022	-282.03	-246.51	-264.27
3	1.5	0.020	-297.87	-259.72	-278.83
4	2.5	0.0234	-267.80	-260.00	-263.90
5	3.5	0.0209	-266.41	-212.27	-239.34
6	4.0	0.0209	-240.09	-216.55	-228.32
7	5.0	0.0175	-195.48	-180.07	-187.78
8	6.5	0.014	-153.64	-133.53	-143.60
9	7.5	0.0109	-129.00	-116.84	-122.90
10	9.0	0.009	- 81.74	- 30.39	- 56.07
11	11.5	0.004	- 41.51	- 24.18	- 32.85

* These are the strain gage numbers as shown in Figure 4.3

Table 4.2: White Ash Creek Structure - Deflection Comparison for Load Level 2 and Position 1

Deflection at section	Number of trucks	Measured deflection *	Theoretical Deflection			
			Finite Strip Method*		Finite Element Method [43]	
				% diff.		% diff.
Central section	1	0.024	0.043	44	0.083	71
	2	0.044	0.058	24	0.104	58
West section	1	0.021	0.034	38	NA	NA
	2	0.038	0.055	31	NA	NA

* The deflection values are at the crown with respect to the bottom of the structure.

** The deflections are in inch. units

Table 4.3: Comparison of Experimental and Analytical Results in a Non-Stiffened Model Subjected to Horizontal Displacement d=0.05 in.

Variable		At location θ from the crown line						
		-30	-20	-10	0	10	20	30
Axial Thrust	Expt.	-0.40	-1.77	-5.32	-0.74	-5.59	-1.94	-1.94
	Theo.	-1.73	-1.53	-1.45	-1.56	-1.45	-1.53	-1.73
Bending Moment	Expt.	8.02	13.26	17.17	17.79	16.83	13.08	7.24
	Theo.	7.28	12.63	15.88	17.04	15.88	12.63	7.28
Deflect-ion	Expt.	0.04	0.07	—	0.12	0.11	0.08	—
	Theo.	0.056	0.102	0.130	0.140	0.130	0.102	0.056
Combined Stress	Expt.	-1479	-2465	-3248	-3277	-3045	-2436	-1363
	Theo.	-1367	-2346	-2941	-3156	-2941	-2346	-1367
% Difference in stress		7.5	4.8	9.5	3.7	3.4	3.7	0.3

Table 4.4: Comparison of Measured and Analytical Stresses in a Model With Corrugated Stiffeners Subjected to Horizontal Displacement d=0.05 in.

Gage Location *	Measured Stress (psi)	Average Measured stress	Analytical stress (psi)	% Error
1	-3609	-3609	-3163	12.35
2	2869	2869	3107	8.30
9	-3435	-3435	-3172	7.70
10	2898	2898	3098	6.90
39	3335	3335	3370	1.10
37	-4247	-4247	-4470	5.23
33	-3725	-4022	-4470	11.14
35	-4319			
34	2812	2827	3132	10.79
36	2841			
17	-5203	-5218	-5727	9.76
21	-5233			
25	5580	5602	6091	8.73
29	5623			

* The strain gage locations are shown in Figure 4.19

Table 4.5: Comparison of Measured and Analytical Deflections in a Soil-Steel Structure Model (P=500 lbs.)

A) Model Without Stiffeners

Load Type	Deflection at the central crown section		
	Measured	Analytical	% diff.
Uniform	0.009	0.003	67
Strip/Line	0.010	0.0071	29
Patch	0.027	0.015	44

B) Model with corrugated stiffeners

Load Type	Deflection at the central crown section		
	Measured	Analytical	% diff.
Uniform	0.005	0.002	60
Strip/Line	0.011	0.0053	52
Patch	0.014	0.0112	20

Note :- Deflections are in inches.

Table 5.1: Theoretical Effective Width Based on Extreme Fibre Stress

Obs. No.	α Deg.	R in.	Applied d_o	σ max psi	We in.	Stiffener Type
1	90	32.45	0.05	-5432	9.5	Corrugated sheet stiffeners
2	120	26.50	0.05	-3697	8.90	
3	45	196.00	0.10	-4795	26.55	
4	90	106.07	0.10	-2198	24.60	
5	30	289.78	0.10	-14740	42.90	
6	105	113.44	0.10	-2387	41.55	
7	120	103.92	0.10	-1456	40.30	
8	30	173.87	0.10	-27045	24.25	Tee-section stiffeners
9	60	150.00	0.10	-4543	24.70	
10	30	289.78	0.10	-21720	61.60	
11	60	150.00	0.10	-10249	58.13	
12	120	86.60	0.10	-4661	48.85	
13	60	150.00	0.10	-6140	34.85	I - section stiffeners
14	120	69.28	0.10	-4406	26.10	
15	30	347.73	0.05	-17806	69.00	
16	60	180.00	0.05	-8611	62.80	
17	120	103.92	0.05	-3800	56.00	

Table 5.2: Effective width of stiffener based on extreme fibre stress

$$w_p = 12.85(w)^{0.37}(f)^{0.72}\left(\frac{A}{S}\right)^{0.28}\left(\frac{\sin\alpha/2}{\alpha/2}\right)^{1.67}$$

Obs. No.	Stiffener Width w - in	Eccentricity of Stiffener f - in	Spacing of Stiffeners S - in	Radius of Shell R_t - in	Alfa α deg.	Actual Effective w_e	Predicted w_p	% Error $p=\frac{w_e-w_p}{w_e}\times 100$	Corrugation Profile	Stiffener Type
1	7	0.250	27	60.00	45	11.00	10.89	1.0	68mmx13mmx1.32mm	
2	7	0.250	27	26.50	120	8.90	8.67	2.6		
3	15	0.566	84	196.00	45	26.55	26.36	0.7	125mmx26mmx3.35mm	
4	15	0.566	84	106.07	90	24.60	23.62	4.0		
5	6	0.895	84	173.87	30	24.25	23.10	4.7	125mmx26mmx3.35mm	
6	6	0.895	84	150.00	60	24.70	25.40	-2.8		
7	24	1.092	108	121.24	120	40.30	41.05	-1.9	150mmx51mmx4.67mm	
8	24	1.092	108	113.44	105	41.55	41.90	-0.8		
9	24	1.092	108	289.78	30	42.90	47.88	-11.6		
10	6	1.403	84	150.00	60	34.85	35.10	-0.7	125mmx26mmx3.35mm	
11	6	1.403	84	69.28	120	26.10	27.00	-3.5		
12	10	2.182	108	289.78	30	61.60	57.01	7.5	150mmx51mmx4.67mm	
13	10	2.182	108	150.00	60	58.13	54.32	6.5		
14	10	2.182	108	86.60	120	48.85	44.48	8.9		
15	10	2.643	108	347.73	30	69.00	68.87	0.2	150mmx51mmx4.67mm	
16	10	2.643	108	180.00	60	62.80	65.63	-4.5		
17	10	2.643	108	103.92	120	56.00	53.73	4.0		

Table 5.3: Effective Width of Stiffener Based on Rigidity

No.	R_t in	α deg.	W in	S in	$\frac{I_s}{I_o} = \frac{\rho_s}{\rho_o}$	I_s/I_o Ratios by			Remarks
						I_{sum}/I_o	I_{eff}/I_o	I_{comb}/I_o	
1	210	60	24	108	2.61	1.21	2.51	2.95	
2	148.5	90	24	108	2.40	1.21	2.46	2.95	
3	132.35	105	24	108	2.30	1.21	2.42	2.95	shell with
4	196	45	15	84	2.37	1.18	2.30	2.83	corrugated sheet
5	106.1	90	15	84	2.29	1.18	2.23	2.83	stiffeners
6	94.54	105	15	84	2.12	1.18	2.20	2.83	
7	34.375	83.75	7	26.5	2.17	1.19	2.20	2.82	model
8	150	60	10	108	5.65	3.95	7.24	9.15	shell with
9	106.10	90	10	108	5.40	3.95	7.05	9.15	Tee-section
10	94.54	105	10	108	5.09	3.95	6.92	9.15	stiffener
11	34.375	83.75	4	26.5	8.02	6.42	9.27	11.28	model
12	117.59	45	6	84	7.02	6.06	10.46	12.62	shell with
13	90	60	6	84	6.98	6.06	10.38	12.62	I-beam
14	63.63	90	6	84	6.68	6.06	10.18	12.62	stiffener
15	56.72	105	6	84	6.48	6.06	10.04	12.62	

Table 5.4: Effect of Stiffener Spacing on Structure During Side filling. (soil-steel structure with thrust beams)

Variable		Structure Type			
		No stiff.	S = 9'	S = 6'	S = 3'
Stiffener material added		---	72%	70%	70%
Combined Stress at (psi.)	Unstiff. zone	1072	190	178	140
	% Reduction	---	82	83	87
	Stiffened zone	1072	597	480	375
	% Reduction	---	44	55	65
Crown Deflect. (Inch.)	δ	0.295	0.050	0.048	0.041
	% Reduction	---	83	84	86

R = 185 in.

α = 80°

P = 252 lb.

(Applied displacement constant along the longitudinal edge but applied force per strip is varying)

Table 5.5: Effect of Stiffener Spacing on Structure During Side filling. (soil-steel structure without thrust beams)

Variable		Structure Type			
		No stiff.	S = 9'	S = 6'	S = 3'
Stiffener material added		---	72%	70%	70%
Combined Stress at (psi.)	Unstiff. zone	1072	190	170	147
	% Reduction	---	82	84	86
	Stiffened zone	1072	596	473	376
	% Reduction	---	44	56	65
Crown Deflect. (Inch.)	δ	0.295	0.052	0.049	0.044
	% Reduction	---	82	83	85

R = 185 in.

α = 80°

P = 252 lb.

(Applied displacements are variable along the supports)

(Applied uniform horizontal force = 1.56 lb/in.)

Table 5.6: Experimental Effective Width of Stiffeners

I_o = Total M.I. of shell without stiffeners, in^4

I_s = Total M.I. of shell with stiffeners, in^4

P_o = Total measured horizontal force for shell without stiffeners, lbs.

P_s = Total measured horizontal force for shell with stiffeners, lbs.

Type of stiffener (1)	$\left(\frac{I_s}{I_o}\right) = \left(\frac{P_s}{P_o}\right)_{expt}$ (2)	$\left(\frac{I_s}{I_o}\right)_{sum}$ (3)	$\left(\frac{I_s}{I_o}\right)_{comb}$ (4)	Weff. in. (5)
Corrugated W = 7 in.	2.17	2.08	2.71	8.51
Tee-Section W = 4 in.	5.34	4.84	8.56	4.00

Where,

$\left(\frac{I_s}{I_o}\right)_{expt}$ = Experimental bending rigidity ratio

$\left(\frac{I_s}{I_o}\right)_{sum}$ = Ratio of bending rigidities obtained by summation of M.I. of individual elements.

$\left(\frac{I_s}{I_o}\right)_{comb}$ = Ratio of bending rigidities obtained by assuming full participation of shell and the stiffeners

Table 5.7: Deflection Comparison for Stiffened and Non-stiffened Shell During Side Filling

Case	Crown Deflection at			Remarks
	(1)	(2)	(3)	
Unstiffened shell	0.1438	0.1438	0.1438	Magnitude of Applied force is same Total P = 290 lb.
Stiffened (corrugated stiffener)	0.0634	0.0620	0.0632	
Stiffened with Tee stiffeners	0.0410	0.0382	0.0402	
Unstiffened shell	0.01438	0.1438	0.1438	Magnitude of applied displacement d_o is same, d_o = 0.05"
Stiffened (corrugated stiffener)	0.1440	0.1410	0.1435	
Stiffened with Tee stiffeners	0.1340	0.1257	0.1325	

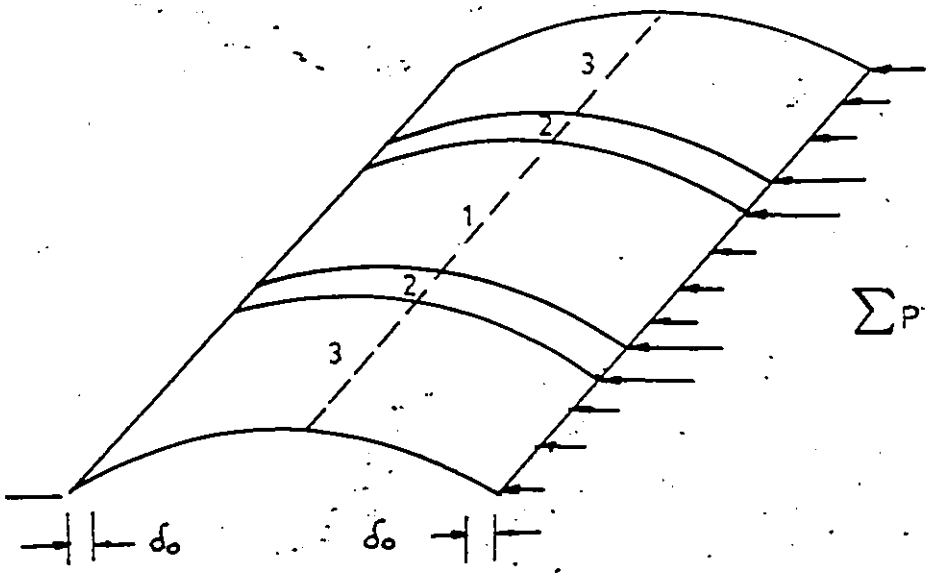

Table 5.8: Effect of Stiffener Spacing on the soil-steel structure under the patch loading.

Parameter		Structure Type			
		No stiff.	S = 9'	S = 6'	S = 3'
Combined stress @ haunch	psi.	-5470	-5340	-4800	-4350
	% drop	---	2.3	12.20	20.47
Axial thrust @ haunch	lb/in.	450	440	393	356
	% drop	---	2.2	12.7	20.9
Bending Moment @ crown	lb.in/in.	185.7	181.7	164.8	150.6
	% drop	---	2.15	11.25	18.9
Bending Moment @ haunch	lb.in/in.	-162.8	-159.2	-143.9	-130.8
	% drop	---	2.21	11.61	19.66
Crown Deflect.	inch.	0.115	0.1125	0.102	0.094
	% drop	---	2.2	11.3	18.26
Average % drop in above parameters		---	2.2	12.00	20.00

R = 185 in. Alfa = 80° Hc = 3 ft. q = 400 lb/ft²

S is the stiffener spacing.

Table 5.9: Reduction of unit forces and deflections in soil-steel structures with different stiffener spacing and radius

Radius R in.	Parameter	Stiffener Spacing (ft. c/c)		
		S = 9	S = 6	S = 3
185	T	0.980	0.870	0.790
	M_1	0.980	0.890	0.810
	M_2	0.980	0.880	0.800
	σ_{max}	0.980	0.880	0.800
	dc	0.980	0.890	0.820
150	T	0.986	0.910	0.770
	M_1	0.983	0.920	0.790
	M_2	0.986	0.910	0.740
	σ_{max}	0.987	0.920	0.779
	dc	0.985	0.900	0.730
120	T	0.997	0.900	0.740
	M_1	0.997	0.940	0.680
	M_2	0.995	0.930	0.660
	σ_{max}	0.999	0.940	0.740
	dc	0.999	0.950	0.730

* T = axial thrust
M_1 = maximum bending moment at crown (+ve)
M_2 = maximum bending moment at haunch (-ve)
σ_{max} = maximum combined stress
dc = crown deflection

** The values of all parameters are considered unity when no stiffeners are provided.

Appendix D

EQUIVALENT STIFFNESS OF SPRINGS

Since the surrounding soil medium has been replaced by the set of equivalent radial and tangential springs with coefficients Kn and Ks respectively, the axial stiffness of each spring (EA)sp has to be expressed in terms of the soil properties (mainly Kn and Ks).

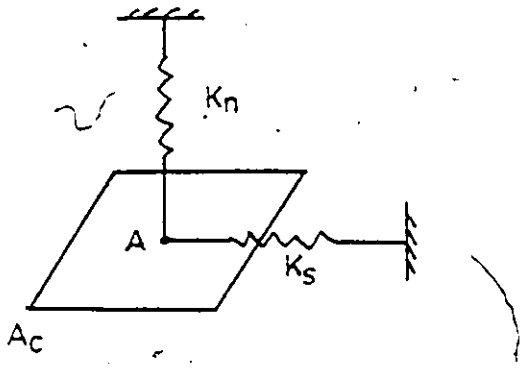

Let Ac be the shell surface area on which the radial and tangential springs of arbitrary length l_i, with modulus of elasticity Es and area of cross section As, are acting at a point A. If a point A undergoes radial (d_w) and tangential (d_v) displacements, the radial and tangential forces acting at A are given by:

$$F_{rad} = Kn\, d_w\, Ac \qquad [D-1]$$

$$F_{tgt} = Ks\, d_v\, Ac \qquad [D-2]$$

Similarly, the axial strains in radial and tangential springs are given by:

$$\delta_{rad} = \frac{d_w}{l_i} = \frac{F_{rad}}{(EA)_{sp}}, \text{ and} \qquad [D-3]$$

$$\delta_{tgt} = \frac{d_v}{l_i} = \frac{F_{tgt}}{(EA)_{sp}} \qquad [D-4]$$

Equating Eq. D-1 with D-3 and D-2 with D-4, the expression for equivalent stiffness of springs can be obtained as shown below.

$$(EA)_{rad} = Kn\, Ac\, l_i \qquad [D-5]$$

or,

$$\left(\frac{EA}{l_i}\right)_{rad} = Kn\, Ac, \text{ and} \qquad [D-6]$$

$$(EA)_{tgt} = Ks\, Ac\, l_i \qquad [D-7]$$

or,

$$\left(\frac{EA}{l_i}\right)_{tgt} = Ks\, Ac \qquad [D-8]$$

Appendix E

CONSISTENT LOAD VECTOR CALCULATIONS

Herein, the use of Eq. 3.45, in calculating the consistent load matrix is demonstrated for the case of uniform vertical load, q, per unit area.

The vertical load, q, can be split into two components, radial (q_w) and tangential (q_o) (Figure 3.18), as given below,

$$q_w = q \cos^2(\alpha/2-\theta)$$

$$q_o = -q \sin(\alpha/2-\theta) \cos(\alpha/2-\theta) \qquad [E-1]$$

Substituting Eq. [E-1] in Eq. 3.45, the following consistent load matrix $\{ P_S \}$ is obtained.

$$\{ P_S \} = \begin{Bmatrix} 0 \\ 0 \\ 0.5\ b\ q\ Qvm \\ (1/12)\ b^2\ q\ Qvm \\ 0.5\ b\ q\ Qwm \\ (1/12)\ b^2\ q\ Qwm \\ 0 \\ 0 \\ 0.5\ b\ q\ Qvm \\ -(1/12)\ b^2\ q\ Qvm \\ 0.5\ b\ q\ Qwm \\ -(1/12)\ b^2\ q\ Qwm \end{Bmatrix} \qquad [E-2]$$

These load vectors are corresponding to the displacement coefficients

$$\{d_i^{(m)}\}^T = \{u_{1m}\ u_{x1m}\ v_{1m}\ v_{x1m}\ w_{1m}\ w_{x1m}\ u_{2m}\ u_{x2m}\ v_{2m}\ v_{x2m}\ w_{2m}\ w_{x2m}\} \qquad [E-3]$$

Where,

$$Q_{vm} = -\frac{1}{2}\left[T_2 \sin(\alpha) - T_3 \cos(\alpha) \right]$$

$$Q_{wm} = \frac{1}{2}\left[T_1 + T_2\cos(\alpha) + T_3\sin(\alpha) - \frac{F}{R}\left(\frac{m\pi}{\alpha}\right)\left\{T_4\sin(\alpha) - T_5\cos(\alpha)\right\}\right] \qquad [E-4]$$

and

$$T_1 = R\int_0^{\alpha} \sin\left(\frac{m\pi\theta}{\alpha}\right)d\theta$$

$$T_2 = R\int_0^{\alpha} \sin\left(\frac{m\pi\theta}{\alpha}\right)\cos(2\theta)\ d\theta$$

$$T_3 = R\int_0^{\alpha} \sin\left(\frac{m\pi\theta}{\alpha}\right)\sin(2\theta)\ d\theta \qquad [E-5]$$

$$T_4 = R\int_0^{\alpha} \cos\left(\frac{m\pi\theta}{\alpha}\right)\cos(2\theta)\ d\theta$$

$$T_5 = R\int_0^{\alpha} \cos\left(\frac{m\pi\theta}{\alpha}\right)\sin(2\theta)\ d\theta$$

Similar equivalent load vectors or the consistent load matrix can be derived for various types of loads.

Appendix F

STIFFNESS MATRIX FORMULATION

A) Shell Strip

The elements of shell strip stiffness matrix are given by

$$[S_{ij}]_{mn} = \int [B]_m^T [D] [B]_n d(\text{area}) \qquad [F-1]$$

where,

[B] = strain matrix (6x12)

$$= \begin{bmatrix} B_{11} & B_{12} & \cdots & B_{1\,12} \\ B_{21} & B_{22} & \cdots & B_{2\,12} \\ \cdot & & & \\ \cdot & & & \\ B_{61} & B_{62} & \cdots & B_{6\,12} \end{bmatrix} \qquad [F-2]$$

[D] = rigidity matrix (6x6)

$$= \begin{bmatrix} [D_p] & [0] \\ [0] & [D_b] \end{bmatrix} \qquad [F-3]$$

$$[D_p] = \begin{bmatrix} D_x & 0 & 0 \\ 0 & D_\theta & 0 \\ 0 & 0 & D_{x\theta} \end{bmatrix} \qquad [F-4]$$

$$[D_b] = \begin{bmatrix} B_x & 0 & 0 \\ 0 & B_\theta & 0 \\ 0 & 0 & B_{x\theta} \end{bmatrix} \qquad [F-5]$$

Eq. [F-1] can further be simplified and written in the following form:

$$[S_{ij}]_{mn} = D_x \int_0^\alpha \int_0^b (B_{1i})_m (B_{ij})_n R\,dx\,d\theta + D_\theta \int_0^\alpha \int_0^b (B_{2i})_m (B_{2j})_n R\,dx\,d\theta + D_{x\theta} \int_0^\alpha \int_0^\alpha (B_{3i})_m (B_{3j})_n R\,dx\,d\theta + B_x \int_0^\alpha \int_0^b (B_{4i})_m (B_{4j})_n R\,dx\,d\theta + B_\theta \int_0^\alpha \int_0^b (B_{5i})_m (B_{5j})_n R\,dx\,d\theta + B_{x\theta} \int_0^\alpha \int_0^b (B_{6i})_m (B_{6j})_n R\,dx\,d\theta \qquad \begin{Bmatrix} j = 1, 12 \\ j = 1, 12 \end{Bmatrix} \qquad [F\text{-}6]$$

Substituting the expressions for B_{ki} and B_{kj} (where k = 1, 6), in Eq. [F-6] and performing the indicated integrals, following stiffness elements are obtained for given values of m and n.

$$S_{11} = 1.2\, D_x \frac{T_1}{b} + \frac{13}{35} D_{x\theta}\, T_2 \frac{b}{R^2}$$

$$S_{12} = \frac{1}{10} D_x\, T_1 + \frac{11}{210} D_{x\theta}\, T_2 \frac{b^2}{R^2} = S_{21}$$

$$S_{13} = -\frac{1}{2} D_{x\theta} \frac{T_7}{R} \qquad S_{31} = -\frac{1}{2} D_{x\theta} \frac{T_7 b}{R}$$

$$S_{14} = \frac{1}{10} D_{x\theta}\, T_7 \frac{b}{R} \qquad S_{41} = \frac{1}{10} D_{x\theta}\, T_7 b \frac{b}{R}$$

$$S_{15} = -\frac{1}{2} D_{x\theta}\, C_F \frac{T_2}{R} = S_{51}$$

$$S_{16} = \frac{1}{10} D_{x\theta}\, C_F\, T_2 \frac{b}{R} = S_{61}$$

$$S_{17} = -1.2\, D_x \frac{T_1}{b} + \frac{9}{70} D_{x\theta} T_2 \frac{b}{R^2} = S_{71}$$

$$S_{18} = \frac{1}{10} D_x T_1 - \frac{13}{420} D_{x\theta} T_2 \frac{b^2}{R^2} = S_{81}$$

$$S_{19} = -S_{13} \qquad S_{91} = -S_{31} \qquad S_{1,10} = -S_{1,4} \qquad S_{10,1} = -S_{4,1}$$

$$S_{1,11} = \frac{1}{2} D_{x\theta} C_F \frac{T_2}{R} = S_{11,1}$$

$$S_{1,12} = -\frac{1}{10} D_{x\theta} C_F T_2 \frac{b}{R} = S_{12,1}$$

$$S_{22} = \frac{2}{15} D_x T_1 b + \frac{1}{105} D_{x\theta} T_2 \frac{b^3}{R^2}$$

$$S_{23} = -\frac{1}{10} D_{x\theta} T_7 \frac{b}{R} \qquad S_{32} = -\frac{1}{10} D_{x\theta} T_{7b} \frac{b}{R}$$

$$S_{24} = S_{42} = S_{26} = S_{62} = 0$$

$$S_{25} = -\frac{1}{10} D_{x\theta} C_F T_2 \frac{b}{R} = S_{52}$$

$$S_{27} = -S_{18}$$

$$S_{28} = -\frac{1}{30} D_x T_1 b - \frac{1}{140} D_{x\theta} T_2 \frac{b^3}{R^2} = S_{82}$$

$$S_{29} = S_{14} \qquad S_{92} = S_{41}$$

$$S_{2,10} = -\frac{1}{60} D_{x\theta} T_7 \frac{b^2}{R} \qquad S_{10,2} = -\frac{1}{60} D_{x\theta} T_{7b} \frac{b^2}{R}$$

$$S_{2,11} = S_{11,2} = S_{16}$$

$$S_{2,12} = -\frac{1}{60} D_{x\theta} C_F T_2 \frac{b^2}{R} = S_{12,2}$$

$$S_{33} = \frac{13}{35} D_\theta T_6 \frac{b}{R^2} + 1.2\, D_{x\theta} \frac{T_5}{b} + \frac{13}{35} B_\theta T_6 \frac{b}{R^4} + 1.2\, B_{x\theta} \frac{T_5}{R^2 b}$$

$$S_{34} = \frac{11}{210} D_\theta T_6 \frac{b^2}{R^2} + \frac{1}{10} D_{x\theta} T_5 + \frac{11}{210} B_\theta T_6 \frac{b^2}{R^4} + \frac{1}{10} D_{x\theta} \frac{T_5}{R^2}$$

$$S_{43} = S_{34}$$

$$S_{35} = \frac{13}{35} D_\theta T_8 \frac{b}{R^2} + 1.2 D_{x\theta} C_F \frac{T_{7b}}{b} + \frac{13}{35} B_\theta C_T T_9 \frac{b}{R^4} + 1.2 B_{x\theta} C_T \frac{T_{7b}}{R^2 b}$$

$$S_{53} = \frac{13}{35} D_\theta T_{8b} \frac{b}{R^2} + 1.2 D_{x\theta} C_F \frac{T_7}{b} + \frac{13}{35} B_\theta C_T T_{9b} \frac{b}{R^4} + 1.2 B_{x\theta} C_T \frac{T_7}{R^2 b}$$

$$S_{36} = \frac{11}{210} D_\theta T_8 \frac{b^2}{R^2} + \frac{1}{10} D_{x\theta} C_F T_{7b} + \frac{11}{210} B_\theta C_T T_9 \frac{b^2}{R^4} + \frac{1}{10} B_{x\theta} C_T \frac{T_{7b}}{R^2}$$

$$S_{63} = \frac{11}{210} D_\theta T_{8b} \frac{b^2}{R^2} + \frac{1}{10} D_{x\theta} C_F T_7 + \frac{11}{210} B_\theta C_T T_{9b} \frac{b^2}{R^4} + \frac{1}{10} B_{x\theta} C_T \frac{T_7}{R^2}$$

$$S_{37} = S_{31}, \quad S_{73} = S_{13}, \quad S_{38} = S_{41}, \quad S_{83} = S_{14}$$

$$S_{39} = \frac{9}{70} D_\theta T_6 \frac{b}{R^2} - 1.2 D_{x\theta} \frac{T_5}{b} + \frac{9}{70} B_\theta T_6 \frac{b}{R^4} - 1.2 B_{x\theta} \frac{T_5}{R^2 b}$$

$$S_{93} = S_{39}$$

$$S_{3,10} = -\frac{13}{420} D_\theta T_6 \frac{b^2}{R^2} + \frac{1}{10} D_{x\theta} T_5 - \frac{13}{420} B_\theta T_6 \frac{b^2}{R^4} + \frac{1}{10} B_{x\theta} \frac{T_5}{R^2}$$

$$S_{10,3} = S_{3,10}$$

$$S_{3,11} = \frac{9}{70} D_\theta T_8 \frac{b}{R^2} - 1.2 D_{x\theta} C_F \frac{T_{7b}}{b} + \frac{9}{70} B_\theta C_T T_9 \frac{b}{R^4} - 1.2 B_{x\theta} C_T \frac{T_{7b}}{R^2 b}$$

$$S_{11,3} = \frac{9}{70} D_\theta T_{8b} \frac{b}{R^2} - 1.2 D_{x\theta} C_F \frac{T_7}{b} + \frac{9}{70} B_\theta C_T T_{9b} \frac{b}{R^4} - 1.2 B_{x\theta} C_T \frac{T_7}{R^2 b}$$

$$S_{3,12} = -\frac{13}{420} D_\theta T_8 \frac{b^2}{R^2} + \frac{1}{10} D_{x\theta} C_F T_{7b} - \frac{13}{420} B_\theta C_T T_9 \frac{b^2}{R^4} + \frac{1}{10} B_{x\theta} C_T \frac{T_{7b}}{R^2}$$

$$S_{12,3} = -\frac{13}{420} D_\theta T_{8b} \frac{b^2}{R^2} + \frac{1}{10} D_{x\theta} C_F T_7 - \frac{13}{420} B_\theta C_T T_{9b} \frac{b^2}{R^4} + \frac{1}{10} B_{x\theta} C_T \frac{T_7}{R^2}$$

$$S_{44} = \frac{1}{105} D_\theta T_6 \frac{b^3}{R^2} + \frac{2}{15} D_{x\theta} T_5 b + \frac{1}{105} B_\theta T_6 \frac{b^3}{R^4} + \frac{2}{15} B_{x\theta} T_5 \frac{b}{R^2}$$

$$S_{45} = S_{36} \quad , \qquad S_{54} = S_{63}$$

$$S_{46} = \frac{1}{105} D_\theta T_8 \frac{b^3}{R^2} + \frac{2}{15} D_{x\theta} C_F T_{7b} b + \frac{1}{105} B_\theta C_T T_9 \frac{b^3}{R^4} + \frac{2}{15} B_{x\theta} C_T T_{7b} \frac{b}{R^2}$$

$$S_{64} = \frac{1}{105} D_\theta T_{8b} \frac{b^3}{R^2} + \frac{2}{15} D_{x\theta} C_F T_7 b + \frac{1}{105} B_\theta C_T T_{9b} \frac{b^3}{R^4} + \frac{2}{15} B_{x\theta} C_T T_7 \frac{b}{R^2}$$

$$S_{47} = -S_{41} \quad , \quad S_{74} = -S_{14} \quad , \quad S_{48} = -S_{10,2} \quad , \quad S_{84} = -S_{2,10}$$

$$S_{49} = -S_{3,10} \quad , \quad S_{94} = S_{49}$$

$$S_{4,10} = -\frac{1}{140} D_\theta T_6 \frac{b^3}{R^2} - \frac{1}{30} D_{x\theta} T_5 b - \frac{1}{140} B_\theta T_6 \frac{b^3}{R^4} - \frac{1}{30} B_{x\theta} T_5 \frac{b}{R^2}$$

$$S_{10,4} = S_{4,10} \quad , \quad S_{4,11} = -S_{3,12} \quad , \quad S_{11,4} = -S_{12,3}$$

$$S_{4,12} = -\frac{1}{140} D_\theta T_8 \frac{b^3}{R^2} - \frac{1}{30} D_{x\theta} C_F T_{7b} b - \frac{1}{140} B_\theta C_T T_9 \frac{b^3}{R^4}$$
$$- \frac{1}{30} B_{x\theta} C_T T_{7b} \frac{b}{R^2}$$

$$S_{12,4} = -\frac{1}{140} D_\theta T_{8b} \frac{b^3}{R^2} - \frac{1}{30} D_{x\theta} C_F T_7 b - \frac{1}{140} B_\theta C_T T_{9b} \frac{b^3}{R^4}$$
$$- \frac{1}{30} B_{x\theta} C_T T_7 \frac{b}{R^2}$$

$$S_{55} = \frac{13}{35} D_\theta T_4 \frac{b}{R^2} + 1.2 D_{x\theta} C_F^2 \frac{T_2}{b} + 12 B_x \frac{T_1}{b^3} + \frac{13}{35} B_\theta C_T^2 T_3 \frac{b}{R^4}$$
$$+ 1.2 B_{x\theta} C_T^2 \frac{T_2}{R^2 b}$$

$$S_{56} = \frac{11}{210} D_\theta T_4 \frac{b^2}{R^2} + \frac{1}{10} D_{x\theta} C_F^2 T_2 + 6 B_x \frac{T_1}{b^2} + \frac{11}{210} B_\theta C_T^2 T_3 \frac{b^2}{R^4}$$
$$+ \frac{1}{10} B_{x\theta} C_T^2 \frac{T_2}{R^2}$$

$$S_{65} = S_{56}$$

$$S_{57} = -\frac{1}{2} D_{x\theta} C_F \frac{T_2}{R} \quad , \quad S_{75} = S_{57}$$

$$S_{58} = S_{2,11} \; , \quad S_{85} = S_{58} \; , \quad S_{59} = S_{11,3} \; , \quad S_{95} = S_{3,11}$$

$$S_{5,10} = S_{12,3} \; , \quad S_{10,5} = S_{3,12}$$

$$S_{5,11} = \frac{9}{70} D_\theta T_4 \frac{b}{R^2} - 1.2 D_{x\theta} C_F^2 \frac{T_2}{b} - 12 B_x \frac{T_1}{b^3} + \frac{9}{70} B_\theta C_T^2 T_3 \frac{b}{R^4}$$

$$- 1.2 B_{x\theta} C_T^2 \frac{T_2}{R^2 b}$$

$$S_{11,5} = S_{5,11}$$

$$S_{5,12} = -\frac{13}{420} D_\theta T_4 \frac{b^2}{R^2} + \frac{1}{10} D_{x\theta} C_F^2 T_2 + 6 B_x \frac{T_1}{b^2} - \frac{13}{420} B_\theta C_T^2 T_3 \frac{b^2}{R^4}$$

$$+ \frac{1}{10} B_{x\theta} C_T^2 \frac{T_2}{R^2}$$

$$S_{12,5} = S_{5,12}$$

$$S_{66} = \frac{1}{105} D_\theta T_4 \frac{b^3}{R^2} + \frac{2}{15} D_{x\theta} C_F^2 T_2 b + 4 B_x \frac{T_1}{b} + \frac{1}{105} B_\theta C_T^2 T_3 \frac{b^3}{R^4}$$

$$+ \frac{2}{15} B_{x\theta} C_T^2 T_2 \frac{b}{R^2}$$

$$S_{67} = -S_{16} \; , \quad S_{76} = S_{67} \; , \quad S_{68} = -S_{2,12} \; , \quad S_{86} = S_{68} \; , \quad S_{69} = -S_{12,3}$$

$$S_{96} = -S_{3,12} \; , \quad S_{6,10} = S_{12,4} \; , \quad S_{10,6} = S_{4,12} \; , \quad S_{6,11} = -S_{5,12}$$

$$S_{11,6} = S_{6,11}$$

$$S_{6,12} = -\frac{1}{140} D_\theta T_4 \frac{b^3}{R^2} - \frac{1}{30} D_{x\theta} C_F^2 T_2 b + 2 B_x \frac{T_1}{b} - \frac{1}{140} B_\theta C_T^2 T_3 \frac{b^3}{R^4}$$

$$- \frac{1}{30} B_{x\theta} C_T^2 T_2 \frac{b}{R^2}$$

$$S_{12,6} = S_{6,12}\,, \quad S_{77} = S_{11}\,, \quad S_{78} = -S_{12}\,, \quad S_{87} = S_{78}$$

$$S_{79} = -S_{13}\,, \quad S_{97} = -S_{31}\,, \quad S_{7,10} = S_{14}\,, \quad S_{10,7} = S_{41}$$

$$S_{7,11} = S_{1,11}\,, \quad S_{11,7} = S_{7,11}\,, \quad S_{7,12} = -S_{1,12}\,, \quad S_{12,7} = S_{7,12}$$

$$S_{88} = S_{22}\,, \quad S_{89} = -S_{14}\,, \quad S_{98} = -S_{41}\,, \quad S_{8,10} = S_{10,8} = 0$$

$$S_{8,11} = S_{1,12}\,, \quad S_{11,8} = S_{8,11}\,, \quad S_{8,12} = S_{12,8} = 0$$

$$S_{99} = S_{33}\,, \quad S_{9,10} = -S_{34}\,, \quad S_{10,9} = S_{9,10}$$

$$S_{9,11} = S_{35}\,, \quad S_{11,9} = S_{53}\,, \quad S_{9,12} = -S_{36}\,, \quad S_{12,9} = -S_{63}$$

$$S_{10,10} = S_{44}\,, \quad S_{10,11} = -S_{36}\,, \quad S_{11,10} = -S_{63}$$

$$S_{10,12} = S_{46}\,, \quad S_{12,10} = S_{64}\,, \quad S_{11,11} = S_{55}$$

$$S_{11,12} = -S_{56}\,, \quad S_{12,11} = S_{11,12}\,, \quad S_{12,12} = S_{66}$$

where

$$C_F = F/R$$

$$C_T = (1 + C_F)$$

and

$$\left.\begin{aligned} T_1 &= R\int_o^\alpha \phi_m\,\phi_n\,d\theta \\ T_2 &= R\int_o^\alpha \phi_m'\,\phi_n'\,d\theta \\ T_3 &= R\int_o^\alpha \phi_m''\,\phi_n''\,d\theta \\ T_4 &= R\int_o^\alpha \phi_{ms}\,\phi_{ns}\,d\theta \end{aligned}\right\} \text{orthogonal}$$

$$T_5 = R\int_o^\alpha \phi_{vm}\,\phi_{vn}\,d\theta$$

$$T_6 = R\int_0^\alpha \phi'_{vm}\,\phi'_{vn}\,d\theta$$

$$T_7 = R\int_0^\alpha \phi'_{m}\,\phi_{vn}\,d\theta$$

$$T_{7b} = R\int_0^\alpha \phi_{vm}\,\phi'_{n}\,d\theta$$

$$T_8 = R\int_0^\alpha \phi'_{vm}\,\phi_{ns}\,d\theta \qquad \text{[F-7]}$$

$$T_{8b} = R\int_0^\alpha \phi_{ms}\,\phi'_{vn}\,d\theta$$

$$T_9 = R\int_0^\alpha \phi'_{vm}\,\phi''_{n}\,d\theta$$

$$T_{9b} = R\int_0^\alpha \phi''_{m}\,\phi'_{vn}\,d\theta$$

in which

$$\left.\begin{aligned} \phi_m &= \phi_u^{(m)}(\theta) = \phi_w^{(m)}(\theta), \quad \phi_{ms} = C_F\phi''_m - \phi_m \\ \phi_n &= \phi_u^{(n)}(\theta) = \phi_w^{(n)}(\theta), \quad \phi_{ns} = C_F\phi''_n - \phi_n \\ \phi_{vm} &= \phi_v^{(m)}(\theta), \quad \phi_{vn} = \phi_v^{(n)}(\theta) \end{aligned}\right\} \qquad \text{[F-8]}$$

and ϕ'_m and ϕ''_m indicate first and second derivative of the basic function w.r. to θ.

Thus, using appropriate basic functions (Eq. 3.8 or 3.16) the stiffness matrix for the shell strip can be derived for m and n values of fourier series terms.

The overall stiffness matrix for a shell strip is given by

$$[S] = \begin{bmatrix} [S]_{11} & [S]_{12} & [S]_{13} & \cdots & [S]_{1n} \\ [S]_{21} & [S]_{22} & [S]_{23} & \cdots & [S]_{2n} \\ \vdots & \vdots & \vdots & \cdots & \vdots \\ [S]_{m1} & [S]_{m2} & [S]_{m3} & \cdots & [S]_{mn} \end{bmatrix} \qquad [F-9]$$

The integrals of equation [F-7] indicate that the odd and even values of m and n are decoupled, and therefore can be written as follows

$$[S]_{m\&n\ odd} = \begin{bmatrix} [S]_{11} & [S]_{13} & [S]_{15} & \cdots \\ [S]_{31} & [S]_{33} & [S]_{35} & \cdots \\ [S]_{51} & [S]_{53} & [S]_{55} & \cdots \\ \vdots & \vdots & \vdots & \end{bmatrix} \qquad [F-10]$$

and

$$[S]_{m\&n\ even} = \begin{bmatrix} [S]_{22} & [S]_{24} & [S]_{26} & \cdots \\ [S]_{42} & [S]_{44} & [S]_{46} & \cdots \\ [S]_{62} & [S]_{64} & [S]_{66} & \cdots \\ \vdots & \vdots & \vdots & \end{bmatrix} \qquad [F-11]$$

B) Element Stiffness Matrix for Spring Elements

Following the similar approach, the element stiffness matrix for normal and tangential springs can be written as follows.

a) i^{th} normal spring

$$[S]^i_{mn} = \left(\frac{EA}{\ell}\right)^i_{eq} \phi_w^{(m)}(\theta_i)\phi_w^{(n)}(\theta_i) \begin{bmatrix} K_{11} & K_{12} & K_{13} & K_{14} \\ & K_{22} & K_{23} & K_{24} \\ & & K_{33} & K_{34} \\ \text{(symmetric)} & & & K_{44} \end{bmatrix} \qquad [F-12]$$

corresponding to out-of-plane displacement coefficients.

b) i^{th} tangential spring

$$[S]^i_{mn} = [E_p]^i_{mn} + [E_w]^i_{mn} \qquad [F\text{-}13]$$

where $[E_p]^i_{mn}$ = stiffness matrix corresponding to in-plane displacement coefficients

$$= \left(\frac{EA}{\ell}\right)^i_{eq} \phi_v^{(m)}(\theta_i)\phi_v^{(n)}(\theta_i) \begin{bmatrix} K_{11} & K_{12} & K_{13} & K_{14} \\ & K_{22} & K_{23} & K_{24} \\ & & K_{33} & K_{34} \\ \text{(symmetric)} & & & K_{44} \end{bmatrix} \qquad [F\text{-}14]$$

$[E_w]^i_{mn}$ = stiffness matrix corresponding to out-of-plane displacement coefficients

$$= \left(\frac{EA}{\ell}\right)^i_{eq} C_F^2 \phi_w^{'(n)}(\theta_i)\phi_w^{'(n)}(\theta_i) \begin{bmatrix} K_{11} & K_{12} & K_{13} & K_{14} \\ & K_{22} & K_{23} & K_{24} \\ & & K_{33} & K_{34} \\ \text{(symmetric)} & & & K_{44} \end{bmatrix} \qquad [F\text{-}15]$$

where $\left(\frac{EA}{\ell}\right)^i_{eq}$ are the equivalent axial stiffness of i^{th} normal or tangential springs as given in Appendix D and

$$K_{pq} = F_p(\eta_i)F_q(\eta_i) \qquad [F\text{-}16]$$

p and q have values from 1 to 4.

$F_p(\eta_i)$ and $F_q(\eta_i)$ are the values of interpolation polynomials (Eq. 3.3) at i^{th} spring location on a shell strip.

Appendix G

FLOW CHARTS

NEWSOIL:- Flow chart for a program to analyse a soil-steel structure under traffic loads.

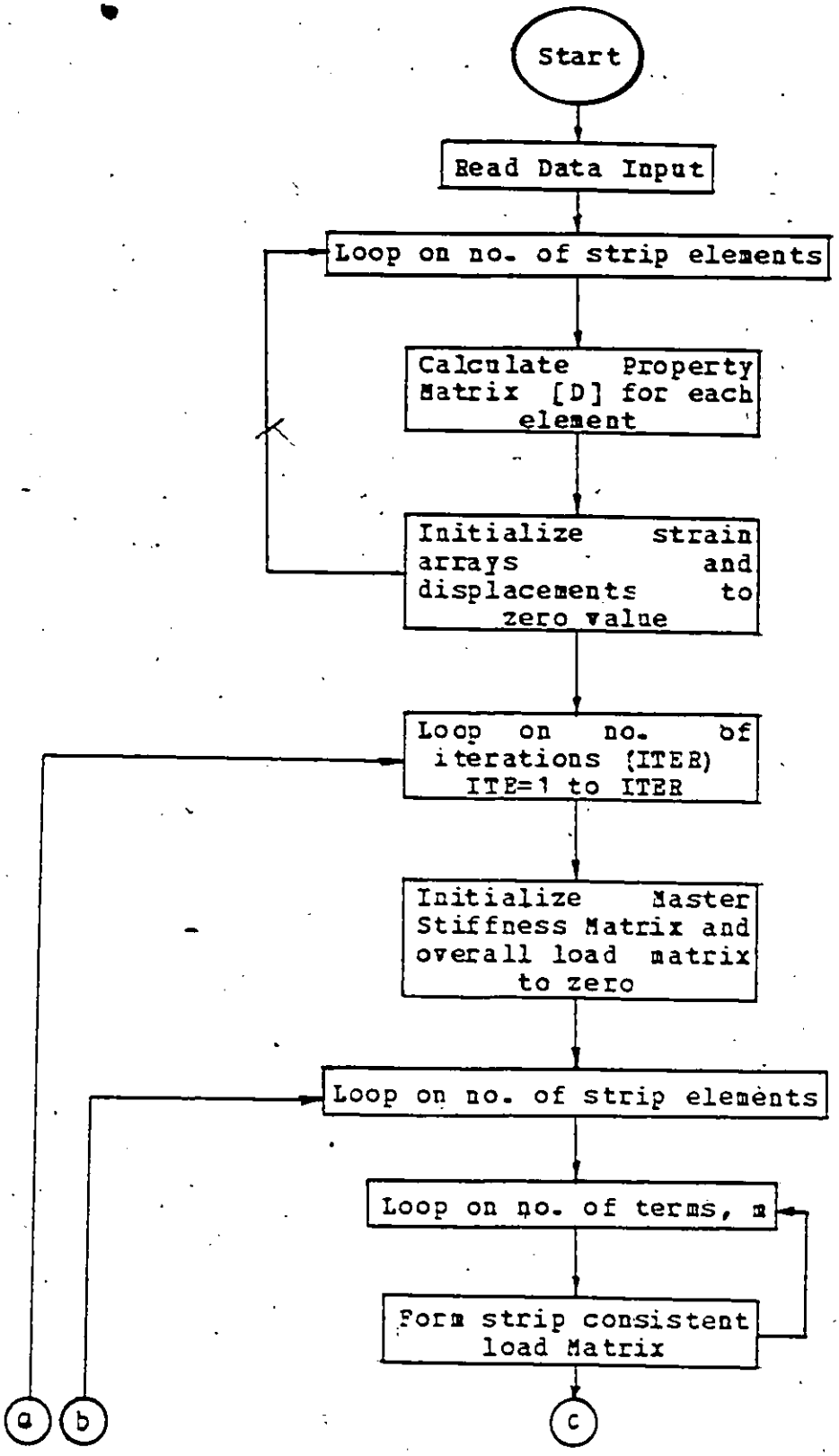

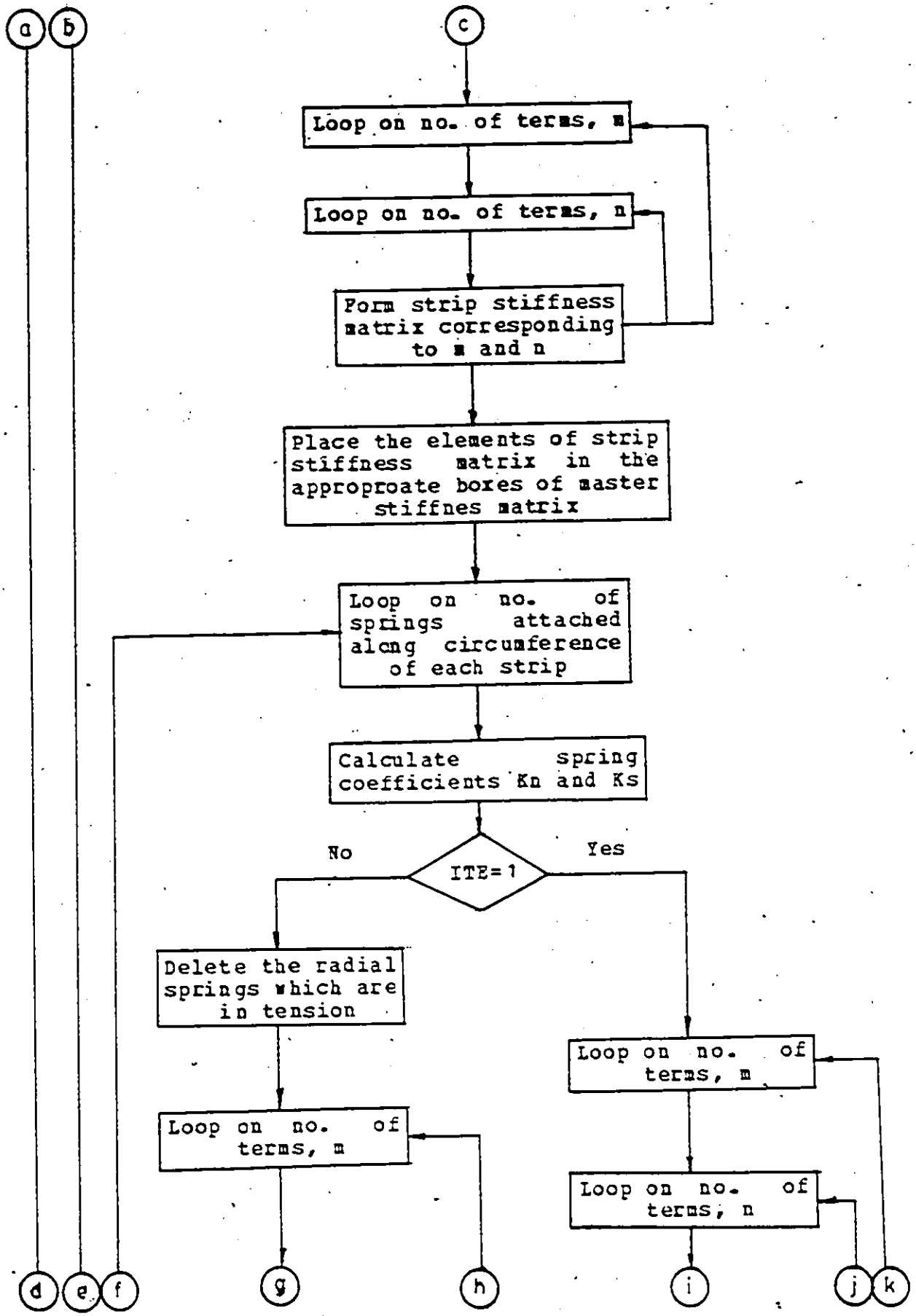
a
b
c
Loop on no. of terms, m
Loop on no. of terms, n
Form strip stiffness matrix corresponding to m and n
Place the elements of strip stiffness matrix in the approproate boxes of master stiffnes matrix
Loop on no. of springs attached alcng circumference of each strip
Calculate spring coefficients Kn and Ks
No
ITE=1
Yes
Delete the radial springs which are in tension
Loop on no. of terms, m
Loop on no. of terms, m
Loop on no. of terms, n
d
e
f
g
h
i
j
k

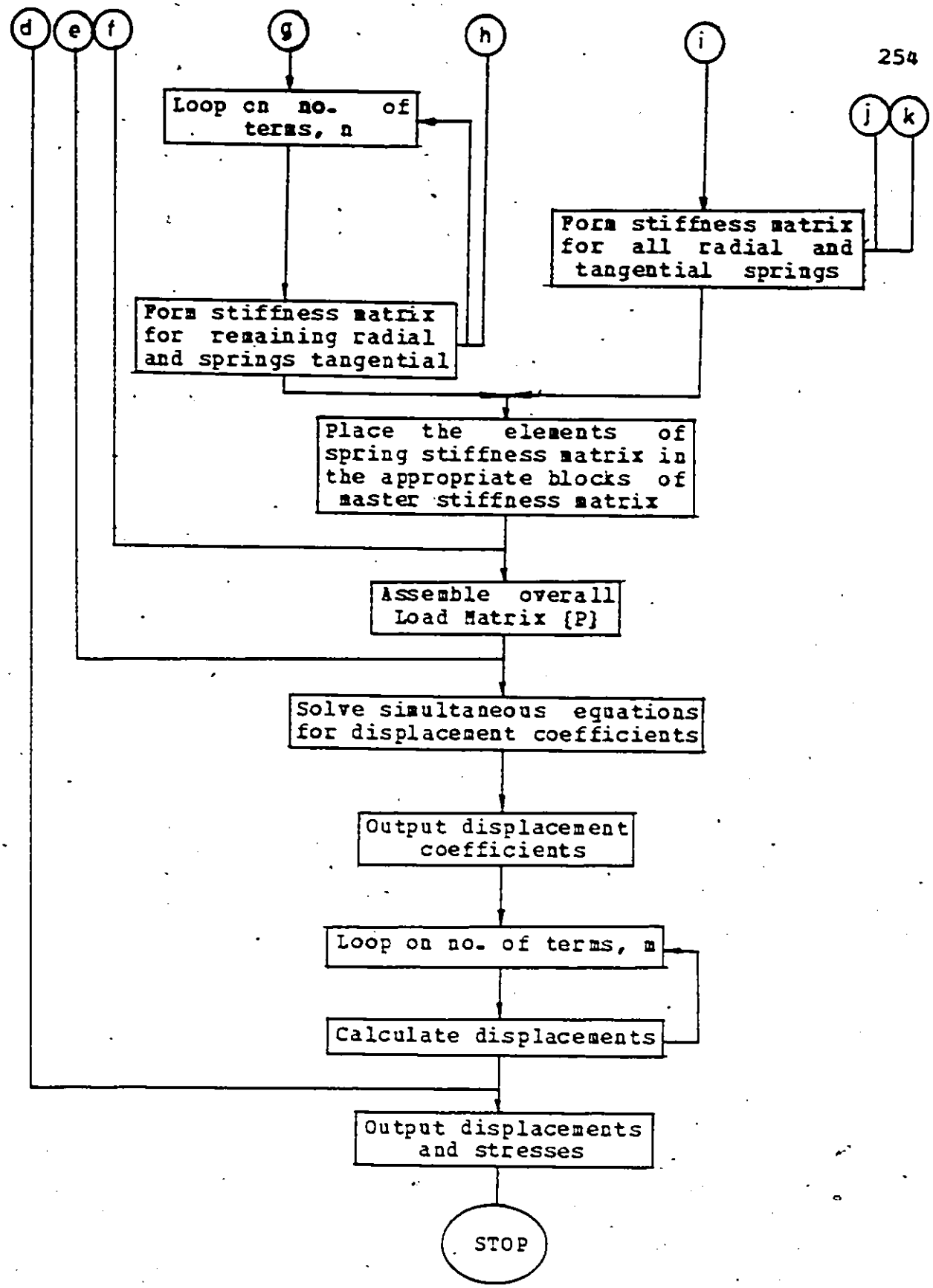
d
e
f
g
h
i
j
k
Loop on no. of terms, n
Form stiffness matrix for all radial and tangential springs
Form stiffness matrix for remaining radial and springs tangential
Place the elements of spring stiffness matrix in the appropriate blocks of master stiffness matrix
Assemble overall Load Matrix {P}
Solve simultaneous equations for displacement coefficients
Output displacement coefficients
Loop on no. of terms, m
Calculate displacements
Output displacements and stresses
STOP

NEWSHELL:- Flow chart for a program to analyse a soil-steel structure during side filling.

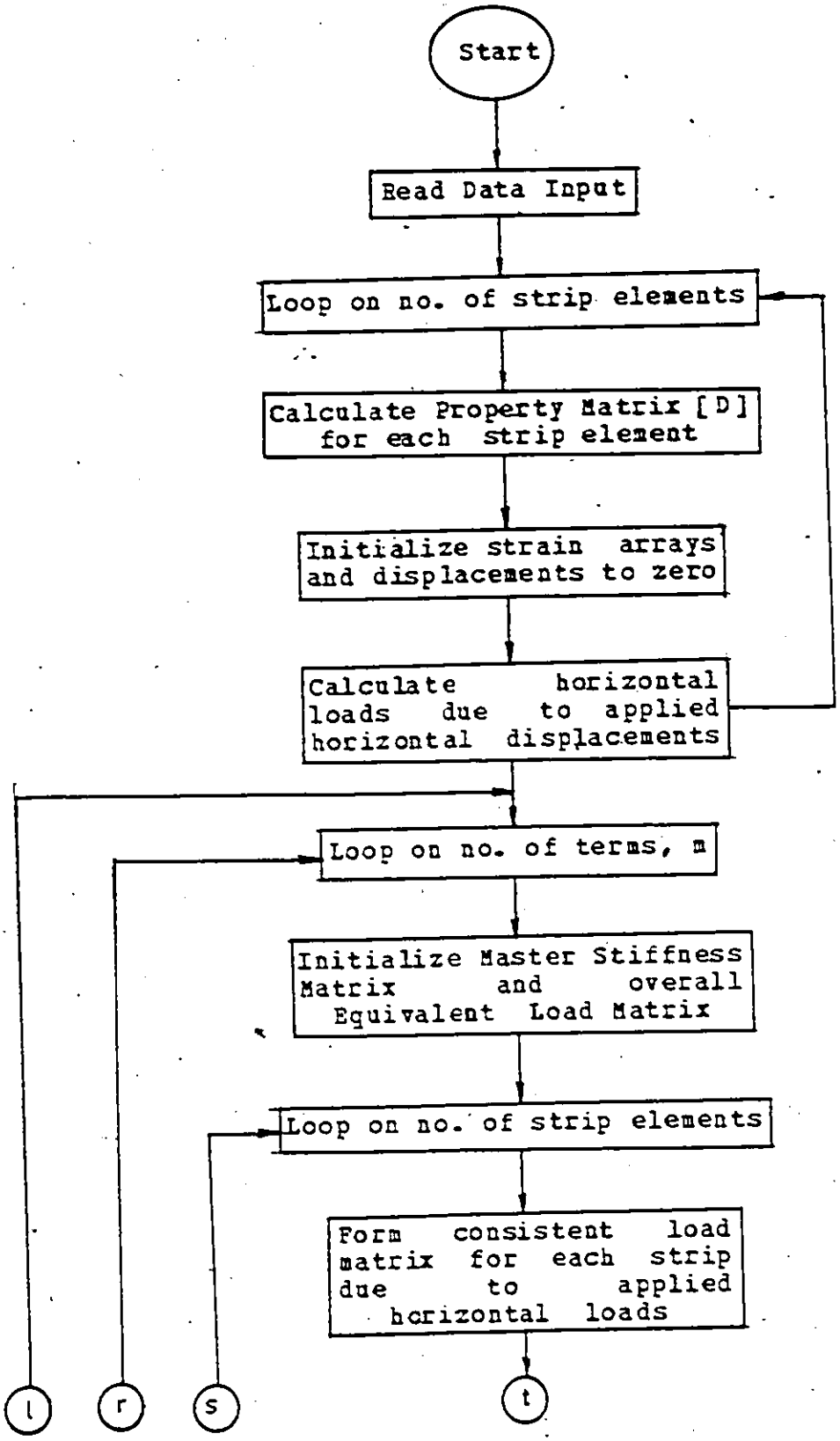

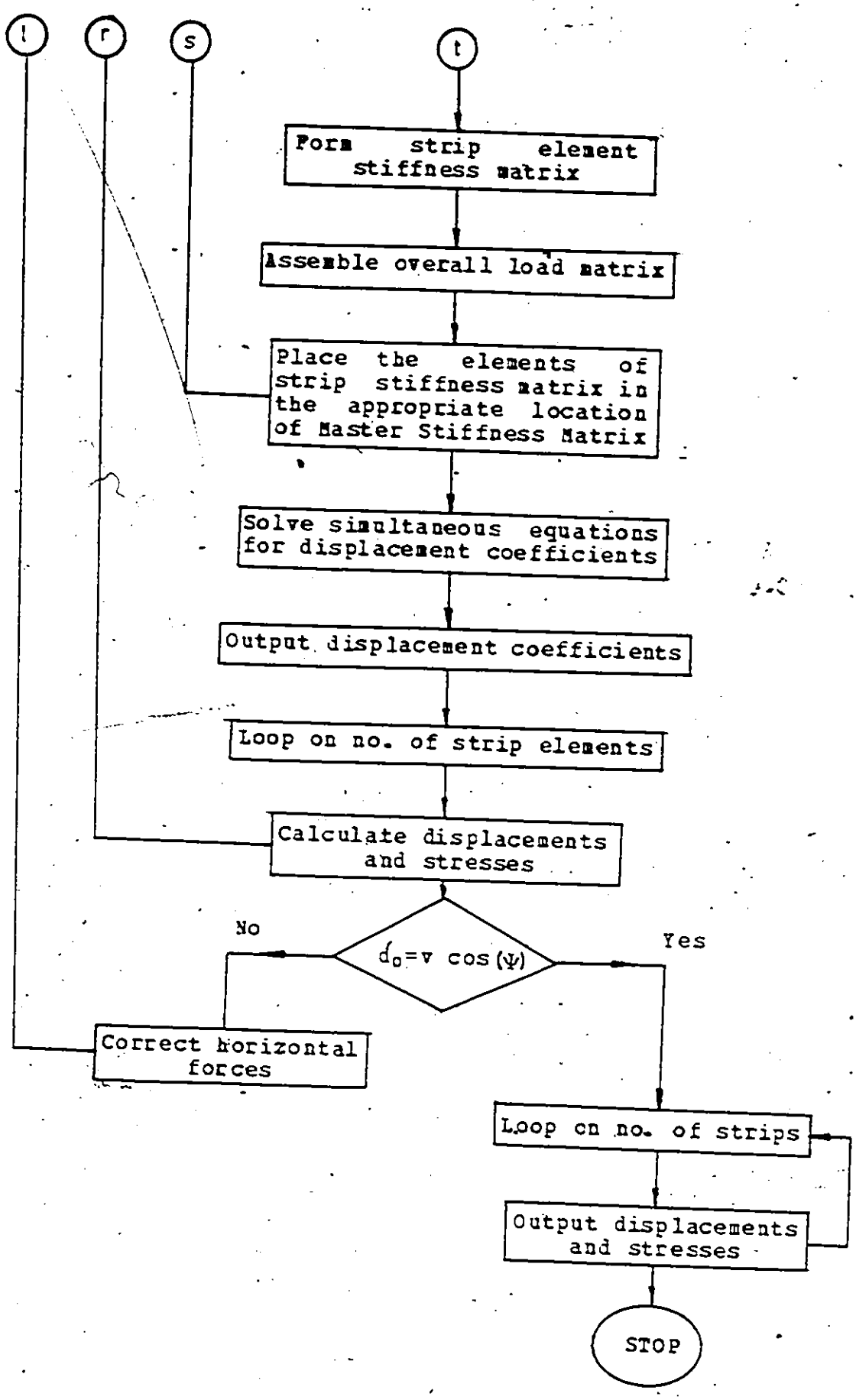
l
r
s
t
Form strip element stiffness matrix
Assemble overall load matrix
Place the elements of strip stiffness matrix in the appropriate location of Master Stiffness Matrix
Solve simultaneous equations for displacement coefficients
Output displacement coefficients
Loop on no. of strip elements
Calculate displacements and stresses
$d_0 = v \cos(\Psi)$
No
Yes
Correct horizontal forces
Loop on no. of strips
Output displacements and stresses
STOP

VITA AUCTORIS

The author was born on June 1st, 1953 in Pimpalner, Maharashtra (India). He completed the secondary school education in 1970 and joined two years pre-professional course at the Pratap College Amalner, India. Then the author joined the college of Engineering in 1972 at the University of Poona, where he was awarded Civil Engineering Merit Scholarship and Sir Dorabji Tata Trust Scholarship for four years. He graduated with a Degree of Bachelor of Engineering in Civil (1st Class with Distinction) in 1976 and joined M/S Engineers India Ltd., New Delhi as Assistant Engineer.

The author was awarded J.N. Tata Endowment Scholarship for Higher Studies in 1980 and he joined the Civil Engineering Department at the University of Windsor, Windsor, Ontario, Canada, as a teaching and research assistant. He graduated with M.A.Sc. degree from the same University in 1981. He was awarded University of Windsor Post Graduate Scholarship for four years. The author prepared this dissertation in partial fulfillment of the requirements for the Degree of Doctor of Philosophy in Civil Engineering.